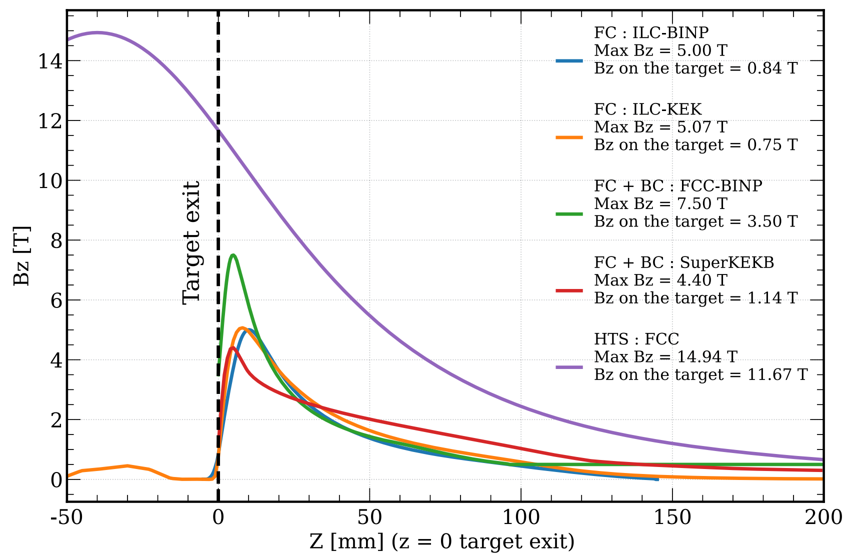

Fig. 7.6 Magnetic field profile of the AMD implemented in the form of the FC and HTS solenoid magnet. BC refers to the bridge coils, which are solenoid magnets surrounding the FC. The following FC models were analysed: BINP design for the ILC, KEK design for the ILC, BINP design for FCC-ee, and KEK design for SuperKEKB. A dashed line indicates the target exit surface

linac, positron and electron bunches are separated using a chicane at 170 MeV and the solenoid focusing is used up to a positron energy of 930 MeV. After the matching section at 930 MeV, the positron beam passes through quadrupole focusing and is accelerated up to the DR energy 2.86 GeV. An energy compressor system (ECS) is used before the DR to increase the number of positrons within the DR energy acceptance. The DR is an important part of the positron source design as its dynamic aperture, longitudinal and transverse acceptance parameters define the final performance of the positron source. The baseline design of the DR is described in Sect. 7.5.

Two AMD designs were investigated during the Feasibility Study: one employing a flux concentrator (FC) based on pulsed magnet technology (currently used in the SuperKEKB collider [357]) and another using a superconducting (SC) solenoid based on high-temperature superconducting (HTS) materials. The latter, an innovative approach for positron sources, will also be tested in the PSI Positron Production (P^3) experiment at SwissFEL [358], which has been designed as a demonstrator for the FCC-ee positron source technologies (see Sect. 7.4.6).

For the classical FC-based approach, several models were evaluated for the FCC-ee positron source design. These included the one designed by BINP for the FCC-ee and ILC projects, the FC developed by KEK for the ILC project, and the FC currently used in the SuperKEKB collider. Due to the conceptual and mechanical constraints of the FC, the peak of the magnetic field is located downstream the target and as a result, the available field on the target is reduced to ∼3.5 T/∼1.1 T (for the BINP/SuperKEKB designs respectively) manifesting a significant drop in capture efficiency. Moreover, the presence of a high transverse magnetic field component (with strong domination of dipole harmonic) makes the trajectories of positrons strongly distorted. As a result, the positron beam receives an offset in the vertical and horizontal planes. This must be mitigated for the positron beam transport in the capture line. Compared to the FC systems used in the SuperKEKB or BINP designs, the FCC-ee requires a higher repetition rate (up to 100 Hz), ideally with stronger magnetic fields and larger apertures. These requirements pose substantial technological and engineering challenges, particularly for high-power sources.

To address these challenges, an SC solenoid based on HTS technology was proposed for positron capture. The HTS solenoid offers several advantages over the FC design. It provides a significantly higher magnetic field at the target exit surface, a larger aperture and greater flexibility in target positioning, as the target can be placed inside the magnet bore. The axial symmetry of the solenoid ensures zero transverse magnetic fields at the magnet axis, eliminating beam distortion issues encountered with the FC option. The comparison of the field profiles for the FC and HTS solenoid designs, as used in the FCC-ee positron source studies, is shown in Fig. 7.6. Based on these considerations and simulation results, the AMD employing the HTS solenoid was selected as the baseline for the FCC-ee positron source.

The capture linac consists of six 3 m long, travelling wave (TW) 2 GHz RF structures with large iris apertures (2a = 60 mm), designed to provide enhanced transverse acceptance for positrons. The baseline design assumes an average RF gradient of 13.3 MV/m. Each accelerating structure is embedded within ten solenoid magnets, forming a solenoidal magnetic channel with a field strength of approximately 0.5 T, which efficiently guides the positron beam through the capture linac aperture. An additional solenoid magnet, referred to as the tuning solenoid, is placed between the AMD and the first accelerating structure. This solenoid increases the magnetic field experienced by the positron beam prior to entering the capture linac, further improving beam focusing and capture efficiency. The RF phases of the capture linac were optimised using the Xopt package [359] to maximise the final positron yield accepted by the DR.

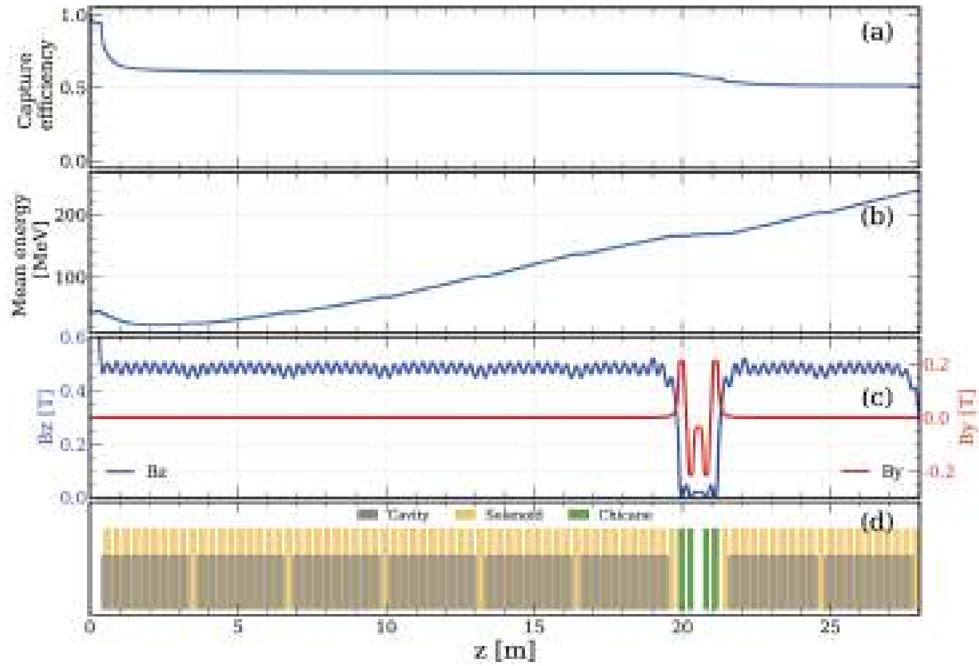

Fig. 7.7 Simulation results of the positron capture section, starting from the target exit surface. The plots illustrate: (a) the evolution of positron capture efficiency, (b) the positron beam energy, (c) the magnetic field profile along the capture section, and (d) the schematic layout of the capture section

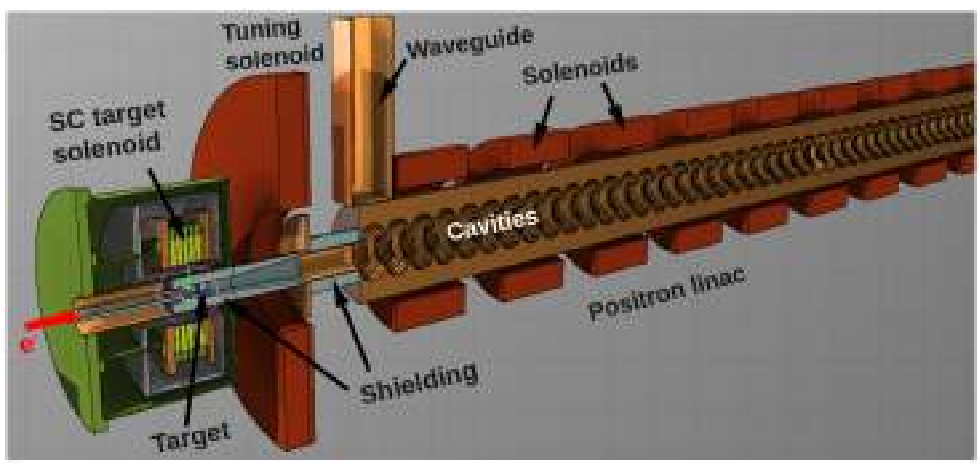

Fig. 7.8 FLUKA geometry model of the positron production target, the AMD with SC solenoid, the tuning solenoid, and the downstream positron capture linac

Figure 7.7 presents the key simulation results for the capture section, including the separator chicane and the first two accelerating structures of the positron linac. At the beginning of the capture section, a 33% drop in capture efficiency is observed, primarily due to the transverse acceptance of the accelerating structures. This is followed by a smaller 9% reduction in efficiency after the separator chicane.

7.4.2 Radiation load studies for target and capture system

The interaction of the electron drive beam with the positron production target gives rise to an intense flux of secondary particles. Only a fraction of the original drive beam energy contributes to the final positron yield, while most of the power is dissipated in the target, the AMD and the downstream capture linac. The resulting thermal load and cumulative radiation damage in the different components require a careful assessment in the engineering design process. This concerns in particular, the design of the production target and the optimisation of shielding components, which protect sensitive components like the SC coils of the AMD.

In order to quantify the impact of secondary radiation fields, radiation transport studies were carried out with the FLUKA Monte Carlo code. The FLUKA geometry model is illustrated in Fig. 7.8. The target was modelled as a stationary tungsten disk with a thickness of 15 mm. The target is surrounded by cylindrical tungsten shielding (13 cm long and 2 cm thick walls), which reduces the heat load and radiation damage in the AMD. The inner radius of the HTS coils of the AMD, placed in a cryostat, was 6.1 cm. A second tungsten shielding with a tapered

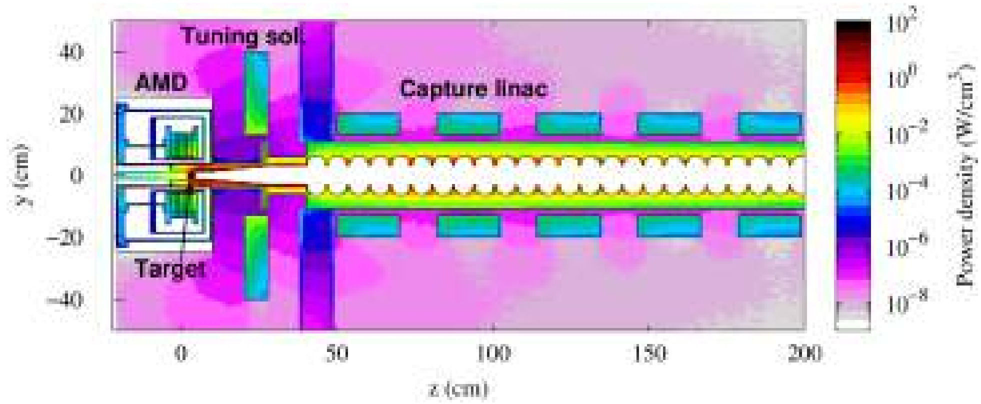

Fig. 7.9 Power density (Z-pole) in the target, AMD, shielding, tuning solenoid and the first RF cells of the capture linac. The peak power density in the target reaches 10 kW/cm^3 (out of the scale of the plot)

aperture was assumed to be located between the AMD and the tuning solenoid, and a third between the tuning solenoid and the first RF structure of the capture linac.

The radiation load studies assumed a 2.86 GeV electron drive beam with four bunches, a bunch charge of 2.37×10^{10} e$^-$, and a repetition frequency of 100 Hz, which results in an average drive beam power of 4.3 kW (Z-pole). The simulated power density distribution in the target, shielding, AMD and the first linac cells is illustrated in Fig. 7.9.

With such electron beam parameters, the target and surrounding shielding absorb around 1.3 kW, which poses a challenge for the target design; possible engineering solutions and cooling options are discussed in the next section. Another issue is the atomic dislocations in the target, which are mostly concentrated along the beam axis. Assuming 185 days of operation per year and a duty factor of around 80%, the radiation transport simulations show that the displacement damage in the target can reach a peak value of 1–2 DPA/year for FCC-ee operation at the Z-pole. Possible mitigation measures need to be determined, e.g., the design of a remote handling system, which would enable regular replacement of the target assembly.

The power deposition in the AMD, including cryostat, HTS solenoid and support structures, is only about 10 W, which demonstrates the effectiveness of the shielding. In particular, the power density in the HTS coils remains below 10 mW/cm^3, which is considered acceptable and is safely below the quench level of the solenoid. The simulations also show that the cumulative displacement damage in the HTS tapes is less than 1×10^{-4} DPA/year (Z-pole), which is not expected to degrade their properties. Furthermore, the total radiation dose to the coils reaches about 6 MGy/year. Since no organic insulation materials are used in the coils, such dose values should not pose a problem for the HTS solenoid, but require further assessment. If needed, a slight increase in the shielding thickness can reduce the dose further.

The capture linac is assumed to consist of six RF structures with 44 cells, which are surrounded by solenoids. About 0.6 kW are deposited in the shielding between the AMD and the capture linac. At the same time, most of the remaining power, i.e., about half of the power originally carried by the electron drive beam, is lost in the linac, mainly in the first structure. The tungsten shielding between the AMD and the linac protects the front face of the linac, but cannot intercept the most energetic secondary particles near the beam axis, which are then lost on the cavity walls. The highest radiation-induced power deposition in a single RF cell is about 70 W, but decreases to about 15 W at the end of the first RF structure. The thermal load due to RF wall losses is estimated to reach similar (or even higher) values as the average radiation-induced power deposition per cell. With an adequate cooling design, the radiation load in the linac is expected to be manageable. The solenoids around the RF structure are assumed to be normal conducting. The integrated dose in the solenoids is estimated to be about 1 MGy/year for operation at the Z-pole, which is considered acceptable. However, the peak dose in the upstream tuning solenoid reaches 5 MGy/year, which must be considered when choosing insulation materials. A better shielding of the tuning solenoid might be needed.

7.4.3 Design and integration of the positron source target

The current baseline design is based on a fixed target made of polycrystalline tungsten (W) with a thickness of 15 mm. The selection of tungsten as a material for the target is due to its high atomic number and its remarkable thermo-mechanical properties at high temperatures. However, to properly dissipate the thermal power produced by the beam impact, a thermal management strategy must be included in the design. For this purpose, a pressurised water cooling circuit is added in the target, as shown in Fig. 7.10a. This consists of a pair of embedded tantalum pipes that transport water from an upstream source and circulate through a 180° elbow inside the tungsten core. This setup will allow the beam-impacted region to properly transfer the 1.26 kW deposited on the target and its

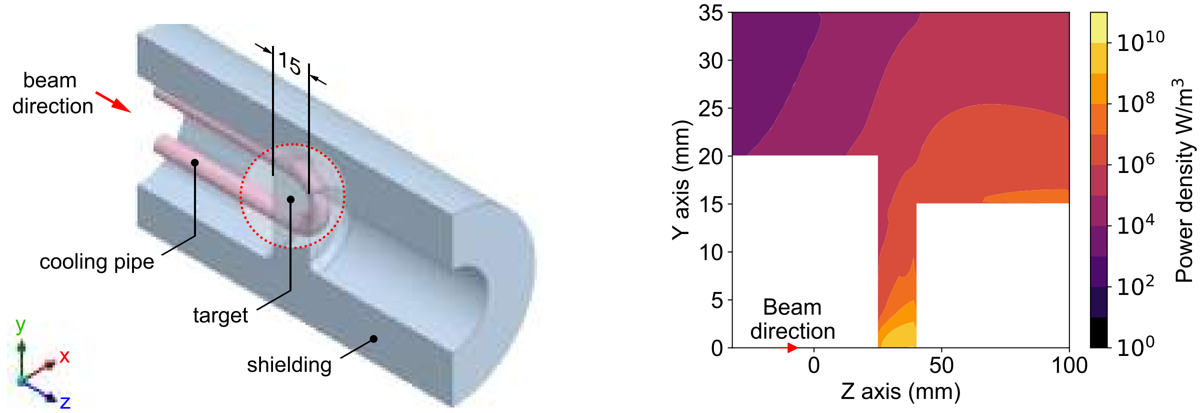

(a) (b)

Fig. 7.10 FCC-ee e$^+$ source target. (a) Baseline design geometry: the detailed zone shows the embedded tantalum cooling pipes. Only one half of the geometry is shown because it is symmetrical with respect to the x-axis and (b) power density deposition map obtained from FLUKA

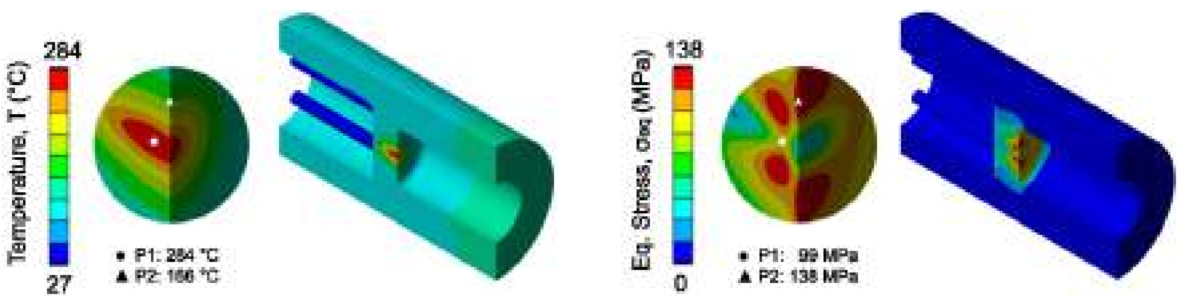

Fig. 7.11 Steady-state thermo-mechanical results: temperature (left) and equivalent stress (right) distributions for the baseline W target. Maximum temperature and stress points are marked with a circle and triangle, respectively

shielding and avoid the direct contact of water with bare tungsten. The power density distribution obtained from Monte Carlo simulations is shown in Fig. 7.10b, where the peak value is 10.4 kW/cm^3 and it takes place along the primary beam axis (z-axis), close to the exit face of the target.

Figure 7.11 shows the steady-state thermo-mechanical results. Note that the location of maximum temperature (P1) is not coincident with the position of maximum equivalent thermal stresses (P2). While P1 is along the beam axis beneath the exit surface, P2 is located at the exit surface at a height above P1. The maximum temperature at P1 is 284 °C. This means that the target is working below the ductile-to-brittle transition temperature (DBTT) for tungsten.[7] In terms of stresses at P1, the 99 MPa registered on the design are due to the constrained material surrounding the target. On the other hand, P2 reaches 166 °C with a maximum equivalent stress of 138 MPa located at the surface level and produced due to the strong thermal gradient. The resulting stress values are below the yield stress at the associated temperatures. The thermal fatigue analysis performed using the Universal Slope method [361] showed that the target is capable of withstanding the extreme service conditions and coping with the expected lifetime of the device, set to 155.4 days/year, which corresponds to 1.34×10^9 thermal cycles[8] with a duty factor of 0.84 [362]. Then, the number of thermal cycles is obtained by including the primary beam frequency of 100 Hz.

From the integration standpoint, the positron source target is a subsystem and its interaction with the required infrastructure is based on the mechanical layout of the P^3 experiment. The current configuration is being used to study the space requirements during the injector complex design. Figure 7.12 shows the tunnel cross section with dimensions of 4×4 m to host the expected services around the beam intercepting device. With the aim of allowing the installation and replacement of the target inside the HTS solenoid, a drift space of around 1.5 m is included. In

[7] For the results presented in this document, the DBTT was set to 400 °C, based on the behaviour of tungsten at high strain-rate loading conditions reported in [360].

[8] The target lifetime is estimated assuming an operation cycle of 185 days/year [13].

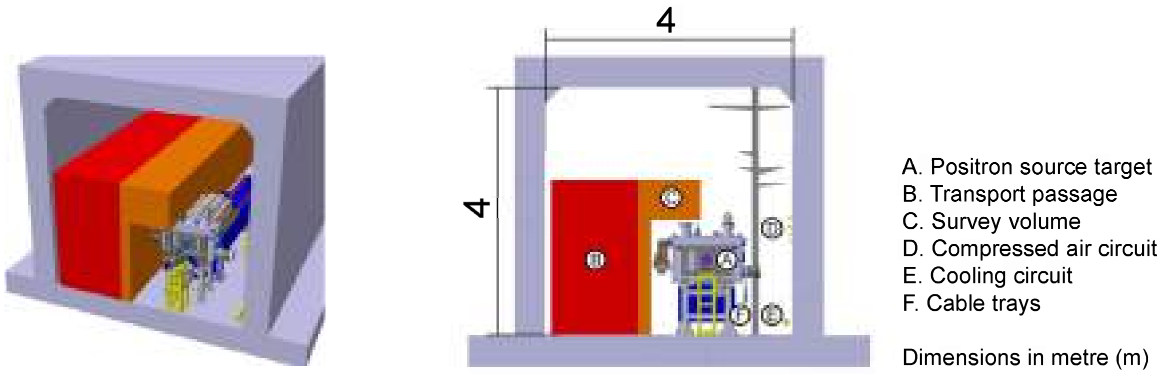

Fig. 7.12 Current layout of the FCC-ee injector complex cavern: tunnel overview (left) and expected utilities around the positron source target (right)

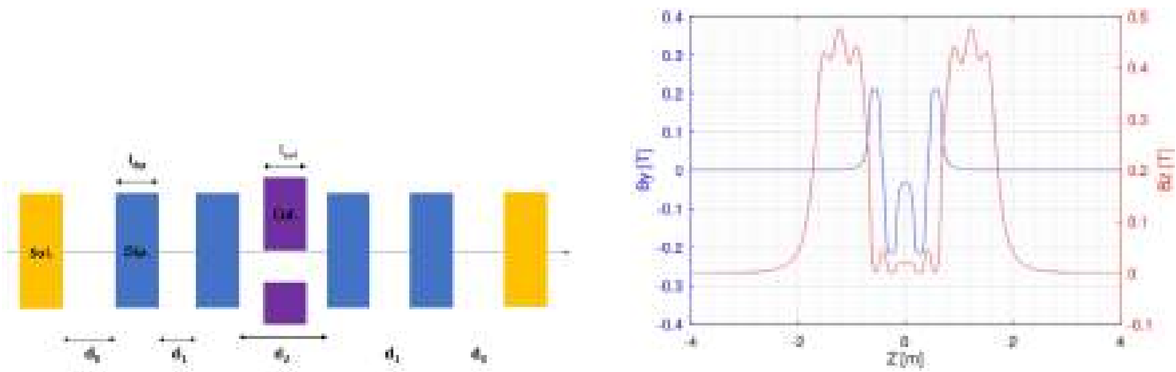

(a) (b)

Fig. 7.13 Separator chicane design. (a) Schematic layout of the chicane and collimator used to stop the electron and photon beams. Sol. refers to Solenoid magnet; Dip. refers to Dipole magnet ($l_{\mathrm{dip}} = 180$ mm) and Col. refers to Collimator ($l_{\mathrm{col}} = 120$ mm) with $d_0 = d_1 = 125$ mm and $d_2 = 350$ mm. (b) On-axis magnetic field of the chicane, including three neighbouring solenoids on each side

addition, an overhead travelling crane with a capacity of 500 kg to handle the target and the surrounding shielding is under consideration. In parallel, a more detailed study of radiation protection where the use of mobile shielding is an option is being carried out. At the same time, an evaluation of the utilities required (e.g., cooling, cabling, handling equipment) needs to be developed. Further integration studies are ongoing to define the requirements in terms of civil engineering. The results of these studies will be incorporated into the model for the general integration of the injector complex.

7.4.4 Positron linac

The positron linac (p-Linac) begins with a chicane equipped with a collimator (beam stopper) at its centre to remove electrons and photons co-propagating with the positron beam. The p-Linac is divided into two sections, each with distinct layouts. In Sect. 1, the layout is the same as that of the capture linac, where the accelerating structures are surrounded by solenoids. In contrast, Sect. 2 employs a simple FODO lattice, with each FODO cell containing two accelerating structures and a phase advance of 76.35°, optimised for minimum positron beam size. The accelerating structures and solenoids used in both sections are identical to those in the capture linac. The separator chicane is situated between the capture linac and Sect. 1, featuring a symmetric layout of four dipole magnets with identical designs but different current settings. A schematic diagram of the chicane, along with the collimator/beam stopper, is presented in Fig. 7.13a.

The dipole yoke in the chicane has a length of 180 mm and a vertical aperture of 70 mm. The beam pipe within the dipoles assumes a rectangular aperture of $\Delta x = 150$ mm and $\Delta y = 50$ mm. The collimator is horizontally offset by -35 mm. To account for field crosstalk between the chicane and the upstream and downstream solenoids, a 3D magnetic field simulation was performed using Maxwell3D. This simulation includes three solenoids upstream and three downstream of the chicane. The resulting on-axis magnetic field is shown in Fig. 7.13b.

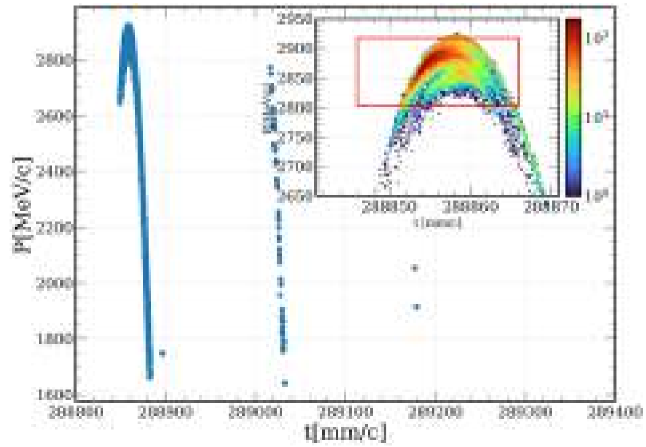

Fig. 7.14 Longitudinal phase space at the end of the positron linac. The inset provides a zoomed view of the main RF bucket. The red region represents the energy and time cut window used to estimate the fraction of positrons accepted by the damping ring

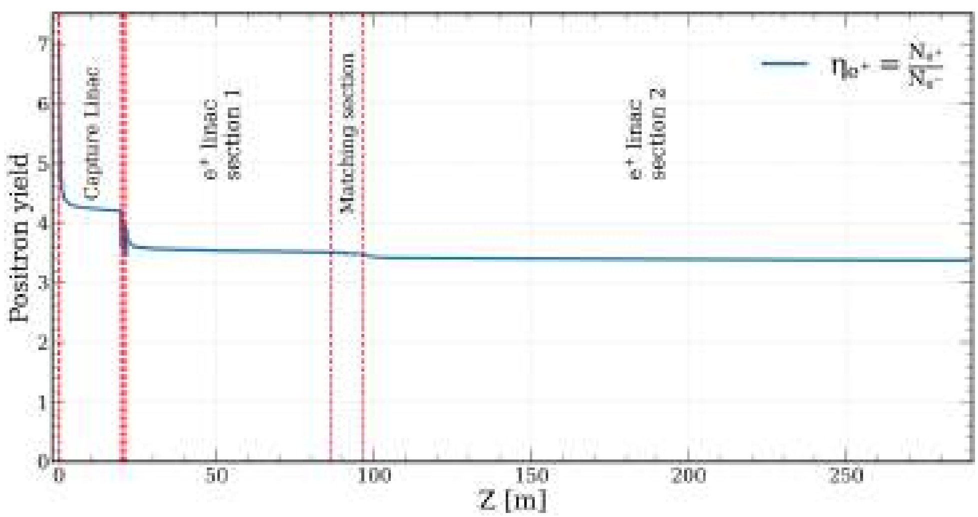

Fig. 7.15 Evolution of the positron yield along the longitudinal axis, from the target exit to the end of the positron linac. The dashed lines indicate the boundaries of the different sections of the positron pre-injector up to the end of the positron linac

Section 1 of the p-Linac contains 20 accelerating structures, with an average RF gradient of 13.3 MV/m. The RF phase is set to −10° off peak, optimised to maximise the final positron yield. At the end of this section, the average energy of the positron beam around the bunch core is approximately 932 MeV. Section 2 contains 52 accelerating structures, with an average RF gradient of 12.8 MV/m. Here, the RF phase is adjusted to 5° off crest for optimal positron yield.

Beam tracking throughout the p-Linac was simulated using RF-Track, including short-range wakefield and space charge effects. To estimate the effective positron yield accepted by the DR, particle selection was applied using energy and time cuts. For all results presented here, an energy window of ±2% around 2.86 GeV (i.e., 2.86 GeV ±57.2 MeV) and a time window of ± 10 mm/c were used. In the next phase of the FCC, positron tracking simulations in the positron linac followed by the injection in the DR should be carried out to have a more realistic estimate of the positron yield accepted.

7.4.5 Simulation results and final performance

Comprehensive start-to-end tracking simulations were conducted to evaluate the performance of the FCC-ee positron source. The final longitudinal phase space of positrons at the end of the p-Linac is shown in Fig. 7.14. Approximately 99% of the positrons reaching the end of the p-Linac are accelerated in the first main RF bucket. Furthermore, about 88% of these positrons fall within the assumed DR acceptance window, demonstrating the effectiveness of the positron source and linac design. The evolution of the positron yield along the longitudinal axis, from the target exit to the end of the p-Linac, is depicted in Fig. 7.15.

Table 7.6 summarises the key parameters and simulation results for the baseline design of the positron source and linac. Beam dynamics simulations confirm that the proposed design ensures reliable positron production, achieving a final accepted yield of 3 N_{e^+}/N_{e^-}. This meets the requirements set by the FCC-ee (Z-pole) with a safety margin of 2.56. To date, no critical issues have been identified that would prevent the use of a superconducting solenoid as

Table 7.6 Parameters and simulation results for the baseline design of the positron source and linac, delivering a positron bunch charge of 5 nC accepted into the damping ring, including safety margins. CS (capture system), CL (capture linac), p-Linac (positron linac), DR (damping ring)

Parameter	Value	Unit
e^- Drive Beam		
Beam energy	2.86	GeV
Repetition rate	100	Hz
Number of bunches per pulse	4	
Bunch charge	3.8	nC
Bunch length (rms)	1	mm
Beam size (rms)	1	mm
Beam power	4.3	kW
Target		
Thickness	15	mm
Production rate	7.07	N_{e+}/N_{e-}
Deposited power	1	kW
PEDD	5.8	J/g
Capture System		
AMD peak field (@Target)	15 (12)	T
Solenoid strength	0.5	T
AMD/CS aperture	60	mm
Average energy @CL	173	MeV
Positron yield @CS (before chicane)	4.2	N_{e+}/N_{e-}
Positron Linac		
Positron yield @p-Linac	3.4	N_{e+}/N_{e-}
Positron yield accepted @DR	3.0	N_{e+}/N_{e-}
Average energy	2.87	GeV
Bunch length (rms)	2.84	mm
Energy spread (rms)	0.87	%
Spot size x/y (rms)	5.28 / 2.78	mm
Normalized emittance x/y (rms)	13.1 / 13.0	mm·rad
Geometric emittance x/y (rms)	2.36 / 2.32	mm·rad

the AMD, along with the proposed capture system and positron linac, in the baseline design. For comparison, in a similar layout using an FC-based capture system (SuperKEKB model), the accepted positron yield is approximately 1.5 N_{e+}/N_{e-}. This lower yield would likely result in use of a thermionic gun to deliver the required electron drive beam bunch charge ($\geq$ 5 nC), significantly increasing the target power load.

Simulations incorporating imperfections in the positron source systems were also conducted. The imperfections considered, from the target to the end of the p-Linac, are summarised in Table 7.7, with RMS values reported. The impact of these imperfections is found to be negligible. The average positron yield accepted by the DR decreases by only 1.3%, while the average transverse emittances increase by 0.4% horizontally and 0.8% vertically. These results indicate the robustness of the proposed design.

7.4.6 PSI positron production (P^3) project

The PSI Positron Production (P^3) experiment is a demonstrator for the positron source and the goal is to design and install such a demonstrator in the SwissFEL facility, and experimentally validate a range of novel techniques that, according to simulations, have proven potential to increase the positron yield by one order of magnitude with respect to the state of the art [358]. The P^3 project is driven by the high luminosity requirements of the FCC-ee collider ring and its results will be one of the key outcomes of the feasibility study concerning the injector. The remarkable positron capture capabilities of P^3 are enabled to a great extent, by the usage of a high-temperature

Table 7.7 Summary of imperfections considered from the target to the end of the positron linac, with RMS error values reported for each parameter

Imperfection	Unit	Value
Transverse position error	µm	100
Transverse angular error (solenoids and dipoles)	µrad	200
Transverse angular error (other elements)	µrad	100
Magnetic strength error	%	0.1
RF gradient error	%	1
RF phase error	°	0.1
Beam position error	µm	100
Beam divergence error	µrad	100

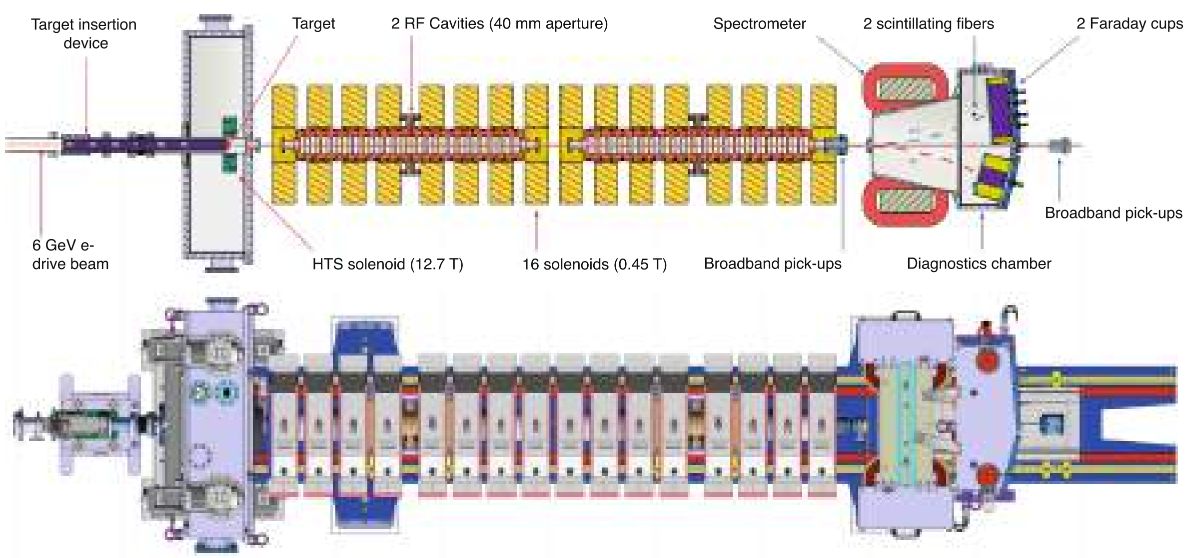

Fig. 7.16 Overview of the technology for the P^3 experiment

superconducting (HTS) solenoid around the target region, as well as a novel standing-wave solution for the RF cavities that provides a large iris aperture.

Figure 7.16 presents a technical drawing of the experiment, illustrating all the technologies developed or under development at PSI and CERN. These technologies have been carefully designed and optimised based on an in-depth study involving advanced beam dynamics simulations. This detailed simulation work made it possible to model and predict the behaviour of particle beams under various conditions, thereby refining the experimental setup and ensuring the optimal performance of each component. The figure also illustrates the integration of these technologies, highlighting key aspects such as the integration of the target in the cryostat that houses the HTS coils, the RF structures surrounded by normal conducting solenoids, and the diagnostics chamber that will allow measurement of the charge and energy spectrum of the positrons generated.

The procurement and assembly of most accelerator and diagnostic components are progressing on schedule, ensuring the timely completion of the project milestones. A key achievement has been the successful demonstration of the HTS solenoid at PSI, which achieved magnetic fields up to 18 T, a significant step forward for this advanced component.

Figure 7.17 shows photos of the P^3 component production process, including the HTS coils and their cryostat, the broadband pickups, and the first accelerating RF structure. Overall, the P^3 experiment is making steady progress, with installation work at SwissFEL proceeding smoothly during scheduled shutdown periods, which take place three times a year. Essential infrastructure components, such as segments of the extraction line and the high-voltage klystron-modulator system, are being installed in the tunnel according to plan. The primary installation phase is expected to conclude by the end of 2025, paving the way for the experiment to begin positron operations in 2026. It is worth noting that the SwissFEL facility is an ideal location for hosting the P^3 experiment, as it can deliver an electron beam energy of up to 6 GeV, matching the maximum drive beam energy required for the FCC-ee positron source. Currently, two beamlines (Aramis and Athos) are operational at SwissFEL, and the

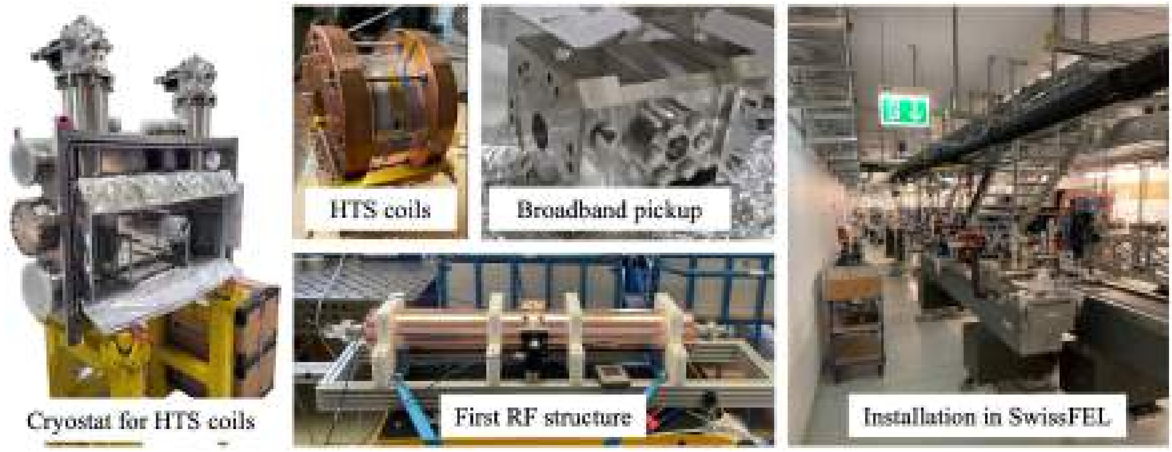

Fig. 7.17 P^3 components production and installation in SwissFEL

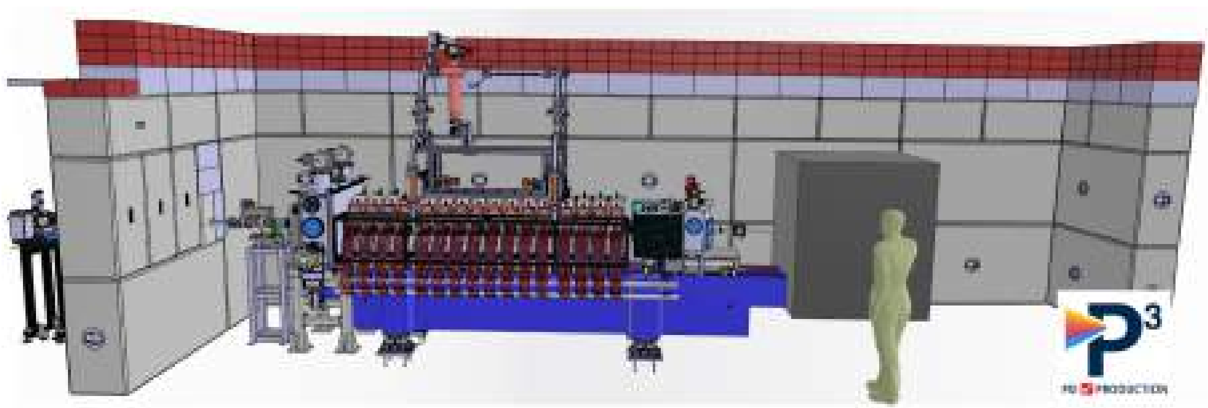

Fig. 7.18 The PSI Positron Production (P^3) Experiment

accelerator tunnel has reserved space for a future third beamline (Porthos). This layout provides sufficient room for the temporary installation of the P^3 experiment and switchyard. Figure 7.18 illustrates the current design of the P^3 experiment in its planned final configuration within the SwissFEL tunnel.

7.5 Damping ring and bunch compressor

The new optimised FCC-ee injector layout imposed a review of the intrinsic structure of damping ring (DR) Transfer Lines (TLs). The presence of two independent linacs for electron and positron beams, and the elimination of the common linac, naturally led to increased DR energy which, to avoid spin resonances, was set at the value of 2.86 GeV.

The main concept driving the DR and TLs design consists of achieving an overall efficiency of the order of 80% in transporting electron and positron beams from the respective linacs, through the DR for emittance cooling, to the end of the TLs conveying extracted beams toward the collider booster. Electron and positron linacs produce beam pulses at 100 Hz, each pulse consists of 4 bunches spaced by 25 nsec, each bunch stores a variable charge intensity up to 5 nC. The DR is mainly needed to reduce the emittance of the incoming positron beam by more than three orders of magnitude, from 2.36×10^{-6} m·rad to about 1.8×10^{-9} m·rad.

However, in the latest injector layout, the DR will also be used for electron beam cooling to cure possible emittance dilution induced by misalignments and space-charge effects. Several options have been studied and evaluated for the DR arcs, such as using multi-bend cells, and FODO cells. One of the options studied is based on a 6-fold symmetry ring, and has multi-bend arc cells. This design is presented as the main option in the following section. An alternative design of the DR has also been studied. A FODO cell is chosen and this alternative DR design, consists of three arcs and three straight sections that locate damping wiggler magnets, the RF cavity and injection/extraction equipment. The ring is about 384 m long, and its energy is 2.86 GeV. The injected beam emittance could be reduced to the required emittance value of 1.76 nm·rad, horizontal damping time is 6.4 ms

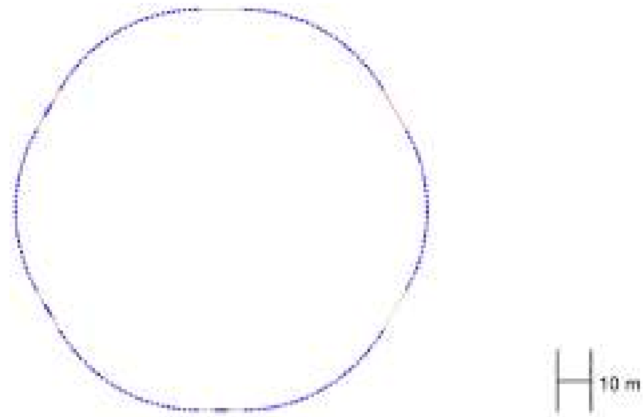

Fig. 7.19 Damping Ring layout. The six-fold symmetry allows having straight sections dedicated for different equipment: RF cavity, injection/extraction septa and kickers and wigglers (to reduce damping time and equilibrium emittance)

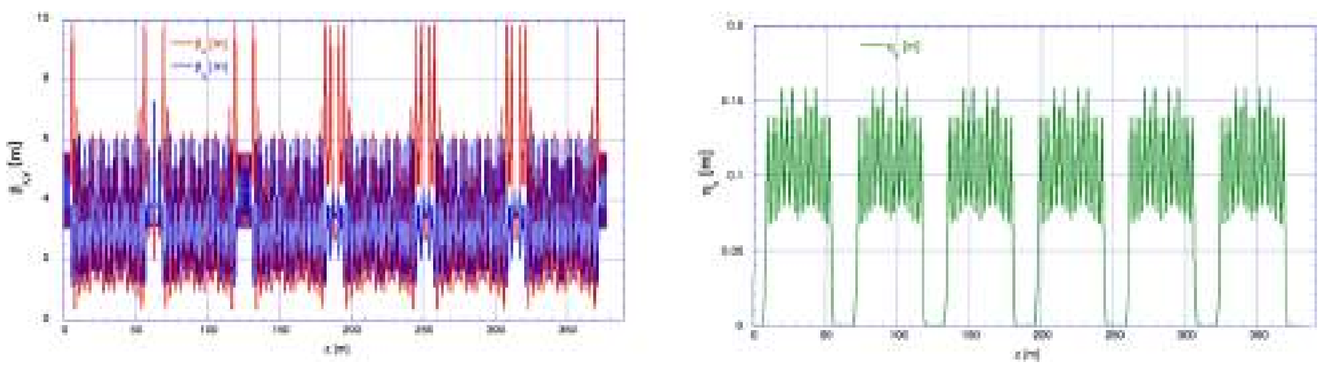

Fig. 7.20 Damping Ring optics: betatron amplitude (left) and dispersion (right)

and the energy loss per turn is 1.13 MeV. The total length of the damping wiggler magnets is about 36.45 m. They have a 2 T magnetic field and are distributed in the three straight sections. It could be possible to lower the magnetic field of the damping wiggler to 1.5 T for optimising the phase advance for minimum emittance (around 135°). However, this may cause even more challenging dynamic aperture optimisation.

7.5.1 New damping ring design

The new DR lattice features a six-fold symmetry, as shown in Fig. 7.19. It consists of six arc cells connected by six straight sessions. Each straight session is used to host three wiggler magnet insertions, one RF cavity module, and two independent injection/extraction sections. Injection and extraction will be implemented in the same branch for the two-particle species in order to avoid changing the polarities of the DR magnets, thus ensuring fast and reliable operation modes for both electron and positron. The injection will be performed using an on-axis scheme.

Arc cells are based on an achromatic multi-bend optics, symmetric with respect to the cell centre. Each half cell provides 30° deflection angle, using 15 bends of five different types. This approach allows keeping the maximum excursion of the horizontal dispersion, optimising damping time, and shaping the H_5 function along the cell to achieve low emittance. A further reduction of the damping time is obtained using three 3.5 m long wiggler magnets, each with a moderate magnetic field intensity of 1.8 T. Straight sections are based on the FODO structure and modified according to their function.

The DR optics is presented in Fig. 7.20, it features moderate betatron oscillation amplitudes achieved with a relatively weak focusing lattice producing low chromaticity per cell and, consequently, wide on- and off-momentum dynamic aperture. Limiting betatron oscillation amplitudes in the transverse planes below a maximum value of the order of 10 m is also beneficial in keeping the ring requirement in terms of stay-clear aperture under control, which is crucial especially for DR operation with positron beam. A complete list of the DR parameters is presented in Table 7.8.

Table 7.8 Damping ring parameters

Parameters	Value
Energy [GeV]	2.86
Circumference [m]	373.46
Arc Cell	multi-bend
Lattice shape	six-fold symmetry
Nat. emittance [nm rad] (WGL on/off)	1.3 / 2.3
Bunch Length [mm]	5.1
Damping time $\tau_{x,y}$ (WGL on/off) [ms]	16.9 / 29.4
Nat. Chromaticity (x/y)	−38.2/-28.3
Nat. energy spread (WGL on/off) [10^{-4}]	7.1 / 5.2
Betatron amplitude max (x/y) [m]	9.66 / 6.49
Betatron amplitude min (x/y) [m]	0.5 / 1.1
Tune (Q_x,Q_y)	27.8707 / 22.3728
Momentum compaction (WGL on/off) [10^{-3}]	1.55 / 1.57
Revolution period [µs]	1.2457
Dipole #, length [m], field [T]	180 , 0.7 1.13, 0.34 0.39
Wiggler #, length [m], field [T]	3, 3.5 , 1.8
Cavity #, length, voltage [MV]	1.5, 4
Max. # Bunch stored, Bunch Curr. [mA]	40 / 4
Store time	5 τ_y
Energy loss per turn (WGL on/off) [keV]	422.2 / 246.7
SR power loss wiggler [kW]	27.83
Kicker rise time [ns]	50

7.5.2 Timing

The maximum number of trains that could be simultaneously stored in the damping ring depends on the revolution period (T_{per}), the train length (Δt) and the kicker pulse rise time (t_K)

$$n_{train} = \frac{T_{per}}{\Delta t + t_K}$$

The storing time (T_{store}) for each train of bunches it is fixed by the requirements imposed from the next steps of the injector chain: the positron vertical emittance must be damped from 2.34 mm·mrad (ϵ^y_{inj}) to 0.18 nm·rad (ϵ^y_{ext});

$$\epsilon_y(t) \sim \epsilon^y_{inj} \mathrm{e}^{-\frac{2t}{\tau_y}}$$

The damping required implies:

$$T_{store} = -\frac{\tau_y}{2} \ln \frac{\epsilon^y_{ext}}{\epsilon^y_{inj}} \simeq 5\tau_y$$

Using the values in Table 7.8 for the revolution period and the linac repetition rate of 100 Hz ($T_{RepRate} = 10$ ms) gives:

$$\tau_y \leq \frac{n_{train} T_{RepRate}}{5} \simeq 20 \text{ ms}$$

with $n_{train} \simeq 10$ that corresponds to $T_{per} \geq$1.25 µs.

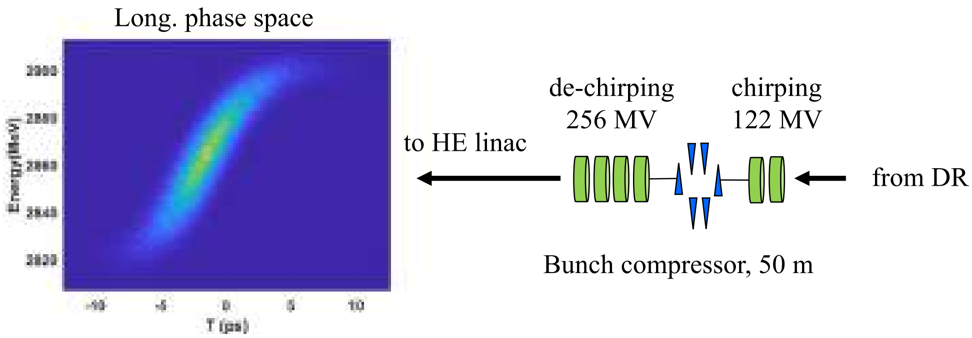

Fig. 7.21 Bunch compressor at 2.86 GeV placed between the DR and the HE-linac. Left: longitudinal phase space after the compression and de-chirping. Right: schematic layout and overall length

7.5.3 Bunch compressor

The bunch compressor is designed to reduce the bunch length of the beam originating from the damping ring, from an initial range of 4–5 mm to a final length of ∼1 mm. Figure 7.21 (right) illustrates the schematic layout of the bunch compressor, which consists of a magnetic chicane formed by four C-shaped bending magnets. Each magnet has a magnetic length of 1.9 m and a maximum magnetic field strength of 1 T. The momentum compaction factor R_{56} is −0.336 m, and the bending angle of each magnet is 11 degrees, resulting in a maximum dispersion of 0.98 m. The distance between dipoles 1 (3) and 2 (4) is 2.9 m, while the separation between dipoles 2 and 3 is 2 m. To induce the necessary energy chirp for compression, two RF structures, providing a maximum accelerating voltage of 122 MV, are employed. Additionally, four RF structures are utilised to partially remove the residual chirp in order to meet the specifications of the high-energy linac (HE-linac). These structures operate with a maximum accelerating voltage of 256 MV. Beam dynamics simulations were performed using the ELEGANT code for a bunch with a maximum charge of 5 nC. Figure 7.21 (left) shows the longitudinal phase space after the compression and de-chirping. The results indicate a residual energy spread of 0.7% after de-chirping, a compression factor of 5.75, and a reduction in the bunch length from 4.6 mm to 0.8 mm. The horizontal emittance growth is approximately 20%, while the vertical emittance growth remains below 1%.

7.6 High energy linac and energy compressor

7.6.1 High energy linac

The high-energy (HE) linac accelerates electron and positron beams from the exit of the chicane downstream of the DR at 2.86 GeV energy up to the transfer line towards the booster ring injection at 20 GeV energy.

Analogous to the e-linac, beam dynamics simulations have been done to study both longitudinal and transverse beam dynamics in the HE-linac. The following beam parameters were used in the simulations: bunch length 1 mm, emittance 1 mm·mrad and 10 mm·mrad in the vertical and horizontal plane, respectively at the start of the HE-linac for a 5 nC electron bunch. The lattice is the same as the electron linac: a FODO lattice with 90° phase advance per cell, one quadrupole, and one BPM per RF structure. The RF structures operate at the peak of the RF electric field (on-crest) to maximise accelerating efficiency and minimise beam quality degradation. The beam tracking simulations described in this document were performed using RF-Track [354].

To evaluate the robustness of the linac design against static misalignments in terms of emittance growth, the same Gaussian-distributed misalignments assumed for the electron linac and reported in Table 7.4 and the BPM resolution of 10 µm were considered.

To mitigate the effects of misalignments, a combination of one-to-one correction and dispersion-free steering (DFS) was applied sequentially, incorporating the randomly distributed errors. In this case, the focus is on the vertical plane, which is much more critical due to the smaller margin between the starting value and the value accepted by the booster. Finally, a maximum emittance growth of 0.6 mm·mrad in the vertical plane was obtained at the end of the linac for 98% or more of the simulation seeds, giving a final emittance of 1.6 mm·mrad below the maximum 2 mm·mrad required at the booster injection. A similar emittance increase is expected in the horizontal plane, which would give a final emittance smaller than 15 mm·mrad, still satisfying the booster requirement (maximum emittance smaller than 20 mm·mrad) in the horizontal plane. These results were achieved by varying the RF structure aperture and optimising the minimum number of sections (resulting in 8 for the HE-linac) in which the linac must be divided to avoid propagating an error in the correction over a long distance. These simulations determined a minimum aperture of the RF structure corresponding to $a/\lambda = 0.12$.

The dynamic effects were investigated using the same approach as the electron linac. The JA was determined by tracking simulations varying the length of the RF structure, impacting the distance among the quadrupoles, the

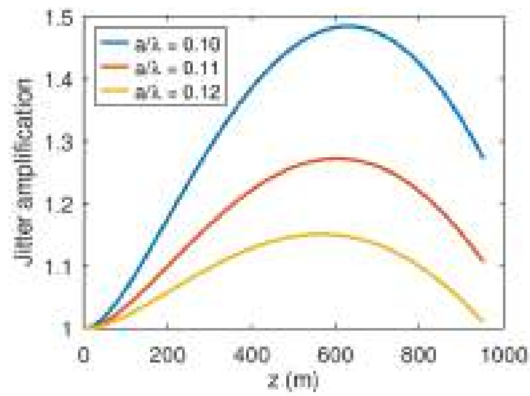

Fig. 7.22 Jitter amplification along the HE-linac for several RF structure apertures. The RF structures are operated on-crest, with a quadrupole spacing of 3.75 m (corresponding to the RF structure length of 3 m)

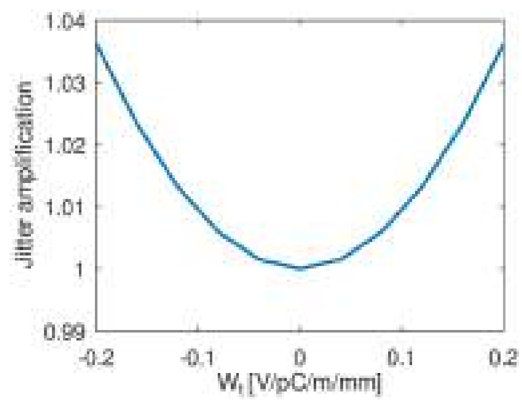

Fig. 7.23 Multi-bunch jitter amplification at the end of the HE-linac

Table 7.9 Summary of the optimised RF and lattice parameters based on the beam dynamics studies

Parameter	Value
Mean RF structure aperture (mm)	13.9 ($a/\lambda = 0.12$)
RF structure length (m)	3
RF structure operating phase	on-crest
Phase advance/cell (degrees)	90
Number of BPM/RF structure	1
Number of quadrupoles/RF structure	1
Distance between the quadrupoles (m)	3.75

phase advance per cell, and the RF structure aperture. Figure 7.22 shows, for example, the JA along the HE-linac assuming a constant RF structure length of 3 m (corresponding to a distance among the quadrupoles of 3.75 m) for several RF structure apertures. In particular, for an RF aperture corresponding to $a/\lambda = 0.12$, a final JA of 1.01 was obtained for 3 m RF structure length. The multi-bunch effects were investigated by imposing a kick from the first to the following bunch, analogous to what was done for the e-linac. The results are shown in Fig. 7.23. The RF structure has been designed to provide a long-range wakefield corresponding to a maximum kick equal to 0.11 V/pC/m/mm for the 5 nC bunch charge. This corresponds to a multi-bunch JA of 1.02.

Single- and multi-bunch JAs give a total JA of 1.03. This allows a very large transverse jitter coming from the upstream sections to be tolerated. The latter is expected to be much smaller than the one at the exit of the gun section, due to the damping in the DR (which is expected to reduce the incoming jitter) and the kickers currently in use (which introduce angle jitter). Table 7.9 summarises the most important lattice and RF structure parameters determined by the beam dynamics simulations. In summary, the RF structure aperture, length, and lattice of the HE-linac fulfil the specifications determined by the transfer line and booster in terms of static and dynamic effects.

Table 7.10 Parameters of the high energy EC assuming the same machine settings for the maximum 5 nC and a minimum 5 pC single-bunch charge. 'Initial' indicates that the parameter is computed at the entrance of the EC chicane and 'final' at the exit of the downstream RF modules. The voltage is 410 MV

Parameter	Q = 5 nC	Q = 5 pC
Initial rms bunch length (mm)	1.00	1.00
Initial single bunch ΔE/E (%)	0.56	0.20
Final rms bunch length (mm)	4.00	1.43
Final single bunch ΔE/E (%)	0.10	0.12

7.6.2 Energy compressor

The Energy Compressor (EC) [363] at the end of the HE-linac is essential to achieve optimal performance along the HE-linac and, at the same time, the beam parameters required by the transfer line and the booster ring. This kind of system, previously utilised in accelerators such as SuperKEK-B to enhance positron capture efficiency in the damping ring (DR), consists of a magnetic chicane followed by RF structures operated at zero-crossing phase. Using the EC presents several advantages:

- Possibility to operate the RF structures of the HE-linac on-crest. This is advantageous for the mitigation of emittance growth and accelerating efficiency.
- It minimises the single-bunch energy spread due to the RF curvature and the longitudinal short-range wakefields.
- It reduces the bunch-to-bunch energy variation due to a very large variation from several nC down to nearly 0 nC bunch charge and associated beam loading effects when using a 'golden' RF pulse during top-up mode operation.
- It reduces the overall bunch-to-bunch energy jitter.
- It manipulates the beam longitudinal phase space to match the booster requirements.

The EC also has some drawbacks:

- It requires more hardware and more space.
- It converts energy jitter and offset to arrival time jitter and offset, which must be within the tolerance of the downstream sections.

While the transfer line and booster requirements can be met without this system, its absence would lead to reduced performance along the HE-linac.

The EC may be utilised exclusively for single-bunch effects, as well as for both single- and multi-bunch effects. In the first case, the R_{56} of the chicane and the integrated voltage of the RF structures are determined by the target bunch length and energy spread, given the incoming chirp. The simulations also incorporate a residual chirp resulting from compression downstream of the DR, estimated at 0.7% for the 5 nC bunch charge. Table 7.10 summarises the results obtained for a maximum and minimum charge of 5 nC and 5 pC, respectively. In this configuration, increasing the integrated voltage can reduce the single-bunch energy spread by a factor of 3 to 4 while maintaining the bunch length. The booster injection does not currently require this, but it is stressed that the system can, in principle, provide it.

Although bunch-to-bunch beam loading compensation can be managed through a low-level RF (LLRF) system, this system must have the capability to modify the RF phase and/or amplitude for each of the infinite combinations of bunch charges in the timescale of the bunch separation (presently 25 ns) for four bunches accelerated during the same RF pulse. Ongoing studies are therefore investigating whether the EC fulfils this task by leveraging a single constant golden pulse optimised by the LLRF, which remains the same for all the possible charge combinations. In this context, the bunch length was identified as a third degree of freedom to fine-tune the single-bunch properties. The bunch length selected is 0.8 mm rms instead of the 1 mm assumed so far. This modification is not detrimental to the other aspects of the design, since a shorter bunch would even be advantageous for static and dynamic effects at the price of a slightly increased single-bunch energy spread of 0.05% at the EC entrance.

Like the previous case, the simulations incorporate the residual chirp resulting from compression downstream of the DR, estimated to be 0.7% for all bunches, and the beam loading effect as a function of the bunch charge calculated assuming the golden pulse discussed in this document, see Fig. 7.30. The optimal R_{56} of the chicane is about 0.55 m and the voltage of the downstream RF structures is equal to 620 MV. This corresponds to a total EC length of less than 90 m including matching sections upstream and downstream of the chicane, the chicane itself, made of normal conducting dipoles, and three RF modules. Table 7.11 summarises the results for the maximum single-bunch charge of 5 nC. The results of the low-charge scenario simulations without modifying

Table 7.11 Parameters of the EC for the maximum 5 nC bunch charge, assuming a target single-bunch energy spread of approximately 0.1%. B_j corresponds to j^{th} bunch along the train. The extra time delay is computed by subtracting an increasing integer number of RF structures periods. The voltage is 620 MV

	B_1	B_2	B_3	B_4
Initial rms bunch length (ps)	0.80	0.80	0.80	0.80
Initial single bunch ΔE/E (%)	0.61	0.61	0.61	0.61
Initial offset centroid ΔE/E from B_1 (%)	0	−0.31	−0.59	−0.93
Final rms bunch length (mm)	4.06	4.07	4.09	4.10
Final single bunch ΔE/E (%)	0.11	0.11	0.10	0.09
Final offset centroid ΔE/E from B_1 (%)	0	−0.01	−0.03	−0.05
Final centroid Δt from B_1 (ps)	0	5.7	11.0	17.3

Table 7.12 Parameters of the EC for a 5 pC bunch charge, assuming the machine parameters optimised for the 5 nC bunch charge (RF structures phasing and strength of the dipoles set using the 5 nC bunch as a reference). The relative energy spread, energy offset, and extra time delay are computed with respect to the B_1 of the 5 nC bunch charge

	B_1	B_2	B_3	B_4
Initial rms bunch length (ps)	0.80	0.80	0.80	0.80
Initial single bunch ΔE/E (%)	0.14	0.14	0.14	0.14
Initial offset centroid ΔE/E from B_1 at 5 nC (%)	1.62	1.97	2.30	2.54
Final rms bunch length (mm)	1.04	1.04	1.03	1.03
Final single bunch ΔE/E (%)	0.13	0.13	0.12	0.12
Final offset centroid ΔE/E reference B_1 at 5 nC (%)	0.14	0.21	0.29	0.36
Final centroid Δt from B_1 at 5 nC (ps)	−29.0	−35.2	−41.0	−44.9

Table 7.13 Spread of the beam parameters at the EC exit for the different charges (assuming the same bunch charge along the four bunches), and considering the maximum single-bunch variation from 5 nC down to 5 pC. The peak-to-peak values are taken for the B_4, which are the maxima

	Initial	Final
Single-bunch rms energy spread @ 5 nC (%)	0.61	0.103±0.009
Single-bunch rms bunch length @ 5 nC (ps)	0.80	4.08±0.02
Single-bunch rms energy spread @ 5 pC (%)	0.14	0.125±0.006
Single-bunch rms bunch length @ 5 pC (ps)	0.80	1.035±0.006
Peak-to-peak centroid energy offset variation from 0-5 nC (%)	±1.74	±0.21
Peak-to-peak centroid Δt variation from 0-5 nC Δt (ps)	0	±31

any machine parameters optimised for the high-charge case are shown in Table 7.12. The shorter single-bunch length compared to the higher charge mode appears to be acceptable for the booster, as lower charges are less susceptible to instabilities.

In conclusion, the EC enables the operation of the HE-linac at settings optimised for beam dynamics and RF structures while ensuring that the target parameters for the downstream lines are matched at its output. The energy jitter and offset caused by substantial bunch charge variations ranging from a few nC to nearly zero are converted into time delays and jitter, which are better tolerated by the transfer line and the booster ring compared to energy variations. Table 7.13 summarises the expected range of parameter variation for the final bunch. Some minor effects, like the variation of the bunch length and the residual chirp from the bunch compressor before HE-linac for the 5 pC charge, are presently neglected. Others are overestimated, such as the single-bunch beam loading, which is included in both the golden pulse calculation (solely the fundamental mode) and the tracking code. Even with these assumptions, the HE-linac and EC design fulfil the requirements of the downstream sections. Further studies are underway to fine-tune the results.

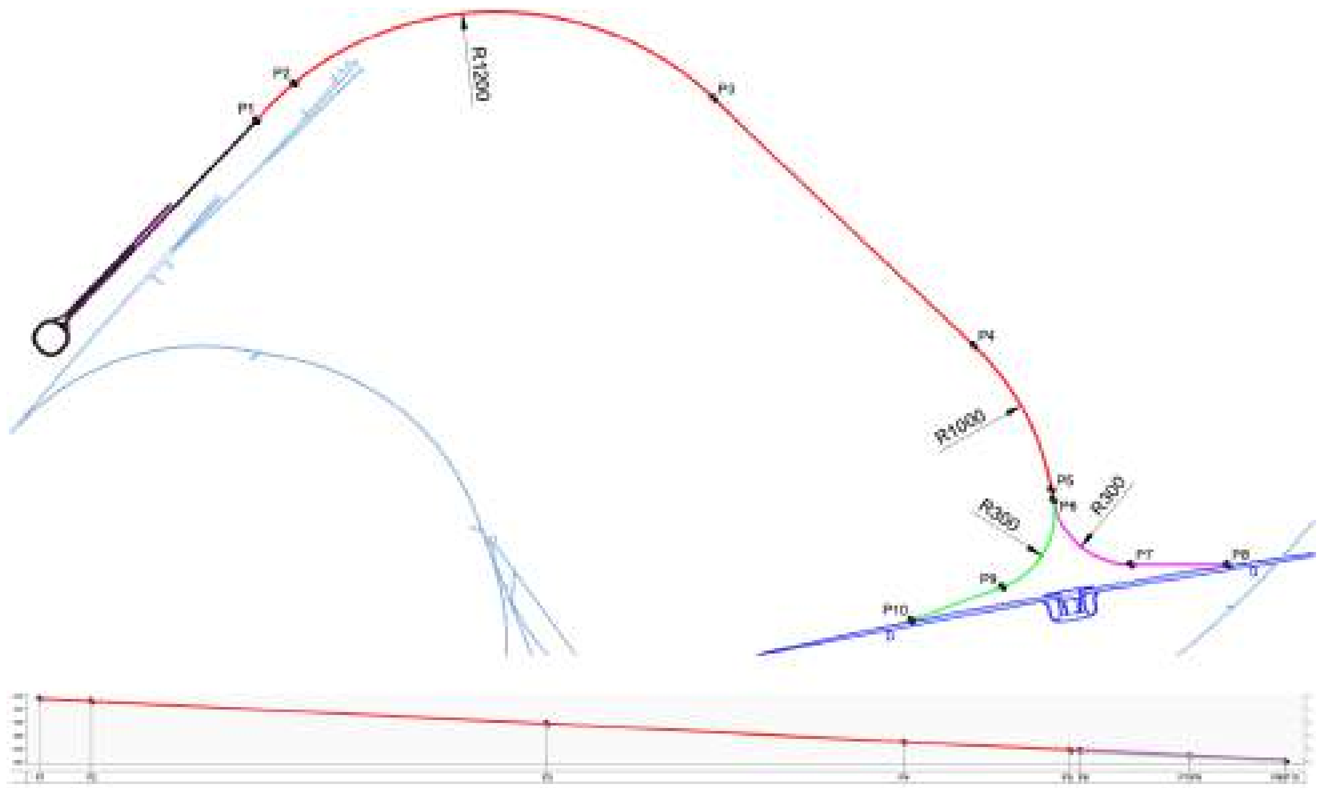

Fig. 7.24 Lepton transfer lines from the injector complex on the surface to the collider tunnel

7.7 Transfer lines from HE-linac to booster

7.7.1 Transfer line geometry

The transfer line geometry has undergone significant changes between MTR and this report. The transfer lines at the MTR stage passed close to the SPS to allow synergy with hadron transfer lines for FCC-hh and for the physics programme in the SPS. The design suggested here provides a direct connection from the output of the HE-linac on the surface at the CERN Prévessin site, see P1 in Fig. 7.24 to the two extremities of the collider tunnel straight section of PA, see P8 and P10, respectively. This design is driven mainly by civil engineering constraints related to scheduling and shaft availability. It also features a symmetric line design for electrons and positrons, ensuring that the beam dynamics impact of synchrotron radiation in the final bending sections is equal for both species. The location of the injector complex allows a very efficient connection between HE-linac and the CERN North Area (NA); see beamlines close to P2 in Fig. 7.24. It remains to be discussed if a beam transfer in the reverse direction from the booster back to, e.g., the NA or a direct line from the HE-linac to the SPS is required and to design the transfer lines accordingly.

7.7.2 Cell design and beam dynamics

As shown in Fig. 7.24, the high-energy linac to booster transport has been designed with a constant negative vertical slope of −3° in the CERN Coordinate System (CSS), combined with horizontal bending in sectors P2-P3, P4-P5, P7-P8 and P9-P10. The slope will be applied and removed at the first and last cells of the line, respectively. To maintain it along the line, the local bending plane must be progressively tilted following the expressions described in Ref. [364]. Figure 7.25 confirms that such a procedure yields the correct beam trajectory. This *twisting reference frame* will introduce a coupling between horizontal and vertical motion. Skew quadrupoles may be needed to control such a coupling, although they have not been included in this initial iteration.

Additionally, the beam transport from the high-energy linac to the booster must be designed to stay within the 'beam quality' budget specified in Table 7.14, which will drive the lattice design choices.

FODO cells have been chosen to design the transfer line due to their simplicity. Later iterations may explore other types of cells, which explicitly aim to minimise the impact of synchrotron radiation (such as theoretical-minimum-emittance cells). The chosen phase advance is 135° as it is close to the optimum for minimising emittance

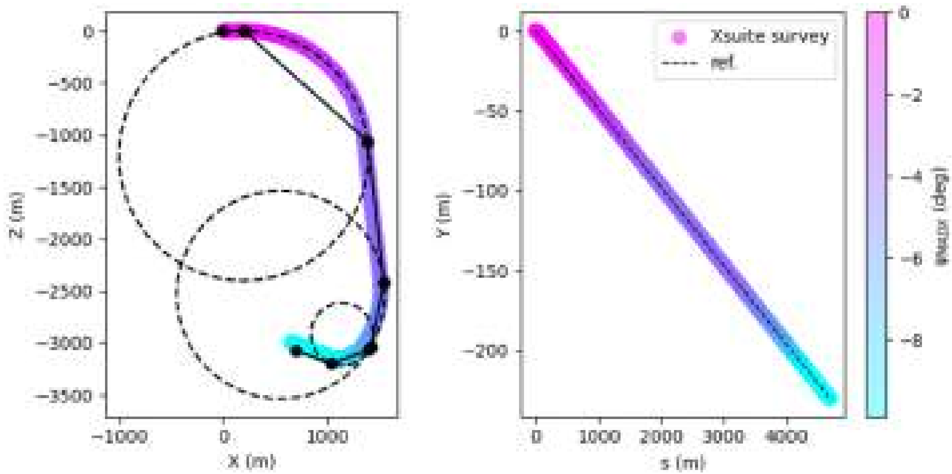

Fig. 7.25 XSUITE survey output and reference trajectory provided by Civil Engineering. The colour bar shows the local roll angle ψ_{MADX}, which is necessary to maintain a constant vertical slope in the global frame

Table 7.14 Summary of Sector Parameters

Sector	Bunch len. (mm)	RMS dp/p (10^{-3})	$\epsilon_{x,N}$ (μm)	$\epsilon_{y,N}$ (μm)
(...)				
HE Linac	1	7.5	16	1.6
E. Compressor	4	1.0	16	1.6
Transfer	TBD	TBD	TBD	TBD
Booster Inj.	4	1	20	2
(...)				

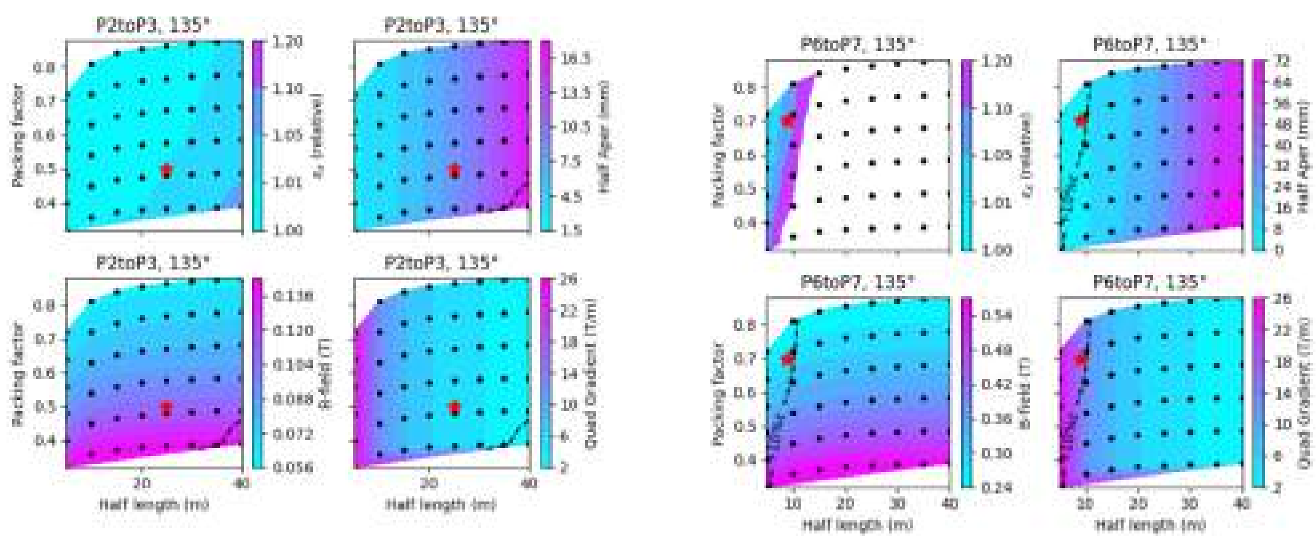

Fig. 7.26 Horizontal emittance blow-up, bending field, quadrupole gradient and aperture as a function of cell half length and dipole fill factor

blow-up [365], while remaining an easy number to work with when designing orthogonal correction schemes. Figure 7.26 shows the horizontal emittance blow-up as a function of the cell length and the dipole fill factor for the sectors P2-to-P3[9] and P6-to-P7 (or equivalently P9-to-P10). The required quadrupole gradients, bending fields

[9]P4-to-P5 has very similar behaviour to P2-to-P3.

Table 7.15 FODO cell parameters

Attribute	Long FODO (P1-to-P6)	Short FODO (P6-to-P8/P10)
Cell length (m)	50	18
Dipole fill factor	0.5	0.67
Dipole field (mT)	130	330
Dipole length (m)	6	6
Dipoles per half cell	2	1
Quadrupole length (m)	1	1
Quadrupole gradient (T/m)	5	14
Cell phase advance (deg)	135	135

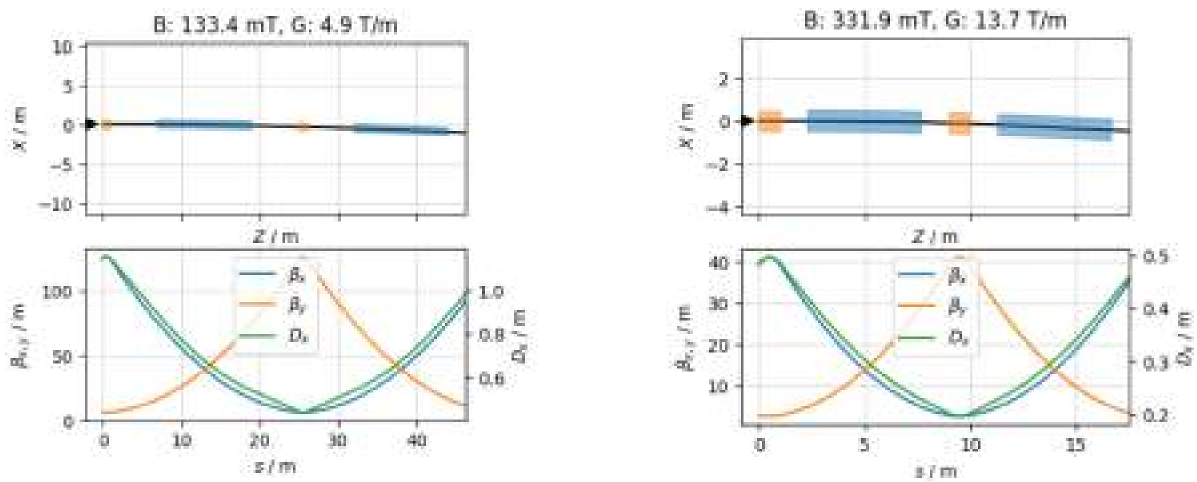

Fig. 7.27 Magnet layout and optics for long and short FODOs (quads in orange and dipoles in blue). Only horizontal dispersion is shown, but a similar vertical dispersion is expected for the cells where the −3 deg, the vertical slope is applied

and apertures are also shown. The aperture required has been calculated with the formula:

$$A_{x,y} = n_\sigma * \sqrt{\beta_{x,y} * \frac{\epsilon_{norm,x,y}}{\gamma}} + D_{x,y} * (2 * \frac{\delta_p}{p} + \delta_{jitter}) + traj * \sqrt{\frac{\beta_{x,y}}{\beta_{max}}} + align \quad (7.1)$$

where $n_\sigma = 6$, $\epsilon_{norm,x/y} = 20/2$ µm, the 1σ momentum spread $\frac{\delta_p}{p}$ is 0.1% (±2σ taken into account and dispersion contribution conservatively added linearly). The trajectory variation is assumed to be ±2 mm at the locations of maximum betatron functions, the momentum jitter δ_{jitter} is assumed to be a maximum of ±0.3%, and there are ±2 mm taken into account for alignment errors.

Based on the parametric scans above, two cells have been chosen to build the line: a long FODO for the shared part of the transport (P1-to-P6) and a short FODO for the separate parts of the transport (P6-to-P8, P6-to-P10). The latter is required due to the tight bending radius of $R = 300$ m, which leads to significant synchrotron radiation. Table 7.15 lists the parameters for each FODO cell. The 135° phase advance is close to the optimum for minimising emittance blow-up [365], while remaining an easy number to work with when designing orthogonal correction schemes.

The schematics and optics functions for both cell configurations are shown in Fig. 7.27. The number of magnets required has been documented in Ref. [366]. For the beginning and end of the line, the bending magnets will bend vertically to introduce (and then remove) the −3° slope present along the entire line descending from the HE-linac to the collider tunnel. In those cells, the dispersion will be vertical but similar in amplitude and shape to the one shown in Fig. 7.27. Under such a configuration, tracking simulations show that both the dp/p blow-up and the bunch length increase remain under 5%. However, further investigations might be needed when including matching sections and errors, which have not been considered in this report.

Table 7.16 Summary of magnet specifications, assuming polarity switching and the FODO parameters from Table 7.15. For ease of manufacturing and costing, the 6 m dipoles have been split into 1 m segments. The number of dipoles quoted refers to the number of 1 m segments

	Unit	Quadrupoles	Dipoles	Correctors
Total number		338	286x6 = 1716	224
# magnets in common line		162	192x6 = 1152	108
Length	m	1	1	tbd
Aperture (diameter)	mm	30	30	30
Gradient	T/m	5-15	-	-
Field	mT	-	150-400	tbd
Deflection	µrad			O(10)
Field homogeneity		$O(10^{-3})$	$O(10^{-3})$	tbd
Polarity switching time	s	O(1)	O(1)	

7.7.3 Magnet technology and technical infrastructure needs

The magnet system of the transfer lines is specified in Table 7.16. The constant transfer energy of 20 GeV opens the door to permanent magnet technology, thus both technologies, electro- and permanent magnets were studied and documented in Ref. [367]. It can be concluded that both magnet technologies are technically feasible. The installation and running cost for the permanent magnet option is well below the electromagnet option. The technical infrastructure needs are also much reduced, however the transfer lines as a whole, contribute less than 10% of the injector complex power requirements. The total power requirements of the transfer lines amount to about 2 MW, compared to about 25 MW for the full injector complex. The permanent magnet option would require about a factor 10 less power for e.g., corrector magnets and ventilation. Operational flexibility is the main aspect to consider when choosing between magnet technologies. If the are beam stability issues in the booster, a transfer energy increase can be beneficial. On the other hand, if the booster could accept a lower energy beam at injection, reducing the transfer energy reduces the power consumption of the whole injector complex which is driven by the HE-linac. The main field of permanent magnets can be tuned by about ±20% by increasing or decreasing a leakage field via mechanical shunts. The shunt modification and subsequent magnetic field measurement require several weeks. Another argument for operational flexibility is the duty cycle of the injector complex, which varies between 5 and 75% depending on the operation mode. In particular, in the low-duty modes, the injector beam can be used for experiments beyond FCC physics and shot-to-shot variability of beam parameters, including the transfer energy, open the door to a very diverse physics programme as discussed in Ref. [368]. At this stage, electromagnets have been chosen as the baseline technology due to the higher operational flexibility for the FCC and any science programme beyond the FCC.

7.8 RF system for linacs

7.8.1 RF accelerating structure

The RF design of the accelerating structures FCC injector complex is optimised to deliver efficient beam acceleration in all 3 linacs: the electron (e-)linac, the positron (p-)linac and the high-energy (HE)-linac. While each linac has some unique operational parameters, they share several common design features: all have a RF structure of total length of 3 m, are configured to accelerate 4 bunches with a separation of 25 ns, and operate with a repetition rate of 100 Hz. The HE- and e-linacs are designed to operate at a frequency of 2.8 GHz, with a bunch charge of 5 nC, while the p-linac operates at a lower frequency of 2 GHz to accommodate its higher bunch charge of 15 nC. This difference reflects the tailored optimisation of each linac to the specific beam dynamics requirements described above. The RF structures have tapered geometries, which effectively balance beam transport with short- and long-range wakefield suppression requirements, $W_t < 0.1$ V/pC/mm/m and a value specific to each linac of $< a > /\lambda$. The detailed parameters and design specifications for all three linacs are summarised in Table 7.17. Similar design principles are applied to all 3 linacs, providing a uniform and scalable approach across all structures. The RF design of the HE-linac, is described as an example, in detail below.

The parametric sweep of iris aperture and thickness was utilised to identify structures that satisfy the long-range transverse wakefield constraint $W_t < 0.1$ V/pC/mm/m for a given $< a > /\lambda = 0.12$ related to the short-range wakefields, ensuring stable beam propagation. The long-range transverse wakefields were calculated using a lookup table, which employs frequency-domain parameters of the 20 lowest higher-order modes (HOMs).

Table 7.17 Accelerating structure parameters for e-, p- and HE-linacs

	e-linac	p-linac	HE-linac	Unit
Frequency	2.8	2	2.8	GHz
Length	3	3	3	m
Average aperture	0.15λ	0.2λ	0.12λ	
Cell aperture: first/last	17.13/14.99	30/30	14.85/10.85	mm
Iris thickness: first/last	10.4/13.7	14.3/20.0	2.84/4.04	mm
V_g/c: first/last	3.14/1.38	2.58/1.92	3.92/1.25	%
r/Q: first/last	3.28/3.67	1.49/1.52	3.63/4.38	kΩ/m
Q: first/last	14,599/13,668	20,977/19,102	16,571/16,039	
Filling time	486	447	460	ns
SLED coupling	15	17	15	
$R_{\text{sh, eff}}$ (4 bunches)	81.69	36	95.65	MΩ/m
Repetition rate	100	100	100	Hz
Klystron power per structure	14.2	14.2	14.2	MW
Average power per structure	3.76	3.68	3.72	kW
Bunch charge	5	15	5	nC
Average loaded gradient (4 bunches)	19.50	13.31	21.06	MV/m
$E_{s,\max}$ (instant.)	77	55	73	MV/m
$S_{c,\max}$ (instant.)	453	298	501	mW/mm^2

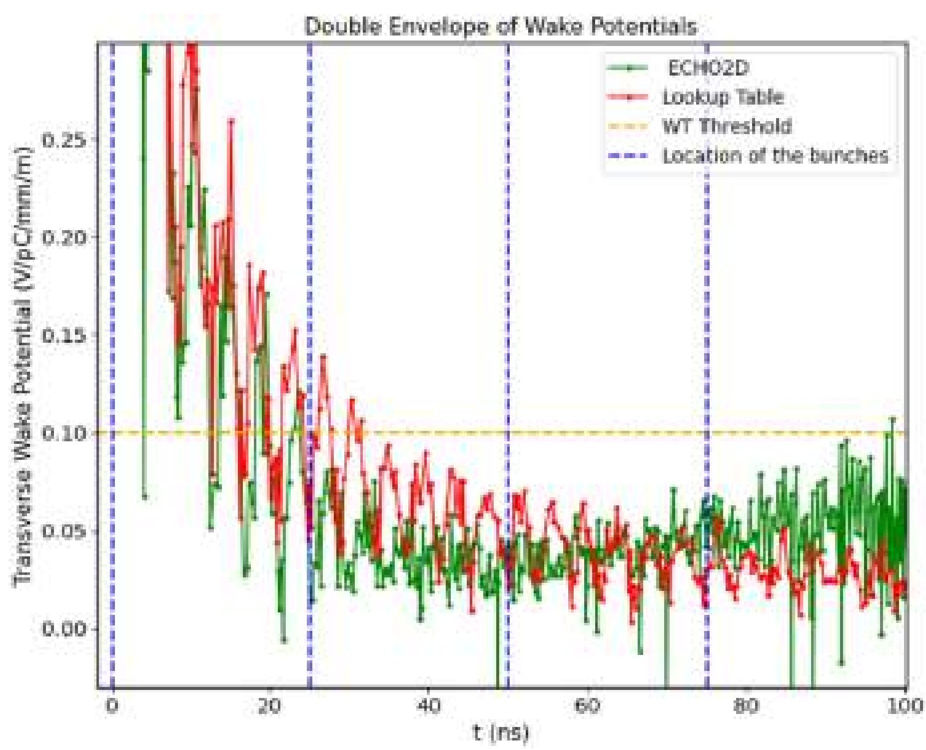

Fig. 7.28 Envelope-of-the-envelope of transverse wakefield potentials for the HE-linac structure, calculated over time using both the lookup table and ECHO2D methods

To achieve more realistic and accurate wakefield predictions and to benchmark the lookup table calculations, the ECHO2D time-domain solver was used for the structure of the final choice. This approach is more accurate, accounting for an infinite number of HOMs and the coupling between cells. The envelope-of-the-envelope approach was applied to the wakefield data from both ECHO2D and the lookup table to rigorously assess worst-case scenarios and long-range wakefield effects. The results are shown in Fig. 7.28.

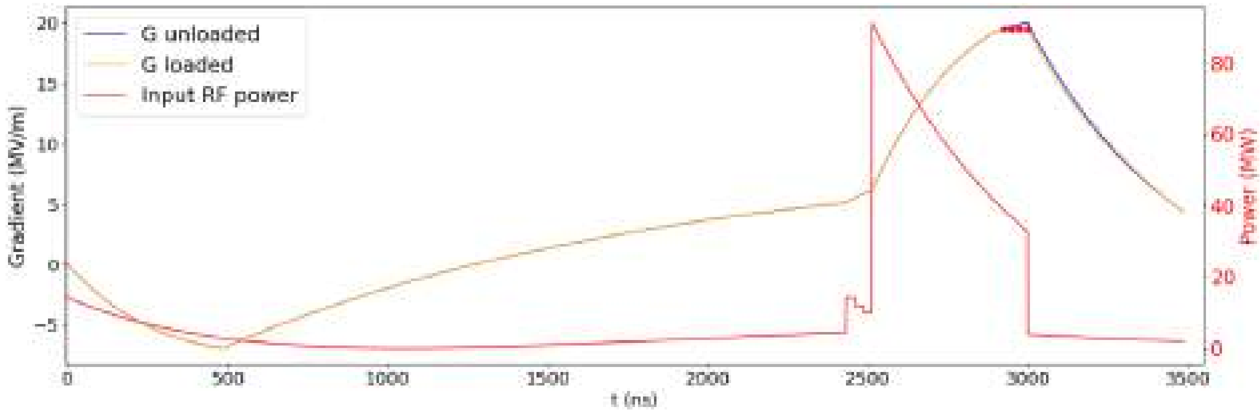

Fig. 7.29 Input RF power and average gradients versus time

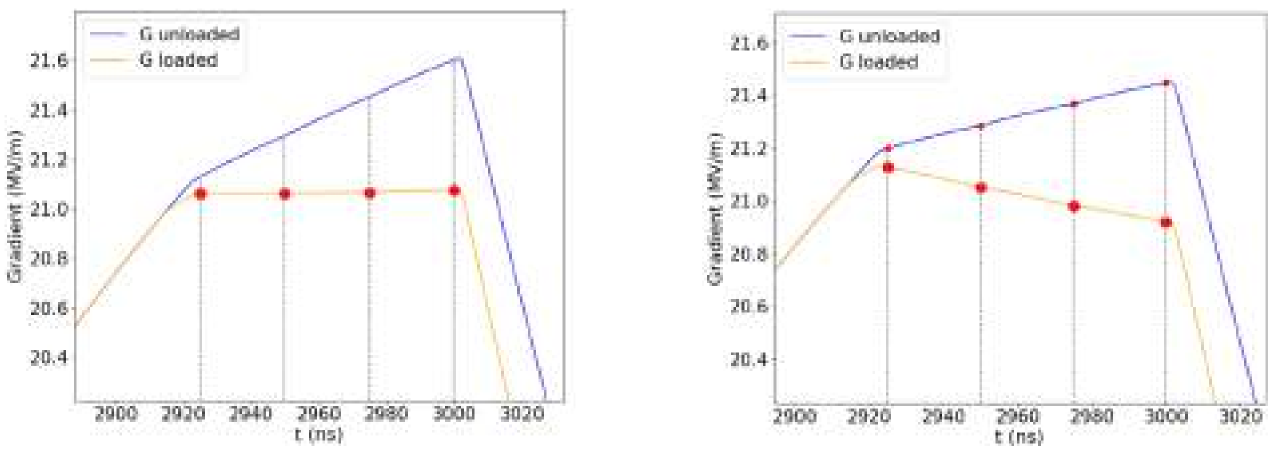

(a) Nominal charge condition.

(b) Top-up operation.

Fig. 7.30 Bunch-to-bunch energy minimisation for the nominal bunch charge (a) and top-up operation (b)

In the design of travelling wave accelerating structures, minimising bunch-to-bunch energy spread is a critical objective for ensuring high beam quality and stable accelerator performance. During collider filling with nominal bunch charge, the input RF power pulse shape is optimised to minimise bunch-to-bunch energy spread, taking into account the beam loading effect. As shown in the red trace in Fig. 7.29, the input RF power is modulated using a step-like amplitude modulation. This approach ensures a constant average loaded gradient for all four bunches. The gradients for unloaded and loaded conditions are represented by the blue and orange traces, respectively. The four red dots indicate the temporal positions of the bunches. In Fig. 7.30(a), the unloaded and loaded gradients are shown in more detail for comparison near the position of the 4 bunches, showing a maximum energy difference of 2.4% between unloaded and loaded gradients on the fourth bunch, highlighting the beam loading effect in HE-linac. However, in top-up operation, where bunch charges vary from 0 to 100% among the four bunches, a single optimal input RF pulse must accommodate both extremes. The ‘golden pulse’ is introduced to address this by averaging the optimised RF pulses for unloaded and loaded voltages. While it does not individually minimise energy variation to ∼0-level, it provides a balanced compromise, reducing energy spread across all possible charge variations. Figure 7.30(b) demonstrates the golden pulse in top-up operation, reducing energy spread to +1.1% and −1.1% for unloaded (4 bunches at 0 bunch charge, small red dots) and loaded cases (4 bunches at nominal intensity of 5 nC, large red dots), respectively. This result underscores the golden pulse’s ability to balance energy spread across bunches, ensuring stable performance even under varying charge conditions in top-up mode.

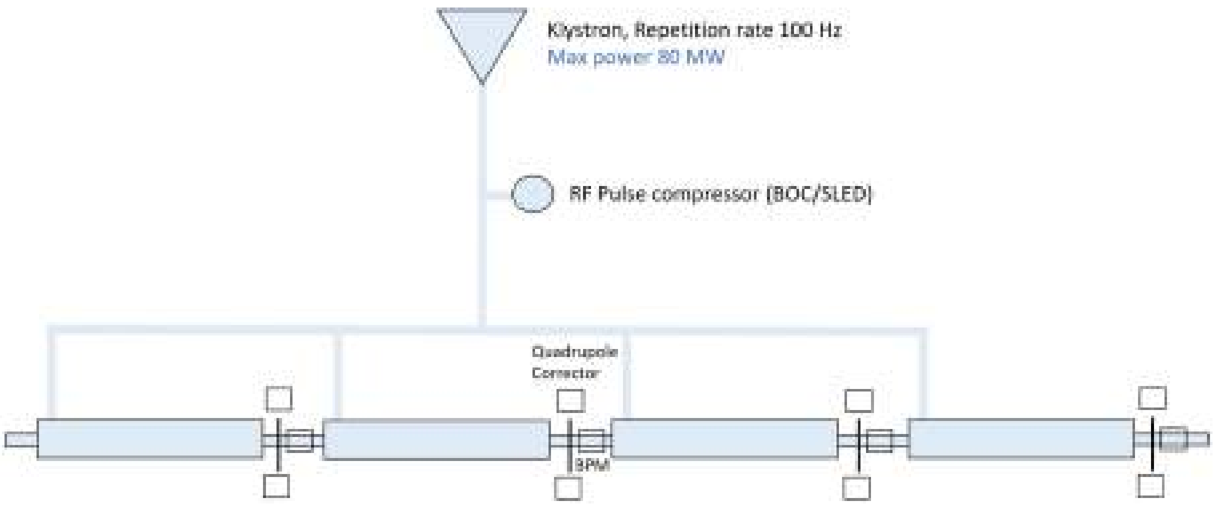

Fig. 7.31 Schematic layout of an RF module for the electron, S2 positron and high-energy linacs

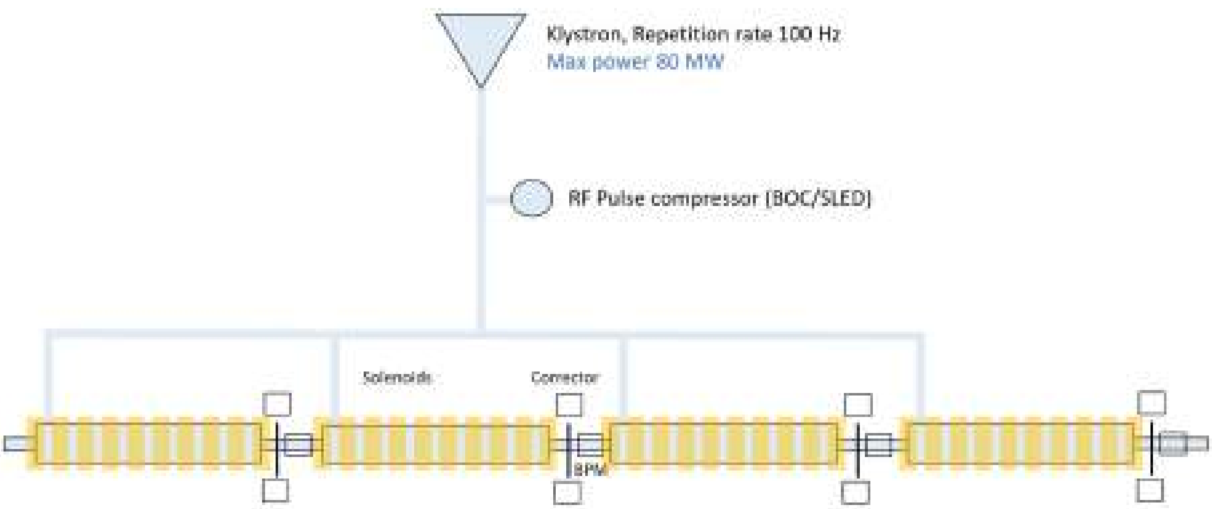

Fig. 7.32 Schematic layout of the RF module for the positron capture and S1 linacs

7.8.2 RF module and RF power

Each RF module of the electron and high-energy linacs consists of one high voltage modulator (HV), one klystron operating at 2806 MHz, one pulse compressor (Barrel-Open Cavity or SLED type) and four accelerating structures with one quadrupole, one corrector magnet and one BPM between each structure. Its total length is 15 m. The choice of an RF module consisting of four structures results from cost and power consumption optimisation. Figure 7.31 shows the schematic layout of such an RF module.

The positron linac has two types of RF modules. The first type equips the end part of the capture linac and the S1 linac. It is about 13 m long, since instead of 4 quadrupoles, it has 40 solenoids, i.e., 10 solenoids per structure for beam focusing. A schematic layout of this type of module is shown in Fig. 7.32. The second type of RF module in the p-linac is similar to the electron and high-energy linac module (see Fig. 7.31). The klystron operates at 2004 MHz in the p-linac.

For the electron and the high-energy linacs, the peak power specification of each klystron is 80 MW. Its repetition rate and RF pulse length are 100 Hz and 3 µs, respectively. For the positron linac, the power specification of the klystron and its repetition rate are also 80 MW and 100 Hz, respectively, but its RF pulse length is 5 µs. Although no klystron exists at the specific frequencies of 2806 MHz and 2004 MHz, many klystrons have demonstrated reliable performance at 2856 MHz with such a power specification and RF pulse length. The development of a conventional klystron at 2806 MHz with a 100 Hz repetition rate is straightforward by retuning its cavities and

Table 7.18 Klystron parameters

Linac	Freq. [MHz]	Peak power specification [MW]	Rep. rate [Hz]	RF pulse length [μs]	Duty factor [10^{-3}]	Average power [kW]	Number required
e-Linac	2806	80	100	3	0.3	24	15
p-Linac	2004	80	100	5	0.5	40	21
HE-Linac	2806	80	100	3	0.3	24	72

Table 7.19 RF module summary table for the injector linacs

	e-Linac	p-Linac	HE-Linac	Unit
RF frequency	2.8	2.0	2.8	GHz
Repetition rate	100	100	100	Hz
Modulator max. peak power	190	190	190	MW
Modulator max. average power	114	152	114	kW
Klystron max. RF power	80	80	80	MW
Klystron RF pulse length	3	5	3	μs
Structures per klystron	4	4	4	
Klystron power per structure	14.2	15.4	14.2	MW
Average loaded gradient	19.5	13.3	21.1	MV/m
Number of rf modules	1 + 14	1 + 6 + 14	72	
Module Length	15	13, 14.8	15	m
Length of all modules	215	304	1080	m

Table 7.20 Comparison of the plug power consumption for the injector linacs assuming 42% or 70% klystron efficiencies

Linac Klystron efficiency [%]	Plug power [MW]	
	42	70
e-Linac	2	1.2
p-Linac	8	6.5
HE-Linac	9.5	6

redesigning its collector. As for the design of a 2004 MHz klystron with such specifications, it would be a completely new development but presents no technical challenges. Several companies have indeed been contacted to assess the feasibility of such conventional klystrons and confirmed that such specifications are achievable. The RF efficiency of such klystrons would be 42%. Their parameters are summarised in Table 7.18.

Both types of klystron operate at 80% of their peak power specification, i.e., at 64 MW. For the electron and high-energy linacs, it is assumed that the RF waveguide system comprises S-band WR284 waveguides and is 25 m long. Taking into account the waveguide losses, the klystron power per structure is then 14.2 MW before pulse compression. For the positron linac, the RF waveguide system comprises the less lossy L-band WR510 waveguides. With a 25 m long waveguide system, the klystron power per structure is 15.4 MW before pulse compression. The specifications of each RF module for all linacs are summarised in Table 7.19.

In recent years, research and development have been conducted on pulsed high-efficiency klystrons, and it is conceivable that more of these klystrons will be available in the near future. A comparison of the plug power consumption for all linacs assuming 42% and 70% klystron efficiencies is shown in Table 7.20. The advantage of operating with high-efficiency klystrons is remarkable for the electron and high-energy linacs but less so for the positron linac since the power consumption of the structure solenoids in the capture and S1 linacs is a substantial fraction of the positron linac total power consumption.

7.9 Availability

This section details results from the enhanced Monte Carlo simulation environment for FCC-ee availability described in Sect. 2.4, focusing on systems specific to the injector complex.

7.9.1 Contributing systems

For availability modelling, the injector chain is divided into two top-level accelerators. The statistical failure rate and blocking duration from subsystems in each accelerator are taken from two representative machines with similar performance characteristics. These are simulated in the injector complex of the FCC-ee to gauge the effect of equivalent availability on global physics performance.

1. **Lower Energy Injectors:** The electron and positron source, linac and damping ring up to an energy 2.86 GeV are modelled from fault data from the SuperKEK-B e^-/e^+ source, injector linac and damping ring between 1998-2023, detailed in Ref. [369].
2. **High Energy (HE) Linac:** with an energy up to 20 GeV is modelled using fault data from the Linac Coherent Light Source (LCLS) at SLAC [370].

Subsystems within each accelerator have been re-categorised for illustration to preserve naming conventions in the CERN complex. These include the relevant supporting technical infrastructure for each accelerator. Only faults leading to downtime in each accelerator were considered, thereby assuming a similar degree of redundancy in the FCC-ee as exists in practice for each representative subsystem.

7.9.2 Inherent resilience to shorter fault types

In the event of an outage in the booster and injector complex, stable beams can be maintained in the main collider rings for a lifetime of 10-15 minutes, depending on energy mode (see Table 2.2). If top-up injection can be restored in this time, normal physics can resume. This significantly reduces the FCC-ee's sensitivity to short-duration fault types in the injector complex and leads to an inherent advantage in availability. The contribution for lost luminosity of subsystems in the injector complex is therefore biased towards those with longer-duration fault types.

7.9.3 Results

The overall contribution to downtime of each accelerator in the injector complex is compared with the booster systems in Fig. 5.14. The lost luminosity contributions in the Z mode from the low energy injectors and HE linac are significant, second only to the booster RF system. The availability of the injector complex will be a challenge for overall FCC-ee performance.

Lower energy injectors The contribution to unavailability and lost luminosity from each subsystem in the low energy injectors is shown in Fig. 7.33. These only contribute to downtime, as the relevant systems have high redundancy, meaning that faults generally block the beam for only short durations. The majority of faults are due to RF breakdowns, which contribute significantly to lost luminosity in Z and W modes, given the lengthy turnaround time required to recover from dumps.

High energy (HE) linac The contribution to unavailability and lost luminosity from systems in the HE linac are shown in Fig. 7.34. RF breakdowns are again the most problematic, representing contributions from S-band klystrons, high-power sub-boosters, waveguides and modulators. The control system is also a high contributor, composed of micros and CAMAC crates as well as the MCC/VMS computing and timing systems. The access system is represented by the Personnel Protection System (PPS). Contribution from the gun laser system is also significant.

7.9.4 R&D opportunities

Opportunities exist for exploiting the injector complex's natural resilience to shorter fault types. If a failed component can be brought back online before the beams in the main collider expire, a lengthy turnaround time may be avoided. This mirrors the opportunities already discussed for the booster in Sect. 5.3.4.

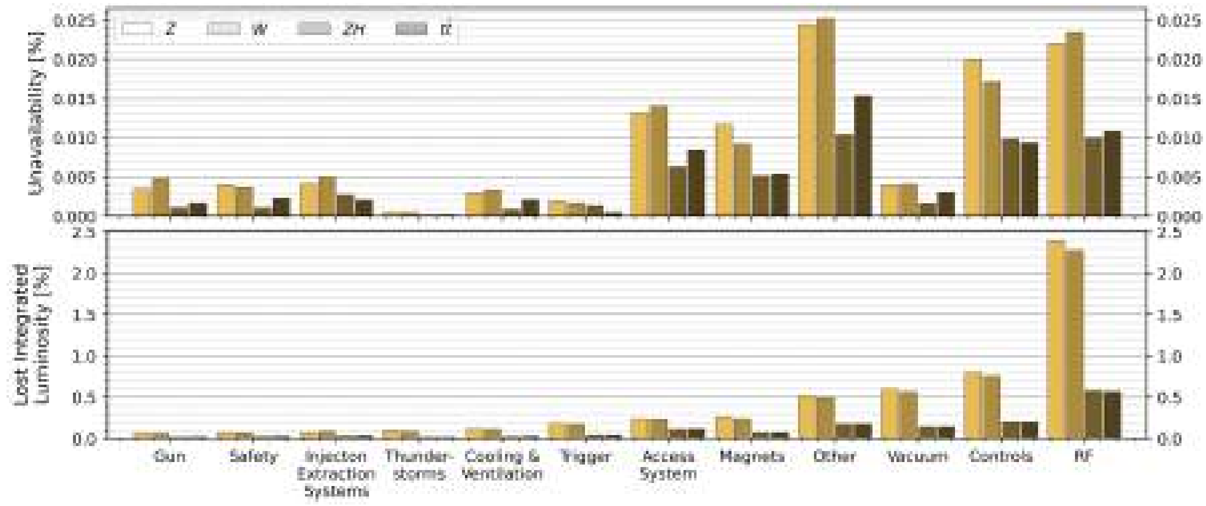

Fig. 7.33 FCC-ee unavailability and lost luminosity contribution of the low energy injectors (up to 6 GeV) determined by applying fault statistics from equivalent equipment at SuperKEK-B [369]. Systems are ordered according to Z mode lost luminosity contribution

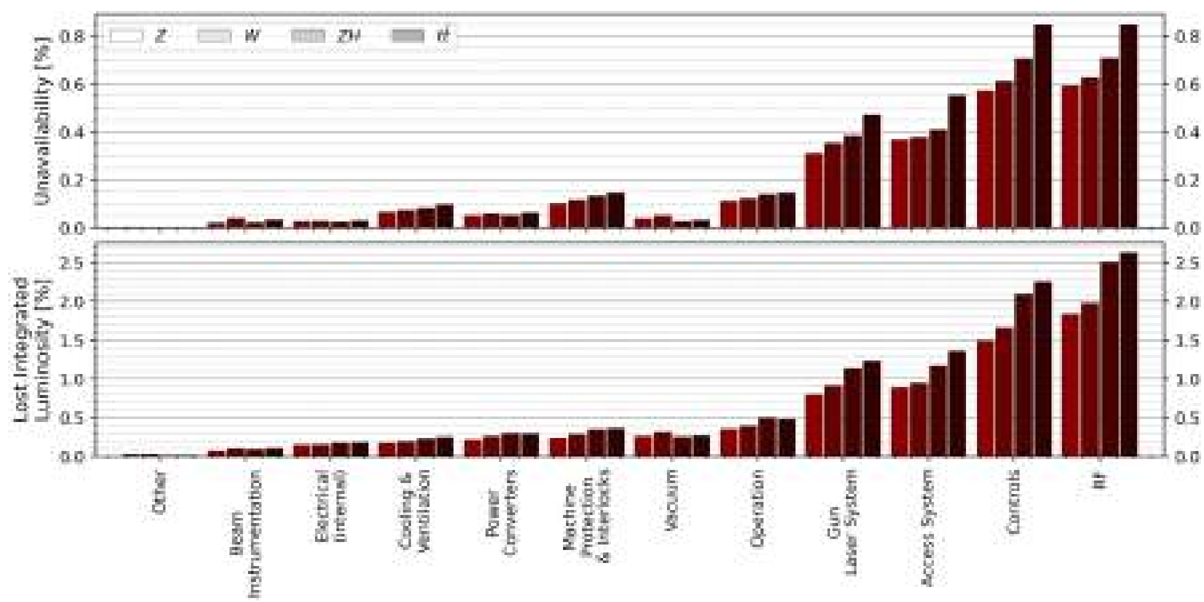

Fig. 7.34 FCC-ee unavailability and lost luminosity contribution of the HE Linac determined by applying fault statistics from the Linac Coherent Light Source (LCLS) at SLAC [370]. Systems are ordered according to Z mode lost luminosity contribution

The short beam lifetime is especially significant for Z mode operation, where the charge imbalance between electron and positron beams in the collider must be less than 5%. Assuming a lifetime of 10-15 minutes, the injection of electrons and positrons must alternate for top-up every 50 seconds. This places significant design constraints on the injector hardware and has profound implications for reliability and availability, as even short interruptions could impact the collider's performance. This requirement limits the breakdown (BD) rate in the injector's accelerating structures. The time required to bring an accelerating structure back into operation after a BD is on the order of a minute. This poses a problem with the injector's availability. An analysis of BDs in the SwissFEL linac is conducted in Ref. [371]. During regular user operation, the RF modules failure rate began to reduce thanks to RF conditioning incidental to nominal operation. This incidental conditioning followed a power law trend that saw the BD rate decrease by over three orders of magnitude in the first three years of user operation, from 10^{-6} to less than 10^{-9} BD per pulse per metre or about two BD per day in the entire linac. Nonetheless, RF BDs continue to account for about half of all broken interlocks in SwissFEL.

Fig. 7.35 Plan view of high-energy linac civil engineering

Given the number of RF structures planned for the FCC injector and scaling, the results obtained for SwissFEL, translate into a reduction of the BD rate from about 850 events per day to about eight events per day after the first four years of operation. The proposed solution, which is to be further investigated, to mitigate these events, is to use some additional RF modules during these BD events. The low probability of having more than two events simultaneously led to the adoption of one additional RF module for the positron and electron linacs and two additional RF modules in the HE linac. Thanks to this approach, the injector's availability due to the BDs could be greater than 99% after a few years of operation.

7.10 Civil engineering

7.10.1 Injector complex

The preferred location for the FCC-ee injector complex is on the existing CERN Prévessin site. Several options for the location of the high-energy linac were explored, with the preferred choice being near the northwest edge of the Prévessin site. A more detailed placement study considering also environmental aspects will be performed in the next phase before confirming the location. The envisaged layout of the facility is shown in Fig. 7.35.

The civil engineering for the high-energy linac will consist of four main elements, namely: the high-energy linac tunnel, the associated e^+ and e^- tunnels, the damping ring and the transfer tunnels/structures to connect the damping ring to the rest of the facility. All these structures will consist of reinforced concrete buried structures extending over a length of about 1.2 km. For shielding purposes, these structures will be built in a series of trenches up to 15 m below the ground level. These so-called 'cut-and-cover' tunnels will be backfilled using the excavated material from the trench formation, and then a surface hall will be constructed above the tunnels. A series of 6 m long vertical mini-shafts of about 0.8 m diameter will connect the tunnels to the surface hall for connecting the klystrons and to allow for the passage of services and cables. A schematic section of this arrangement is shown in Fig. 7.36.

Compared to the other options studied for the high energy linac, the preferred site has a number of significant advantages including:

- The proposed location is quite flat, with a total difference in ground level along the length of the HE-linac of about 5 m
- The proposed location has minimal existing infrastructure. A small number of underground networks will need to be rerouted before construction, and two or three older structures on the Prévessin site will be carefully dismantled or relocated as needed.
- The location and orientation are well suited for a potential future connection of beam lines to the North Area of Prévessin, where fixed-target physics research is conducted.

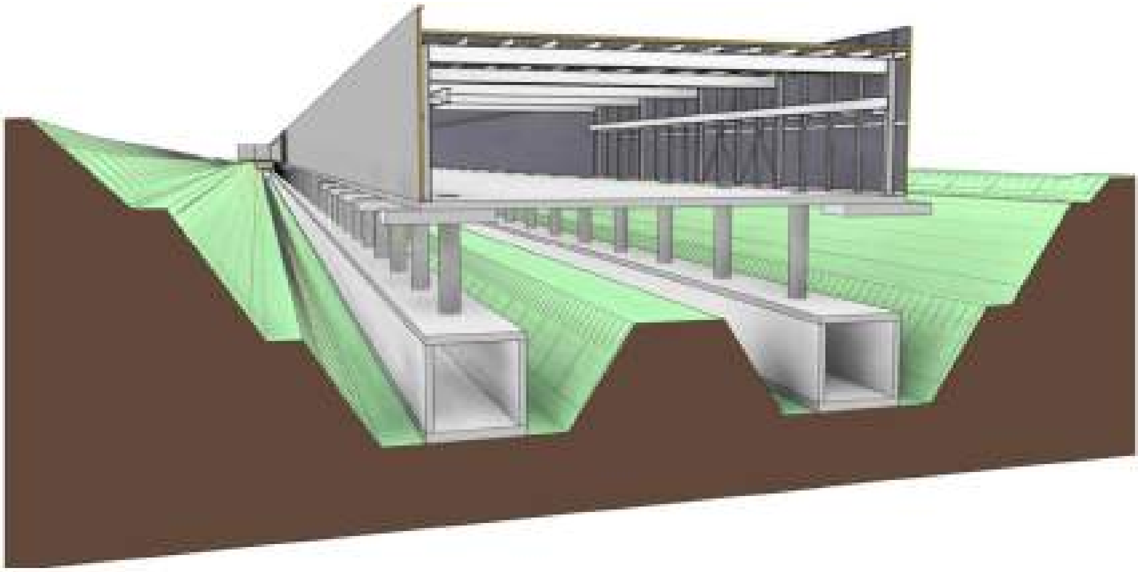

Fig. 7.36 Cross-section of high energy linac civil engineering

Fig. 7.37 Schematic view of transfer tunnels

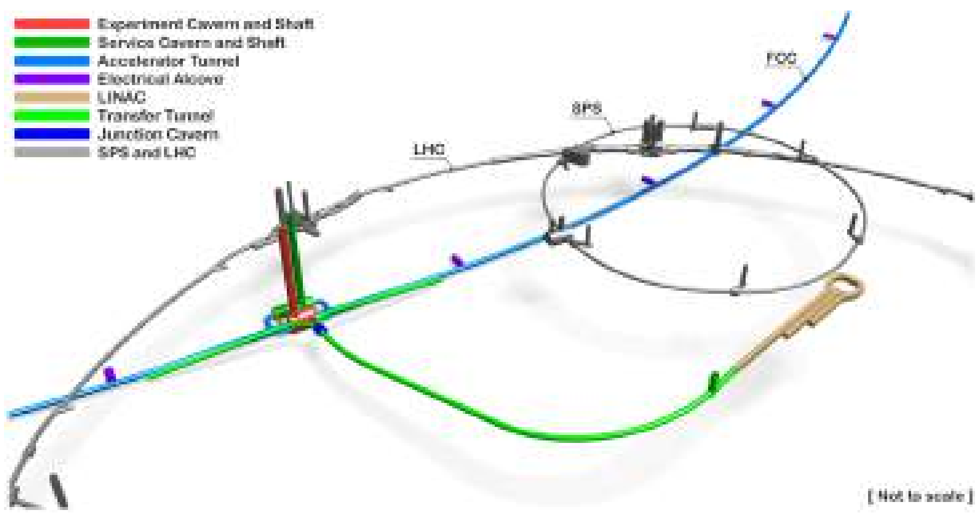

7.10.2 Transfer tunnel

The beam lines from the high energy linac will be connected to the FCC main accelerator tunnel through a transfer tunnel. This transfer tunnel will consist of a single tunnel of internal diameter 3 m and total length of 5560 m. As this tunnel approaches PA of the FCC, the tunnel will bifurcate to provide a clock-wise and anti-clockwise link to the FCC. These two link tunnels will be symmetrical and each 747 m in length. This arrangement is shown schematically in Fig. 7.37 and a plan view is given in Fig. 7.38.

The main characteristics of the transfer tunnel are:

- Three horizontal curves with a minimum radius of 300 m are required
- The tunnel will have a slope of 4.9%.
- Connection of the tunnel to the high energy linac will be made on the CERN Prévessin site at the end of the high energy linac.
- Connections to the FCC main tunnel would be created with 0.8 m diameter drilled horizontal passage for the clockwise and anti-clockwise beam lines. A small personnel access connection would also be created between the FCC and transfer tunnels for emergency access and ventilation. These connections would be constructed in the widened section of the accelerator tunnel either side of PA, where the span of the accelerator tunnel is 14.5 m.

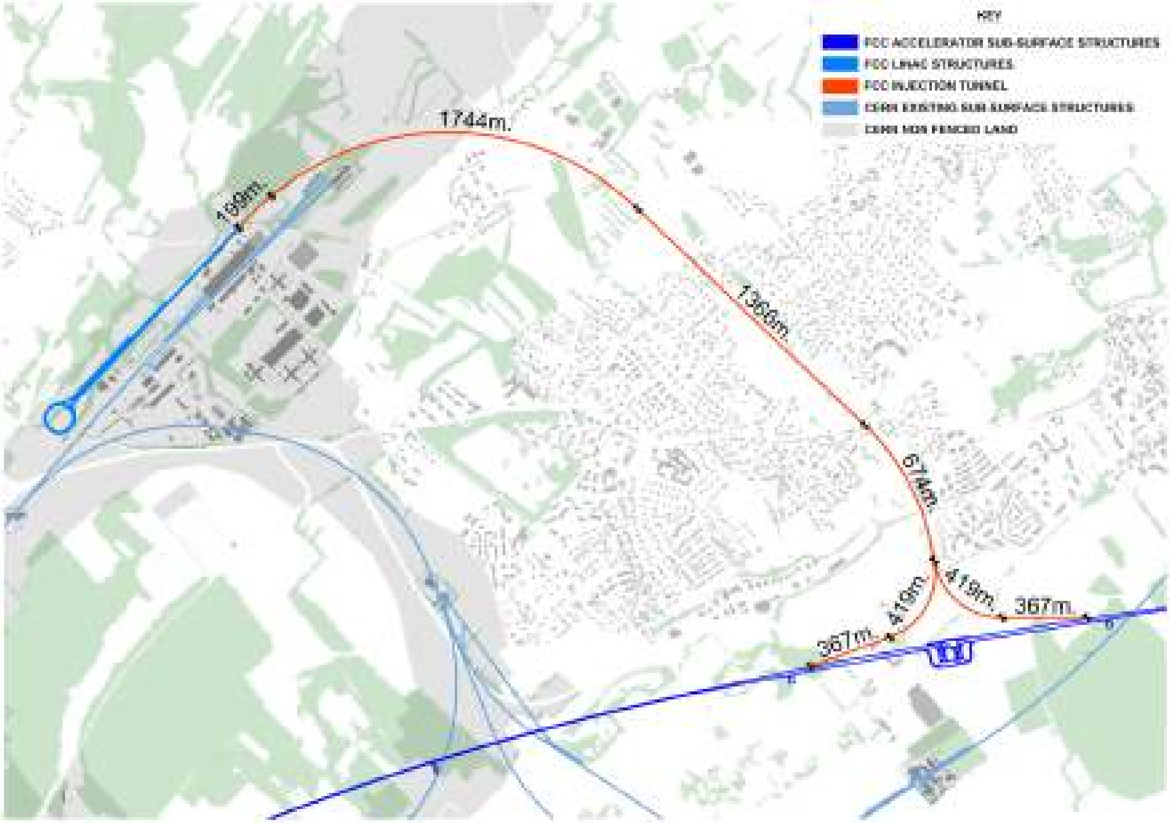

Fig. 7.38 Plan view of transfer tunnels

- A temporary shaft located within the existing Prévessin site would be built to provide access for the construction of the transfer tunnel. This shaft would have a depth of 30 m and an internal diameter of about 10 m to suit the contractor's plant and equipment. The shaft may not be needed for the operation of the FCC. The transfer tunnel will be excavated from this shaft using either a tunnel boring machine or roadheader or a combination of the two.
- A junction cavern of 30 m length and 9 m span will be necessary to accommodate the bifurcation of the tunnel for the clockwise and anti-clockwise injection into the FCC machine.

Geological conditions for tunnelling this small-diameter tunnel are expected to be favourable, with molasse strata serving as the tunnelling medium from the access shaft down to the FCC accelerator tunnel. The connections to the FCC tunnel will be made at a depth of approximately 200 m below ground level. Additional confidence in the feasibility of construction comes from CERN's extensive experience in underground civil engineering projects in this region, including the SPS, LHC, and CNGS, all of which were successfully constructed in the same general area. If a tunnel boring machine (TBM) is used for excavation, reinforced concrete segments will likely be employed for support, similar to the main FCC accelerator tunnel. Alternatively, if a roadheader is used, a two-phase approach will be followed for tunnel support, consisting of an initial lining with rock bolts and shotcrete, followed by a secondary cast in-situ reinforced concrete lining.

7.11 Technical infrastructure

The new injector complex will be integrated in CERN's Prévessin site, requiring additional energy and services. Initially constructed for the SPS accelerator and its fixed-target physics programme, the Prévessin site hosts the SPS North Area and serves as a critical hub for CERN's technical infrastructure. This includes the 400 kV power lines from RTE (France's Transmission System Operator) that supply power to the entire CERN complex, the CERN Control Centre (CCC) responsible for operating all CERN accelerators, the new data centre, and the Ethernet backbone hub. These infrastructures are regularly upgraded to support the evolving demands of CERN's programmes. The new injector complex will become a significant addition to the existing layout. The injector complex consists of five main areas: the e-linac, the p-linac, the damping ring, the HE-linac, and the transfer line to the booster. Each area includes an accelerator tunnel and its associated surface building. Dedicated

Table 7.21 Main electrical loads from the accelerators of the injector complex for the Z and WW modes of operation. Here, the RF numbers for the three linacs assume a commercially available klystron efficiency of 42%

Accelerator loads	Area	Power rating
RF	e-linac	2 MW
RF	p-linac	4 MW
Magnets	p-linac	4 MW
RF	HE-linac	9.5 MW
Magnets & RF	Damping ring	3.2 MW
Magnets	Transfer line	2 MW
Total		**24.7 MW**

Table 7.22 Additional loads of the injector complex

Other loads	Types	Power rating
Accelerator systems	Auxiliary magnets, vacuum, instrumentation, control...	2 MW
General services	AC plugs, lighting, safety systems...	2 MW
Cooling and ventilation	Pumps, motors, fan coils...	3 MW
Total		**7 MW**

technical infrastructures will be established to meet the needs of these areas, which can operate independently. For electricity and cooling, there will be a shared infrastructure. A new electrical substation will connect to the existing main substation to supply power to the complex. Cooling towers, grouped in a dedicated building near the end of the HE linac, will dissipate heat generated by the five areas. Each area will also have its own ventilation systems.

The tunnels will house accelerator system components such as RF cavities, magnets, instrumentation, and beam pipes. The surface buildings will accommodate RF klystrons, high voltage modulators, magnet power supplies, vacuum control systems, and beam instrumentation electronics. These buildings will require power distribution, water cooling, ventilation, control systems, and safety features, including fire detection and alarm systems. Services like electricity, cooling, and control will be distributed from the tunnels to the surface buildings.

Additional technical infrastructures will support the complex, including access systems, smoke extraction, environmental monitoring, radiation protection systems, handling and transport systems, and communication systems. These systems will be integrated into the surface buildings above the tunnels. The injector complex can be operated remotely from the existing CERN Control Centre.

The estimated main accelerator electrical loads for the injector complex are presented in Table 7.21. Complementing the main loads, the additional power demand of other systems is presented in Table 7.22. Considering instead of 42%, as in Table 7.21, a higher klystron efficiency of 55%, a value that seems reasonable given the developments in high-efficiency klystrons (which aim at S-band klystrons with 70% efficiency), it appears possible to save 3.2 MW on the electrical load for the linacs. This consideration would result in a reduced total electrical load for the injector accelerators of 21.5 MW for the Z and WW modes operation, instead of 24.7 MW. For the ZH and $t\bar{t}$ running, the reduction in energy consumption with the linacs operating at 50 Hz instead of 100 Hz is approximately 6.5 MW at a klystron efficiency of 55%, resulting in a total electrical power of 18.2 MW for the injector accelerators.

The injector complex will require a main electrical substation with a capacity of up to 40 MVA. For the Z and WW running with 42% S-band klystron efficiency and 10% margin, its annual energy consumption is estimated at 150 GWh. With a klystron efficiency of 55% and reduced margins, the injector annual energy consumption for Z and WW running decreases to 120 GWh (linac repetition rate of 100 Hz), and for the ZH and $t\bar{t}$ modes of operation to about 93 GWh (linac repetition rate of 50 Hz).

The cooling towers will have a capacity of approximately 25 MW, with an annual water consumption of 200,000 m^3. This water will be sourced from the existing distribution system, which uses water from Lake Geneva. From a technical infrastructure perspective, integrating the injector complex into the Prévessin site is feasible without affecting SPS operations.

7.12 Ongoing studies and possible upgrades

As the study advances there is strong support from Switzerland and PSI to continue and strengthen the CHART collaboration. The injector project team, consisting of PSI and CERN members and external partners, is preparing a comprehensive proposal to be included in the CHART programme for the financial period 2025-2028, complete with detailed resource and cost estimates, to be finalised in early 2025. In the next phase, several critical areas will require focused attention. The updated baseline design includes a 2.86 GeV damping ring, which must be integrated into the forthcoming technical design study.

The current baseline design assumes an RF frequency in the linacs compatible with the main rings to retain operational flexibility. However, the limited availability of suitable power sources on the market presents a challenge, prompting efforts to adopt a commercial S-band frequency for the RF system in the linacs. Additionally, the positron linac will undergo optimisation to shift from the current 2 GHz setup to a more widely available S-band frequency. Reliability and availability of the injector complex will be key factors in the injector's design, particularly for continuous 'top-up' operation, which requires a low-gradient injector configuration with an experimentally validated RF breakdown rate. Assessing the impact of short interruptions caused by RF breakdowns in top-up operations will also be critical for ensuring stable performance.

The involvement of international partners will remain crucial as the injector study progresses towards the technical design and construction stages. A comprehensive technical design report could follow the feasibility study phase, building on the SwissFEL linac technology for RF accelerating structures and related upgrade projects. This report will also benefit from the expertise of international partners who have experience in synchrotron light and positron source operations. Its primary objective will be to establish detailed specifications for the accelerator and technical infrastructure requirements necessary to initiate civil engineering design. These specifications will ensure that all system and subsystem requirements are addressed, making the initial construction phase and mass production of critical components smoother.

A comprehensive TDR for the accelerator and the associated technical infrastructure will be completed should the project move to its next phase. This will be pivotal, enabling further engineering design efforts and finalising all necessary specifications for civil engineering work. This phase is essential to confirm that all design elements undergo rigorous examination and are fully integrated into the project, ensuring a seamless transition to the construction phase. A prototyping phase will be critical in this context. During this phase, RF accelerator structures will undergo exhaustive testing to validate their performance and reliability. Additionally, based on a photo-cathode RF gun, the electron source concept will be demonstrated to support top-up operation for reliably injecting electrons into the collider ring. This demonstration is essential to confirm that the chosen technology can meet operational requirements and integrate smoothly into the overall system.

Furthermore, the P^3 positron production experiment at PSI will be completed and commissioned, with subsequent development focusing on a hybrid scheme expected to reduce the power dissipated on the target while keeping the efficiency of positron production. This development phase will refine the specifications for the positron source, ensuring that all components meet the operational criteria for integration into the injector complex.

Chapter 8

Technical infrastructure for FCCs

8.1 Requirements and design considerations

The infrastructure requirements and the proposed technical solutions for FCC-ee have been defined for the PA31-1.0 layout, which, as described above, features eight points with associated surface areas. Four of the points are experiment points, and four are technical points. The technical infrastructure systems described here are electricity and energy management, cooling and ventilation, integration, geodesy and survey, cryogenic systems, transport and logistics, and computing infrastructures and robotics. The present study focuses on the technical infrastructure related to FCC-ee. However, wherever design choices are made which may impact FCC-hh (in particular, the space requirements and dimensions), constraints from and possible synergies with the hadron collider are taken into account.

8.1.1 Assignment of points

Four of the eight FCC points are designated for experiments: PA, PD, PG, and PJ. Among these, PA and PG are considered as large experimental areas for FCC-hh, whereas PD and PJ are optional sites that may accommodate smaller hadron collider detectors requiring less infrastructure. All four points can accommodate the much smaller experiments of the FCC-ee collider.

The remaining four points are technical. Point PB, the only one located in Switzerland, has been chosen to house the beam dump system. Points PL and PH have been selected to house the booster and collider RF, respectively. Point PF was found less appropriate to house the RF due to difficult access conditions (the access shaft is displaced laterally w.r.t. the FCC ring by several hundred metres) [372], but it could house the collimation system.

The assignment of points PL and PH was made based on constraints from accelerator physics (a preference to concentrate the collider RF at a single point), constraints at the surface areas, and infrastructure constraints (accessibility, resources, electrical network connection, and powering). Since point PL features a relatively complicated surface site with many constraints, it was decided to install the booster RF 800 MHz cryomodules at this point. The Booster RF requires much less infrastructure than the collider RF and can be more easily integrated. Point PH was designed to house the collider RF (400 and 800 MHz cryomodules), which requires substantial infrastructure.

8.1.2 Electricity supply

Electrical power will be provided by the French network and fed into the FCC at three points (PA, PH, and PD). Further distribution is then accomplished via the FCC tunnel. The electrical infrastructure is designed to support all FCC-ee configurations seamlessly, eliminating the need for additional substations between different operational stages. The proposed setup also includes the possibility of operating the machine without one sub-station (PA or PD). The PH substation, which has the main RF loads (200 MW), is mandatory for beam operation. This setup will ease the maintenance and repairs as all substations will be connected together through the HV network. RTE (Réseau de Transport d'Électricité) has launched a study on how to connect the FCC to the French network. The requirements of the FCC project are not considered significant by RTE, and will not impact the French electrical network operation.

8.1.3 Cooling and ventilation

The potential sources of cooling water in the area are lake Geneva and the Rhône and Arve rivers. As a baseline, the required cooling water will be taken from Lake Geneva via the existing infrastructure, which has enough capacity to supply the FCC. Pipework within the tunnel will connect the remaining points to PA, PD, or PJ to ensure their respective water supply. The drainage flow rates correspond to around 30 m^3/h in the RF points and a maximum of 11 m^3/h in the remaining points.

A semi-transverse ventilation scheme has been adopted for the FCC tunnel, with air supplied through a dedicated duct running along the entire sector and extracted either via the tunnel itself or through an emergency extraction duct. To ensure continuous airflow in case of a duct failure, air is supplied to each sector from both endpoints, with the same configuration adopted for the extraction system.

8.1.4 Cryogenic systems

The cryogenic system design of FCC-ee follows the requirements of the superconducting devices, which are distributed throughout the machine. Whilst the technical points PB and PF do not feature any cryogenic needs, the technical points PH and PL are associated with the radiofrequency (RF) system, which needs to be operated at 2 K and at 4.5 K. These RF points have the largest cryogenic installations due to their high concentration of heat loads. Additionally, each experiment point – PA, PD, PG, and PJ – requires a dedicated cryoplant to support the cooling needs of the detector magnet and the magnets in the machine detector interface (MDI) region.

8.1.5 Transport and logistics

In the first phase of the analysis, an inventory was established detailing the type, quantity, dimensions, and weight of the components to be transported. Simultaneously, the number of personnel requiring transport to their workplace in the tunnel was determined, and evacuation studies were conducted.

Based on these input data, two vehicle concepts have been studied: the first for the transport of the equipment, including the accelerator components, and a second for the transport of personnel throughout the installation, operation and dismantling phases.

The vehicle for transporting materials will be electric, fed by batteries. Charging stations will be installed all along the tunnel. The design comprises a trailer carrying the material, pulled by a tractor hosting the batteries. The trailer is equipped with two robotic arms capable of handling and manoeuvring the components up to their final location.

As the market already offers valid solutions, the personnel vehicle will be based on an existing system. This will then be customised to meet the specific requirements and constraints of the FCC tunnel. The personnel vehicles will be electric and powered by batteries. The personnel transport will consist of a mixture of individual and scheduled transport systems. Its characteristics will be defined to ensure the safe evacuation of people present in a sector at the appropriate time.

For safety reasons, vehicle overtaking must be possible at any location in the tunnel, which imposes a constraint on the width of the vehicles.

In addition to technical solutions for material and personnel transport, a logistics study is being conducted. This study develops logistics scenarios based on various boundary conditions, such as the number of shafts available for material transfer and the number of vehicles used for underground transportation.

For each scenario, key performance indicators (KPIs) are generated, including the number of magnets that can be installed per day and the total installation time required for the accelerator. Potential bottlenecks in material flow are also identified. These indicators serve as an objective tool for evaluating and comparing different scenarios, enabling the selection of the most suitable approach for the overall project.

8.1.6 Geodesy

The size of the FCC requires a refined and extended geodetic infrastructure, including reference frames and a gravity field model. The geodetic infrastructure must be compatible with each phase of the project. This comprises the generation of a primary surface geodetic network. To this end, Swisstopo and IGN are increasing the density of their national geodetic networks. In order to meet the vertical alignment accuracy, a refined model of the gravity field is being prepared.

8.1.7 Communications, computing, and data services

Three different infrastructures will be deployed to enable data, telephone and radio networks. They are all built on top of a fibre optics infrastructure. Regarding the IT infrastructure, the FCC will feature two redundant data centres on the Meyrin and Prévessin sites.

8.1.8 Surface areas

Based on the design choices above and input from the infrastructure and equipment groups, the needs for infrastructure and buildings at the eight surface points have been compiled. The tables summarise the key elements (element, location, construction type, size, capacity) by domain (safety, electricity, and energy management, cooling and ventilation, geodesy and survey, cryogenic systems, transport and logistics, computing infrastructures). The contents of these inventory tables are the basis for the layout of the surface points [373].

8.1.9 Underground areas

Integration studies of the underground areas, including the tunnel, main caverns and service caverns, shafts and alcoves, have been performed. Equipment sensitive to radiation will be placed in alcoves. There are seven alcoves per arc. The alcoves are linked to transport lay-by zones, which allow transport vehicles to park, pass and overtake each other.

In addition to the alcoves, there are service caverns at the eight points. The current civil engineering design for the service caverns at technical areas is 60 m long, 25 m wide and 15 m high. These caverns will each be divided into three levels to provide additional floor area on the upper levels. The service caverns are mainly occupied by power supplies, cooling and ventilation equipment, as well as cryogenics equipment.

8.2 3D integration studies

The 3D integration studies of the FCC-ee have been detailed for all the areas of the underground tunnels and caverns, fitting the requirements from the work packages (e.g., civil engineering, infrastructure, general services, transport, safety, optics, accelerators requirement, etc.). This section presents the results of the configuration and layout of the accelerators and infrastructure systems that were studied for the feasibility study report. This is an evolution of the previous studies made for the conceptual design report [13, 306]. The 3D integration studies take into account the configurations of both the FCC-ee and the FCC-hh to ensure space compatibility.

8.2.1 General layout of the FCC

The FCC is a 90.6 km circumference tunnel including eight access points equally spaced above the accelerator tunnel and currently named as point PA, PB, PD, PF, PG, PH, PJ and PL (see Fig. 8.1). The points PA, PD, PG and PJ will host the detectors in dedicated civil engineering areas. They are mentioned as large experiment

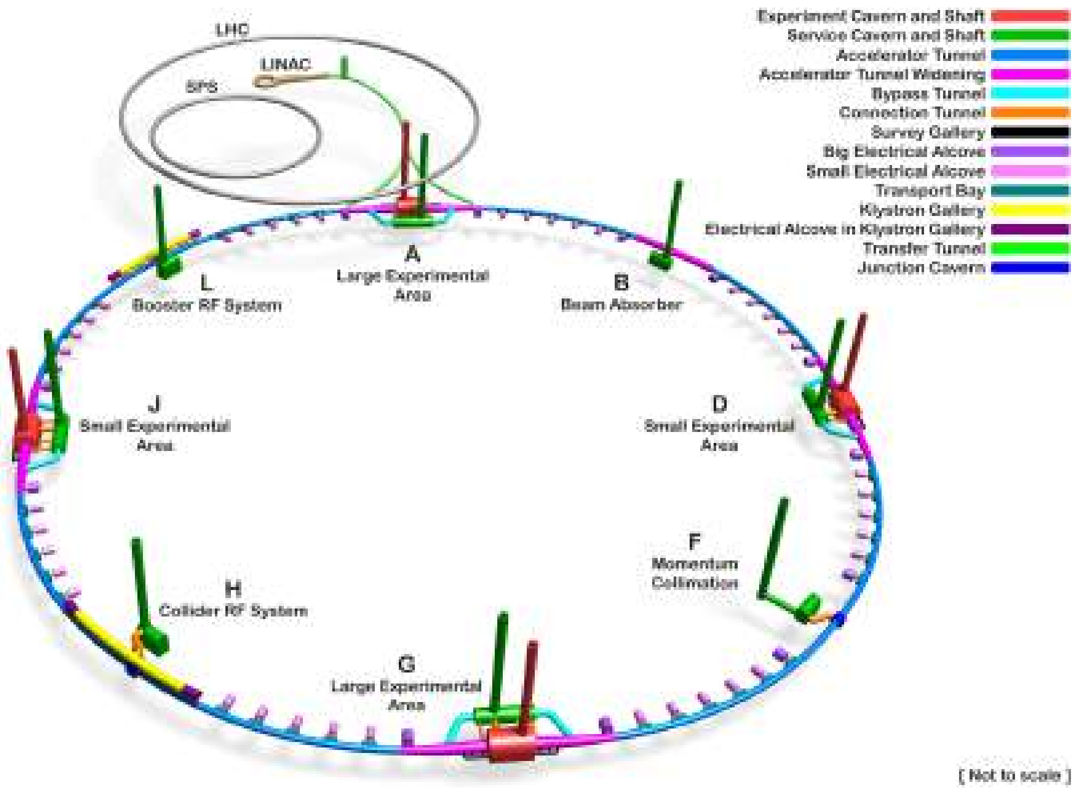

Fig. 8.1 FCC-ee schematic view

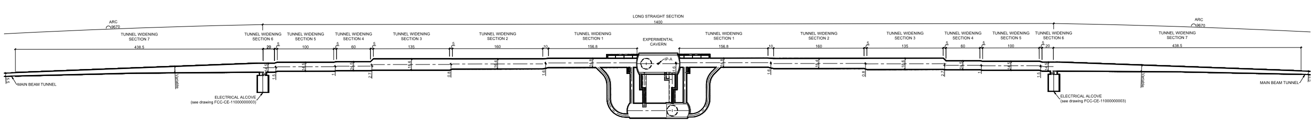

Fig. 8.2 FCC underground - civil engineering in point PA

points for points PA and PG and small experiment points for points PD and PJ. The points PB, PF, PH and PL are mentioned as technical points hosting different accelerator parts.

For the FCC-ee machine,

- The point PB will host the extraction system from the booster, transfer line and injection system to the collider, and the extraction systems and transfer lines to the dumps for both the collider and the booster,
- The point PF will host the collimation systems (betatron and momentum),
- The point PH will host the collider RF system,
- The point PL will host the booster RF system.

For the FCC-hh machine,

- The point PB will host the collider injection lines and the extraction lines to the dumps,
- The point PF will host the betatron collimation system,
- The point PH will host the momentum collimation system,
- The point PL will host the RF system.

8.2.2 Integration of point PA and point PG

Point PA and point PG will serve as large experimental points, hosting detectors in the cavern in both the FCC-ee and the FCC-hh phases of operation. The cavern size and extent meet the needs of the detectors for both FCC-ee and FCC-hh. In addition, for the FCC-ee, the long straight sections (LSS) on either side of point PA and point PG will host the beamstrahlung dumps and the polarimeter system (see Fig. 8.2 and Fig. 8.3). The LSS of point PA will also host the end of the transfer line from the injector linac, into the booster.

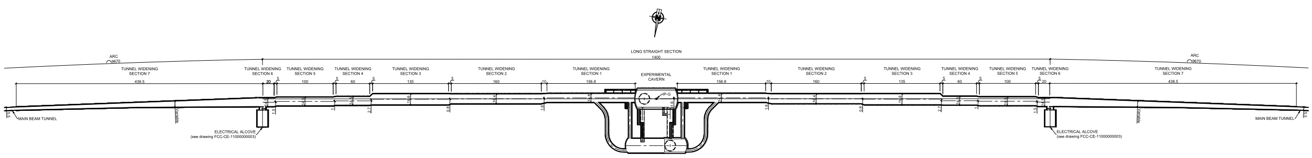

Fig. 8.3 FCC underground - civil engineering in point PG

Fig. 8.4 FCC-ee point PA and point PG - general overview

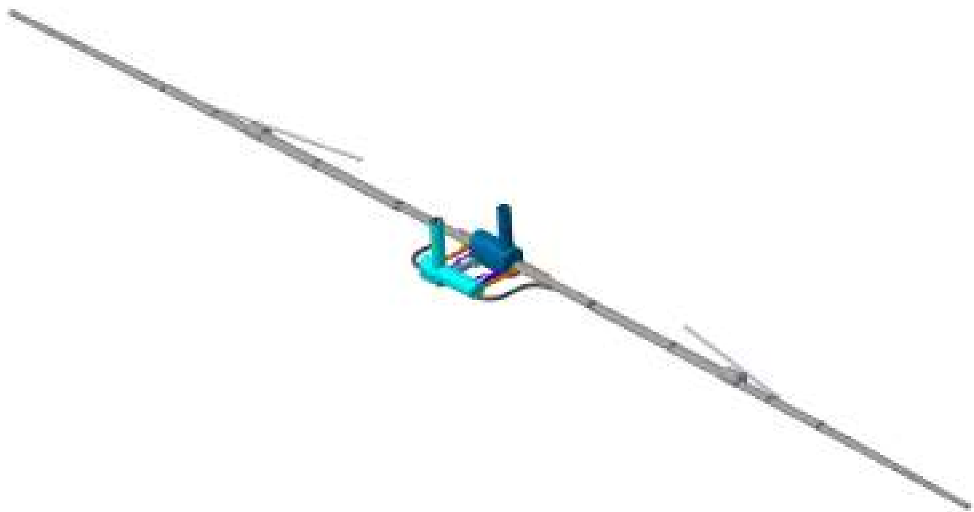

Fig. 8.5 FCC-ee point PA - top overview with optics

Fig. 8.6 FCC-ee point PA - experiment cavern cross-section

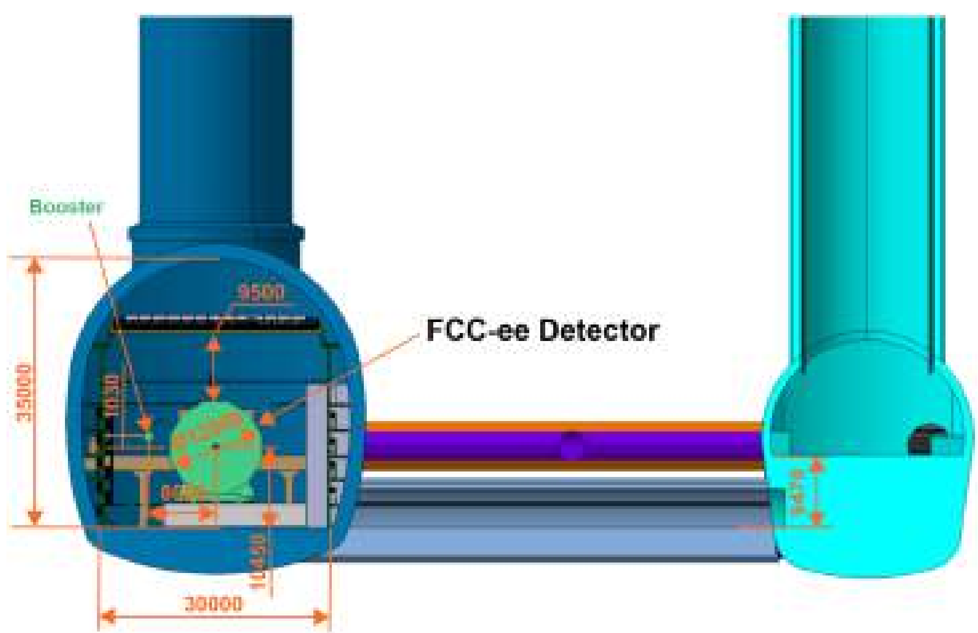

Figures 8.4 to Fig. 8.12 are the results of the 3D integration studies for the point PA and the point PG.

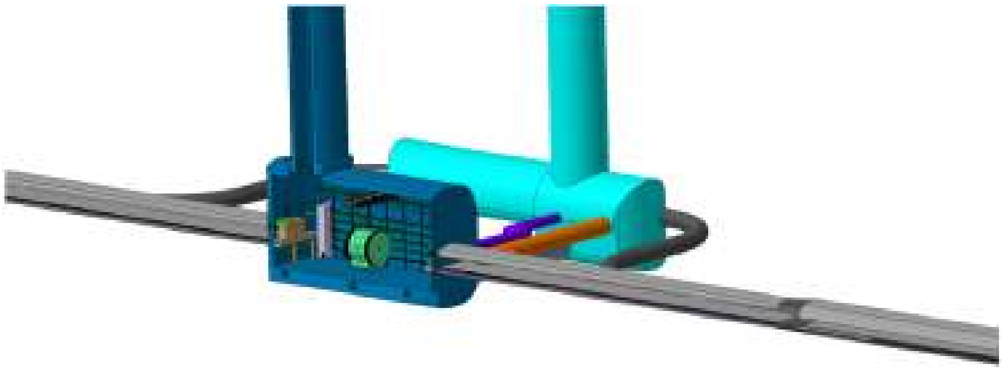

Fig. 8.7 FCC-ee point PA - experiment cavern iso view

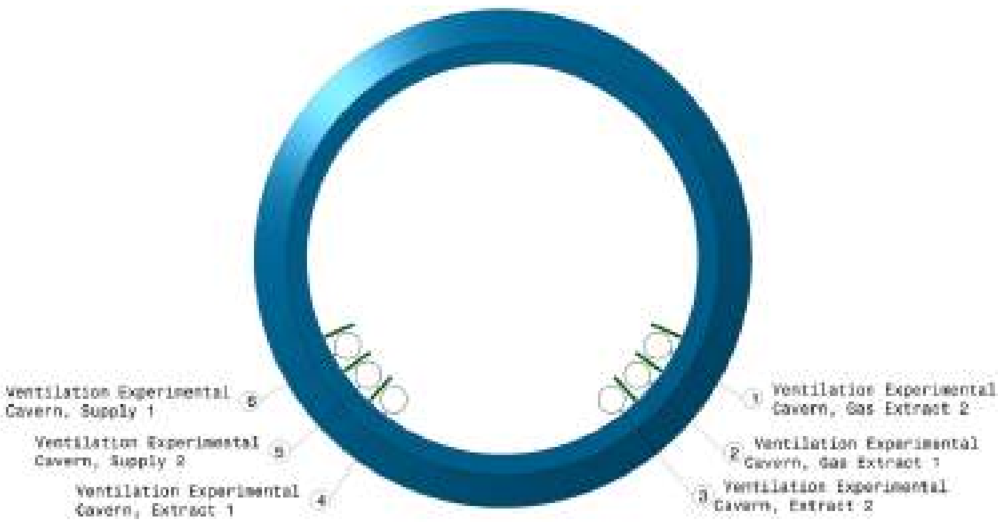

Fig. 8.8 FCC-ee point PA - shaft of the experiment cavern

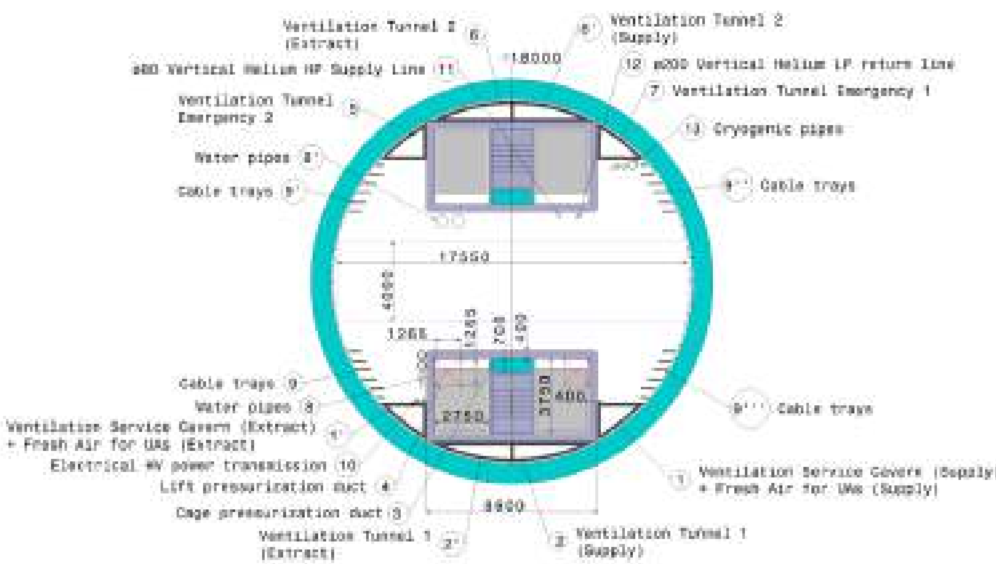

Fig. 8.9 FCC-ee point PA - shaft of the service cavern

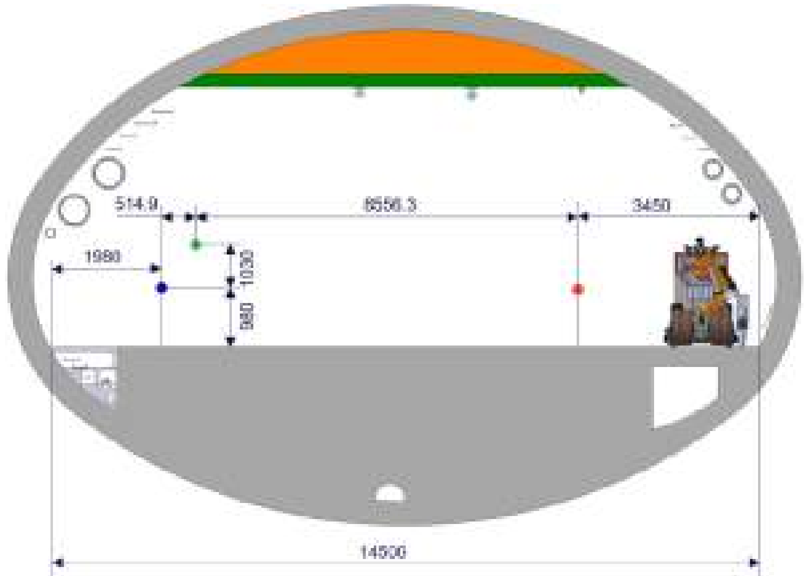

Fig. 8.10 FCC-ee point PA - tunnel cross-section with booster

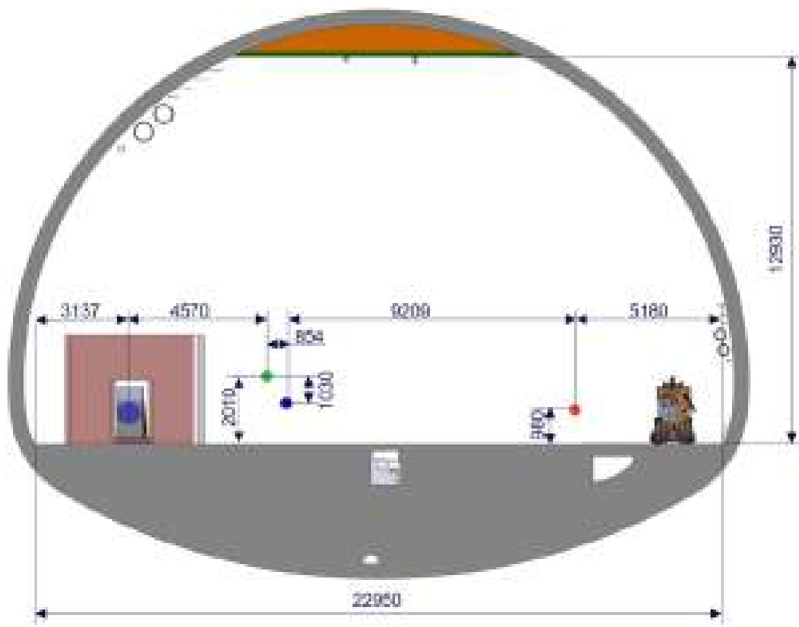

Fig. 8.11 FCC-ee point PA - tunnel cross-section with dump

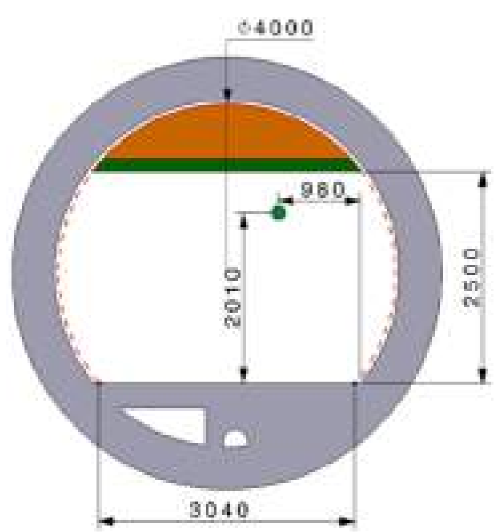

Fig. 8.12 FCC-ee point PA - booster injection tunnel

8.2.3 Integration of point PB

Point PB will house the FCC-ee beam dump and injection from the booster into the collider. In the next phase of operation, FCC-hh will house the beam dump system. The civil engineering volumes meet the needs of FCC-ee (see Fig. 8.13).

Figures 8.14 to Fig. 8.16 are the results of the 3D integration studies for the point PB.

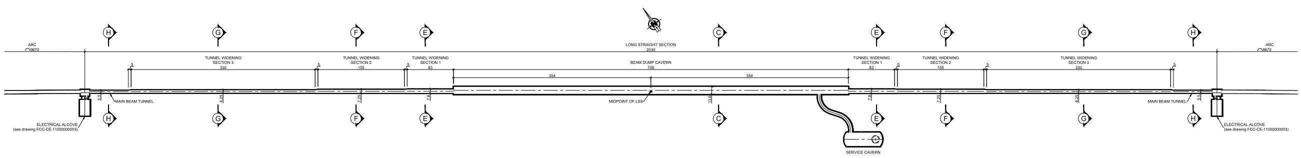

Fig. 8.13 FCC underground - civil engineering in point PB

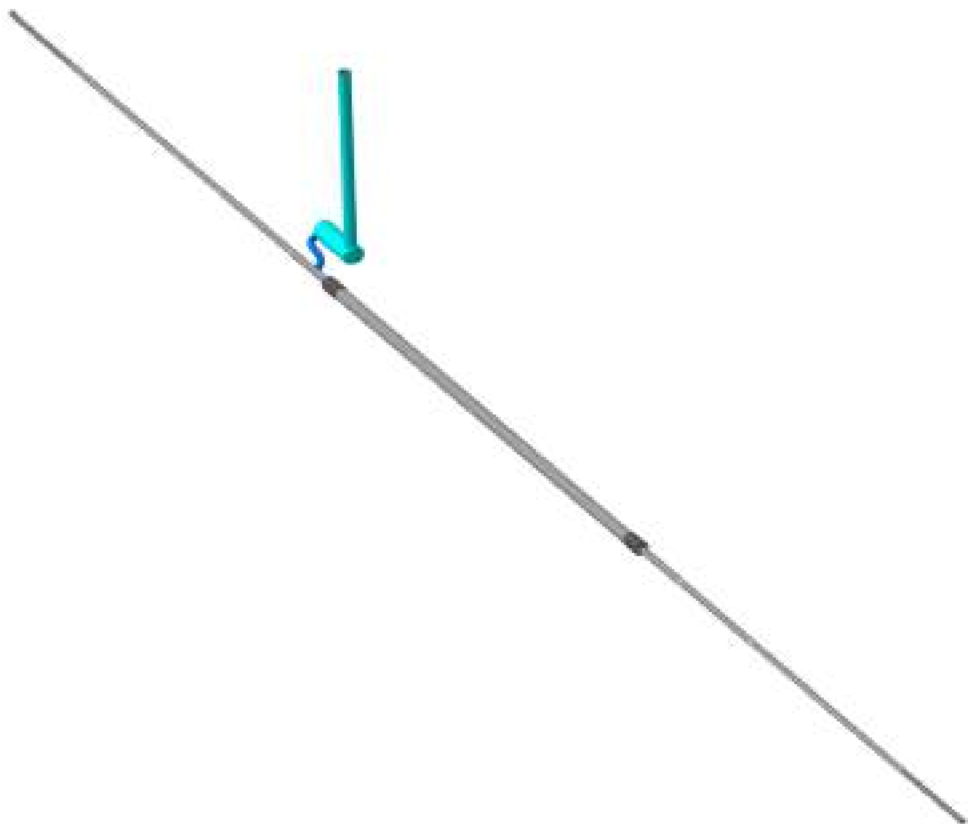

Fig. 8.14 FCC-ee Point PB - general overview

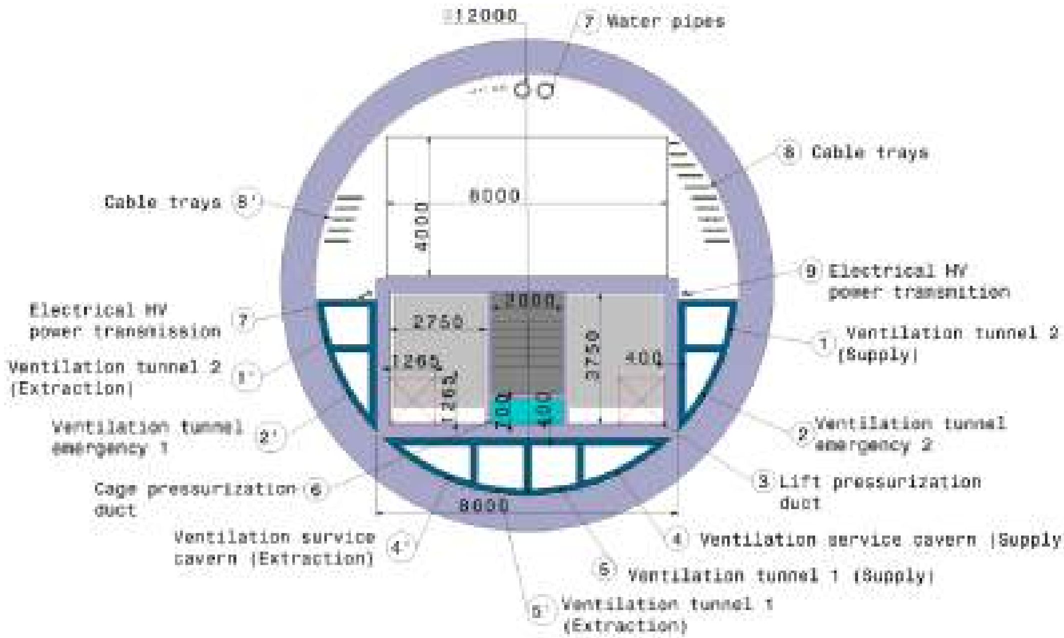

Fig. 8.15 FCC-ee Point PB - shaft of the service cavern

Fig. 8.16 FCC-ee Point PB - tunnel including the dump

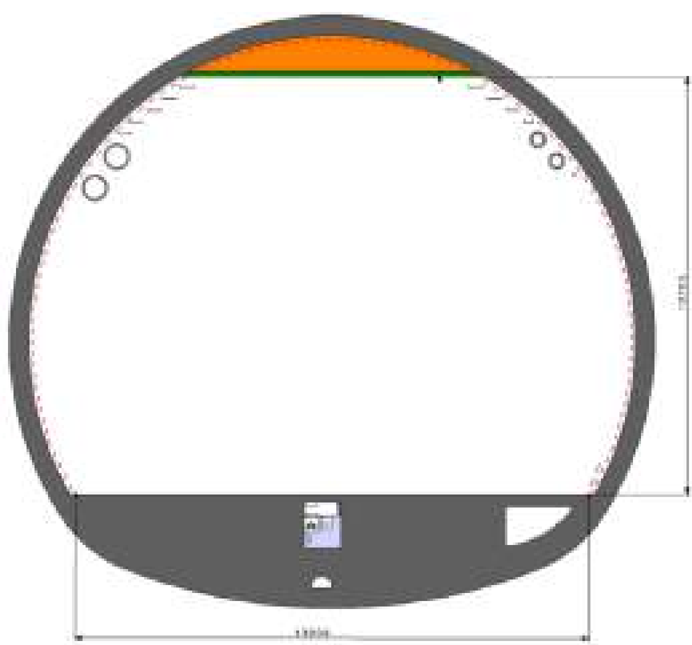

8.2.4 Integration of point PD and point PJ

Point PD and point PJ will serve as small experimental points, hosting detectors in the cavern in both the FCC-ee and the FCC-hh phases of operation (see Fig. 8.17 and Fig. 8.18). The cavern size and extent meet the needs of the detectors for both FCC-ee and FCC-hh. In addition, for the FCC-ee, the long straight section (LSS) on either side of point PD and point PJ will host the beamstrahlung dumps.

Figures 8.19 to Fig. 8.23 are the results of the 3D integration studies for points PD and PJ.

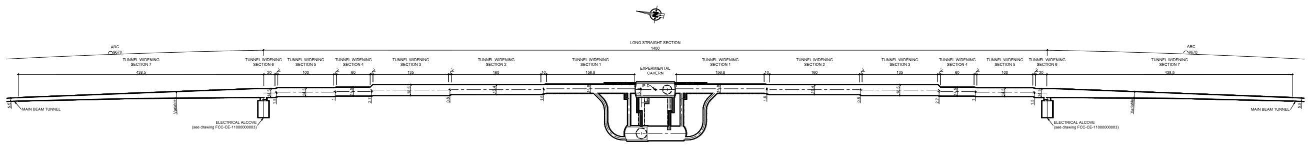

Fig. 8.17 FCC underground - civil engineering in point PD

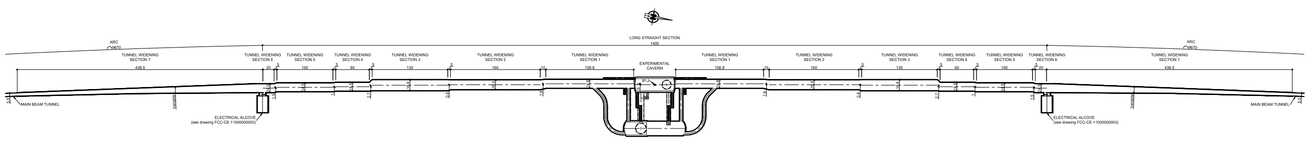

Fig. 8.18 FCC underground - civil engineering in point PJ

Fig. 8.19 FCC-ee point PD and PJ - general overview

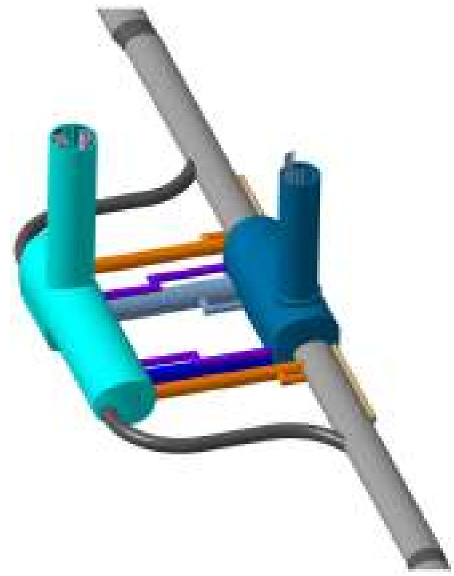

Fig. 8.20 FCC-ee point PD and PJ - shaft of the experiment cavern

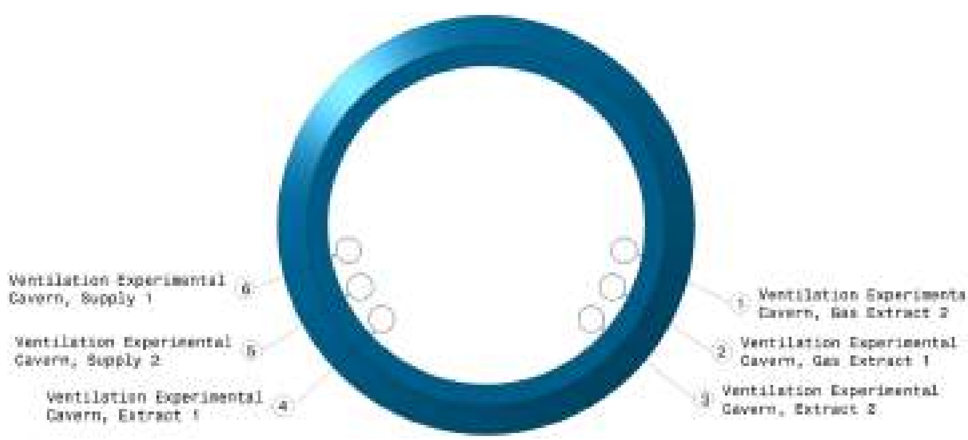

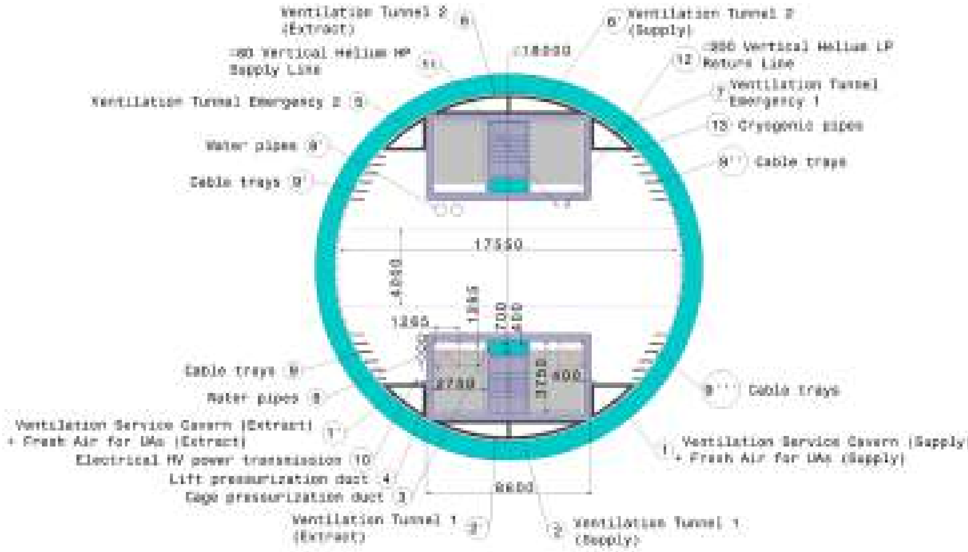

Fig. 8.21 FCC-ee point PD and PJ - shaft of the service cavern

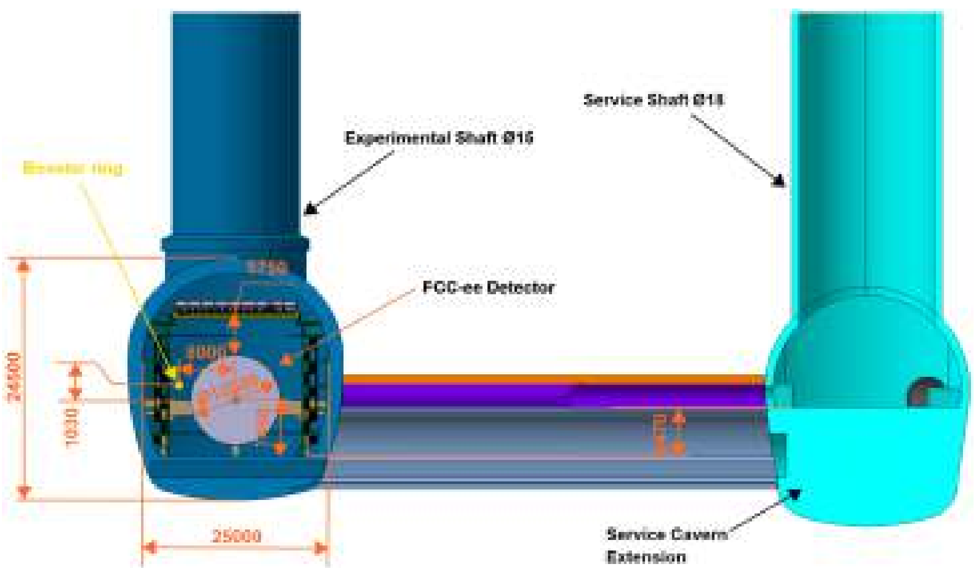

Fig. 8.22 FCC-ee point PD and PJ - experiment cavern cross-section

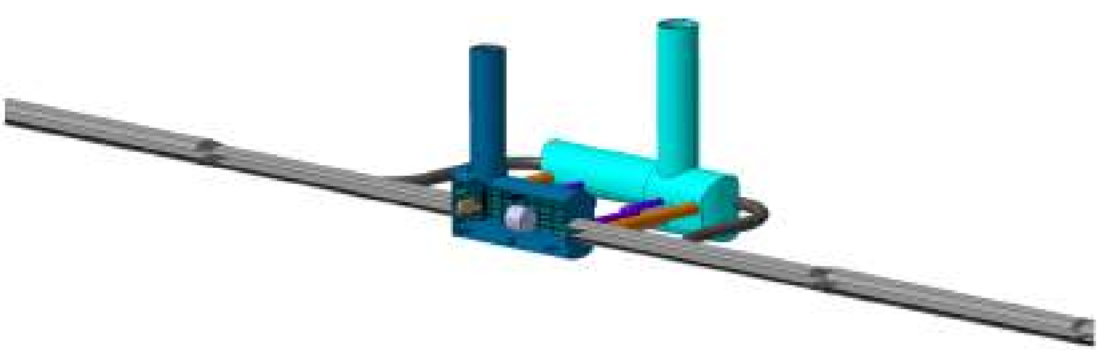

Fig. 8.23 FCC-ee point PD and PJ - experiment cavern iso view

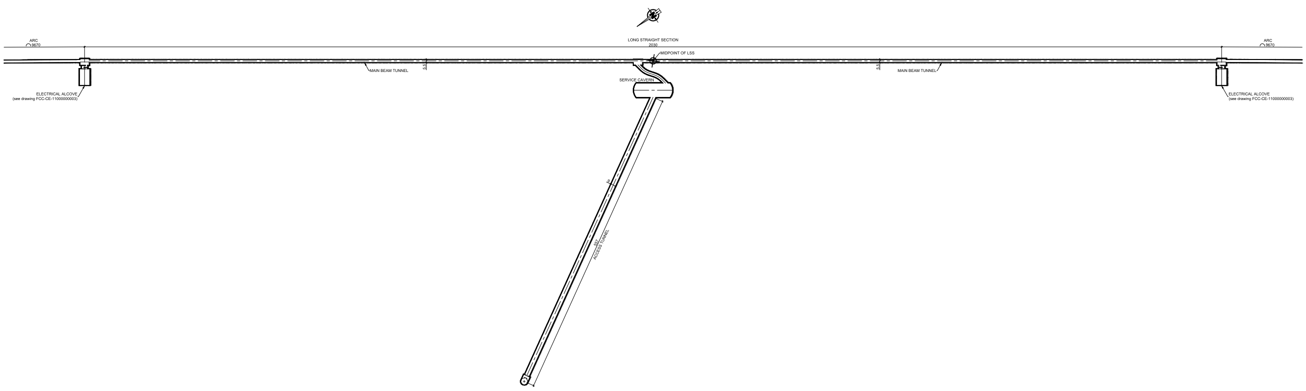

Fig. 8.24 FCC underground - civil engineering in point PF

Fig. 8.25 FCC-ee point PF - general overview

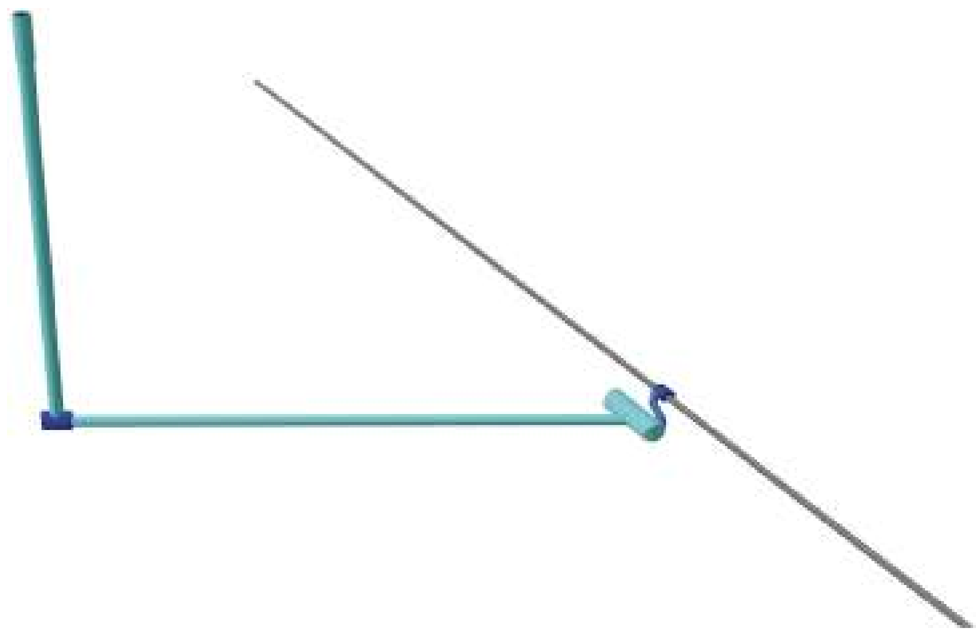

8.2.5 Integration of point PF

Point PF will house FCC-ee betatron and momentum collimation systems. In a next phase of operation, FCC-hh will house the beam dump systems. The civil engineering volume meet the needs of FCC-ee (see Fig. 8.24).

Figures 8.25 and 8.26 are the results of the 3D integration studies for the point PF.

8.2.6 Integration of point PH and point PL (RF systems)

The RF systems of the FCC-ee will be located in point PH for the collider and point PL for the booster (see Fig. 8.27 and Fig. 8.28).

Configuration and layout of collider RF systems - point PH Figures 8.29 to Fig. 8.33 are the results of the 3D integration studies for point PH.

For radiation safety, the distance between the klystron gallery and the machine tunnel is 10 m and shielding is installed in the klystron gallery. The vertical cores house the waveguides and electrical cables. For fire protection, there are partition walls every 400 m in the klystron gallery, and a smoke extraction system on the ceiling. There is a stairway connection between the klystron gallery and the machine tunnel every 280 m.

Configuration and layout of booster RF systems - point PL Figures 8.34 to Fig. 8.37 are the results of the 3D integration studies for point PL.

Fig. 8.26 FCC-ee point PF - shaft of the service cavern

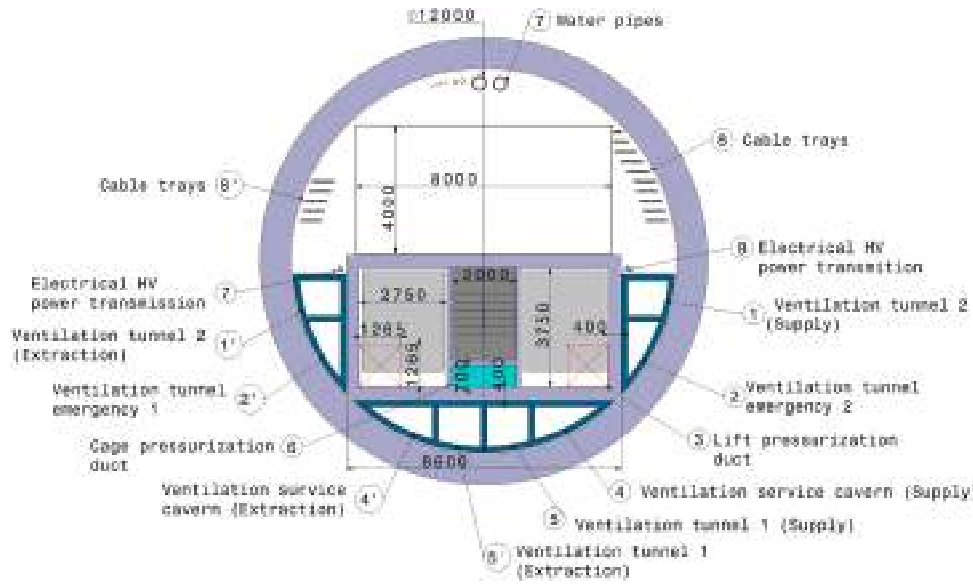

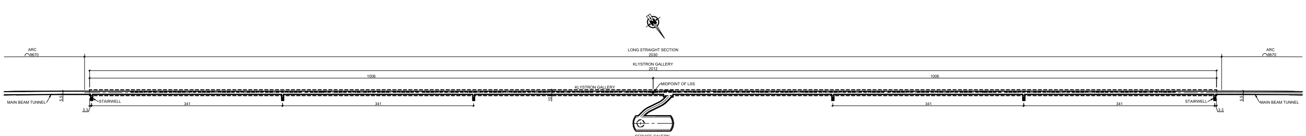

Fig. 8.27 FCC underground - civil engineering in point PH

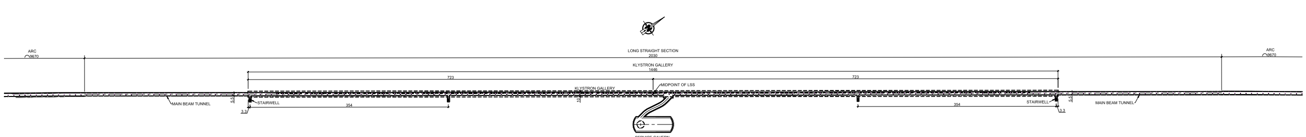

Fig. 8.28 FCC underground - civil engineering in point PL

Fig. 8.29 FCC-ee point PH - general overview

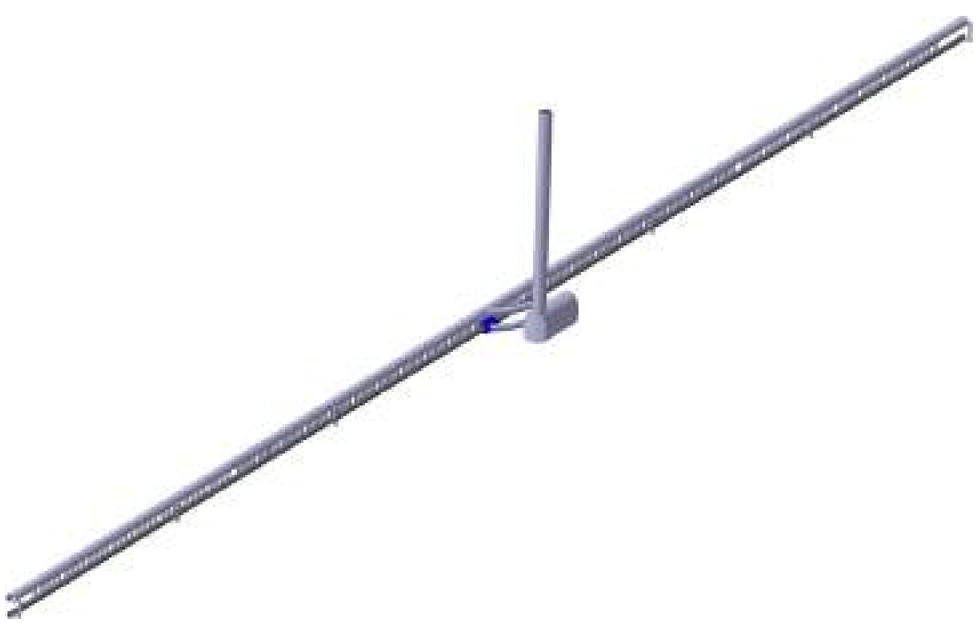

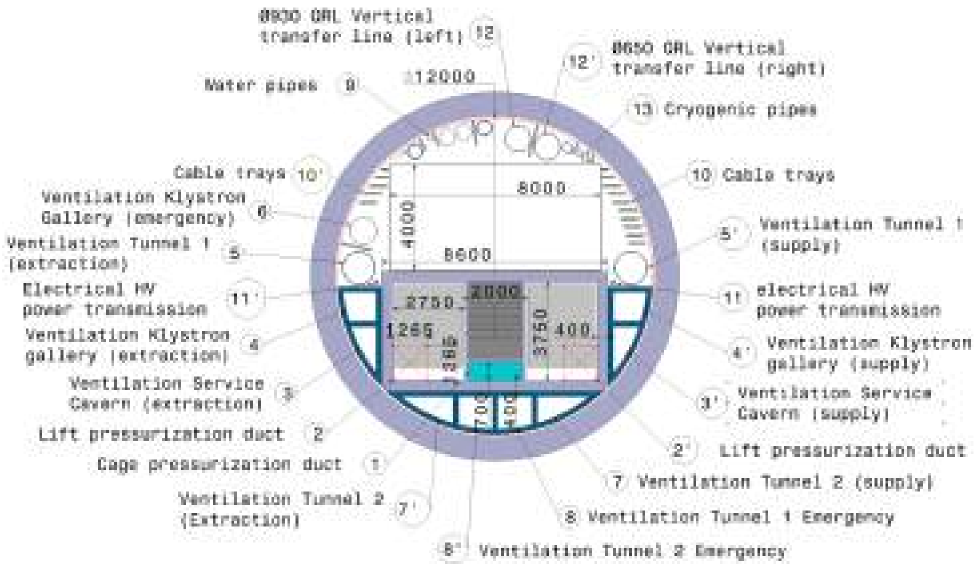

Fig. 8.30 FCC-ee point PH - shaft of the service cavern

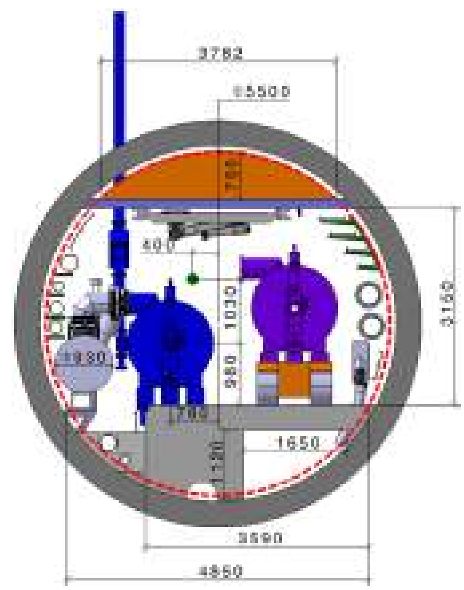

Fig. 8.31 FCC-ee point PH - tunnel cross-section with FCC 800 MHz cavity

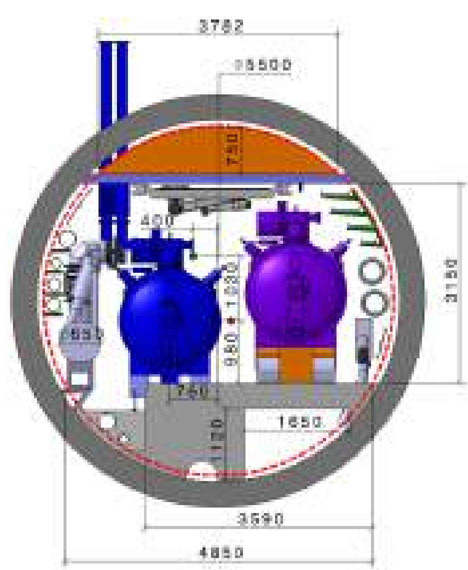

Fig. 8.32 FCC-ee point PH - tunnel cross-section with FCC 400 MHz cavity

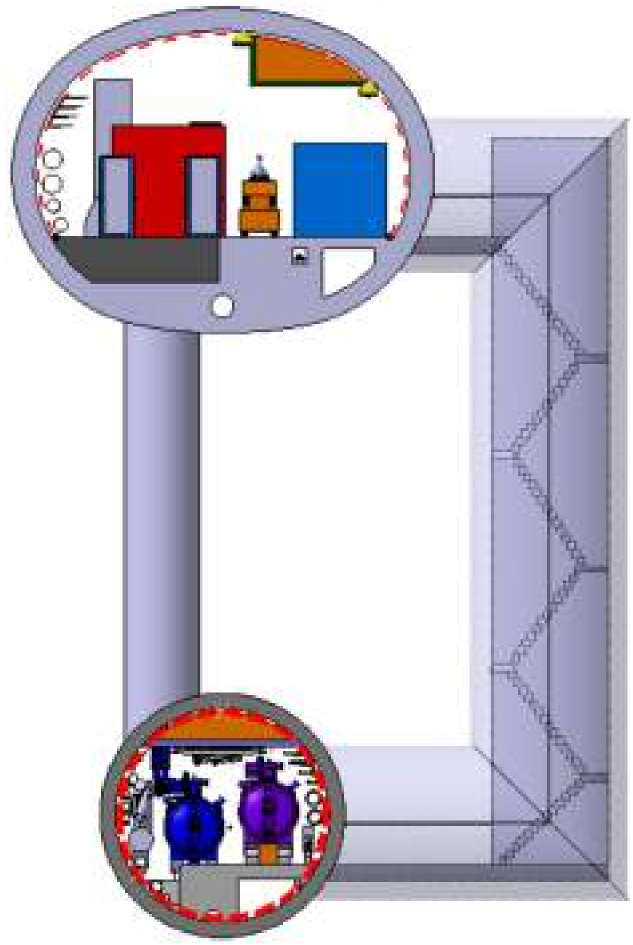

Fig. 8.33 FCC-ee point PH - tunnel and gallery cross-section

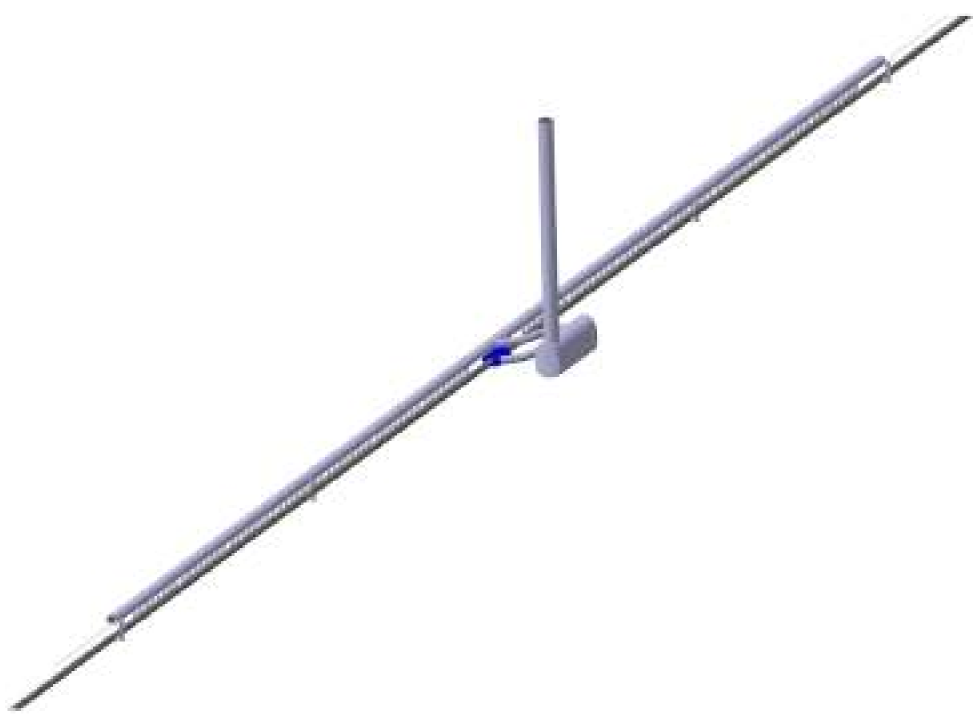

Fig. 8.34 FCC-ee point PL - general overview

Fig. 8.35 FCC-ee point PL - shaft of the service cavern

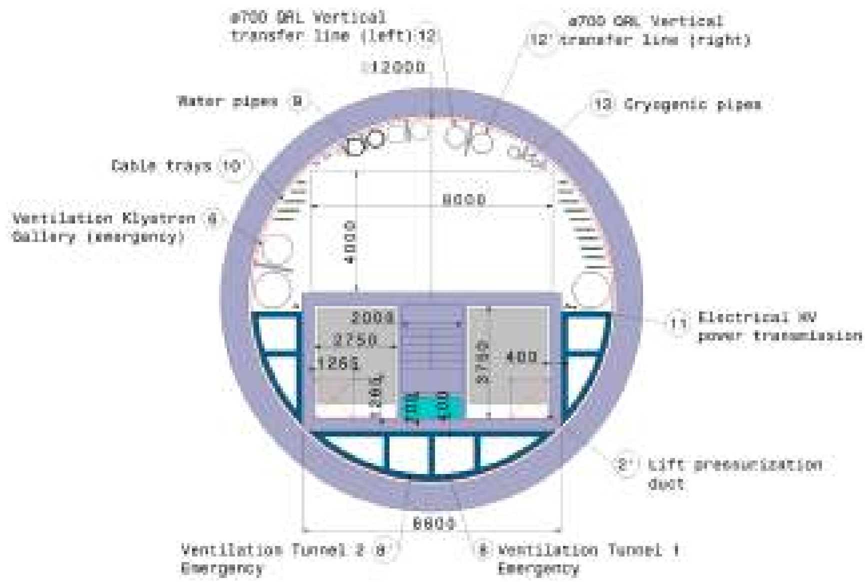

Fig. 8.36 FCC-ee point PL - tunnel cross-section with booster 800 MHz cavity

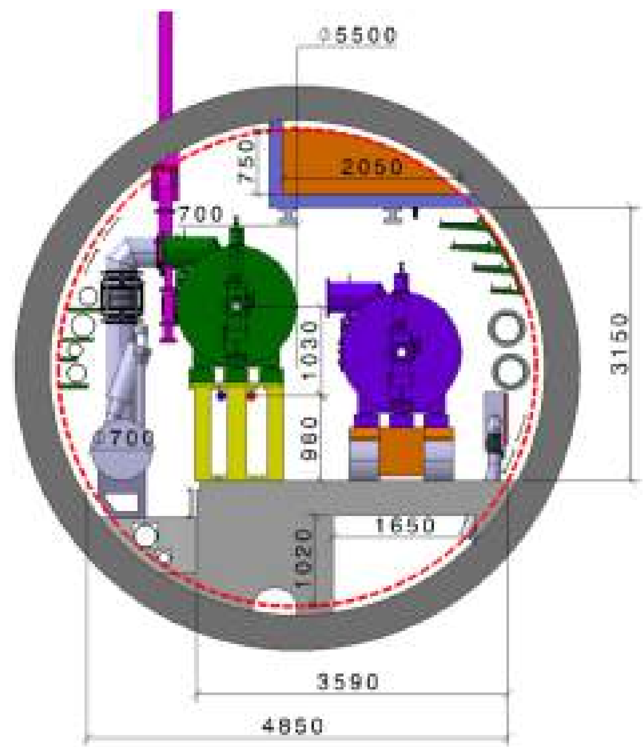

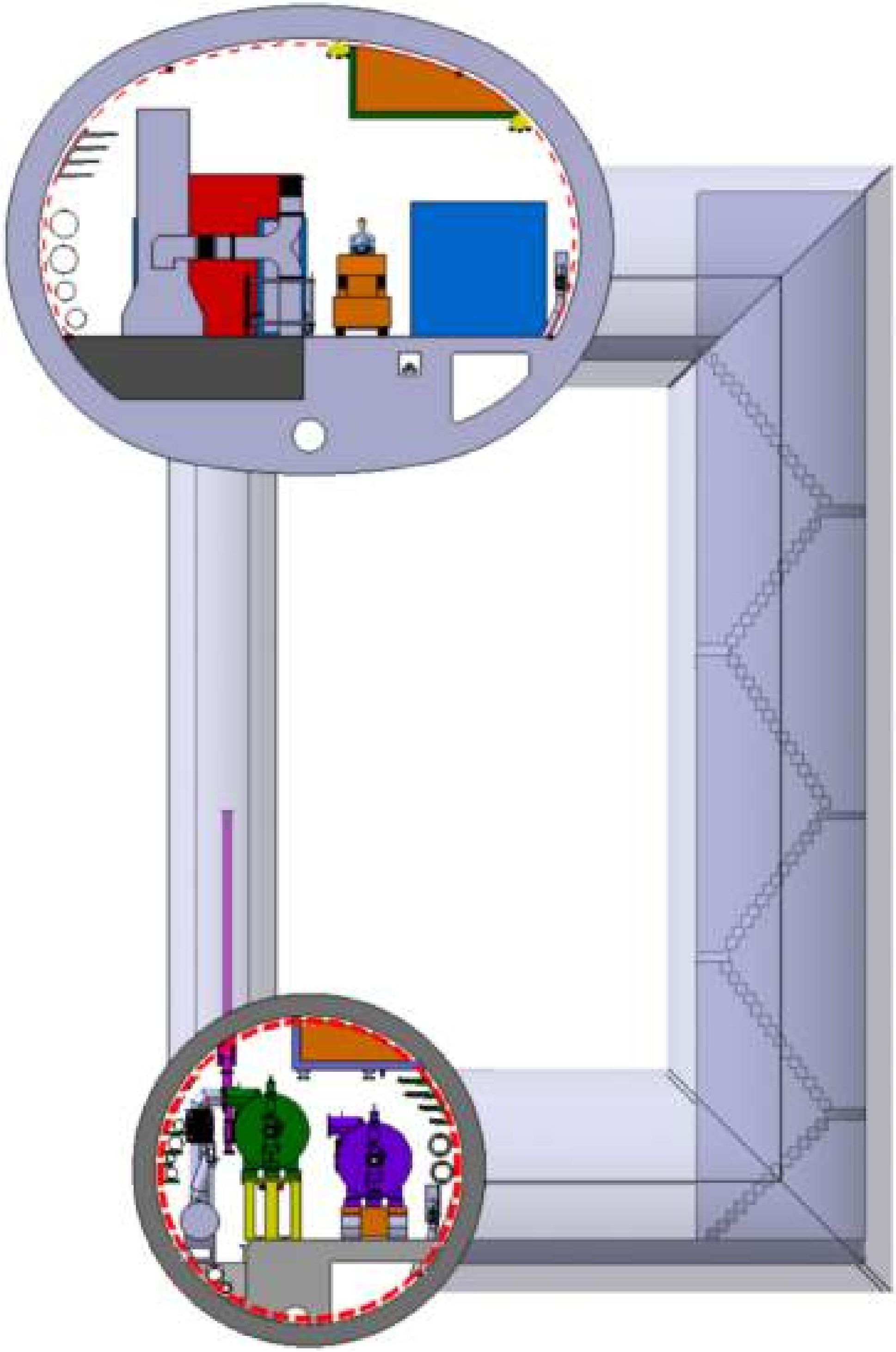

Fig. 8.37 FCC-ee point PL - tunnel and gallery cross-section

8.2.7 Integration of the arcs

The machine tunnels will house the FCC-ee accelerator and, in the following phase of operation, the FCC-hh accelerator. The civil engineering volume meet both accelerators needs.

Since the publication of the conceptual design report [13], the collider and booster have been lowered to give more space above the beam lines for safety requirements. After collecting updated requirements from all the stakeholders, the space requirements were reviewed with respect to installation and maintenance accessibility. A

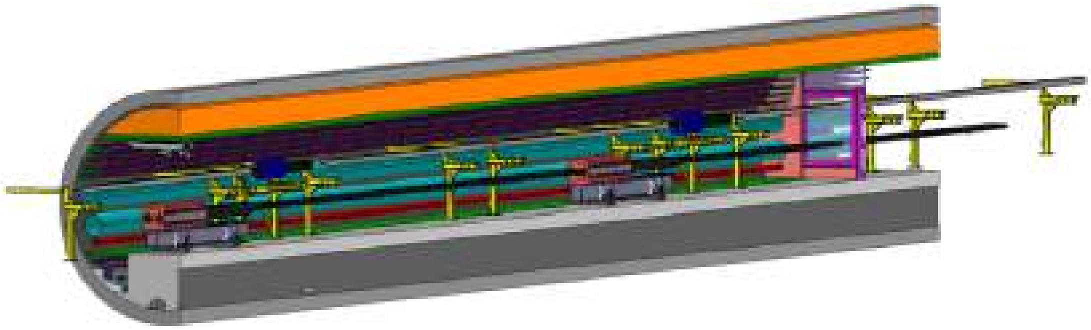

Fig. 8.38 FCC-ee layout in the arcs - longitudinal view

Fig. 8.39 FCC-ee layout in the arcs - cross-section view

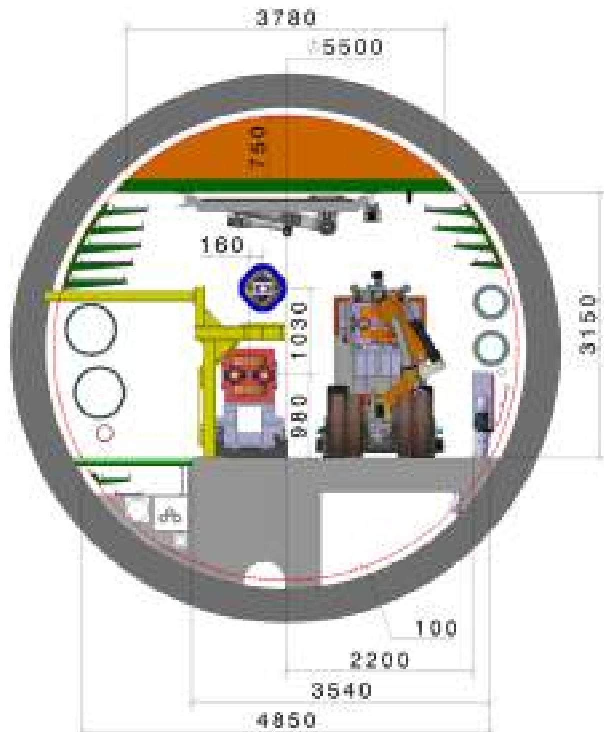

robot was added to the ceiling of the tunnel for better control of installation and maintenance of both magnets and support services.

Figures 8.38 and 8.39 are the results of the 3D integration studies for the arcs based on one of the baseline scenarios of a half-cell layout (see Fig. 3.71 and Fig. 3.72). The optimisation of the arc-supporting structures to maximise their performance, easing the installation and maintenance while minimising cost is facilitated by the FCC-ee Arc Half Cell Mock-up (see Sect. 3.10).

8.2.8 Integration of the alcoves

In addition to the technical and experiment points, there will be 56 alcoves distributed around the ring (7 per arc). These alcoves will mainly house electronics and power supplies, which need to be shielded from ionising radiation. The alcoves integrate the electrical equipment to supply a sector of the FCC, including systems installed in the alcoves themselves, plus the tunnel infrastructure like lighting, general services and a secured network. The entrance of the alcoves will also serve as a parking area for the transport vehicles (see Figs. 8.40 and 8.41). Figures 8.42 to Fig. 8.45 are the results of the 3D integration studies for the alcoves.

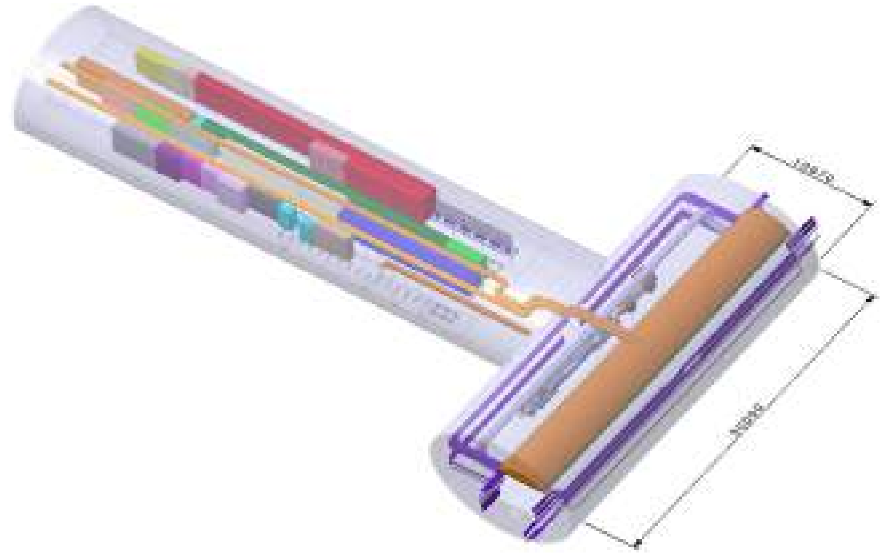

Fig. 8.40 FCC-ee alcove in the arcs with big parking area

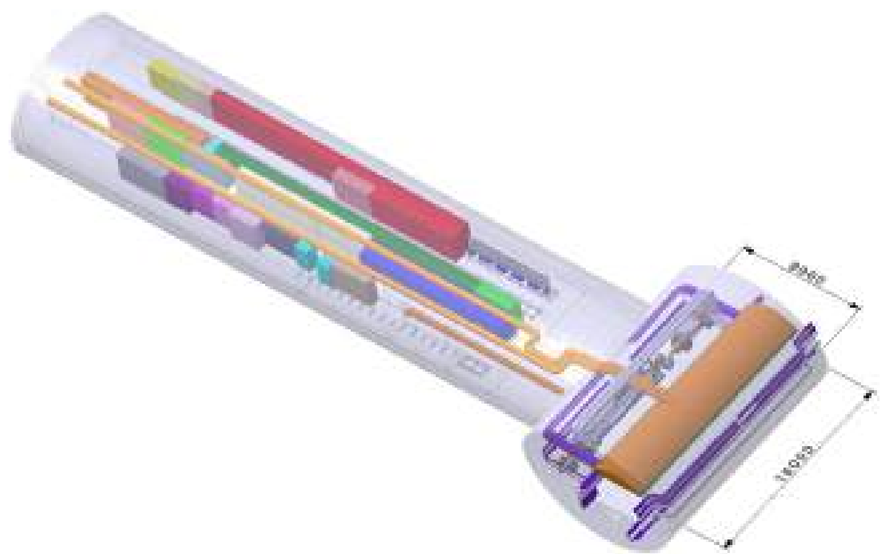

Fig. 8.41 FCC-ee alcove in the arcs with small parking area

The integration of power converters in the alcoves and the routing of cables in the machine tunnel present significant challenges due to space constraints and the high number of circuits involved. Power converters are installed in both small and big alcoves. Table 8.1 provides an overview of the number of converters in the alcoves and the number of cables in the cable trays.

There are five cables trays of varying sizes located above the booster supporting structure. The layout of the cables in the cable tray must respect the normal cabling rules. The proposed radiation shielding must reduce the radiation level to be low enough for the cables to survive for the entire lifetime of operation.

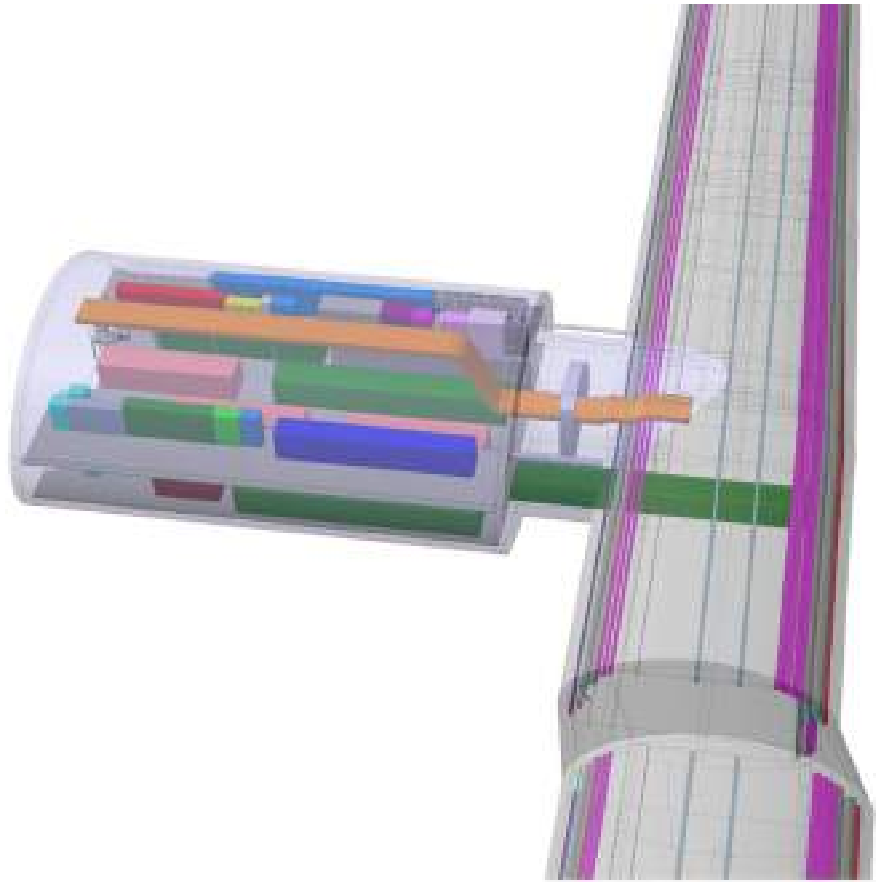

Fig. 8.42 FCC-ee alcove at point PA and PG

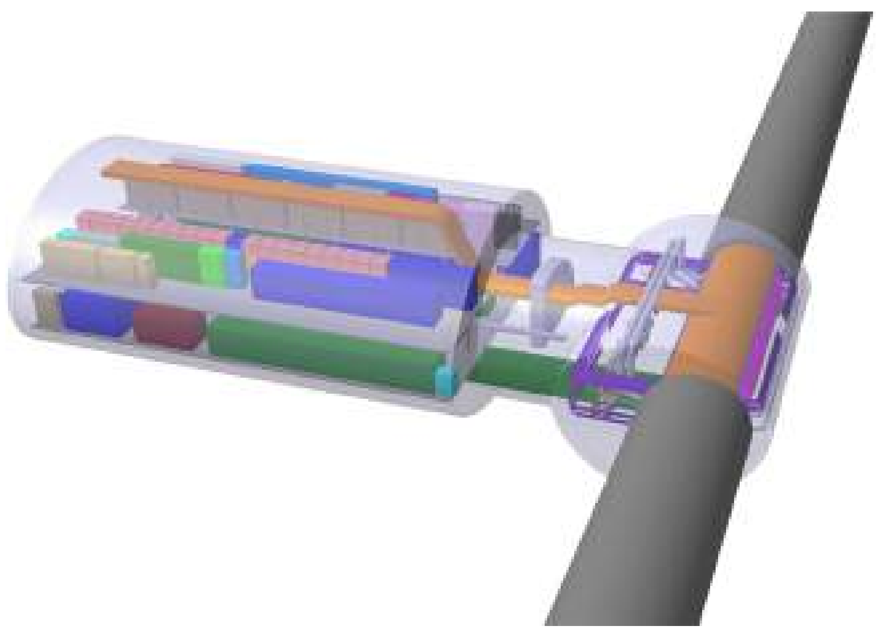

Fig. 8.43 FCC-ee alcove at point PB

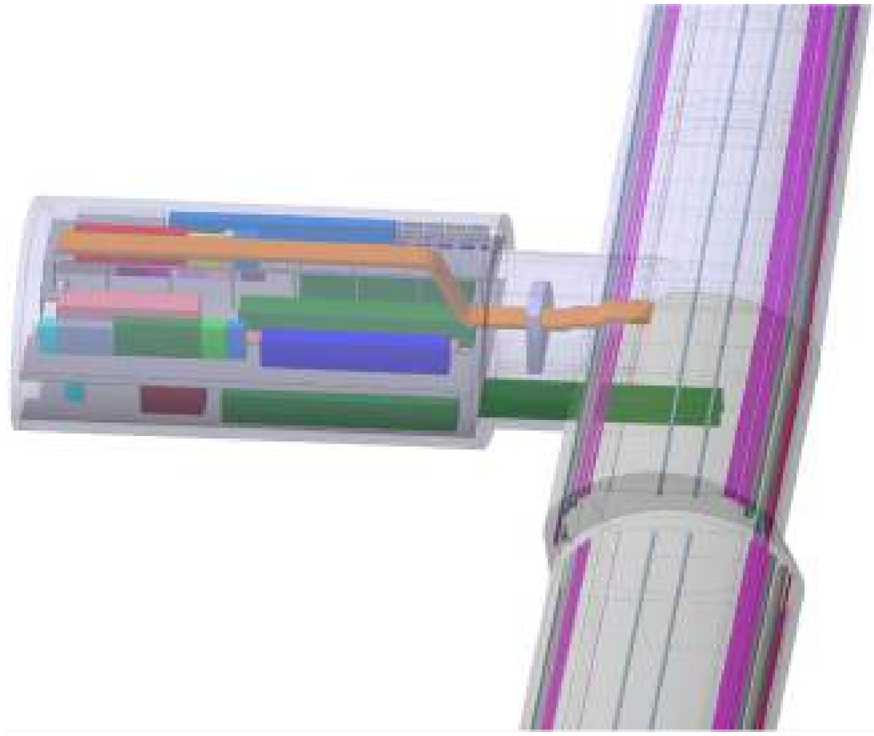

Fig. 8.44 FCC-ee alcove at points PD and PJ

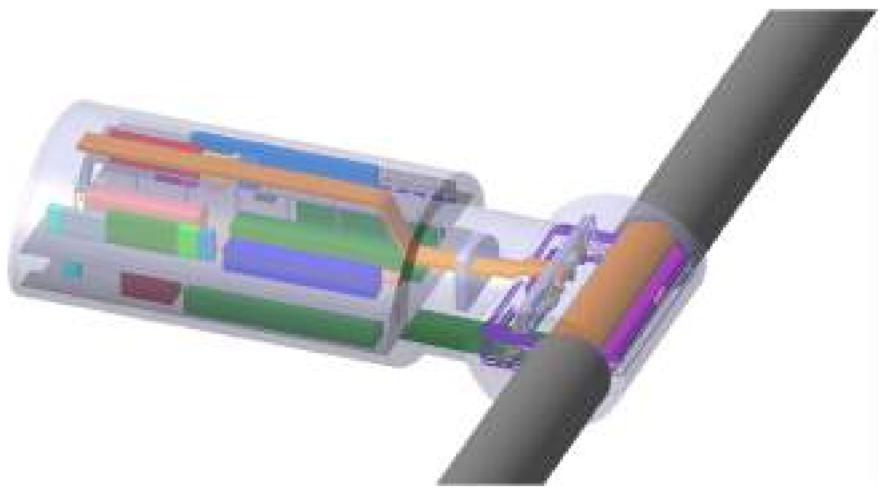

Fig. 8.45 FCC-ee alcove at point PF

8.2.9 Next phase for the integration studies

The integration studies have been made with the pre-design of volumes and will evolve with detailed technical design in the next phase of the FCC studies. Optimisation of the 3D integration studies with respect to the requirements from work packages will continue for all the areas following the identified technical and space needs:

- Optimisation of the large experiment points PA and PG [374, 375] and small experiment points PD and PJ [376], integrating more detailed detectors design in the experiment caverns,
- Optimisation of the technical point PB [377], integrating more detailed mechanical design of the accelerators and transfer lines,
- Optimisation of the technical point PF [378], integrating more detailed mechanical design of the collimation systems,
- Optimisation of the technical point PH and PL [379, 380], integrating the more detailed mechanical design of the radiofrequency and cryogenic systems and enlarging the space for transport and safety in the passage part of the tunnel,

Table 8.1 Quantities of converter racks in the alcoves and cables in cable trays at the exit of an alcove

Magnet	Quantity of racks in		Cables	
	Big alcove	Small alcove	Size (mm^2)	Quantity
Collider Dipole	27	-	1x500	2
Collider Quadrupole (F and D)	46	-	1x300	4
Collider Sextupole (F and D)	42	84	1x70	28
Collider Dipole Tapering	1	2	1x6	16
Collider Quadrupole Tapering	1	2	1x10	16
Collider Horizontal Corrector	2	3	1x10	60
Collider Vertical Corrector	2	3	1x16	60
Collider Skew Quadrupole	2	3	1x10	60
**Collider Straight Section*	*18*	-	-	-
**Collider Injection*	*n/a*	*n/a*	*n/a*	*n/a*
Booster Dipole	35	-	1x500	2
Booster Quadrupole (F and D)	86	-	1x185	8
Booster Sextupole Focusing	4	-	1x240	2
Booster Sextupole Defocusing	11	-	1x185	4
**Booster Dipole Tapering*	*1*	*2*	*1x4*	*8*
**Booster Quadrupole Tapering*	*1*	*2*	*1x6*	*8*
**Booster Horizontal Corrector*	*3*	*6*	*1x25*	*36*
**Booster Vertical Corrector*	*3*	*6*	*1x25*	*36*
**Booster Quadrupole Corrector*	*3*	*5*	*1x16*	*30*
**Booster Skew Quadrupole*	*3*	*5*	*1x16*	*30*
**Booster Straight Section*	*23*	-	-	-
**Booster Injection*	*n/a*	-	*n/a*	*n/a*
Total	**314**	**123**	-	***410***

*Magnet specifications not yet fully defined or inexistent – values extrapolated

- Optimisation of the arc half-cell [381], including the optimisation of the arc-supporting structures studied by the FCC-ee Arc Half Cell Mock-up (Sect. 3.10) to maximise their performance, ease the installation and maintenance while minimising cost.
- Optimisation of the alcoves [382], updating the control and powering racks layout with respect to technical specification evolutions.

8.3 Cooling and ventilation

8.3.1 Introduction

The cooling systems for the FCC mainly concern several water systems for the machine and its infrastructure, including accelerator and detector equipment (electronic racks, cryogenic plants, water-cooled magnets, RF equipment, etc.). Raw water will be used to fill the cooling circuits in some firefighting systems and as make-up water for the cooling towers. Chilled water is needed to extract the heat load from air in ventilation systems. Demineralised water would be employed to cool sensitive equipment like magnets, synchrotron radiation absorbers, and power converters.

The ventilation systems for the FCC should ensure the necessary conditions of humidity and temperature in the tunnel during operation, providing a supply of fresh air for personnel working within the facilities and heating for the working environment. The extraction systems must be capable of purging the air in the tunnel before access is allowed, as well as removing smoke and gases during an emergency.

Other systems comprise several and varied applications, some unrelated to cooling and ventilation. The compressed air systems for the FCC would provide compressed air to end clients requiring it, including the dampers

Fig. 8.46 Distribution of raw water coming from point PA, Lake Geneva

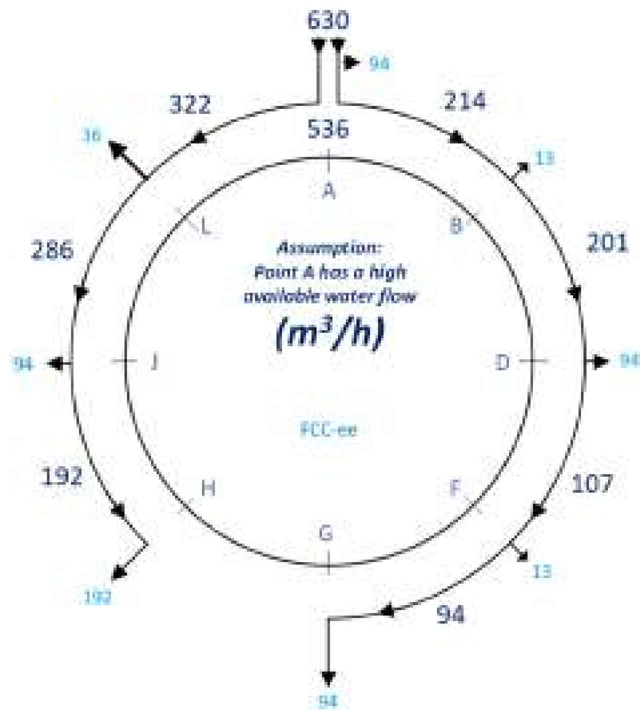

Table 8.2 Maximum make-up and effluent water of cooling towers (m^3/h)

Point	PA	PB	PD	PF	PG	PH	PJ	PL
Make-up water for cooling towers	94	13	94	13	94	192	94	36
Effluent water from cooling towers and filters	13	2	13	2	13	26	13	5

employed in the FCC tunnel. Effluent water from the cooling towers and filters would be concentrated in salts and returned to a water treatment plant. Drinking water would be needed for sanitary purposes. Finally, a drainage network would evacuate the water drained from the surface facilities and underground areas.

Cooling systems

Water supply The FCC accelerator would need to be supplied with water at the eight surface points. The main water consumers are the cooling towers, but water is also needed for the fire-fighting systems, the demineralised water production plant and all the cooling plants in the surface buildings as well as in the tunnels and caverns.

As a baseline, raw water is supplied from point PA to the rest of the accelerator, as represented in Fig. 8.46. Lake Geneva, located near PA, also serves as a water source for other accelerators within the CERN complex. Pipes running through the FCC tunnel sectors distribute water to one or more contiguous points: one branch supplies water from point PA to points PB, PD, PF, and PG, while another branch supplies water from point PA to points PL, PJ, and PH. Table 8.2 presents the approximate maximum raw water flow rates required, along with the effluent water generated at the cooling towers and filters.

An alternative design to this baseline could include the Rhône and Arve rivers as potential water sources for the FCC. In that case, point PA would feed points PL and PB with water from Lake Geneva, point PD would feed points PF and PG with water from the Arve river and point PJ would feed point PH with water from the Rhone river. This would effectively decrease the piping and pumping system sizes.

Firefighting water is available across each surface site, as well as in the service and experiment caverns. An additional flow rate of 240 m^3/h per point is allocated for firefighting purposes. Each surface site is equipped with water tanks capable of storing the estimated water supply needed for one hour.

In addition to the cooling towers and firefighting systems, the demineralised and chilled water circuits also require periodic refilling, with an estimated maximum demand of 0.5 m^3/h.

Water transfer between points is managed through a pumping station at point PA and booster pumps positioned at the bottom of the shaft at point PF, as illustrated in Fig. 8.47, which also depicts the approximate surface and underground elevations, along with shaft depths.

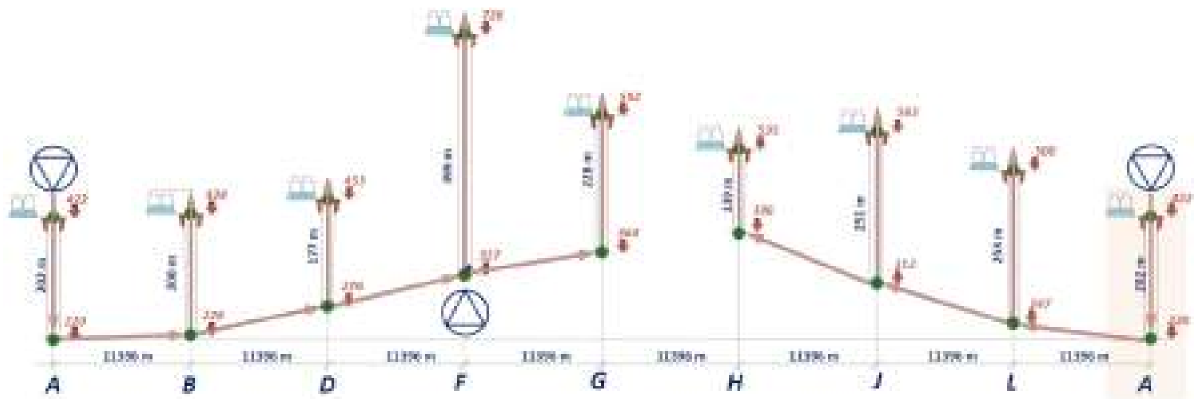

Fig. 8.47 Pumping stations and booster pumps of the raw water system

Table 8.3 Cooling demands (MW) of the primary circuit

Point	PA	PB	PD	PF	PG	PH	PJ	PL
Cryogenics						34.0		10.0
Experiments	0.5		0.5		0.5		0.5	
General Services	2.0	2.0	2.0	2.0	2.0	2.0	2.0	2.0
Power Converters						4.5		0.1
Chilled Water	5.8	5.2	5.8	5.2	5.8	11.3	5.8	5.8
Underground	42.5	1.0	42.5	1.0	42.5	48.9	42.5	2.7
Total power required	50.8	8.2	50.8	8.2	50.8	100.7	50.8	20.6

Table 8.4 Cooling capacity (MW) of the primary circuit

Point	PA	PB	PD	PF	PG	PH	PJ	PL
Number of cells per cooling tower	6	2	6	2	6	8	6	3
Cooling capacity per cell	10.0	10.0	10.0	10.0	10.0	15.0	10.0	11.0
Total cooling capacity	60.0	20.0	60.0	20.0	60.0	120.0	60.0	33.0

Primary cooling circuits The cooling towers will remove most of the heat generated by the accelerator equipment, the detectors and the technical areas. There will be a set of field erected, open wet cooling towers per surface site.

The evaporative cooling towers are of the mechanical-induced draft counter-flow type. Ventilation fans are positioned at the top of the cells, ensuring easy access for maintenance. Each tower consists of multiple cells with identical cooling capacity, with one cell per tower reserved for backup purposes (N + 1 redundancy). The towers are designed to operate with water treated with anti-corrosion and biocide chemicals. The cooling towers comply with the following parameters and conditions:

- Outside air wet bulb temperature: 21 °C.
- Cooling tower inlet temperature: 40 °C.
- Cooling tower outlet maximum temperature: 25 °C.

The cooling power to be installed at each point has been determined based on the users' cooling requirements. Certain equipment, particularly cryogenic systems, will be cooled directly by the primary circuit, while other equipment will be connected to the primary systems via heat exchangers (secondary circuits). In most cases, the secondary circuits will operate in a closed loop using demineralised water.

Table 8.3 gives an overview of the cooling requirements by type of equipment: each row represents a different type of equipment, except for the 'Underground' row, which groups all equipment cooled from the same primary circuit and is located underground. In addition, Table 8.4 provides the cooling tower complex capacity per point, including the backup cells. Figure 8.48 shows the cooling tower complexes per point, including the backup cells.

The cooling towers operate continuously in open air with the ambient conditions present in Geneva and its surrounding area, with only a short stoppage each year to carry out maintenance. The baseline strategy implemented

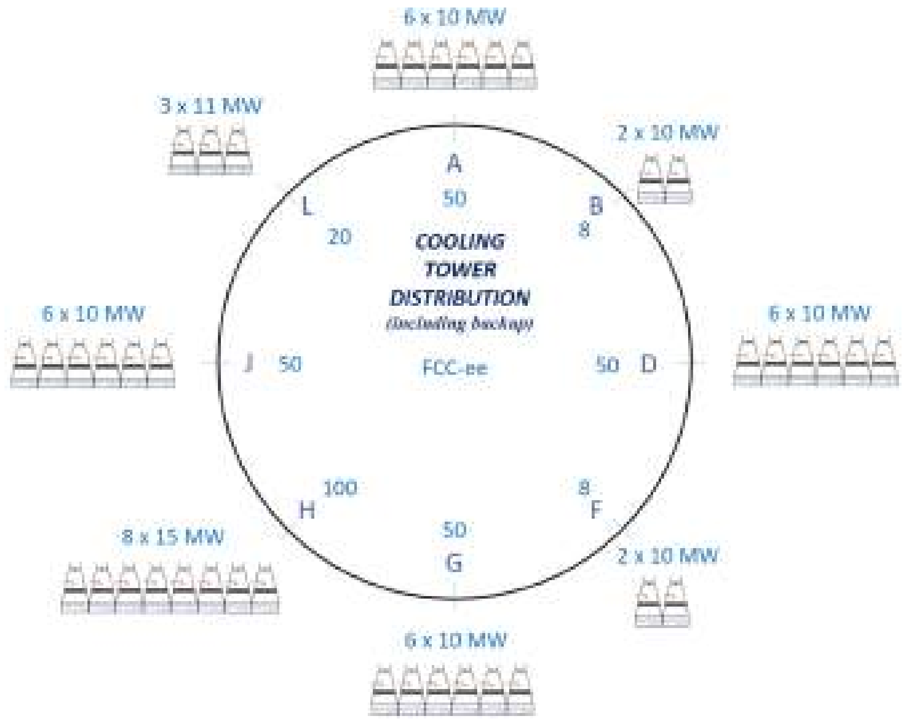

Fig. 8.48 Cooling tower complex for FCC-ee, including the backup cells

to reduce water consumption in the cooling tower is the recycling of its blowdown water. To do so, its conductivity is first reduced to values of around 20 µS/cm. The resulting water is then mixed with normal raw water, which is eventually used as a low-conductivity make-up water for the cooling towers.

An alternative to the baseline design is the adoption of hybrid cooling tower technology, which combines the advantages of both wet and dry cooling methods to enhance performance and reduce the environmental impact. In this system, the wet cooling tower - similar to the baseline design - uses water to absorb heat from the process, releasing it through evaporation. Dry air-water heat exchangers supplement this. The airflows from the wet and dry sections are mixed before reaching the fan stack, helping to reduce or eliminate the visible water vapour plume typically observed in wet cooling towers, particularly under certain weather conditions. However, hybrid cooling towers require a larger surface area and entail higher costs.

Demineralised water cooling circuits The secondary circuits are connected to the primary system through heat exchangers. In most cases, the secondary circuits use demineralised water in a closed loop. Demineralised water cooling circuits are grouped according to the typology of the equipment to be cooled and to the equipment pressure ratings. Since the underground areas are up to 400 m below ground level (case of point PF), it is necessary to install an underground cooling station in the service cavern at all points. Here, heat exchangers separate the circuit coming from the surface (with a static pressure of up to 40 bar) from the underground distribution circuit. For operability and maintenance purposes, both surface and underground cooling stations are accessible during accelerator running. Figure 8.49 shows the demineralised water distribution in the FCC tunnel, the water being supplied at the experiment points. The types of underground equipment cooled by demineralised water are listed in Table 8.5. The magnets, alcoves and SR absorbers rows correspond to equipment located in the tunnel. The other four columns refer to equipment located close to the access points.

The heat loads from the accelerator's radio frequency system come directly from the RF equipment. Furthermore, the cryogenic installation, which cools part of the equipment to cryogenic temperatures, is cooled by primary water, not demineralised water. The first fill of the demineralised water circuits can be done by a CERN-owned on-truck demineralised water production station and leave the topping up of the circuits to smaller local demineralisers at each point. Alternatives include renting an on-truck production station or designing the local demineralisers to carry out the first fill too. In this case, the production station would be underutilised, operating at reduced capacity most of the time.

Chilled water cooling circuits Chilled water at 6 °C is needed for air dehumidification and cooling purposes and for the cooling of electrical equipment with specific temperature requirements.

The water is cooled by industrial air-cooled or water-cooled chillers. The maximum heat load to be removed by chilled water per point is given in Table 8.6, together with the flow needed for a temperature difference of 6 K

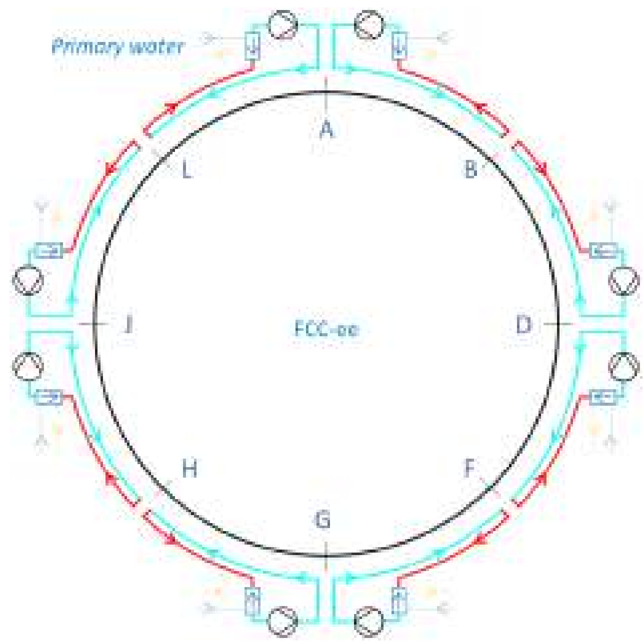

Fig. 8.49 Demineralised water distribution in the FCC tunnel

Table 8.5 Demineralised water cooling demands (MW) per underground user

Point / Sector	PA / PL-PA PA-PB	PB	PD / PB-PD PD-PF	PF	PG / PH-PJ PJ-PL	PH	PJ / PH-PJ PJ-PL	PL
Magnets	2×7.1		2×7.1		2×7.1		2×7.1	
Alcoves	2×0.9		2×0.9		2×0.9		2×0.9	
SR Absorbers	2×12.5		2×12.5		2×12.5		2×12.5	
Experiment Area	0.5		0.5		0.5		0.5	
Power Converters	1.0	1.0	1.0	1.0	1.0	1.0	1.0	1.0
RF						45.7		0.7
Cryogenics*	0.01*		0.01*		0.01*	2.2*	0.01*	1.0*
Total power	42.5	1.0	42.5	1.0	42.5	48.9	42.5	2.7

* Cryogenic equipment uses primary water quality in its secondary circuit.

Table 8.6 Chilled water cooling demands (kW) and supply water flow rate (m^3/h) per point

Point	PA	PB	PD	PF	PG	PH	PJ	PL
Cooling power	4895	4322	4875	4322	4895	9367	4875	4757
Flow rate	703	620	700	620	703	1345	700	683

between the supply and return chilled water temperature. The number of chillers and power per chiller is shown in Table 8.7: all of them have similar cooling demands except for point PH, which has a higher demand due to hosting the most power-intensive RF section.

The distribution of chilled water in the tunnel is designed as shown in Fig. 8.50. The selection of refrigerant for the chillers will be guided by both technological compatibility and environmental sustainability, with careful consideration of ongoing research developments. This decision will be made at a later stage, ensuring it reflects the latest advances and best practices. Additionally, the potential integration of mixed water production at 12 °C, which is not currently planned, will be assessed based on user requirements and implemented if deemed necessary to optimise efficiency and performance.

Table 8.7 Chilled water cooling capacity (kW) per point

Point	PA	PB	PD	PF	PG	PH	PJ	PL
Number of chillers	6	6	6	6	6	7	6	6
Cooling power of chiller	1000	900	1000	900	1000	1800	1000	1000
Total cooling power	6000	5400	6000	5400	6000	12,600	6000	6000

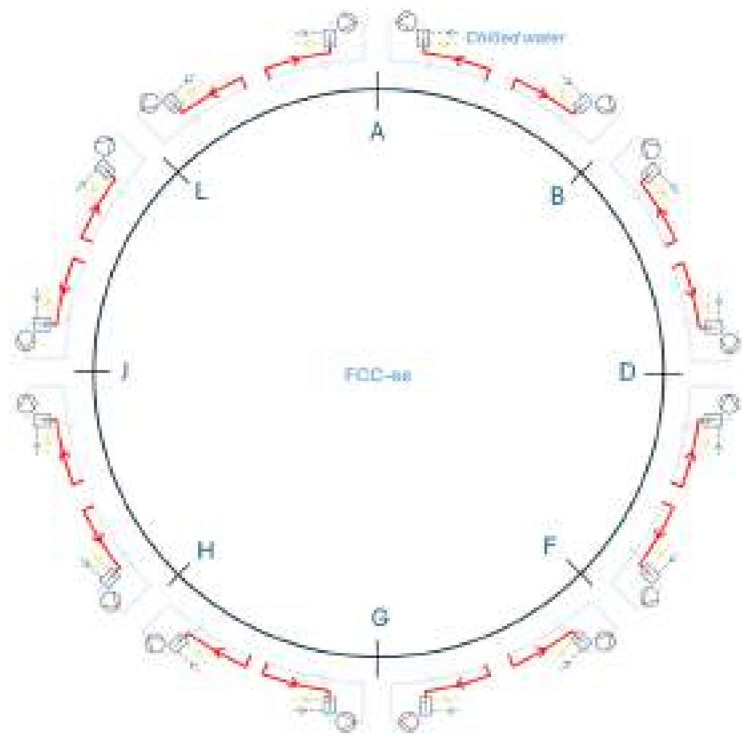

Fig. 8.50 Chilled water distribution in the FCC tunnel

8.3.2 Ventilation systems

Design principles and heat loads The FCC ventilation systems supply a sufficient amount of fresh air to meet the air quality and thermal requirements: the ambient temperature is suitable for the accelerator and auxiliary technical equipment. In addition, the air supplied is dehumidified to prevent condensation on equipment and structures.

In the current design, the underground areas are generally ventilated by air-handling units located on the surface, accessible at all times. Redundant units (N + 1) are planned everywhere to avoid affecting accelerator operation in case of breakdown. Additionally, fan coils provide local cooling wherever necessary. Tables 8.8, 8.9 and 8.10 present the air heat loads in all surface sites, in the underground areas and for each sector of the tunnel, respectively.

Tunnel ventilation For the FCC tunnel, a semi-transverse ventilation scheme has been adopted. The air is supplied through a specific duct running throughout the sector and extracted either through the tunnel itself or by an emergency extraction duct. Air is supplied to each sector from both endpoints to ensure air supply even in case of a duct failure; the same configuration has been adopted for the extraction (Fig. 8.51).

The air supply duct runs in the concrete floor slab and supplies air to the tunnel about every 100 m via diffusers at floor level. A closed circular segment in the upper part of the tunnel is used for emergency extraction. The structure consists of 70 mm thick steel panels, secured to the tunnel lining using post-drilled anchors, and is equipped with passive fire protection on both sides. Inlet diffusers and extraction grills are strategically offset to ensure optimal air distribution within the tunnel and to prevent direct airflow shortcuts between supply and extraction points.

Fire-resistant dampers are installed at every connection between diffusers and extraction grills, enhancing ventilation control in the event of a fire or helium release. These dampers help manage airflow within the affected tunnel compartment, improving safety and containment.

Table 8.8 Heat loads on air (kW) on the surface, per point

Point	PA	PB	PD	PF	PG	PH	PJ	PL
Cryogenics*	13		13		13	1400*	13	402*
Experiment Areas	50		40		50		40	
General Services	500	500	500	500	500	500	500	500
Power Converters*						2250*		35*
Shaft pressurisation	300	150	300	150	300	150	300	150
Fresh air for Underground	150	50	150	50	150	150	150	150
Total heat load to Chilled water	1013	700	1003	700	1013	800	1003	800

* Cryogenics and power converters heat loads that are extracted without chilled water.

Table 8.9 Heat loads on air (kW) underground, per point

Point	PA	PB	PD	PF	PG	PH	PJ	PL
Cryogenics	10		10		10	145	10	60
RF						4600		75
Experiment Areas	50		40		50		40	
Power Converters	220	220	220	220	220	220	220	220
CV Zone Underground	200		200		200	200	200	200
Total heat load to Chilled water	480	220	470	220	480	5165	470	555

Table 8.10 Heat loads on air (kW) for each arc of the tunnel

Magnets	Cables*	Synchrotron radiation absorbers	Alcoves	Total heat load to Chilled water
352	2500*	250	300	3402

* Heat load from the cables extracted without chilled water.

To further control the spread of smoke and helium gas, each tunnel sector is divided into 28 compartments, separated by fixed fireproof panels and automatic doors. This design prevents smoke propagation in case of fire and mitigates the spread of helium gas in the event of an accidental leak from accelerator equipment.

Under normal conditions, there are four different working modes for tunnel ventilation.

- *Run mode*: the accelerator is in operation, and most of the electrical systems are powered; a high heat load is transferred to the air in this mode. Additionally, radiation protection aspects are taken into consideration.
- *Access mode*: technical personnel can work in the tunnel, and therefore, occupational safety requirements are considered.
- *Economy mode*: a minimum airflow is employed in situations without personnel access, reducing the airflow. In this mode, the dew point of the air is controlled, but wider ranges of dry temperature are accepted to save energy.
- *Flushing mode*: used to renew the air underground completely and takes place when moving from Run to Access modes. The extracted volumes are filtered before release.

The airflow requirements under normal and emergency conditions are presented in Table 8.11. When the accelerator is in operation with full heat loads, the maximum dry temperature is limited to 32 °C and the maximum dew point is limited to 12 °C, inside the tunnel. In this mode, the nominal supply temperature is of 17 °C. In flushing mode, the minimum supply temperature is 15 °C. If the external temperature is below 0 °C, the airflow will be reduced to maintain the 15 °C supply temperature. For the access mode, the temperature inside the tunnel is set between a minimum of 18 °C and a maximum of 26 °C, while respecting the regulations regarding air renewal. In all operating modes, environmental sustainability and energy efficiency are key priorities. As a general

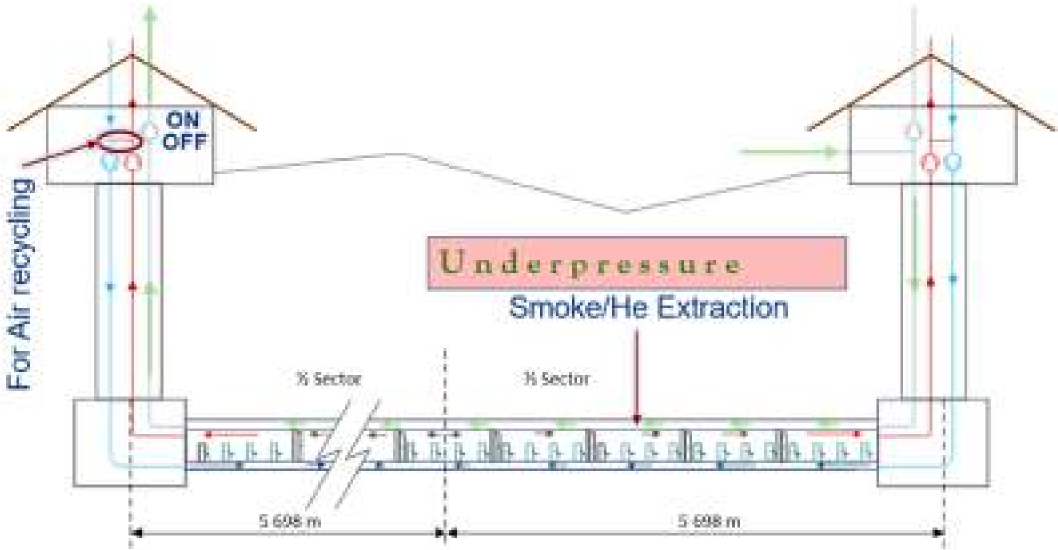

Fig. 8.51 Operation of the ventilation elements in one sector of the tunnel during normal operation. Smoke and helium extraction in green, general extraction in red and air supply in blue

Table 8.11 Airflow conditions for the tunnel ventilation

	Air supply	Regular extraction	Emergency extraction
Run and Access mode	2×27,000 m^3/h per sector.	2×27,000 m^3/h per sector.	Standby under pressure operation, no extraction.
Flushing mode	100,000 m^3/h per sector.	100,000 m^3/h per sector.	Standby under pressure operation, no extraction.
Emergency conditions	10,000 m^3/h in affected compartments (max. 2). 3500 m^3/h in adjacent compartments (max. 2). 2160 m^3/h in the rest of the compartments.	Max. 54,000 m^3/h Sharing between the two shafts depends on affected compartment location.	10,000 m^3/h in affected compartments (max. 2). 3500 m^3/h in adjacent compartments (max. 2).

principle, the ventilation system is designed to minimise electrical consumption by incorporating free cooling and air recycling strategies.

In run and access modes, airflow is supplied through an inlet duct integrated into the tunnel floor slab. In flushing mode, however, air is not delivered via this duct but is distributed longitudinally across the entire tunnel cross-section.

An alternative approach to tunnel ventilation would be to extend the longitudinal airflow concept of flushing mode to both run and access modes, resulting in a fully longitudinal ventilation scheme. This solution would simplify system controls, enhance robustness, and free up space required for the integration of the inlet duct. However, before implementation, the system's performance under degraded conditions and emergency scenarios must be carefully assessed to ensure full compliance with safety standards.

Experiment areas ventilation The ventilation system for the experiment areas (experiment caverns at points PA, PD, PG, and PJ) consists of a ventilation system on the surface with a supply and extraction unit and the possibility of recycling 100% of the air or the option to supply a controlled percentage of fresh air. The ventilation principle for the experiment caverns is represented in Fig. 8.52. No additional local cooling systems are planned.

The nominal airflow conditions are presented in Table 8.12. During operation, the experiment areas will have a temperature distribution of 18/32 °C from floor to ceiling. The same parameters as for the FCC tunnel are applicable in flushing and access modes.

RF areas ventilation The RF system is cooled mainly by the demineralised water circuits in the underground klystron galleries of points PH and PL. A considerable heat load nevertheless remains to be extracted: 4600 kW in point PH and 75 kW in point PL.

Table 8.12 Airflow conditions for the experiment areas ventilation

	Air supply	Regular extraction	Gas extraction
Run and Access mode	50,000 m^3/h to 70,000 m^3/h	50,000 m^3/h to 70,000 m^3/h	Switched off
Flushing mode	50,000 m^3/h to 70,000 m^3/h	50,000 m^3/h to 70,000 m^3/h	Switched off
Fire emergency (gas extraction)	Up to 70,000 m^3/h	Up to 70,000 m^3/h	Switched off
Gas emergency (gas extraction)	20,000 m^3/h	Switched off	20,000 m^3/h

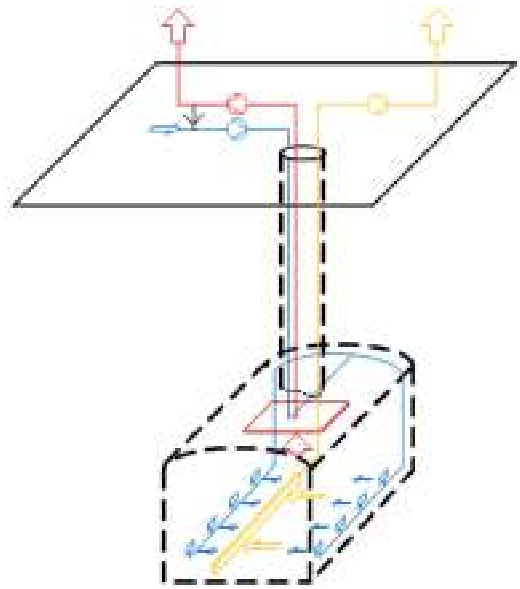

Fig. 8.52 Ventilation systems of the experiment cavern. Smoke and helium extraction in orange, general extraction in red and air supply in blue

Table 8.13 Airflow conditions for the RF areas ventilation

	Air supply	Regular extraction	Emergency extraction
Run and Access mode	30,000 m^3/h	30,000 m^3/h	Switched off
Emergency conditions	<30,000 m^3/h	<30,000 m^3/h	10,000 m^3/h in affected compartments (max. 2). 3500 m^3/h in adjacent compartments (max. 2).

The ventilation design features main ventilation from the surface, supplemented by a fresh air supply, and local cooling with fan coils cooled by chilled water. Table 8.13 presents the airflow requirements for each of the modes; flushing is not needed because contaminants are not present in the klystron gallery equipment.

Technical areas ventilation Dedicated ventilation systems serve the technical zones around each point and the connecting galleries between areas. These areas comprise the service caverns and connecting galleries at all points.

The design of each ventilation system differs because the general demands and heat loads vary significantly between the points. A difference is made between the technical areas in experiment points (points PA, PD, PG, PJ), the technical areas in technical points (points PB and PF), and the technical areas in RF points (points PH and PL). The ventilation solutions proposed under normal and emergency conditions are presented in Table 8.14. Finally, other ventilation systems pressurise airlocks to create pressure cascades for safety purposes.

Surface buildings ventilation Each surface building will be ventilated by a dedicated air-handling unit. Where the building size requires it, it is planned to have several units in the same building, each of them taking care of a part of the building. At present, it is not considered necessary to have redundant units in these buildings. Should this be needed, it can easily be implemented. All surface buildings will be equipped with a mechanical system on the roof to extract smoke, designed and certified for operation at 400 °C for a minimum period of 2 h.

Table 8.14 Airflow conditions for ventilation of the technical areas

	Air supply	Extraction	Emergency extraction
Technical Areas in Experiment points	Fresh air for UAs, 20,000 m^3/h. Ventilation for Service Cavern, 40,000 m^3/h.	Extraction through the Service Cavern, 60,000 m^3/h.	Emergency extraction through the Ventilation system for Service Cavern, 60,000 m^3/h.
Technical Areas in Technical points	Ventilation for Service Cavern, 40,000 m^3/h.	Extraction through the Service Cavern, 40,000 m^3/h.	Emergency extraction through the Ventilation system for Service Cavern, 40,000 m^3/h.
Technical Areas in RF points	Ventilation for Service Cavern, 40,000 m^3/h.	Extraction through the Service Cavern, 40,000 m^3/h.	Emergency extraction through the Ventilation system for Service Cavern, 40,000 m^3/h.

8.3.3 Other systems

Drinking water Drinking water will be used by personnel. It is planned that this will be provided by the local water network at each point.

Reject water and sumps Discharging effluent water into local disposal networks or small water bodies presents challenges due to its high salinity levels. To address this, a centralised treatment system is proposed, in which all effluent water is transported through the tunnel to a treatment plant at point PA.

An alternative approach would involve local treatment of effluent water at each point. Implementing minimum or zero liquid discharge (ZLD) technologies could significantly reduce the volume of effluent by concentrating the salts into solid pellets. However, this solution would introduce higher costs and increased surface area requirements due to the complexity of these treatment systems.

Compressed air The compressed air for all equipment and actuators will be provided by compressed air stations located on the surface at each point. These will supply both surface and underground areas. A level of redundancy of N + 1 is planned to ensure the reliability and maintainability of the plant.

Sumps and clear water Two separate pump systems to lift clear water and sewage will be installed underground at each point. They will be connected to the point's local drainage network. All underground equipment (tunnel and caverns) must have redundancy in order to avoid affecting operation in case of a breakdown. The sump pumping capacities for the tunnel at the points are 30 m^3/h, and the experiment caverns have an additional 30 m^3/h of sump pumping capacity. Alarms for 'high level' and 'level too high' will be implemented in all basins.

The key parameters of the clear water, including temperature and pH, will be systematically monitored prior to discharge. If the clear water fails to meet the required quality standards or poses a risk of environmental contamination, appropriate mitigation measures will be implemented. These measures may include the activation of retention basins at designated discharge points to ensure compliance with environmental regulations.

8.4 Power consumption and electricity distribution

8.4.1 Energy consumption of the FCC-ee machine

Overall power demand Since FCC-ee is a large-scale accelerator, accurately identifying and understanding its electrical loads is essential for designing a robust electricity infrastructure and assessing overall energy consumption. The accelerator's main electrical loads include the radiofrequency (RF) systems, magnets, cryogenic systems, cooling and ventilation, experiments, and general services, which cover all general-purpose energy needs. The total power demand varies depending on the operation mode of the machine (Z, WW, H, and $t\bar{t}$).

The collider radiofrequency system represents the largest electrical load, requiring 146 MW across all operation modes. It consistently supplies 50 MW per beam to compensate for synchrotron radiation losses. The global efficiency of the RF chain is 68%, with the goal of having klystron amplifiers operating at 80% efficiency. The power demand for the magnets and their powering chains depends on the beam energy, starting from 6 MW in Z mode, increasing to 39 MW in H mode, and reaching 89 MW in $t\bar{t}$ mode.

The cryogenic power demand remains relatively low at 13 MW up to H mode but becomes significant at 35 MW in $t\bar{t}$ mode. The cooling and ventilation systems require between 25 MW and 33 MW, while the power demand of the experiments and data centres is estimated to be 10 MW for all four experiments, with an additional 4 MW

Table 8.15 Power demand by technical system, in MW

Beam energy, GeV	Z	W	H	$t\bar{t}$
	45.6	80	120	182.5
Collider radiofrequency	146	146	146	146
Booster radiofrequency	2	2	2	2
Collider cryogenics	1.2	11.5	11.5	27.6
Booster cryogenics	0.35	0.8	1.5	7.4
Cooling and ventilation	25	26	28	33
Collider magnets	6	17	39	89
Booster magnets	1	3	5	11
4 experiments, PA, PD, PG, PJ	10	10	10	10
4 datacentres, PA, PD, PG, PJ	4	4	4	4
General services	26	26	26	26
Total power during beam operation	222	247	273	357

Table 8.16 Power demand by operation mode, in MW

Beam energy mode	Z	W	H	$t\bar{t}$
Shutdown	30	33	34	41
Technical stop	67	78	81	108
Short downtime	74	98	125	209
Commissioning	144	163	177	233
Machine Development	96	121	147	231
Beam operation	222	247	273	357

allocated for local data centres, given that detailed technical designs are not yet available. Finally, general services are expected to require up to 26 MW, based on scaling from LHC consumption.

These estimates will form the basis for the development of the FCC-ee's electrical infrastructure, ensuring it can accommodate the varying power demands while optimising efficiency and sustainability. Table 8.15 shows the estimate of the maximum power demand for the four different modes of operation.

Operational model The energy consumption is estimated based on the accelerator operational model. The power demand depends on the time of year and the machine's state. The machine schedule defines the different periods during the year, and the power demand varies from the minimum during the shutdown to the maximum during beam operation.

The schedule consists of six distinct periods: shutdown, commissioning, physics operation, short downtime (without access to the machine), technical stops (or long downtime), and machine developments. The power demand calculated for each period is shown in Table 8.16.

The machine schedule comprises 120 days of shutdown, 30 days of commissioning, 20 days of machine development, 10 days of technical stops and 185 days for physics, see Table 8.17.

The machine availability is expected to be at least 80%. Unlike other accelerators, FCC-ee does not lose time for acceleration, meaning that its operational efficiency is determined solely by technical downtime and the associated time required for beam refilling and recovery. Based on empirical data from similar machines, the effective efficiency factor is estimated to be approximately equal to the hardware availability (80%), with an additional 5% reduction to account for beam recovery after a failure.

Of the 185 days allocated for physics operation, an estimated 46 days are lost due to downtime, leaving 139 days for colliding beams.

The downtime is categorised into three types: long stops due to major failures, such as the loss of cryogenic conditions or RF cavity conditioning; downtime with machine access, allowing repairs and maintenance; and downtime between cycles, which includes beam dumps and refilling that do not require machine access.

Table 8.17 Distribution of operating modes in time

Period type	Duration
Shutdown	120 days
Commissioning	30 days
Physics Operation	185 days
Beam colliding	139 days
Downtime	46 days
Machine development	20 days
Technical Stops	10 days

Table 8.18 Power demand by point, $t\bar{t}$ mode

Point	Type	Max power [MW]
Point PA	Experiment	23
Point PB		20
Point PD	Experiment	23
Point PF		20
Point PG	Experiment	23
Point PH	Collider RF	194
Point PJ	Experiment	23
Point PL	Booster RF	30

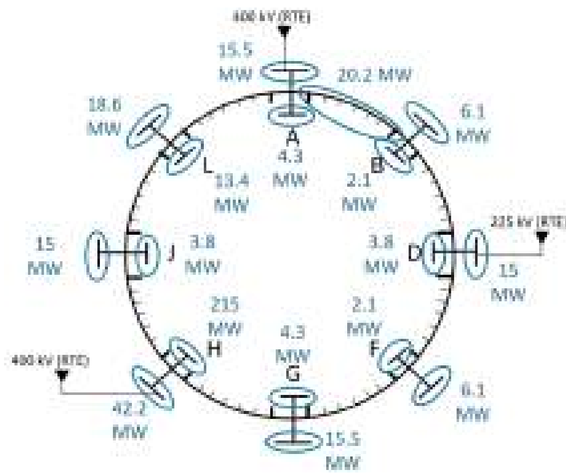

Fig. 8.53 Load mapping of the FCC-ee machine

Power demand by points As the distribution of the power demand is not uniform across the points (see Table 8.18), the installed power and its position need to be known to be able to design the electrical infrastructure. The load survey performed in the first phase of the study provided the following localised power requirements:

- Surface at each point: between 6.1 and 42.2 MW,
- Underground at each point: between 2.1 and 215 MW,
- Tunnel between points: around 20.2 MW.

This first analysis allowed the creation of a load mapping of the FCC-ee machine for the design of its electrical network, see Fig. 8.53.

Energy consumption With the schedule and the expected power demand for the various periods, the annual energy consumption can be calculated, see Tables 8.19 and 8.20 for Z and $t\bar{t}$ operation respectively. The energy consumption varies from 1.07 TWh/year for Z mode operation to 1.77 TWh/year for $t\bar{t}$ mode operation. For comparison, the complete CERN complex energy consumption in 2024 was 1.3 TWh/year. This yearly consumption is expected to increase after the completion of the HL-LHC project.

Table 8.19 Energy Consumption, Z mode

Z mode	Duration, days	Power, MW	Energy, GWh
Beam colliding	139	222	740
Downtime	46	67	75
Commissioning	30	144	103
Machine development	20	96	46
Technical Stops	10	67	16
Shutdown	120	30	86
Total Z mode operation			1070

Table 8.20 Energy consumption, $t\bar{t}$ mode

TT mode	Duration, days	Power, MW	Energy, GWh
Beam colliding	139	357	1200
Downtime	46	108	157
Commissioning	30	233	168
Machine development	20	231	111
Technical Stops	10	108	26
Shutdown	120	41	117
Total $t\bar{t}$ mode operation			1770

Grid connections To provide power to the machine which is spread over many points, the strategy is to connect three points to the high-voltage European grid and to create an internal transmission network through the tunnel to distribute it to the other points. These connections will be rated at the same level of 220 MVA at each point. These points are PH, PA, and PD (see Fig. 8.54) and will be connected to the French grid, operated by RTE. RTE confirmed that, beside a minimum additional infrastructure to connect the new FCC points, no further upgrades or power stations are required in the existing French grid.

PH needs a dedicated substation for the collider RF systems. PA can be powered through an existing CERN substation. PD is needed to cover the other parts of the machine, for redundancy with PA and for the future operation of FCC-hh.

In addition to that, all the points will be connected at much lower power to the local distribution grids: SIG (Services Industriels de Genève) for the point in Switzerland (PB), and ENEDIS for points located in France, except for point PG which will be connected to Energie et Services de Seyssel. These connections are needed for the civil engineering works, and later they will be used as backup sources. The voltage level of these connections will be at medium voltage (20 kV in France, 18 kV in Switzerland), and they will be in general rated at 14 MW, to cover the TBM loads in the civil engineering works phase.

8.4.2 FCC electrical grid

Transmission network The FCC can be powered from the French national grid, operated by RTE (France's Transmission System Operator, Réseau de Transport d'Électricité), through three access points (PA, PD, and PH) at two possible voltage levels (400 kV or 225 kV). Power will be distributed to the other access points via an internal high-voltage (HV) transmission network, which will be implemented using HV cables installed within the accelerator tunnel. These cables will link all access points, ensuring power transmission from one point to the adjacent ones.

Following verification with RTE, it has been confirmed that operating two or three high-voltage supplies of the FCC in parallel will not be permitted by the grid operator, as this would introduce the risk of uncontrolled or unwanted power transfers between connection points.

As a result, the option of operating the HV grid of the FCC as a closed loop, initially considered feasible, has been discarded at this stage of the study. Instead, the three high-voltage supplies will be operated in an antenna configuration, with each connection radially supplying other points in the accelerator. In the normal configuration, three distinct sectors have been defined, each powered by a single RTE connection: PA will supply PB, PJ, and PL; PD will supply PF and PG; while PH will operate standalone, as the RF systems at this location represent the largest power load of the machine.

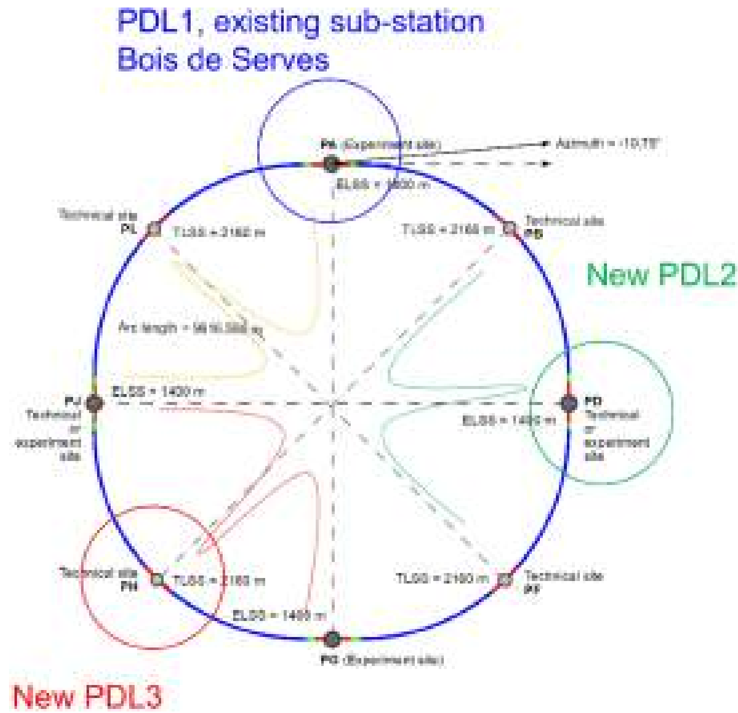

Fig. 8.54 High Voltage grid connections, PDL as delivery points

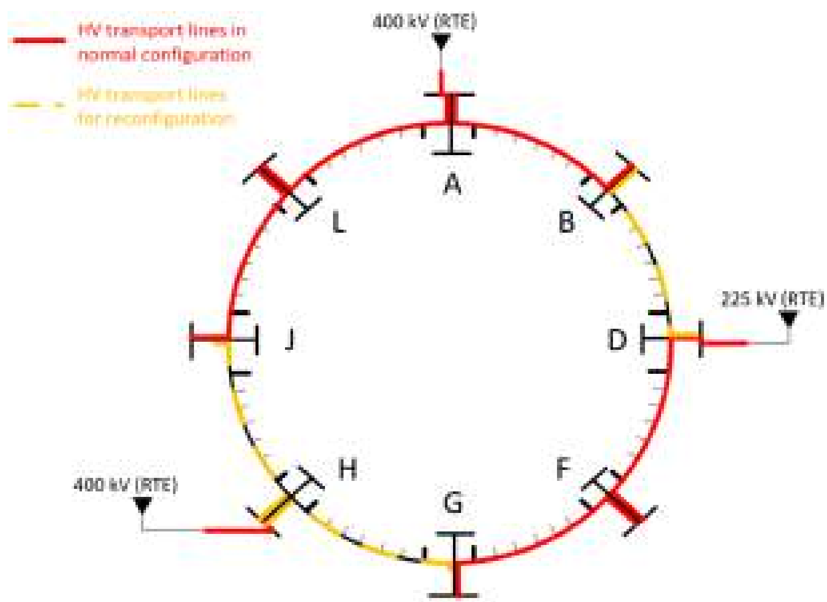

Fig. 8.55 General single line diagram of the transmission network of FCC

Even if the HV cables between PB and PD, between PG and PH, and between PH and PG will not be loaded during normal operation, they can be used as a backup supply in case part of the HV network is unavailable. The possible continuity of service based on the [N-1] principle has been analysed by simulating different failures in the network and reconfigurations to overcome these failures have been determined. The only scenario in which the machine will cease operation without the possibility of network reconfiguration is the loss of supply from PH, as the RF loads at this location are too high to be compensated by other power sources. Apart from this case, the network is designed to allow reconfiguration, ensuring that the accelerator can continue normal operation in the event of a failure of one HV source or one HV branch. The list of possible HV network failures that the system can withstand, along with the corresponding reconfiguration strategies, is summarised in Table 8.21.

This analysis also provides the minimum criteria for dimensioning the sources and lines of the HV network, in addition to the load requirements. Finally, to also cope with the objective of keeping the same HV grid for the

Table 8.21 Transmission network configuration modes to overcome failures

	PA - PB	PB - PD	PD - PF	PF - PG	PG - PH	PH - PJ	PJ - PL	PL - PA
Normal configuration	ON	OFF	ON	ON	OFF	OFF	ON	ON
Loss of PA	ON	ON	ON	OFF	ON	ON	OFF	ON
Loss of PD	ON	ON	ON	OFF	ON	ON	OFF	ON
Loss of PA - PB	OFF	ON	ON	ON	OFF	OFF	ON	ON
Loss of PD - PF	ON	OFF	OFF	ON	ON	OFF	ON	ON
Loss of PF - PG	ON	OFF	ON	OFF	ON	OFF	ON	ON
Loss of PJ - PL	ON	OFF	ON	ON	OFF	ON	OFF	ON
Loss of PL - PA	ON	OFF	ON	ON	OFF	ON	ON	OFF

future FCC-hh, it was decided that all the HV cables will be sized equally to a nominal rating of 115 MVA, to allow the infrastructure to be compatible with the FCC-hh load.

Selection of the voltage level, the location and the technology of the HV transmission network The selection of the operating voltage of the transmission network has been based on a study aimed at optimising infrastructure and operational costs. As a result, the voltage will be stepped down from 400 or 225 kV, to a lower level, see Fig. 8.55.

For the radiofrequency (RF) systems, the voltage will be stepped down to the required level for the main RF power conversion system, which is currently planned to be 40 kV. While adopting 40 kV for the entire transmission network would offer some benefits in terms of material uniformity, an initial analysis clearly indicated that this voltage level is not optimal due to the large cable cross-sections required, leading to high space occupancy in the tunnel and significant power losses. For these reasons, 40 kV was discarded from the beginning of the study.

To determine the most suitable internal transmission voltage, the analysis considered three reference voltages, selected from standard values used by European Grid Operators: 63 kV, 90 kV, and 132 kV. The study was conducted for these three voltage levels, allowing extrapolation to evaluate performance trends across different voltage ranges. For each voltage level, two options have been considered: i) substations installed on the surface or underground (in the technical galleries of the accelerator); ii) air-insulated substations (AIS) or gas-insulated substations (GIS).

The following parameters were included in the analysis, with the aim of evaluating the impact of the different alternatives on all the main aspects of the total lifetime cost of the network:

- OPEX[10] of the HV lines: electrical losses of the lines depending on their operation over the full FCC machine (based on the operating models of the phases of FCC-ee, and on a simplified estimation of the same models for FCC-hh).
- CAPEX[11] of the HV lines: initial cost of the cables, the accessories and the installation works required.
- OPEX of the HV substations: electrical losses of the transformers depending on their operation over the full FCC machine programme and the cost of the maintenance of the substations.
- CAPEX of the HV substations: initial cost of the substations, and equivalent financial value of their space occupation.

The values of CAPEX and OPEX of each case have been assessed based on detailed studies of the substations and the lines at the different voltage levels, but also with estimated financial values of the space occupied and energy cost.

This comprehensive analysis gave the total lifetime cost for each scenario, with the variation trends illustrated in Fig. 8.56. The study concludes that selecting a 63 kV transmission voltage and using GIS substations installed on the surface are the optimal choices within the range analysed. Additionally, manufacturers are demonstrating a clear trend toward reducing the greenhouse gases used in GIS mixtures, significantly improving the environmental sustainability of this technology. The final technical solution was developed based on these findings.

This analysis will be kept running in the future phases of the FCC study, as some parameters have a significant impact and can change the conclusions.

Main high voltage substations The design of the HV substations has been developed according to the results of the analysis shown on Fig. 8.56.

[10] Operational expenditure.

[11] Capital expenditure.

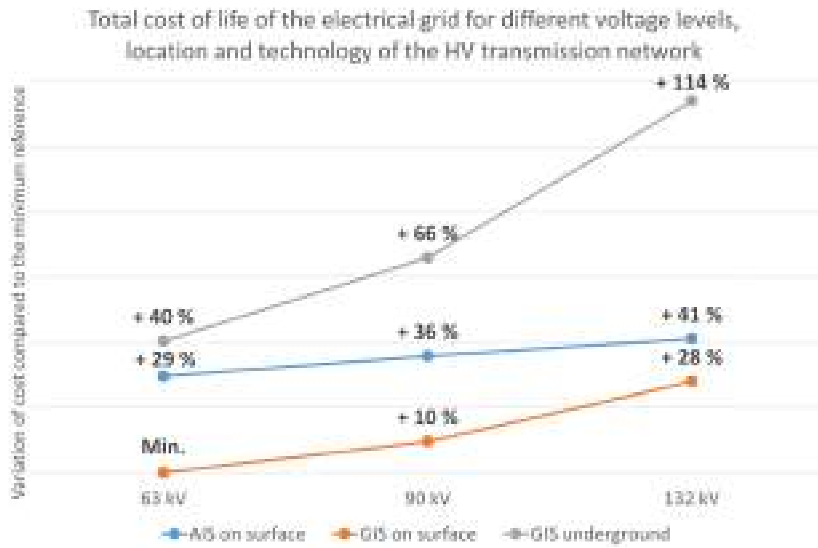

Fig. 8.56 Trend of the variation of the total lifetime cost of the electrical grid for different voltage levels, locations and technologies of the HV transmission network

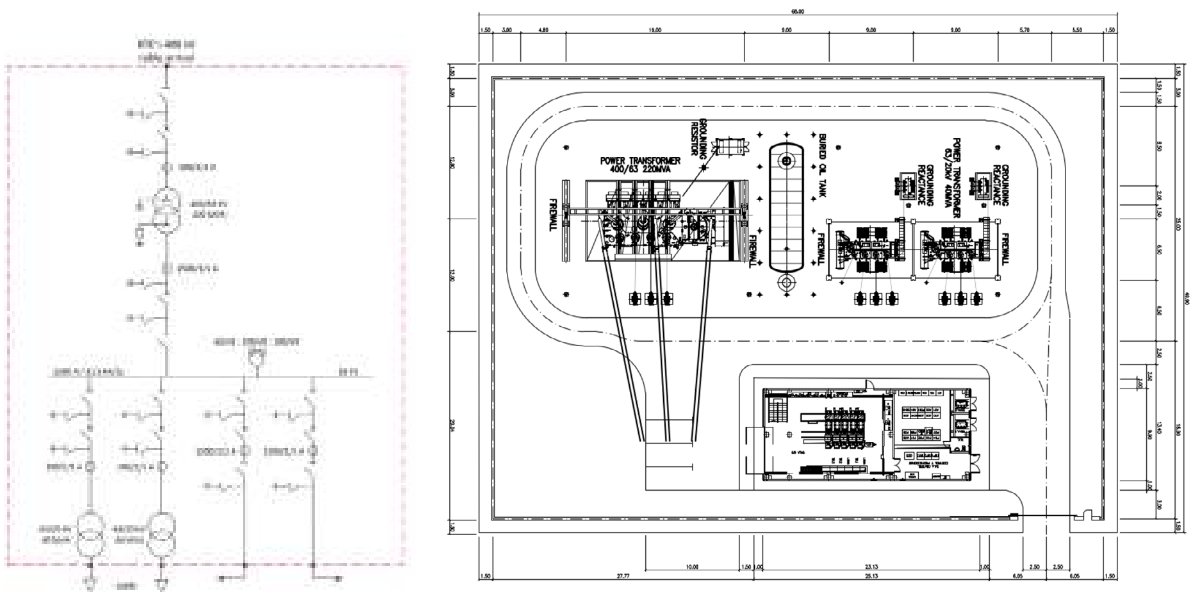

(a) Single line diagram. (b) Layout.

Fig. 8.57 Typical 400/63 kV substation

A 400/63 or 225/63 kV GIS substation (Fig. 8.57) will be installed with a main stepdown transformer of 220 MVA in the three points connected to the European grid. The main switchgears and auxiliary systems will be housed inside a dedicated building, while the transformer will be installed nearby, protected by firewalls and equipped with all necessary safety systems to manage potential oil spills. These include a containment pit, oil separator, retention basin, and fire protection measures, ensuring safe operation and environmental compliance. It is worth noting that in PH an additional bay will be available in the 400 kV switchgear, to supply an additional 150 MVA 400/40 kV transformer that will be dedicated to the power conversion system for the FCC-ee RF system.

A 63 kV GIS substation (Fig. 8.58) will be installed at all the other access points, as shown in the single line diagram of the transmission network in Fig. 8.58a. Also, in this case, the main switchgear will be housed with the auxiliary systems in a building. At each point, the 63 kV GIS substation will supply two 40 MVA 63/20 kV transformers that will be the sources of the distribution networks for each point.

In each access point connected to the grid, the total surface area of the HV substation will be approximately 10,000 m^2; in each of the other points, it will be approximately 4000 m^2, these requirements are already included

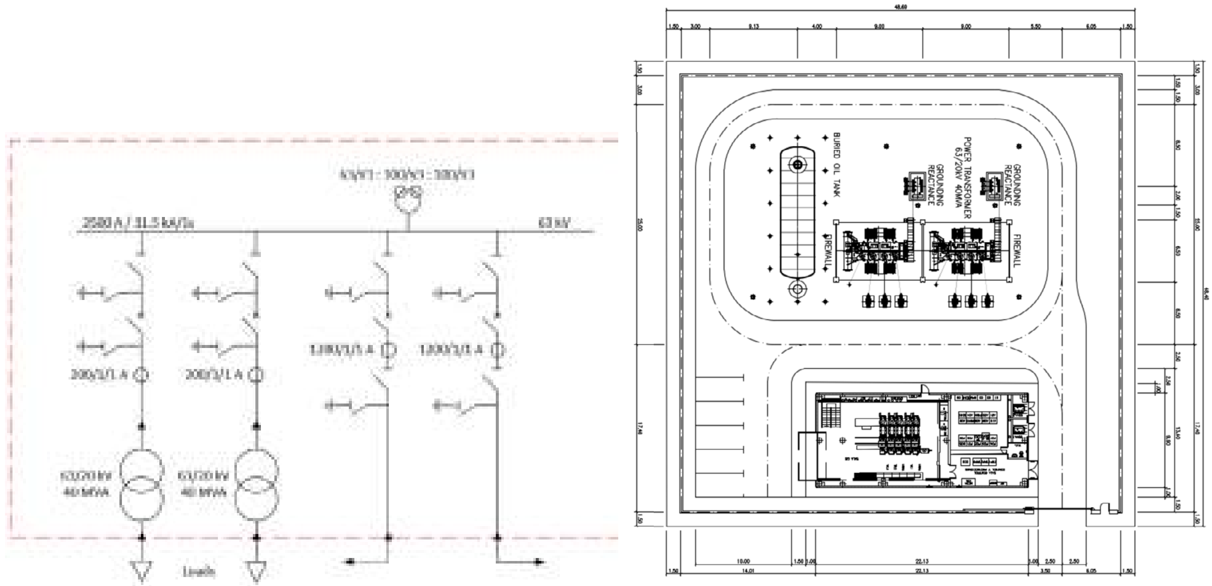

(a) Single line diagram. (b) Layout.

Fig. 8.58 Typical 63 kV substation

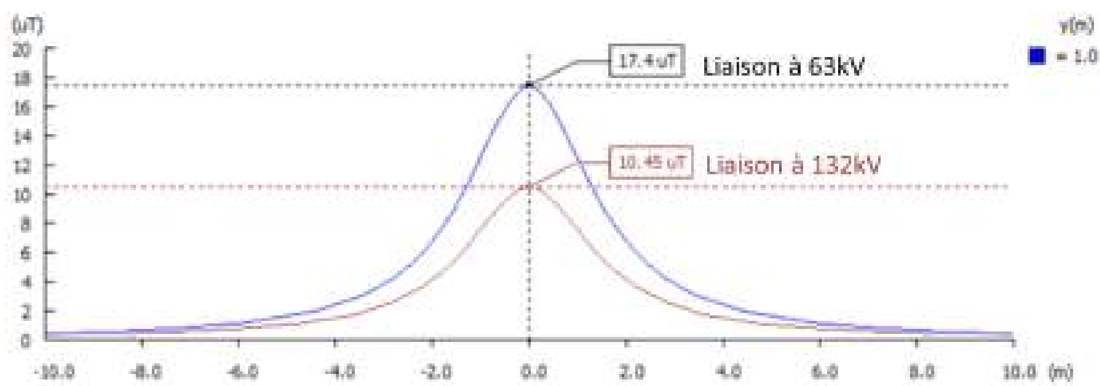

Fig. 8.59 Comparison of magnetic field simulations for cables (63 kV in blue, 132 kV in red)

in those considered by the civil engineering team for the surface occupation and the layouts of the different sites.

Installation of HV cables in the accelerator tunnel As the installation of HV transmission networks rated at tens or hundreds of MVA (Fig. 8.60) is not a standard solution adopted in the underground accelerator facilities (e.g., in LHC today only cables of up to 18 kV and rated at 15 MVA are installed for the electrical distribution), a detailed and specific feasibility analysis has been performed, in order to confirm the absence of showstoppers and to provide requirements for civil engineering.

The final report of this analysis confirms the feasibility of installing such cables in the underground areas of the accelerator. It provides models and datasheets of cables with their related losses, different installation methods with their constraints and the required space and civil engineering works to install and house the cables. It also includes a cost estimate and a tentative schedule for the installation. All the details can be found in Ref. [383], but a summary is presented in Table 8.22.

Two important points deserve to be mentioned: the cable runs in a concrete duct of 520×500 mm in the machine tunnel requiring a specific volume, as can be seen in Fig. 8.61; and the cables along a tunnel sector need junction chambers every approximately 1-1.5 km, requiring a significant space in the tunnel of approximately 1200×500×16,000(length) mm as shown in Fig. 8.62. This second point is important, as it was decided to create the junction chambers corresponding to each alcove (in the current baseline, every 1.6 km), housing them in the transport parking areas to ease their construction and future accessibility.

Fig. 8.60 Specification of the proposed 63 kV cable

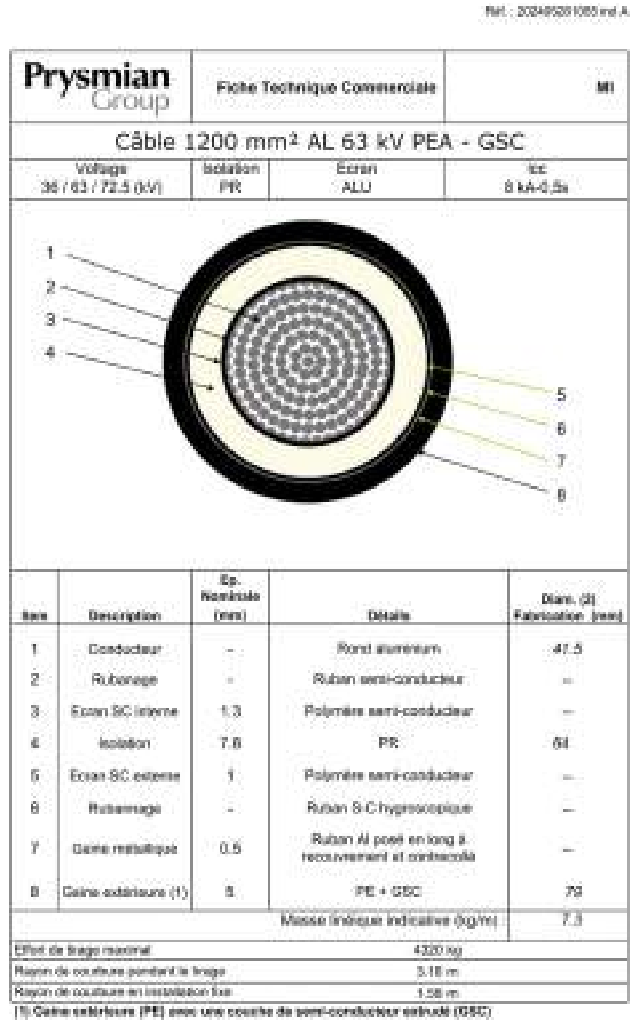

Table 8.22 Summary table of the requirements of the HV lines

	63 kV	132 kV
Proposed cable	3× 1200 mm^2, Aluminium cable	3× 630 mm^2, Aluminium cable
Proposed space occupation in the tunnel	Concrete duct of 520×500 mm.	
Proposed quantity of junction chambers	13 junction chambers (including 1 earthing junction chamber)	
Proposed space occupation of junction chambers	With earthing of screens: duct of 1500×500 mm with a length of 9.5 m.	With earthing of screens: duct of 1800×500 mm with a length of 12 m.
Preferred installation method	Within PEHD ducts with the so-called cable train pulling method.	
Cost of installation	Lower cost	+ 4% compared to 63 kV
Schedule estimation of installation (per line between two points)	160 days	170 days
Level of magnetic field in the tunnel	See magnetic field graphs on Fig. 8.59.	

Distribution networks The power is locally dispatched to the electrical loads of the surface and underground facilities by the medium and low voltage distribution networks available at each point.

The various loads can be classified based on their function and criticality, and each category has a dedicated distribution network with specific features, as shown in Table 8.23. The functional separation of the networks was one of the criteria in the study of the distribution at each point. This was to ensure users' power quality (in

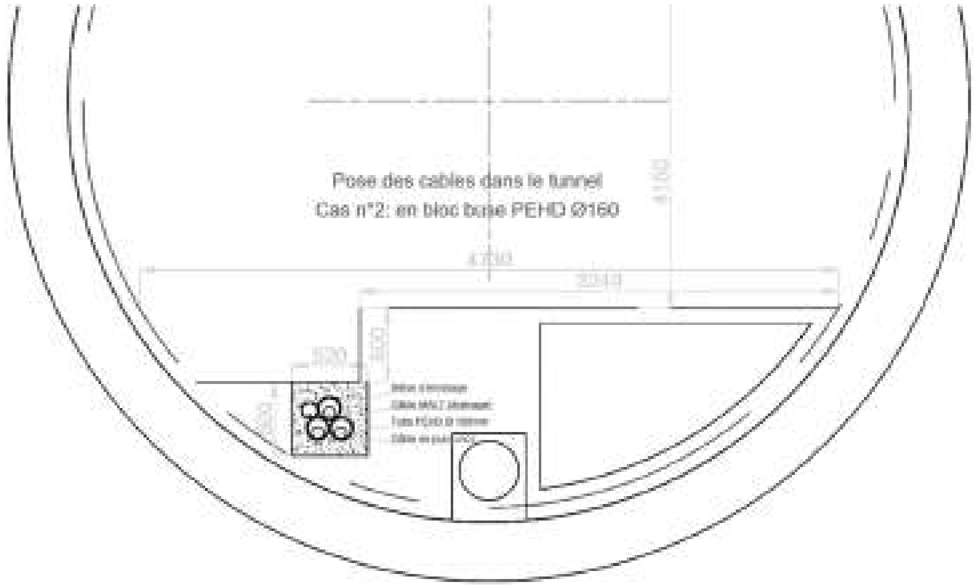

Fig. 8.61 Proposed space occupation of the cables in the machine tunnel

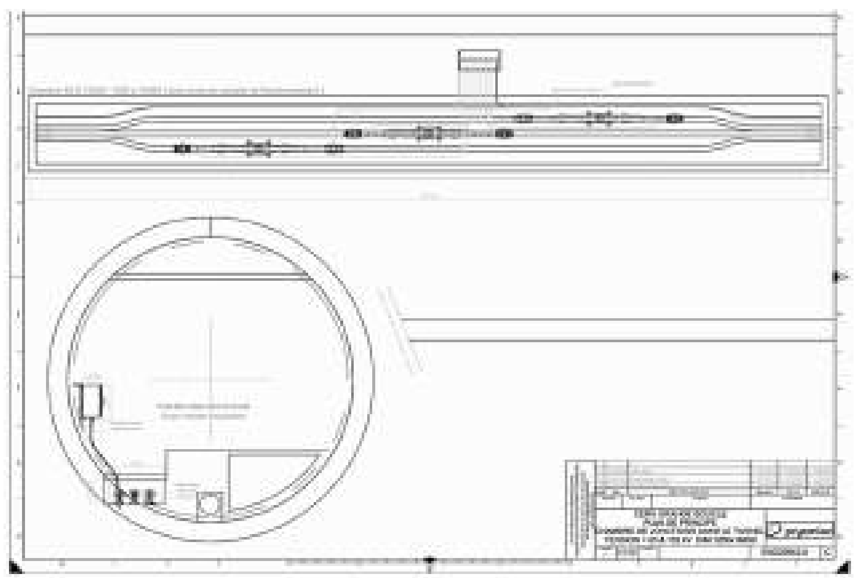

Fig. 8.62 Proposed space occupation of the junction chambers in the machine tunnel

particular, to minimise potential disturbances from power electronics) and to enhance reliability, operability, and maintainability of the grid.

The distribution network concept is the same for all points. The HV transmission network supplies two 63/20 kV transformers to create two main types of networks at 20 kV: General Services (GS) and Machine. The power is dispatched through two medium voltage substations (one in a surface building, the other in the underground service cavern) to 20/0.4 kV transformers that supply the low voltage switchboards in charge of local distribution to the terminal loads.

The GS and machine networks can be coupled at the 20 kV substations to allow a backup supply: the size of the main 20 kV transformers, busbars and links (primary and backup) has been set to allow full reconfiguration and nominal operation in case one element of the network is unavailable as a result of maintenance or failure. For these reasons, and also to cope with the load forecast of the FCC-hh, the two main transformers of each point have been sized at 40 MVA, and the main 20 kV links at 20 MVA.

An example is shown in the single line diagram of the distribution network of point PA shown in Fig. 8.63, and the layout of the 20 kV substations on the surface at the same point is shown on Fig. 8.64.

Secured and uninterruptible networks Based on the load categories of Table 8.23, there is a secured network (Fig. 8.65) with backup sources available at each point to power critical loads within a few seconds of the main

Table 8.23 Network types and characteristics

Network type	Loads type (non-exhaustive list)	Power unavailability duration in case of degraded scenario
Machine	Power converters, RF, cooling pumps, fan motors, etc.	Until return of main supply
General Services	Lighting, outlets	Until return of main or secondary supply
Secured	Personnel safety-related loads (lighting, pumps, elevators)	10-30 s
Uninterruptible	Personnel safety (evacuation and anti-panic lighting, fire-fighting system, oxygen deficiency, evacuation)	Interruptions are not allowed; continuous service is mandatory
	Machine safety (sensitive processing and monitoring, beam loss, beam monitoring, machine protection)	

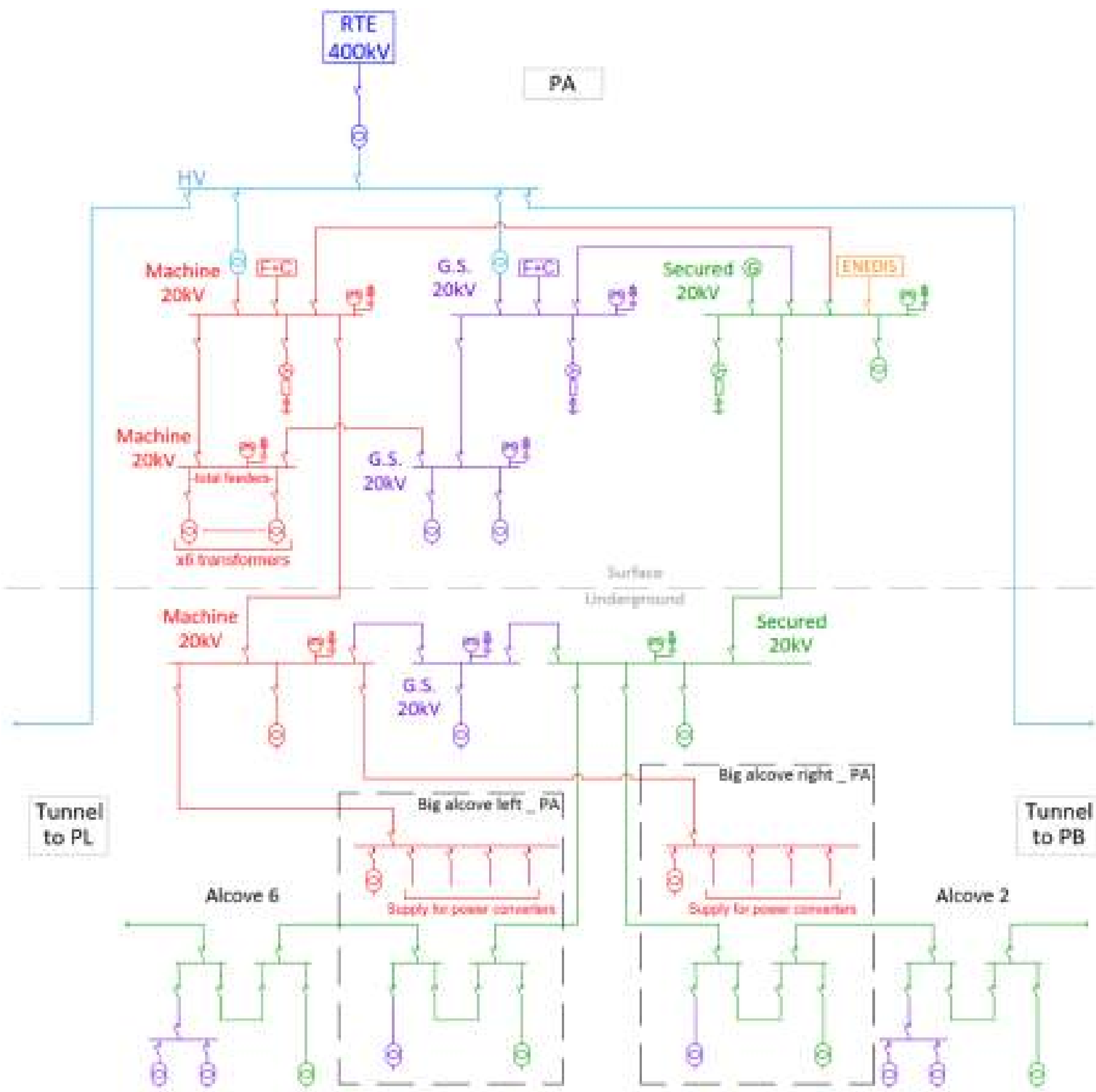

Fig. 8.63 Conceptual electrical distribution for point PA

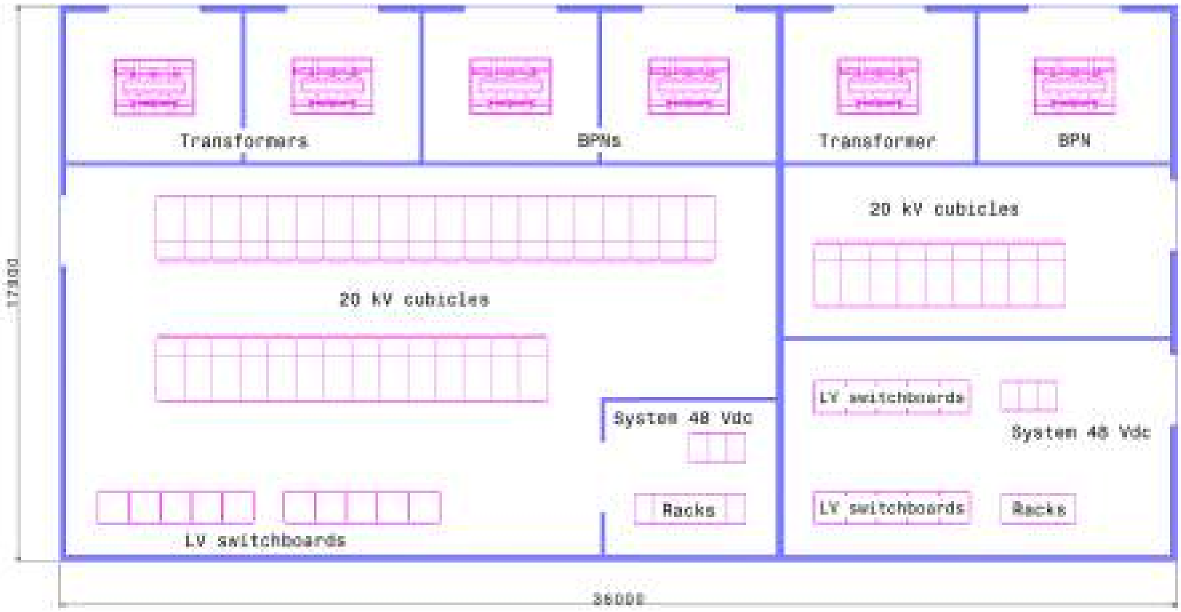

Fig. 8.64 Layout of the 20 kV substation of point PA

supply becoming unavailable. The first priority backup sources have an emergency power station installed on the surface close to the substation (the baseline is a diesel generator, alternatives like hydrogen-based groups are under evaluation). As an alternative, there will be a connection to the medium voltage utility deployed during the construction phase which will be kept available.

The backup sources will be at 20 kV and will be connected to the surface substation, on a busbar where only critical loads are hosted; from there, a cable running down the shaft will connect to the equivalent in the underground substation. From the underground substation, the secured network will be distributed to each alcove through a 20 kV line, and each secured load in the tunnel will be powered from its closest alcove.

The distribution from the secured substation in the tunnel must be done at medium voltage, as stepping down to low voltage would result in excessive voltage drop in the circuits running along the sector. In this sense, a possibility for optimisation was identified during the study, and to avoid duplicating the 20 kV cables in the tunnel (one for the normal network, one for the secured power), it is proposed to use the same link deployed for the general services, applying a load shedding logic in case of power outage. The aim is to minimise the space occupation and ease integration in this tight area.

In all the substations (surface, underground, alcoves) there will be a coupling between the critical loads 20 kV busbar and the general services busbar; in normal operation, the coupling will be closed, and the link between the substations will serve both critical and not-critical loads. In case of a failure, maintenance or any other unavailability of the main source, the electrical network will be supplied using the backup power sources: in this case, the couplings between the secured network and the general services network will be automatically disconnected, and in the tunnel the same 20 kV link will only keep the loads related to the safety of people live.

The secured network of one access point covers all the facilities of the point itself at medium voltage and extends up to half a sector to the left and right in the tunnel. To enhance the reliability of the system, there is an MV coupling to the last alcoves of each half sector: this stays open during normal operations. If a part of the network connected to one point is not operational, all the secured network busbars can be powered from the adjacent points through the tunnels by closing this coupling.

The secured network described so far is specifically designed to support electrical loads related to personnel safety. If a similar level of backup is required for systems associated with the accelerator or experiments, a parallel infrastructure with equivalent characteristics will need to be developed and implemented. For loads that cannot accept a brief interruption of a few seconds, whether they are safety-related or critical to operation, an uninterruptible power supply (UPS) system supported by batteries will be made available. This system will be strategically installed in buildings, service caverns and alcoves, to ensure a continuous power supply with the necessary autonomy. This infrastructure will serve critical loads of systems like vacuum, machine protection, cryogenics, RF, control, IT.

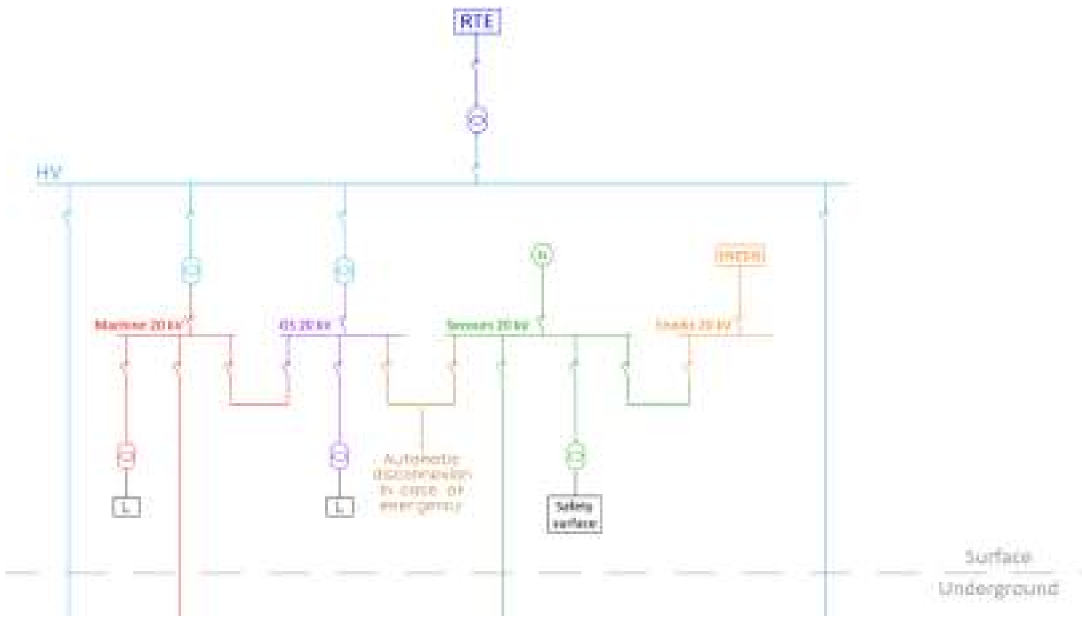

(a) On surface,

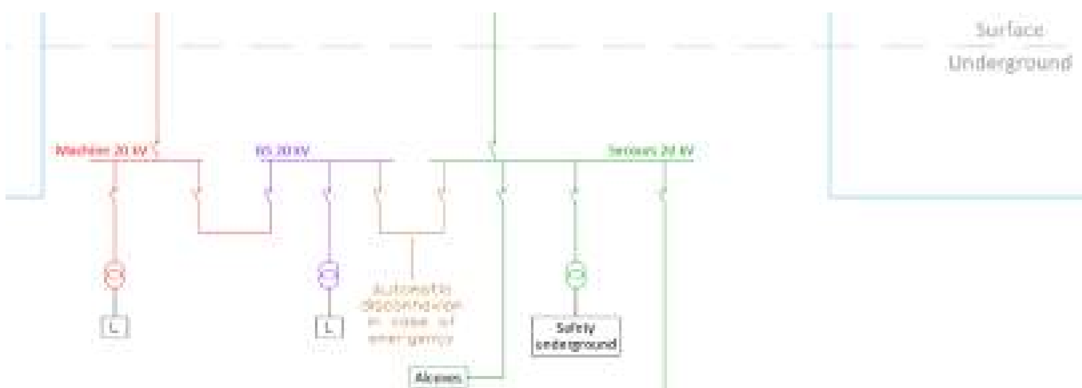

(b) underground,

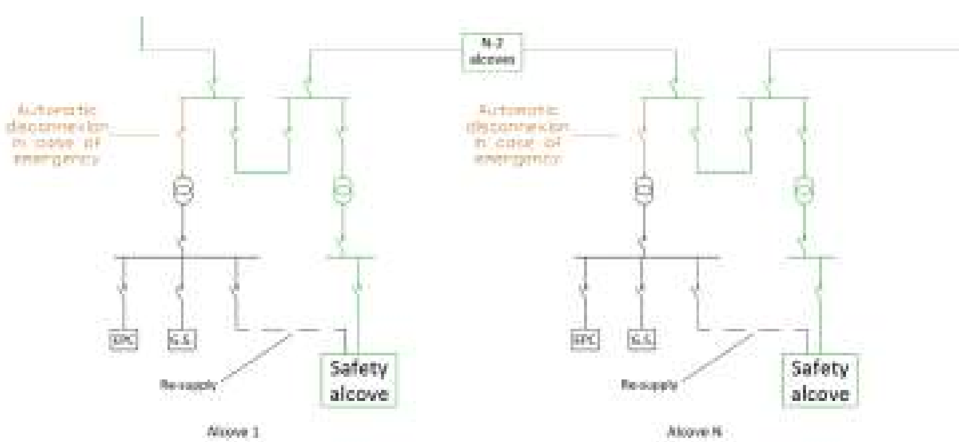

(c) in the tunnel.

Fig. 8.65 Conceptual electrical distribution for the secured network

8.4.3 RF powering

The RF system requires a power source capable of delivering a stable, high-quality DC high voltage. In existing implementations, such as the LHC and other accelerators, this is typically achieved by supplying a small group of RF amplifiers with a power converter operating in the MW range. However, for FCC-ee, this approach has been deemed economically unfeasible due to the large number of power converters and the extensive surface infrastructure that would be required at point PH. To address this challenge, a centralised power conversion strategy has been adopted, utilising a modular multilevel converter (MMC) to efficiently meet the system's power requirements.

Given that the RF system's power demand exceeds 100 MW, a thyristor-based converter was considered but ultimately found to be impractical due to power quality issues. If such a converter were implemented, a large-scale reactive power and harmonic compensation system would be required to maintain acceptable power quality. In contrast, the MMC solution offers significant advantages: it requires minimal or no harmonic filtering on the AC side and provides flexible reactive power control. This capability could potentially be leveraged to partially compensate for the reactive power consumption of the accelerator, further optimising energy efficiency.

8.4.4 Arc powering and alcoves

Power is distributed through the alcoves along the tunnel from the underground 20 kV substations. The alcoves serve multiple functions: they house equipment that must be protected from radiation, as well as local distribution systems for the arc, including accelerator systems, cooling and ventilation, safety systems, lighting, and power boxes. Additionally, they accommodate the power converters responsible for supplying the magnets in the arc.

The current baseline design includes seven alcoves per arc, with two larger alcoves positioned at the ends of the LSS (long straight section) of each point. These larger alcoves will host the power converters for the main arc magnets (dipoles and quadrupoles), as they require more space. The remaining alcoves will be spaced every 1600 m, each covering a sector extending 800 m on either side, distributing power accordingly.

The machine and general service networks will be separately available only in the first alcoves at the LSS ends, as the power converters in these locations have significantly higher loads and must be powered using dedicated transformers connected to a separate machine network. However, for the other alcoves, where power requirements for converters and other accelerator systems are much lower, it has been decided to supply them only from the general service network to avoid installing two separate 20 kV links in the tunnel.

To achieve this optimisation, the functional separation criteria outlined in Table 8.23 have been suspended for the alcoves. Instead, the choice is based on the assumption that the electrical parameters of the installed systems, particularly the power converters, will comply with specific requirements for connection to the network, including resilience to voltage and frequency variations and low total harmonic distortion (THD).

A similar synergy has been adopted for the safety-related loads and the secured network in the alcoves. These will be supplied through the same 20 kV link running through the tunnel, using a load-shedding logic to prioritise general services when necessary.

Following these technical choices, one 20 kV cable will run through the tunnel to the first smaller alcove from the alcoves at the end of the LSS at each access point, connecting it and continuing to the next, up to the end of the arc at the next access point (see Fig. 8.66. In the nominal configuration, each access point will supply the alcoves of half sectors to the left and to the right, with the one in the middle having an open coupling between the two sides. Closing this coupling, and having the 20 kV cable running from one point to the other, will allow re-supplying all the alcoves from only one point if the other is unavailable.

Electrical equipment in the alcoves The power distribution of the alcoves has been studied and sized based on the load requirements identified for the FCC-ee arc. The 20 kV cable coming from the arc will arrive at a switchgear divided into two busbars for secured and other loads. The switchgear will be connected to 20/0.4 kV transformers powering various low voltage switchboards, from where all the circuits going to the alcove and the tunnel are supplied. A redundant UPS will provide the required backup to create an uninterruptible network for the critical loads, and a redundant power supply will be dedicated to the emergency lighting.

In addition to the power converters, a certain number of racks will be installed, supplied through ad-hoc busbar trunking systems, and hosting the systems required for the accelerator and the services in a sector. Today, the number of these racks is estimated at 13 units, but could evolve in accordance with the evolution of the systems' requirements. Figure 8.67 shows the typical single-line diagram of the power distribution of an alcove.

A preliminary study has been conducted for the so-called big alcoves at the end of the LSS, concerning the powering of the power converters and of the loads of the half sector. The principles that have been applied are the same as used for the other alcoves, and the single line diagram is shown on Fig. 8.68.

Fig. 8.66 Arc and alcoves powering layout concept

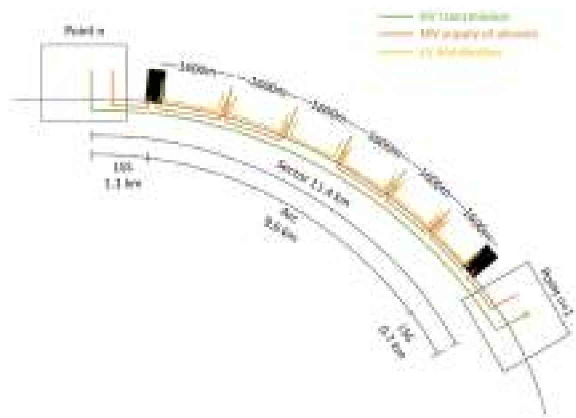

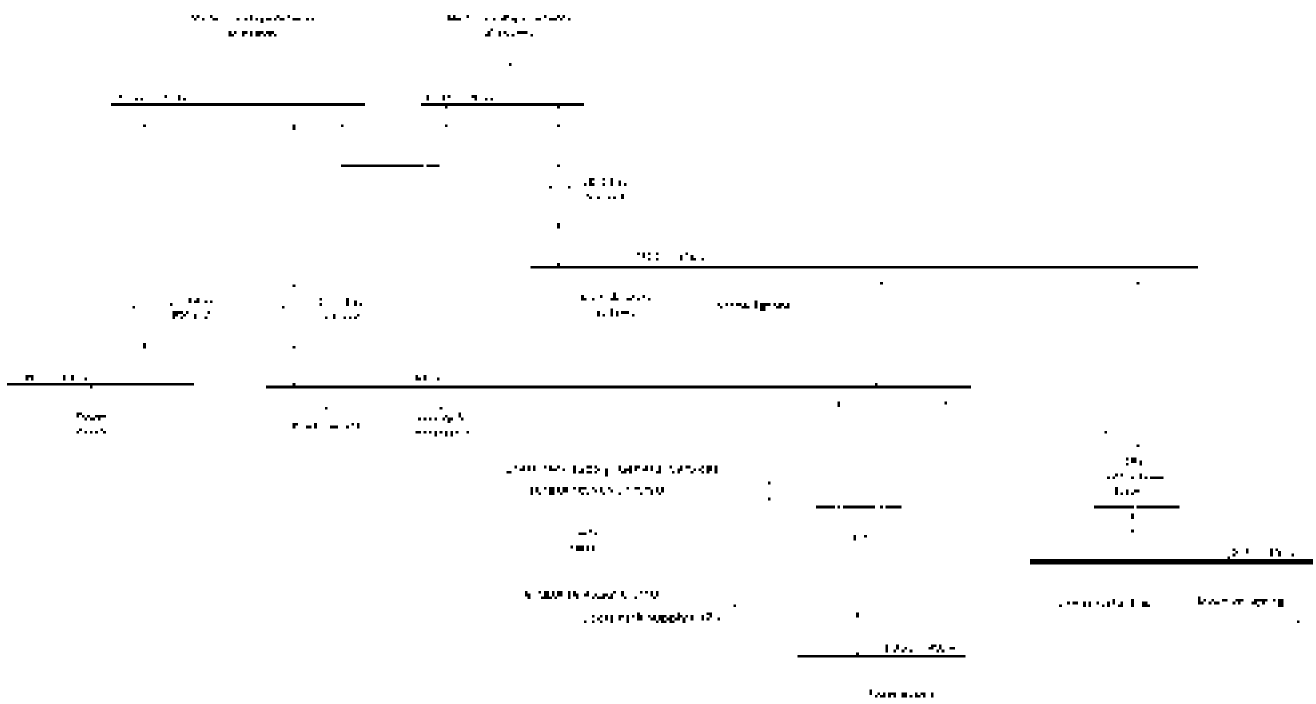

Fig. 8.67 Typical single line diagram of the power distribution of an alcove

Electrical equipment in the arc The list of equipment and circuits for powering the arc (see Fig. 8.69) includes:

- One power outlet box on the general service network every 50 m, powered from only the closest alcove (maximum length of the circuit: 800 m), without redundancy.
- One power outlet box on UPS network every 50 m, with secured redundant powering from both alcoves to the right and left (maximum length of the circuit: 1600 m).
- One normal light every 5 m, powered from only the general service network of the closest alcove (maximum length of the circuit: 800 m), with a circuit connected in parallel to the secured switchboard of the same alcove supplying 1 light out of 5 (to create a set of minimum lighting every 20 m).

In addition, the list of electrical equipment related to safety in the arc includes:

- One electrical emergency button (AU) every 50 m.
- One emergency light every 14 m, with secured redundant powering from both alcoves on the right and left (maximum length of the circuit: 1600 m).

The list of the cables composing these circuits is given in Table 8.24.

The quantification of these cables is of great importance in the assessment of the space required for the cable trays and other containment systems (e.g., cablofil, duct) that need to be installed in the arc.

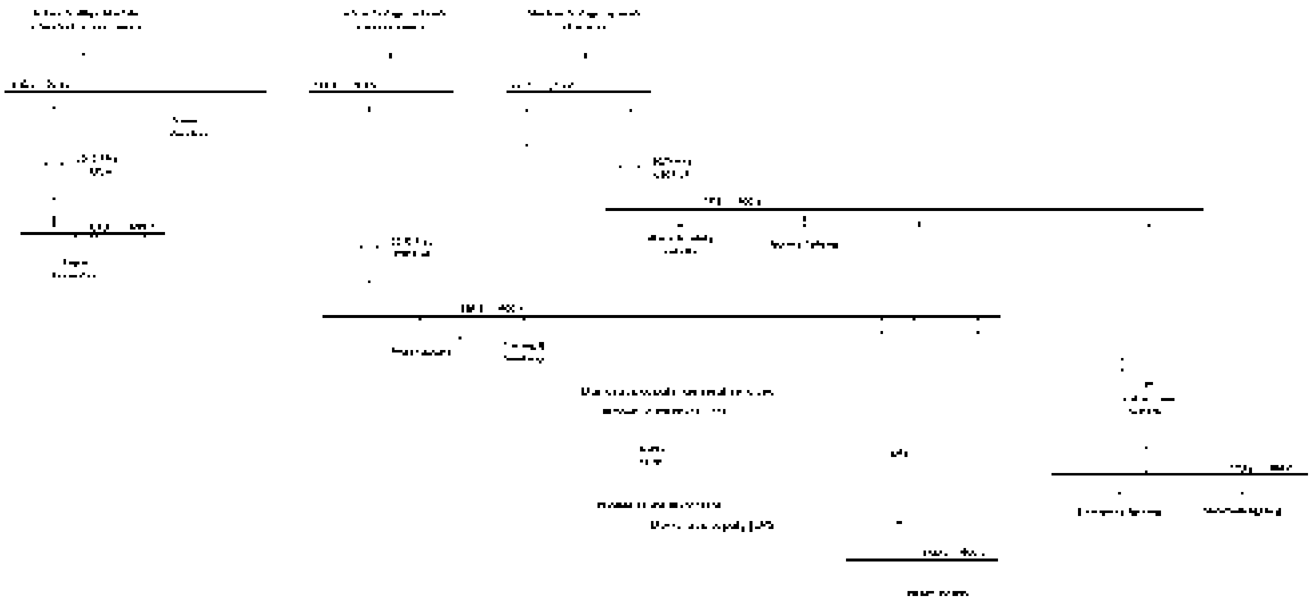

Fig. 8.68 Typical single line diagram of the power distribution of a big alcove at the end of LSS

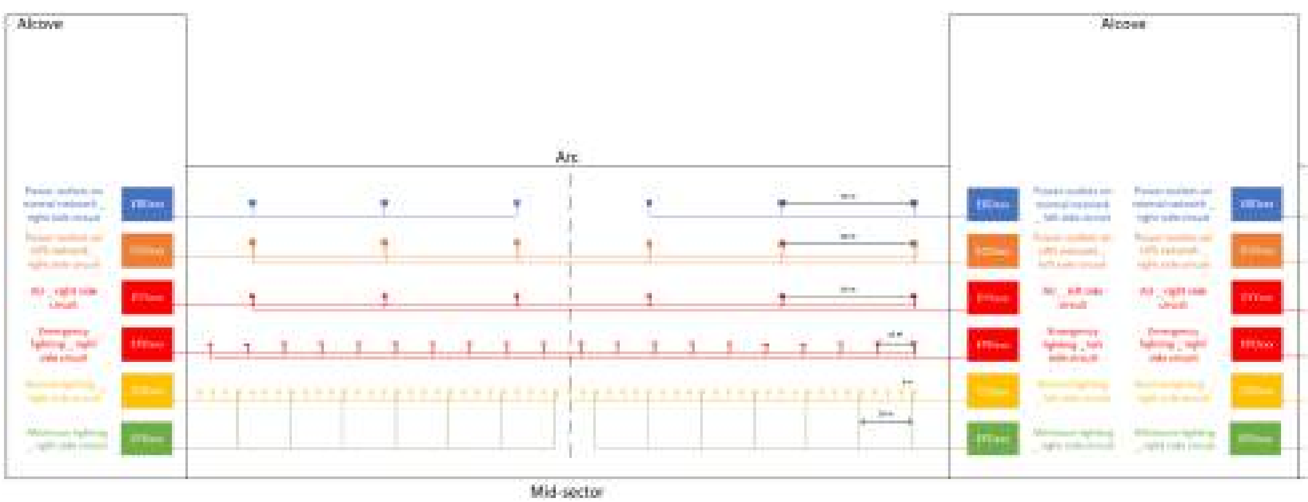

Fig. 8.69 Electrical distribution in the arc

For the same reason, the signal and control cables and the optical fibres used by other systems and installed in the arc have also been estimated. This process started from the various system's owners when available, or from extrapolation from previous accelerator projects at CERN when the information was not available. The list of these cables is given in Table 8.25.

The collection of the powering and cables' requirements in the tunnel will be constantly updated in the next stages of the study to consider every possible modified or new request and to adapt the technical solution accordingly. Furthermore, the use of optical fibres should be prioritised over copper cables to minimise space occupancy when developing users' cable requirements.

The information summarised in Table 8.24 and Table 8.25 allows the selection and dimensioning of the cable containment systems to be installed (mainly cable trays). This is one of the most important factors for the determination of the layout and cross section of the arc tunnel. The number and dimensions of cable trays are:

- Twelve 500 mm wide and 60 mm high cable trays for: DC cables (five cable trays considered), MV power cables, LV power cables, signal cables and optical fibres.
- Two 200 mm wide, 60 mm high and fire-resistant cable trays for safety systems.
- One 520×500 mm concrete duct for the HV cables.

Table 8.24 Estimation of the power cables in the arc

User	Load	Cable tray	Cable type	Size (mm)	Number of lines in the tunnel
Powering	MV power of alcoves	MV	$3\times(1\times400\ \mathrm{mm}^2) + (1\times120\ \mathrm{mm}^2)$ Cu	3×d = 50 + d = 21	1
	Power outlets on GS network	LV	$3\times(1\times150\ \mathrm{mm}^2) + (1\times95\ \mathrm{mm}^2)$ Cu	3×d = 21 + d = 18	1
	Power outlets on UPS	LV	$3\times(1\times150\ \mathrm{mm}^2) + (1\times95\ \mathrm{mm}^2)$ Cu	3×d = 21 + d = 18	2
	Classic lighting	LV	$(5\times10\ \mathrm{mm}^2)$ Cu	d = 22	1
	Emergency lighting	Safety	$(5\times2.5\ \mathrm{mm}^2)$ Cu, flat	24x6	2
	Emergency stops link (AU)	Safety	$14\times(2\times1\ \mathrm{mm}^2)$ Cu	d = 21	2

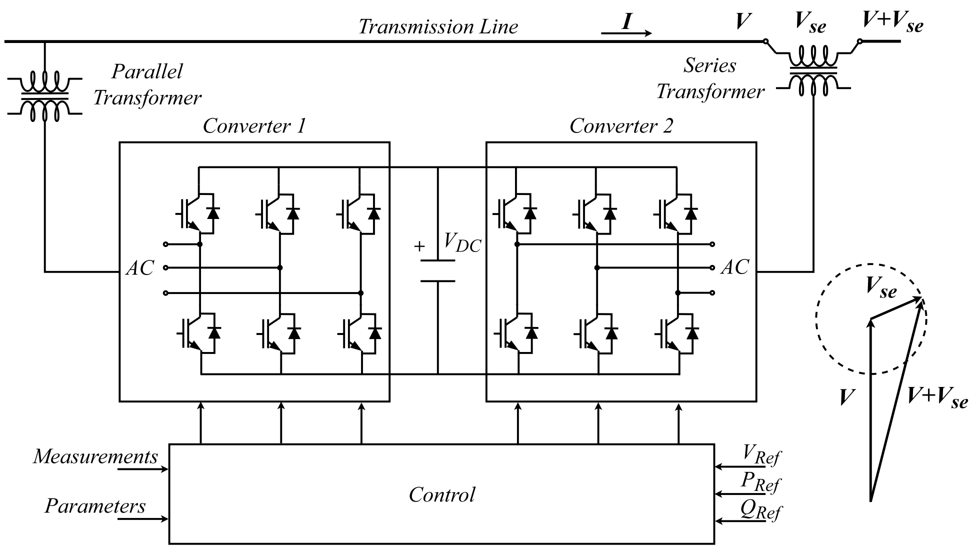

Fig. 8.70 Diagram of a unified power flow controller (UPFC) used to enhance controllability of the FCC network

8.4.5 Control of FCC grid

AC network control using unified power flow controllers Unified power flow controllers (UPFCs) are power-electronic-based network controllers capable of performing voltage control, power flow control, reactive power compensation, and protection against network perturbations. The versatility of these systems makes them highly suitable for controlling and stabilising the FCC AC transmission network, offering an alternative to systems such as static var compensators (SVCs) or DC networks.

A UPFC consists of two back-to-back converters, each connected to the network via a transformer. One converter is connected in parallel, enabling reactive power or voltage control at the associated network node. The other converter is connected in series, allowing active and reactive power flow control, voltage control, and voltage dip mitigation by injecting a specific voltage between the network and the loads. Figure 8.70 illustrates the basic structure of the UPFC.

The application of UPFCs in the FCC network can be tailored to specific protection and reactive power compensation requirements. In the high-voltage transmission ring, UPFCs can be installed at each network connection point to manage the accelerator's reactive power using the parallel converter. At the same time, the series converter provides protection against voltage dips and prevents undesired power flows, particularly under closed-loop operation.

At the medium-voltage level, UPFCs enable voltage control and protect access points from voltage dips. To optimise equipment efficiency, protection can be focused on critical sections of the network by connecting the series transformer to selected feeders. This approach creates a dedicated machine network, effectively decoupling it from general services, following the model already employed in CERN's existing infrastructure.

Compared with existing compensating equipment such as SVCs, UPFCs offer enhanced functionality. While they perform the same tasks of reactive power compensation and voltage control, UPFCs are more robust to network perturbations, exhibit faster response times, and, through the series converter, provide load protection against transients - an advanced feature not currently available in SVCs.

Table 8.25 Estimation of the control and signal cables, and optical fibres crossing the arc

User	Load	Cable tray	Cable type	Size (mm)	Number of lines in the tunnel
Fibre optics	Backbone	FO	3 cables (×24 fibres)	d = 25	1
	Underground	FO	9 cables (×24 fibres)	d = 25	2
	BI (only BPMs)	FO	13 cables (×12 fibres) +8 cables (×24 fibres)	d = 25	4
	Sensing	FO	2 cables (×6 fibres)	d = 25	1
Vacuum	ion pumps	Signals	1×0.63(HV) + 2×0.25 mm^2 Cu	d = 10.7	28
	NEG (power)	Signals	3×2.5 mm^2 Cu	d = 13	16
	Penning	Signals	3-axis 0.8/8.4 mm Cu	d = 10.3	12
	Pirani	Signals	1× (4×1 mm^2) Cu	d = 6.5	12
	BA power	Signals	6× (2×0.75 mm^2) Cu	d = 14.5	6
	BA collector	Signals	3-axis 0.5/5.7 mm Cu	d = 7	6
	Sector valve	Signals	6× (2×0.75 mm^2) Cu	d = 14.5	6
	Profibus	Signals	2× (1×0.35 mm^2) Cu	d = 8	1
Access & Alarms	Sector doors	Safety	13× 2×0.5	d = 17	1
	Fire doors - magnet	Safety	2×1.5	d = 10.5	3
	Fire doors - position contacts	Safety	2×1	d = 5	3
	Fire doors - flashing lights	Safety	4×1.5	d = 10.5	3
	Call points - break-the-glass	Safety	2×1	d = 5	2
	Call points - telephones	Safety	1× 4×0.6)	d = 7.4	2
	Evacuation - voice alarm	Safety	2×2.5	d = 13	2
Cooling & Ventilation	Fancoils	Signals	1×70 mm^2	d = 16.6	16
	Dampers	Signals	1×35 mm^2	d = 12.1	21
	Valves & other equipments	Signals	1×35 mm^2	d = 12.1	3
Radiation protection	Radiation detectors ($t\bar{t}$ phase only)	Safety	2×CEH50 + 2× (2×0.22 mm^2)	d = 9.5	2
Magnet	WIC fieldbus	Signals	1×50 mm^2	d = 14	4
Protection	BIS fibres	FO	1 duct	d = 25	1
Power Converters	DC cables				
Others	Unknown				

At this stage of the project, the exact compensating requirements are not fully defined. However, it is anticipated that the reactive compensation needs for each access point will be approximately 10 MVAr. Regarding voltage dip compensation, most of the recorded voltage dips at CERN exhibit a depth of less than 30% of the nominal voltage. With this figure in mind, and assuming a power rating of 10 MVA for the loads to be protected at each access point, the UPFC must be designed to inject up to 3 MVA during such events. Based on these considerations, the total installed UPFC power per access point can be estimated at approximately 15 MVA.

DC distribution alternative Recent developments in power electronics have enabled the use of DC for power transmission and distribution. Compared with conventional AC distribution, DC networks offer lower transmission losses, as only active power flows through the cables and the skin effect is absent. Additionally, DC networks provide precise power flow control and mitigate perturbations originating from the AC network.

The use of DC to transmit power from network connection points to accelerator loads is under consideration. In this transmission scheme, loads are supplied by high-voltage converters with energy buffers that decouple them

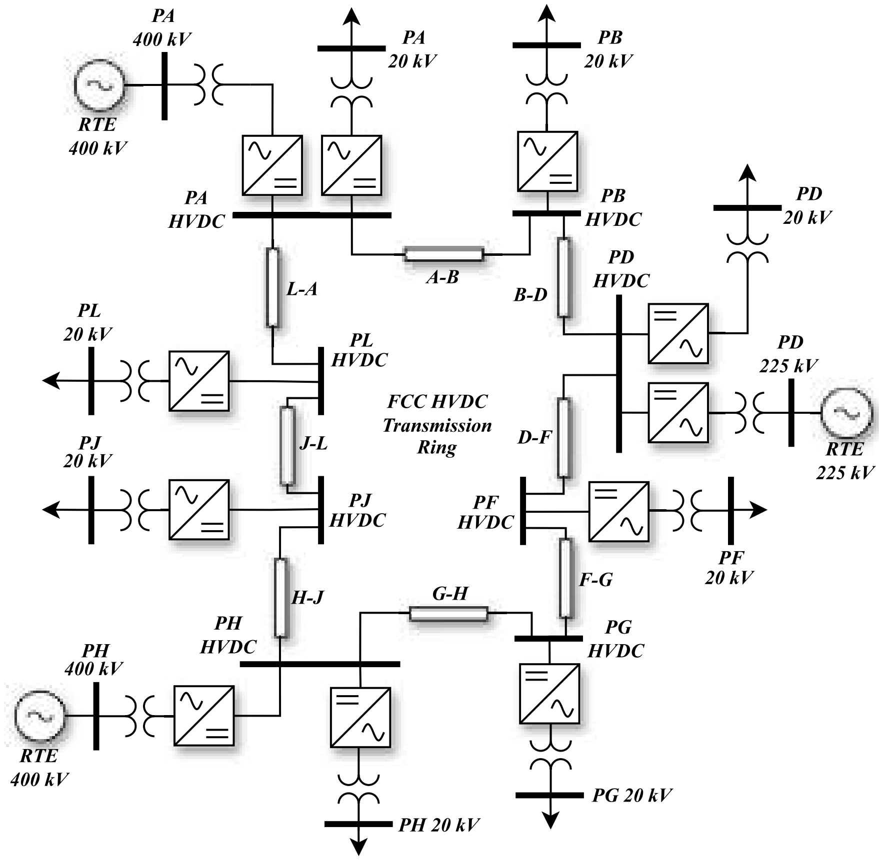

Fig. 8.71 High Voltage DC network used as an alternative to conventional AC distribution along the accelerator ring

from network dynamics. This configuration enables the local generation or absorption of reactive power as required by the loads, protecting them from network perturbations. To implement these features, the network configuration shown in Fig. 8.71 is proposed.

It consists of eleven power converters: three operating as rectifiers and eight as inverters. A key feature of this configuration is the closed-loop operation of the transmission ring, which guarantees precise control of power flows. This operational mode enables adjustments to the power drawn from the main connection points, optimising flow and ensuring resilience in the event of a feeder outage. In such scenarios, any point on the accelerator can still be supplied by at least two feeders located on opposite sides of the ring.

8.4.6 Energy storage systems

The use of energy storage systems (ESS) is being evaluated for the FCCee and FCChh. The primary objectives of ESS are:

- Providing energy to critical systems (e.g., safety or cryogenics) during electrical outages lasting from minutes to hours (some of these systems currently rely on diesel generators).
- Storing lower-cost energy from renewable sources (local or otherwise) for later use.
- Temporarily storing the energy of FCC-hh magnets during the deceleration phase of the acceleration cycle and returning it during the next cycle.

Technologies such as batteries, supercapacitors, flywheels, electrolysers, fuel cells (hydrogen-based), and gravitational energy storage systems have been preliminarily analysed and compared for the above-mentioned applications.

A collaboration has been established to explore the integration of hydrogen as an energy storage system (ESS) vector to support one or more functions within the accelerator complex. Hydrogen-based systems are particularly well-suited for both short and long-term energy storage, offering the advantage of decoupling energy storage capacity - determined by the hydrogen mass - from charging speed, defined by electrolyser capacity, and power output, which is set by the fuel cell capacity.

The heat generated by electrolysers and fuel cells is available at high temperatures, which can enhance the usability of waste heat. For instance, this heat can be used to increase the temperature of water used for cooling various equipment, thereby improving the efficiency and transportability of waste heat over longer distances.

Additionally, the heat recovered can be leveraged to drive absorption cooling cycles, contributing to the cooling needs of magnets, power converters, tunnels, and other infrastructure.

In principle, hydrogen-based ESS technology offers high flexibility and adaptability across a wide range of applications. However, it has some drawbacks, including relatively low conversion efficiency and the requirement for robust hydrogen storage systems. Nevertheless, the co-generation of usable heat and cooling can partially offset these efficiency limitations, making hydrogen a promising candidate for integration into the FCC infrastructure. Studies on the feasibility and implementation of hydrogen ESS within the FCC are ongoing and will be further intensified in the future.

For the FCC-hh superconducting magnets, preliminary assessments suggest that batteries appear to be the most suitable ESS technology for recovering energy during the ramp-down phase of the cycle and re-injecting it into the magnets during the next acceleration cycle.

8.5 Cryogenic systems

Cryogenic infrastructure is essential for various components of the accelerator. The experiment points PA, PD, PG, and PJ will each be equipped with two cryoplants: one dedicated to the detector magnet (detector cryoplant) and another to the machine detector interface (MDI) region magnets (interaction region (IR) cryoplant). These systems ensure the required low-temperature environments for the sensitive components in the experiment regions.

While the technical points PB and PF do not require cryogenic refrigeration, the technical points PH and PL are associated with the radiofrequency (RF) system, which necessitates operation at 2 K and 4.5 K to efficiently accelerate particles to the required energies. Each technical point features a long straight section (LSS) of 2032 m, symmetrically distributed around the interaction point (IP). The RF system, composed of a string of superconducting cavities and klystrons, is housed within these LSS regions and requires dedicated cryogenic refrigeration to maintain the necessary low-temperature conditions for efficient operation.

Installation of the cryogenics for the cooling of the superconducting RF systems will follow the same strategy defined for the cryomodules to be operated in the technical points PH and PL.

A new RF layout was proposed in June 2024 with the aim of simplifying the overall installation of the SRF system. As described in Sect. 3.4.3, it consists of installing and, from the beginning, operating all the 2-cell 400 MHz cavities for the Z, WW and H mode, with each cavity powered at 500 kW in continuous wave (CW) mode. In other words, all the cryomodules necessary for the operation of FCC-ee at the energies of Z, WW and H levels will be installed at once and operated with the heat loads corresponding to the Z energy. This is valid for both 400 MHz and 800 MHz cryomodules.

This new layout significantly simplifies the design and staging of the cryogenic system. There will only be two stages: one for the Z, WW and H operation, with cryoplants operated to cover heat loads at H energy, and another one for $t\bar{t}$ operation (Fig. 8.72, with the same cryogenics scenario. This major modification drove the update of the cryogenic system with respect to the CDR, and the corresponding results can be found in the following sections.

8.5.1 Cryogenics for superconducting RF systems

Layout and architecture The general cryogenic layout of the FCC-ee RF system is shown in Fig. 8.73. Cryoplant locations are indicated using small circles near the experiment and technical points.

Aiming to optimise the integration of the machine, the RF systems of the collider and the booster have been split between two points. Point PH contains the collider RF, while point PL contains the booster's. This separation is also optimised from the cryogenic point of view as the booster and the collider present different heat load profiles. The booster ramps up the energy of the particles from injection energy to collider energy while the collider maintains a constant energy. Both the dynamic and static loads vary greatly. Moreover, the booster is composed solely of bulk Niobium 800 MHz cavities operating at 2 K, whilst the collider is mainly composed of coated elliptical 400 MHz cavities operating at 4.5 K. For the collider at point PH, there is an exception at the $t\bar{t}$ stage, where 800 MHz cavities are installed to further increase the accelerating gradient achieved with the 400 MHz cavities.

Figures 8.74 and 8.75 show the cryogenic plant architectures for point PH and PL respectively. For certain stages that contain two cryoplants, the cryogenic plant architecture includes an interconnection box (QUI) that couples the refrigeration equipment to the cryogenic distribution line. The interconnection box facilitates a level of redundancy amongst the refrigeration plants and eases maintenance procedures. The other elements that are shown in the figures are the warm compressor station (WCS) and the upper cold box (UCB), located on the surface. Also included is the lower cold box (LCB), located in the cavern. This split box architecture has a temperature cut of 40 K between the two cold boxes, which reduces the hydrostatic losses incurred due to the depth of the tunnel.

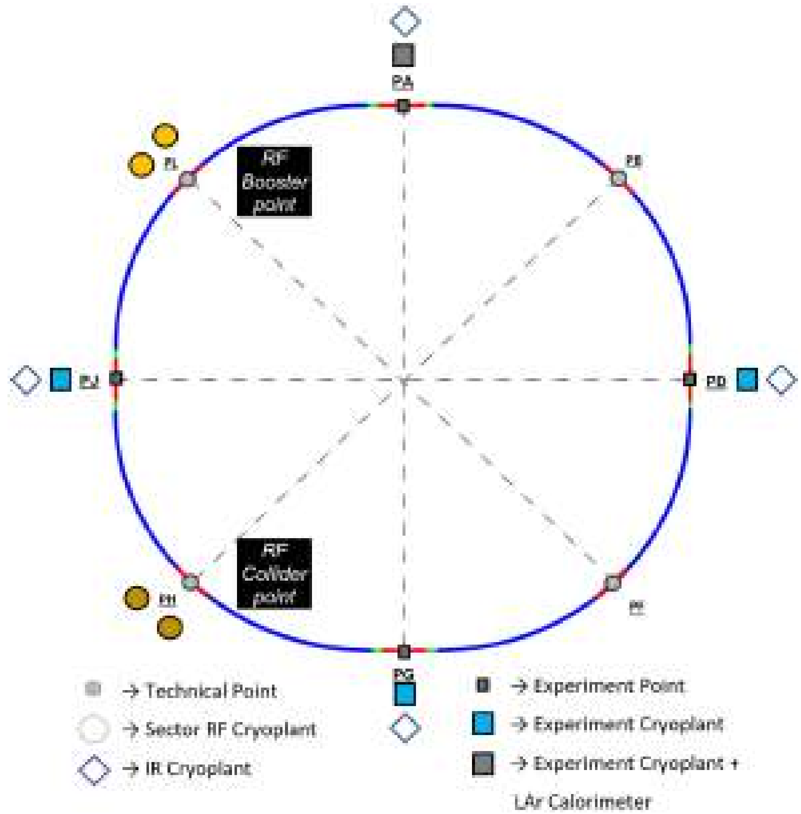

Fig. 8.72 FCC-ee collider cryogenic system layout for $t\bar{t}$ operation

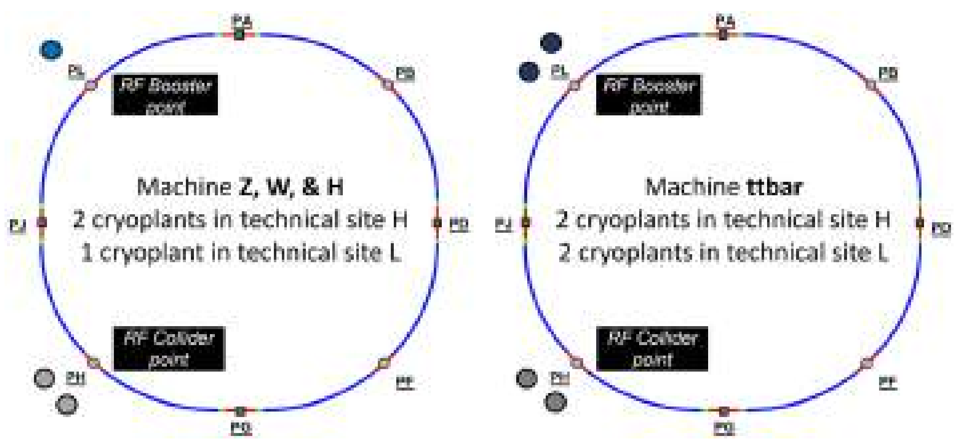

Fig. 8.73 General cryogenic layout for the technical points

Temperature levels In view of the high thermodynamic cost of refrigeration at 2 K and 4.5 K, the thermal design of cryogenic components aims to intercept the largest fraction of heat loads at higher temperatures, hence the use of multiple staged temperature levels. These are:

- 50 K – 75 K for thermal shield as the first major heat intercept, sheltering the cavity cold mass from the bulk of heat inleaks from the environment.
- 4.5 K normal saturated helium for cooling 400 MHz superconducting cavities.
- 2 K saturated superfluid helium for cooling the 800 MHz superconducting cavities.

The cryomodules (CM) and cryogenic distribution line (QRL) combine several low temperature insulation and heat interception techniques which will have to be implemented on an industrial scale. These techniques include low-conduction support systems made of non-metallic fibreglass/epoxy composite, low-impedance thermal contacts under vacuum for heat intercepts, and multi-layer reflective insulation for wrapping the cold surface.

Heat loads Inward static heat leaks (inleaks) arise from the ambient temperature environment and depend on the cryomodule design. The current design adopts a fully segmented architecture for both the booster and the

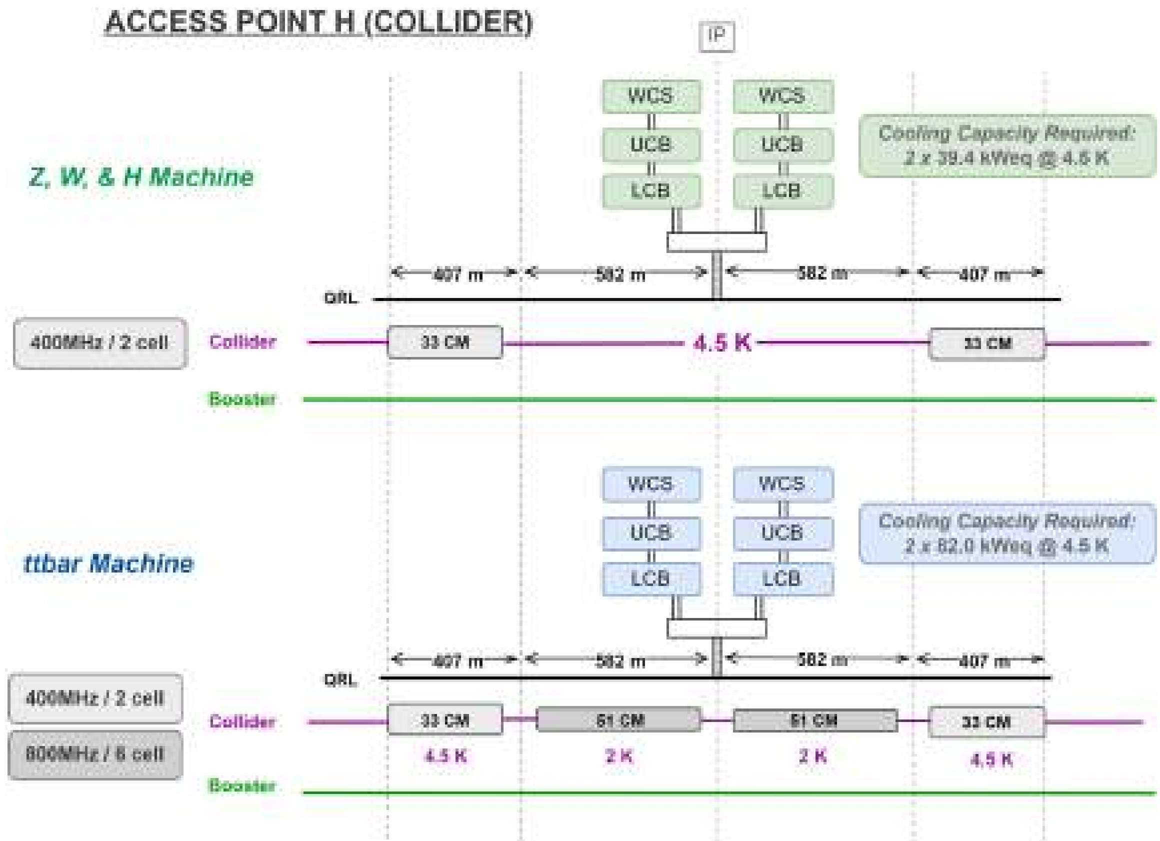

Fig. 8.74 Cryogenic plant architecture at point PH (RF collider)

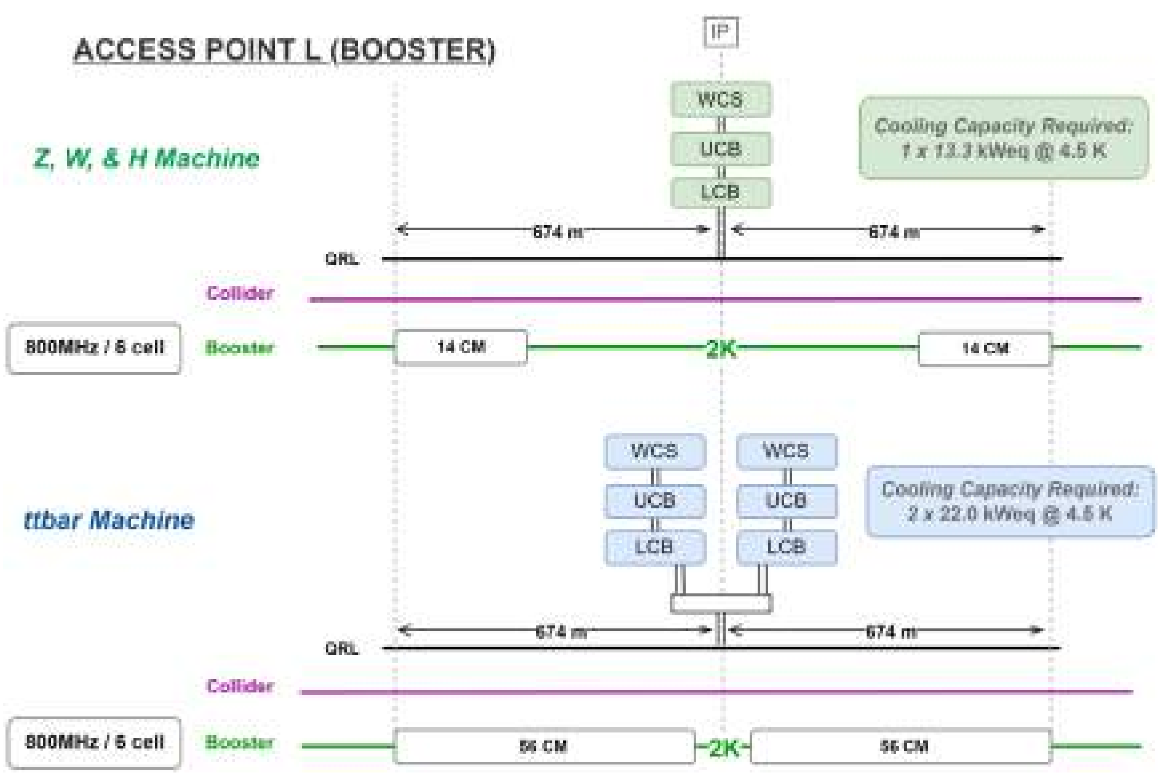

Fig. 8.75 Cryogenic plant architecture at point PL (RF booster)

Table 8.26 Collider heat loads at point PH (as of October'24)

FCC-PH (collider)	Z, WW, & H	$t\bar{t}$	
Freq [MHz]	400	400	800
Temperature [K]	4.5	4.5	2.0
No. of cryomodules	66	66	102
No. of cavities (×4)	264	264	408
Static losses to the thermal shield / CM (no margins) [W]	218	218	120
Static losses to the helium bath / CM (no margin) [W]	131	131	37.3
Dynamic losses / cavity (no margins) [W]	128	129	27.1
Dynamic losses / CM (no margins) [W]	512	516	108.5
Total static losses to the thermal shield (with uncertainty factor) [kW]	21.6	21.6	18.4
Total static losses to the helium bath (with uncertainty factor) [kW]	13	13	5.7
Total dynamic losses (with overcapacity factor) [kW]	50.7	51.1	16.6

Table 8.27 Booster heat loads at point PL with an assumed duty cycle of 15% (as of October'24)

FCC-PL (Booster)	Z, WW, & H	$t\bar{t}$
Freq [MHz]	800	800
Temperature [K]	2.0	2.0
No. of cryomodules	28	112
No. of cavities (×4)	112	448
Static losses to the thermal shield / CM (no margins) [W]	103	103
Static losses to the helium bath / CM (no margin) [W]	37	37
Dynamic losses / cavity (no margins) [W]	3	3
Dynamic losses / CM (no margins) [W]	12	12
Total static losses to the thermal shield (with uncertainty factor) [kW]	4.3	17.3
Total static losses to the helium bath (with uncertainty factor) [kW]	1.6	6.2
Total dynamic losses (with overcapacity factor) [kW]	0.5	2.0

collider, where each cryomodule has an independent connection to the cryogenic distribution line. Additionally, this distribution line is positioned externally to the cryomodule. The thermal calculations for the cryomodules are based on the thermal performance data of similar cryogenic assemblies.

The heat loads in the RF cryomodules are dissipated in the cavity baths at 4.5 K and 2 K. These heat loads are determined by both the thermo-mechanical design of the cryomodule and the heat dissipation from the cavities during operation.

Table 8.26 presents the heat load values for point PH, while Table 8.27 provides the corresponding values for point PL. The reported values (excluding margins) originate directly from the SRF group. For the booster, these values are expected to increase, as the final RF cavity voltage and duty cycle have not yet been determined. The heat loads given in Table 8.27 for the booster assume a duty cycle of 15%. However, duty cycle values across different working points will range between 15% and 90% and still require finalisation.

Additionally, the reported heat loads do not account for all margins or the dynamic heat loads resulting from dissipation in the fundamental power coupler and higher-order modes (HOMs). These values are valid for an installed quality factor of 3.0×10^{10} for the 800 MHz cavities and 2.7×10^{9} for the 400 MHz cavities.

Notably, at the $\mathrm{t\bar{t}}$ stage for both point PH (collider) and point PL (booster) there will be 800 MHz / 2 K cavities. These 800 MHz cavities have different heat loads at the different points. While the static heat loads are similar, the dynamic losses are very different with 27.1 $\mathrm{W/cav_{collider}}$ and 3 $\mathrm{W/cav_{booster}}$. The dynamic losses are very different since the collider operates in continuous waves with 27.1 $\mathrm{W/cav_{collider}}$ while the booster dynamic

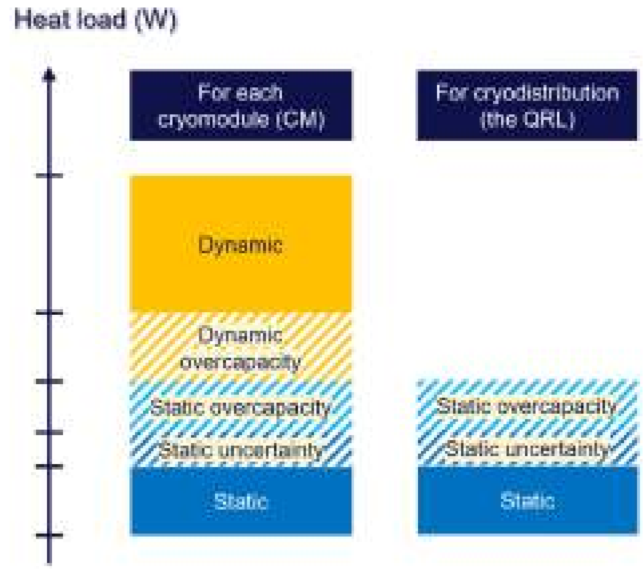

Fig. 8.76 Uncertainty and overcapacity margins on the raw heat loads

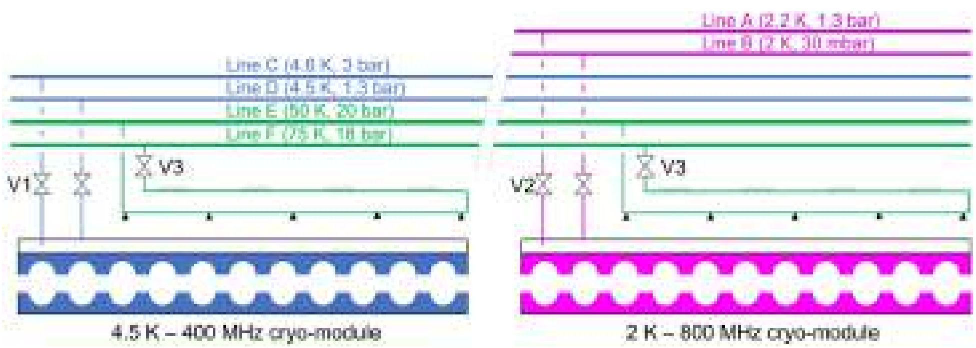

Fig. 8.77 Cryogenic flow scheme for the cryomodules. Here the cryogenic plant is located to the right of the 800 MHz section

losses are dependent on the duty cycle. This value is likely to increase following the expected increase of the booster duty cycle.

Dimensioning the cryoplants requires adding margins to the raw heat loads, by defining and applying two factors, the uncertainty and the overcapacity. The uncertainty, evolving during the project lifetime, is set to 50% for the feasibility study and covers the design uncertainties of the cryo facility. It is applied to the static heat loads. The overcapacity, stable during the project lifetime, is also set to 50% for the feasibility study, and ensures nominal performance of the cryo facility by covering specific risks such as reduced performance induced by ageing and operational flexibility. The overcapacity is applied to both the dynamic heat loads and the static heat loads after the uncertainty factor. Figure 8.76 shows a visual representation of how the margins were applied.

8.5.2 Cooling scheme and cryogenic distribution

The cooling scheme for the cryomodules is represented in Fig. 8.77. The 4.5 K cavity cold masses are immersed in saturated helium baths, which are supplied by line C. The saturation pressure is maintained by line D, which recovers the evaporated vapour. The 2 K cavity cold masses are immersed in saturated helium baths, which are supplied by line A. The low saturation pressure is maintained by pumping the vapour through line B. Each cryomodule has a dedicated thermal shield and heat intercept circuit cooled in parallel between line E and F.

Table 8.28 gives the size of the main cryogenic distribution system components. The cryogenic distribution line (QRL) was designed for the final $t\bar{t}$ stage, making it oversized for the Z, W, and H stages. This design choice was made to lower installation complexity and costs. A visual cross-sectional view of the QRL can be seen in Fig. 8.78. A front view of the lengths of the QRL along with other connecting components in the service cavern and LSS sections can be seen in Fig. 8.80 and Fig. 8.79.

2 K system optimisation Refrigeration of the RF cavities in a 2 K saturated bath involves low-density helium (He) with process pressures in the 30 mbar range. A series of compressors are required to achieve these pressure levels. Whenever high mass flow rates of helium need to be treated, performing a large fraction of the compression at

Table 8.28 Dimensions of the main cryogenic distribution line components

Component	Diameter [mm] Point PH	Diameter [mm] Point PL
Line A: 1.3 bar, 2.2 K	80	60
Line B: 30 mbar, 2.0 K	345	265
Line C: 3 bar, 4.6 K	120	20
Line D: 1.3 bar, 4.5 K	200	20
Line E: 20 bar, 50 K	80	60
Line F: 18 bar, 75 K	80	60
Vacuum jacket (400 MHz)	550*	-
Vacuum jacket (800 MHz)	830*	600*

* +100 mm for bellows and flanges.

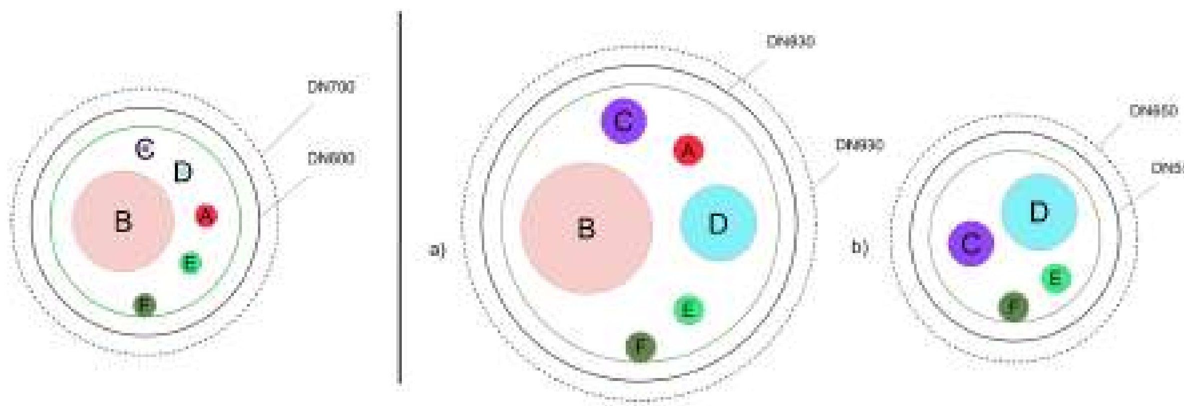

Fig. 8.78 Cross sections of point PL (left) and point PH (right) cryogenic distribution line. a) for the cooling of 800 MHz cryomodules. b) for the cooling of 400 MHz cryomodules

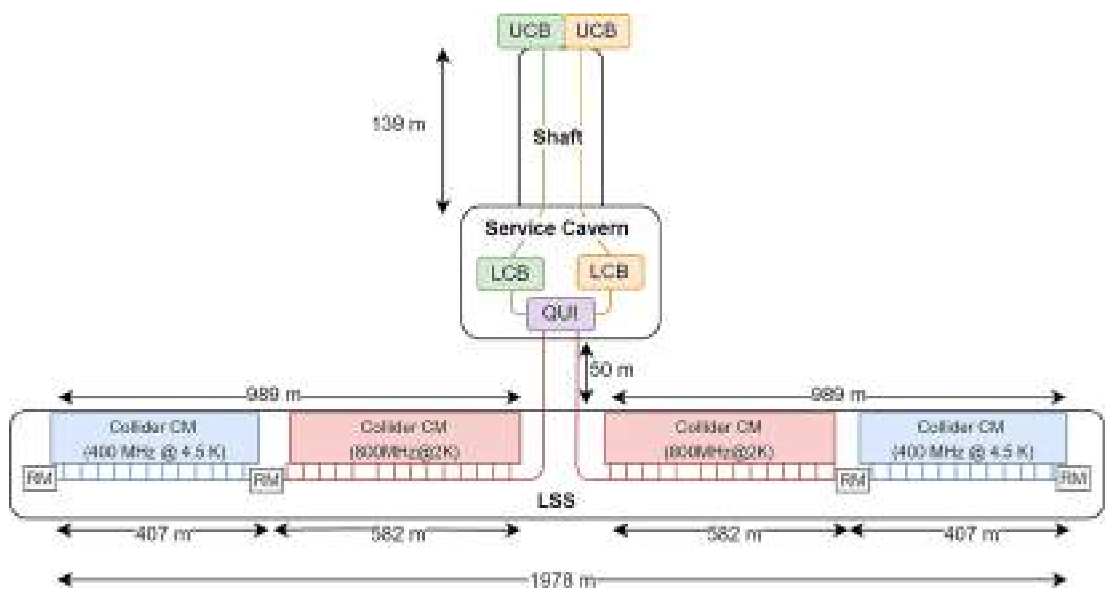

Fig. 8.79 Collider (point PH) cryogenic plant distribution architecture at the $t\bar{t}$ stage

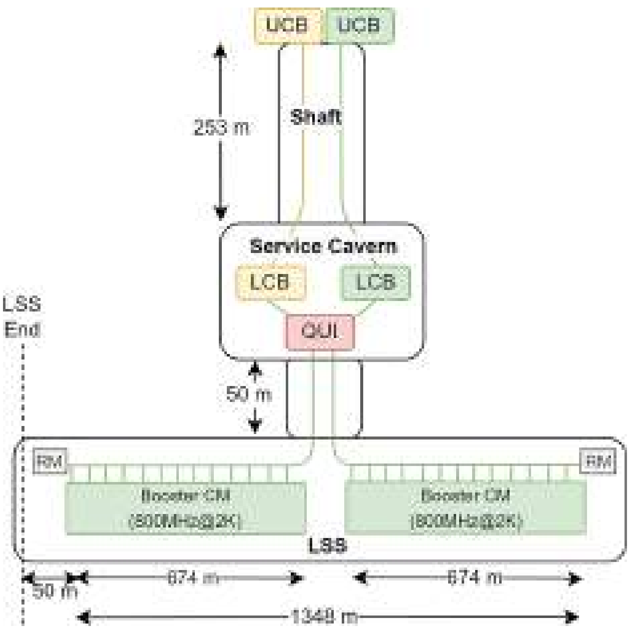

Fig. 8.80 Booster (point PL) cryogenic plant distribution architecture at the $t\bar{t}$ stage

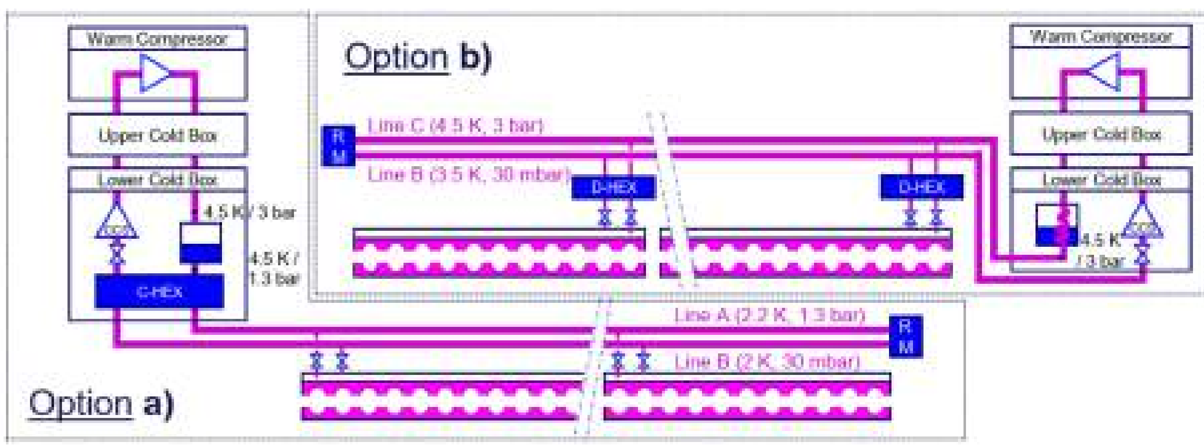

Fig. 8.81 FCC-ee 2 K system distribution architecture options studied, a) and b). CCS being the Cold Compressor System, RM the Return Module, C-HEX the Centralised Heat Exchanger and D-HEX the Distributed Heat Exchanger

low temperatures allows operating with a higher density, effectively limiting the size of the compressors. During $t\bar{t}$ operation of FCC-ee, about 550 g/s or 250 g/s [384] per train will need to be pumped at points PH and PL, respectively. In both cases, a cold compressor system (CCS), composed of a series of centrifugal compressors, will be required to provide the compression back to semi-atmospheric levels ($\approx$ 400 mbar). From previous studies, it is considered that a CCS of 12 kW at 1.8 K is feasible [385, 386]. This translates into a mass flow rate of about 500 g/s with one train of four compressors at a suction pressure of 16 mbar. Addressing FCC-ee needs, the suction pressure of such a CCS can be increased as the saturation temperature desired is 2 K. This leads to slightly higher densities and, hence, allows operation with slightly more than 500 g/s mass flow rates.

The lower the design suction pressure of a CCS is, the more compression stages may be required to reach semi-atmospheric levels, further increasing the system's complexity. Since the cavities are cooled by a saturated He-II bath [387], the furthermost 2 K cryomodule will need to be at the saturation pressure of helium at 2 K, that is, at 31 mbar. The pressure drop along the distribution line to that cryomodule needs to account for this and must be minimised so that the suction pressure at the inlet of the CCS is kept as high as possible. The design goal is to limit the total pressure losses such that the suction pressure of the CCS stays above 22 mbar. Out of the 9 mbar of available pressure drop, 7 mbar is left as a margin for heat exchangers, elbows and valves, and 2 mbar is set as a design criterion for sizing the very low pressure (VLP) return line or line B in Fig. 8.81. The choice of 2 mbar provides a good compromise for the CCS suction pressure and the overall size of the VLP line. Limiting the

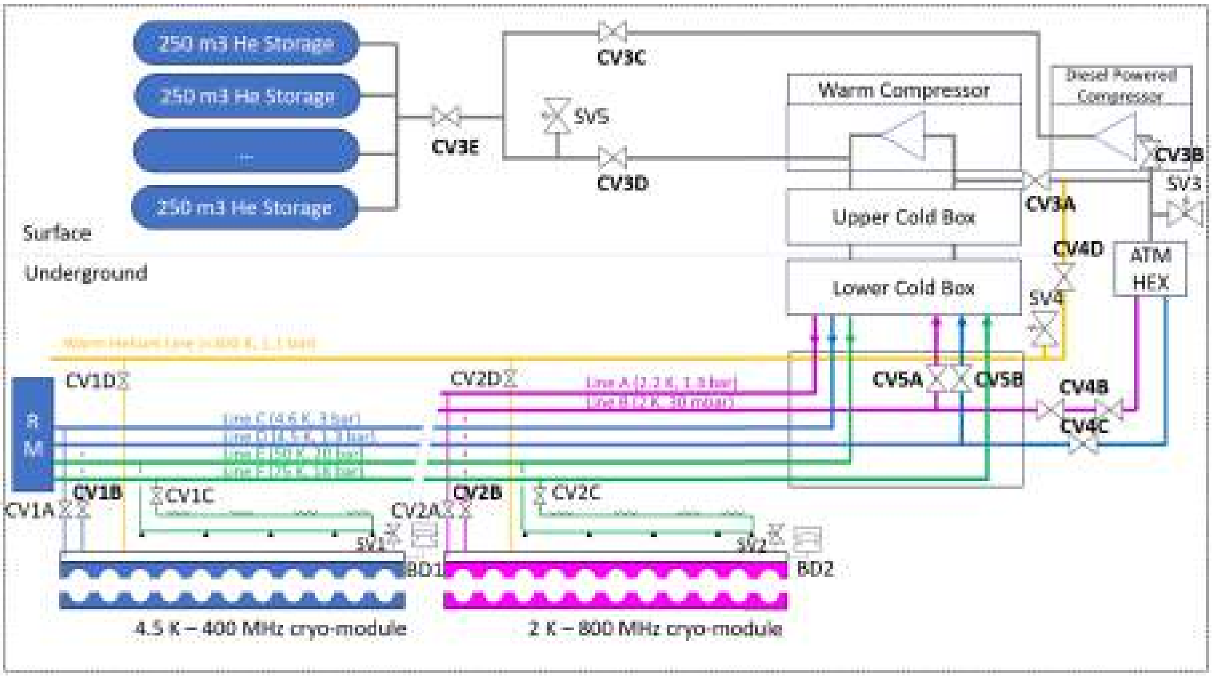

Fig. 8.82 FCC-ee proposed helium recovery system (HRS) concept

pressure drop further could hinder the already difficult distribution line integration in the 5.5 m diameter tunnel, where the space is very limited due to the presence of both booster and collider machines.

Ensuring a thermodynamically well-adapted architecture is essential to reduce the high cost associated with such a system. Several architectures have been assessed and compared so far, with the goal of finding the optimum choice when considering both energy and integration constraints. Figure 8.81 shows the two main options that are being considered.

The current calculations for the cryoplants and QRL are based on the preliminary architecture choice of the C-HEX design. An energetic optimisation was performed [388] to justify the preliminary architecture choice. The conclusions of the study showed that choosing a D-HEX based architecture means only a 1.3% increase in total cryoplant size and energy consumption of FCC-ee. The main gain of the C-HEX option is the smaller size of the VLP return line, as well as the central location of one single HEX, reducing the number of components in the tunnel and easing the overall integration. This conclusion is subject to achieving high-efficiency on a C-HEX twice as big as the current state of the art. The current calculations for the cryoplants and QRL are based on the C-HEX design.

Helium recovery system The latest available cryomodule inventory values are 55 kg of He at 2 K per 800 MHz cryomodule, and 116 kg of He at 4.5 K per 450 MHz cryomodule [387]. Because the SRF cavities are low-pressure rated devices, the risk of inventory loss in a non-nominal scenario is high. Without a recovery system the pressure inside the helium tank of the cryomodules would start building up, in the case of non-nominal operation, eventually reaching the set pressure of the pressure relief valve first, then ultimately the burst disc. The latter is the main safety component, preventing the cavity from sustaining any mechanical damage. The scenarios that could lead to such a situation are:

- **Scenario 1:** Isolated cryomodule(s) from the cryoplant due to a malfunctioning valve.
- **Scenario 2:** Loss of the full sector cooling capacity (e.g., due to a power outage).
- **Scenario 3:** Beam vacuum break.
- **Scenario 4:** Insulation vacuum break.

Scenarios 3 and 4 generate very high mass flow rates due to the large heat load that appears after a vacuum break. Therefore, these are to be addressed with the pressure relief devices alone. The helium recovery system (HRS) will cover Scenario 1 and 2, which consist of only inherent static heat loads. The concept proposed for such a system is depicted in Fig. 8.82 and has been presented in detail in [388].

Table 8.29 Point PH cryoplants and their staging, including an overcapacity margin factor of 1.5

	Z, WW, & H	$t\bar{t}$
Type	C1	C1+ (Upgrade of C1)
Schema	See Fig. 8.83 (a)	See Fig. 8.83 (b)
50-75 K, kW per cryoplant	23.7	37.5
4.5 K, kW per cryoplant	36.4	36.6
2.0 K, kW per cryoplant	-	13.0
Nominal equivalent cooling capacity at 4.5 K per cryoplant [kW_{eq}]	39.4	82.0
Number of cryoplants required	2	2

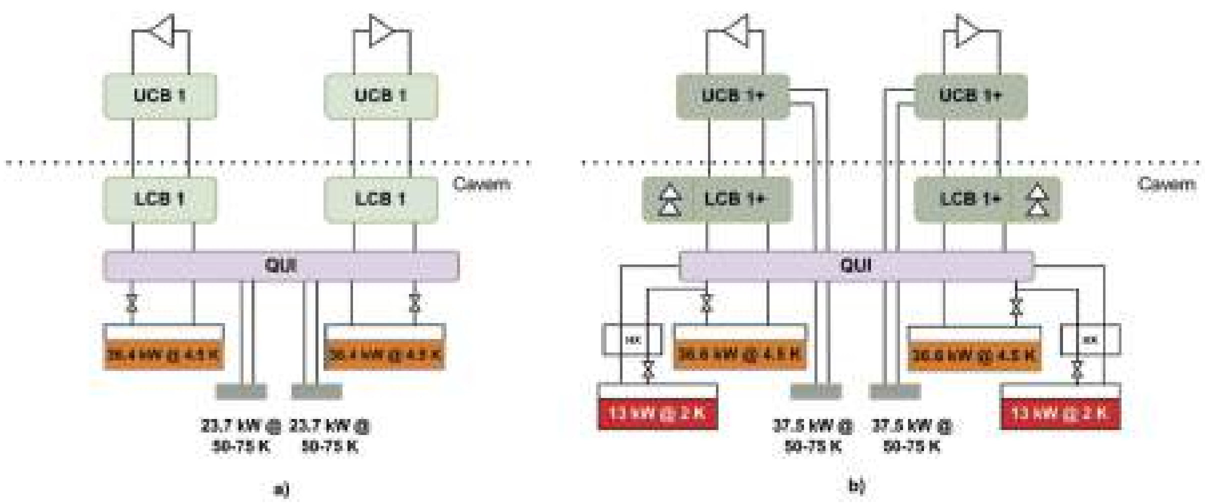

Fig. 8.83 Point PH cryoplant architecture at Z, WW and H (a), and $t\bar{t}$ (b)

Table 8.30 Point PL Cryoplants and their staging, including an overcapacity margin factor of 1.5

	Z, WW, & H	$t\bar{t}$
Type	B1	B2
Schema	See Fig. 8.84 (a)	See Fig. 8.84 (b)
50-75 K, kW per cryoplant	14.4	16.9
4.5 K, kW per cryoplant	-	-
2.0 K, kW per cryoplant	3.6	6.1
Nominal equivalent cooling capacity at 4.5 K per cryoplant [kW_{eq}]	13.3	22.0
Number of cryoplants required	1	2

8.5.3 Cryogenic plants

Table 8.29 and Table 8.30 give the nominal cooling capacity per cryogenic plant required at the various temperature levels for the technical points, including an overcapacity margin factor of 1.5.

8.5.4 Cryogen inventory and storage

The cryogenics system for the RF points will require helium and nitrogen. Nitrogen will only be needed for the regeneration of absorbers and dryer beds. Consequently, one standard 50 m^3 liquid nitrogen (LN_2) reservoir is planned for each point PH and point PL. The helium inventory is mainly driven by the cryomodule cold mass baths and the cryogenic distribution system. The combined helium inventory of point PH (collider) and point PL

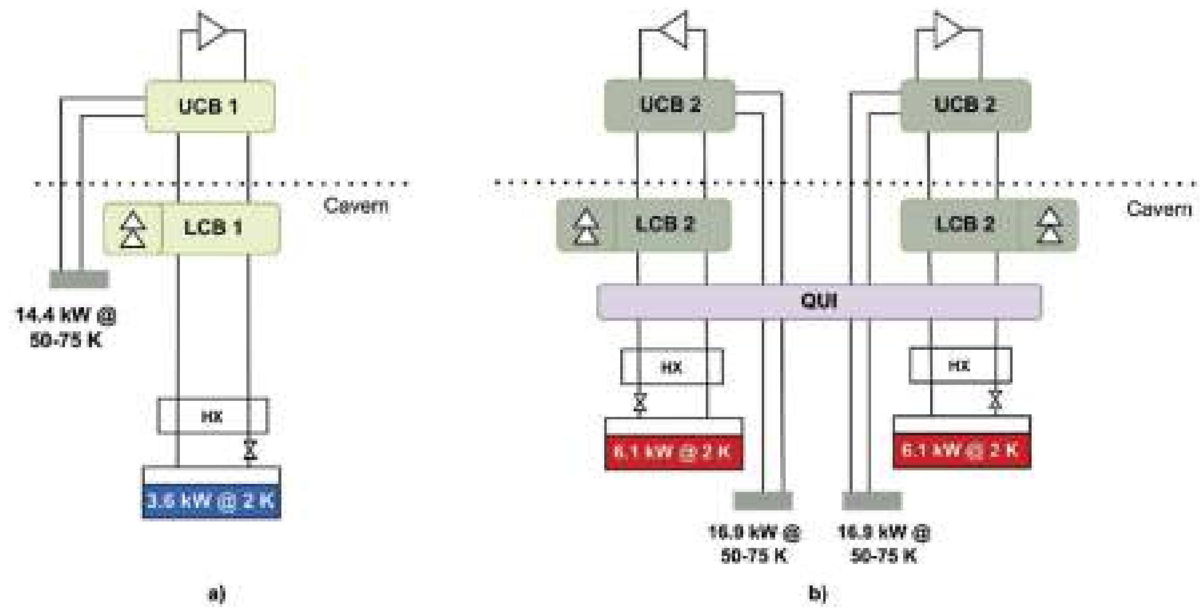

Fig. 8.84 Point PL cryoplant architecture at Z, WW and H (a), and $t\bar{t}$ (b)

Table 8.31 Inventory of helium and its storage for the FCC-ee RF points

Machine	Z, WW & H	$t\bar{t}$
Cryomodules (t)	9.2	19.4
Distribution (t)	5.0	6.0
Cryoplant (t)	3.2	7.2
Total (t)	17.4	32.7
No. of 250 m^3 MP storage tanks at point PH (collider)	21	34
No. of 250 m^3 MP storage tanks at point PL (booster)	4	12
Total No. of storage tanks (+1 auxiliary tank)	26	47

Table 8.32 Static and dynamic heat load sharing for the different FCC-ee phases

FCC-ee Machine	Z, WW & H		$t\bar{t}$	
Point	PH	PL	PH	PL
Static heat loads at 4.5 K [kW$_{eq}$]	24.8	10.4	54.8	32.5
Dynamic heat loads at 4.5 K [kW$_{eq}$]	54.0	2.9	109.2	11.6
Total heat loads at 4.5 K [kW$_{eq}$]	78.8	13.3	164.0	44.1
Dynamic heat load percentage	68%	22%	67%	26%

(booster) is 17.4 tons for the Z, WW, and H stage and 32.7 tons for the $t\bar{t}$ stage. The storage will be provided using 250 m^3 medium-pressure (MP, 18 bar) storage tanks, the total number of storage tanks required can be found in Table 8.31.

8.5.5 Economic mode for energy savings

One of the particularities of the FCC-ee is the large difference between the static and the dynamic heat loads that the cryogenic system must handle. The dynamic heat loads represent between 22% and 68% of the total heat loads depending on the machine stage and RF point. See Table 8.32, where details are given.

Due to the proportion of large dynamic heat loads and the requirement to maintain the RF cavities at cryogenic temperatures (<5 K) throughout the years between the long shutdowns (LS), the cryogenic systems must be designed in such a way that the electrical and water consumptions are optimised throughout the year.

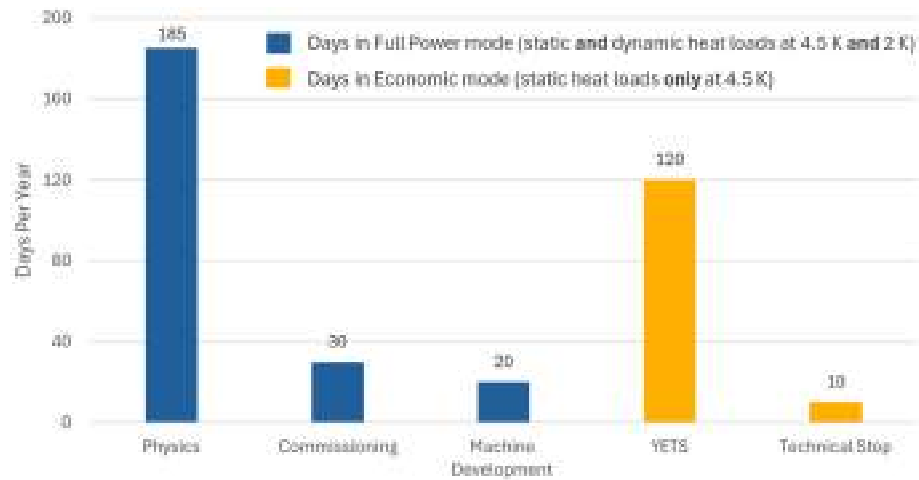

Fig. 8.85 FCC-ee yearly cryogenic operation modes between long shutdown periods

Table 8.33 Cryogenic system electrical energy consumption per year

PL and PH plants	Z, WW & H	$t\bar{t}$
Full power [MW elec]	20.3	45.8
Eco power [MW elec]	7.6	12.9
Elec energy/year [GWh] no eco mode	177.4	401.0
Elec energy/year [GWh] with eco mode	138.1	298.3
Electrical energy savings per year	22%	26%

The cryogenic system must deliver full power during the physics, commissioning, and machine development (MD) periods. During these periods the RF cavities need to be fully operational at top energy. During the end-of-year technical stops (YETS) and the technical stops (TS), all RF cavities (including the 800 MHz cavities at 2 K) will be switched off and maintained at 4.5 K using an economic mode of the cryogenic plant. During this economic mode, there will be only static heat loads from the RF cavities. In the current evaluation of the FCC-ee yearly operation [4], around 36% of the time could be operated with such a cryogenic economic mode as depicted in Fig. 8.85.

To allow these energy savings, the cryoplants must be designed taking into account these different operation modes. The coefficients of performance (COP) of the cryoplants must be optimised for the full power mode and the economic mode, where a reduced cryogenic power will be delivered. To achieve this objective in partnership with the cryoplant manufacturers, different solutions will be studied and developed. For instance, specific piping and some additional cryogenic equipment will be needed, such as smaller warm compressors with variable frequency drives and specific turbines that could be operated efficiently during this economic mode. A COP-1 of 220 W_{elec}/W at 4.5 K for the full power mode and a COP-1 of 250 W_{elec}/W at 4.5 K for the economic mode were considered for this report.

Because of the economic mode, the cryogenic system will consume less power during the YETS and TS periods. The energy consumption per year for the FCC-ee cryogenic system is shown in Table 8.33. The table includes both scenarios with and without the implementation of an economic mode. By using the economic mode, electrical energy savings of up to 26% can be achieved. Note that the cooling water system dedicated to cryogenics will also be alleviated in about the same proportion.

8.5.6 Cryogenics for experiments and MDI region

Concept The experiment points PA, PD, PG and PJ each have a detector cryoplant that covers the needs of the detector magnet, as well as a second IR cryoplant for the machine detector interface (MDI) region magnets.

Figure 8.86 shows the loads expected for the detector and IR cryoplants. In yellow is the 2 T detector solenoid, which will be cooled by a dedicated detector cryoplant. The other loads, represented in blue, will be covered by the IR cryoplant. These loads remain under study, but could include the MDI magnets, which contain focusing quadrupoles (QC**), compensating and screening solenoids, as well as the crab sextupoles (SY**). One of the detectors will also include a liquid argon calorimeter and its associated liquid nitrogen cryoplant.

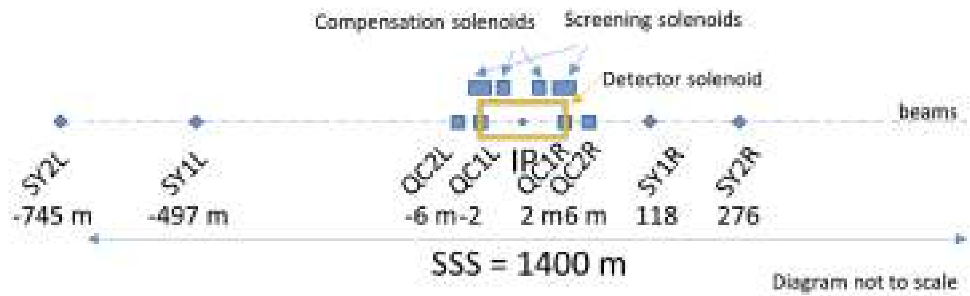

Fig. 8.86 Interaction region superconducting electrical loads

Basic parameters The current working scenario has the following cryoplants:

- Four cryoplants for the detector solenoids. CMS-like 1.5 kW_{eq} at 4.5 K plants are considered as an envelope case following the latest FCC experiment sites civil engineering and technical infrastructure review
- Four cryoplants for the IR area magnets. Further details on heat loads and the mechanical design of the cryostat will define the cryoplant size and architecture.
- One nitrogen liquefier for the detector containing the liquid argon calorimeter. An ATLAS-like 20 kW at 80 K plant is considered at this stage.

8.5.7 Cryogenics for alternative solutions

An alternative solution currently under study aims to exchange all the short straight section (SSS) warm magnets (arc quadrupoles, arc sextupoles and correctors) with superconducting ones based on ReBCO HTS tapes. The main goal of this alternative solution is power reduction. It also envisages nesting the quadrupoles and the sextupoles. Saving space and relaxing the RF system requirements and costs. The proposal involves 2900 distributed cryostats, each being 3.5 m long, affecting some 11% of the entire machine. The operating temperature is currently defined at 40 K [389]. The adoption of this solution would have a large impact on the amount of cryoplants and distribution lines that would be needed.

8.6 Transport

8.6.1 Equipment transport requirements

The transport of equipment within the underground facilities is a key activity during the installation phase. Given the current stage of the study, some of the data collected remains partial. Therefore, assumptions have been made based on similar existing projects. The identified requirements have been consolidated in the document Transport Requirements [390].

The types of items considered in the preliminary transport study include:

- Accelerator components (magnets, supports, beamstrahlung dump system);
- Power converters;
- Electrical equipment;
- Cryogenic equipment;
- Cooling and ventilation equipment.

Among these, the collider and booster ring components have the greatest impact on the design of the transport vehicles. To keep underground installation time as short as possible, certain components, such as quadrupoles and sextupoles, will be pre-assembled on a supporting structure at the surface and then transported as a single unit (QSS unit), as illustrated in Fig. 8.87.

The weight of the QSS unit is expected to be close to 14.5 t for a length of 7 m, which represents the maximum load that the vehicle will lift. The dipoles will be transported stacked in groups of three, with an overall weight close to 16 t and a length of approximately 12 m. The beamstrahlung dump system is also significant in terms of weight and dimensions, a specific preliminary study has been conducted on this topic and is summarised in the present report Sect. 8.6.1. The other elements considered are more standard (mainly pipes, racks and cable reels) and will be transported by electric tractors and trailers as is usual for CERN accelerators.

Overhead cranes and shafts Overhead cranes will be installed in almost every surface building and within the service caverns to facilitate handling operations during both the installation and operation phases.

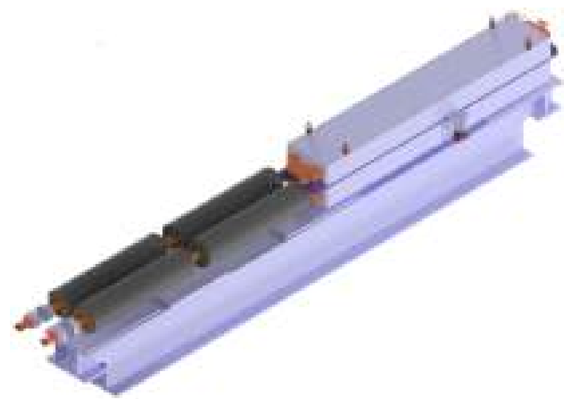

Fig. 8.87 Quadrupole with two sextupoles and the supporting girder (QSS unit)

Table 8.34 List of overhead cranes

Building	Location	Capacity [t]
Assembly hall SX†		120
Head-Shaft building SD†		75
Head-Shaft building SD‡		25
Tunnel and service areas ventilation building SU	Surface	7.5
Experiment ventilation building SUX†		7.5
Cooling plant SF		3.5
Power converters building SR		5
Compression station SH†		20
Service cavern	Underground	20

† Only in the experiment points

‡ Only in the technical points

This type of equipment is generally preferred over floor-based handling machines, such as forklifts or telehandlers, as it offers several advantages. In terms of safety, the suspension point is located above the object being handled, reducing the risk of accidental collisions or tipping. From an operational perspective, overhead cranes provide greater positioning precision, ensuring more controlled and efficient handling. The use of overhead cranes eliminates the need for wide aisles for manoeuvring and high floor load capacities, leading to potential cost savings in infrastructure design and implementation.

Table 8.34 contains the list of the overhead cranes foreseen to be installed in the facilities of the experiment and technical points.

The overhead cranes will comply with the relevant European Directives (currently the Directives 2006/42/EC [391], 2014/30/EU [392] and 2014/35/EU [393]) and the CERN Safety Rules. According to the expected frequency of use (intensive during the installation phase, very low during the operation phase) and the load spectra (the maximum load will rarely be lifted), they will be considered as light/medium duty overhead cranes and classified as A4-M4 according to the FEM (European Materials Handling Federation) guide 1.001.

The hoist design will incorporate specific features to ensure that the crane is suitable for handling fragile components with high precision in positioning. The hoist will be equipped with two ropes, ensuring that the hook is lifted and lowered without horizontal drift, thereby minimising the risk of unintended movement. Additionally, all motors will be driven by inverters, allowing for smooth acceleration and precise control during lifting and lowering operations.

The speed values will be set in the following ranges:

- Lifting speed: 8 to 10 m/min;
- Cross-travel speed: 12 to 15 m/min;
- Long-travel speed: 15 to 20 m/min.

Table 8.35 Characteristics of shaft cranes

Overhead crane	Sites	Capacity [t]	Lifting height [m]
Assembly hall crane	PA, PD, PG, PJ	120	253
Head-shaft building crane type A	PB, PH, PL	25	253
Head-shaft building crane type B	PF	25	400
Head-shaft building crane type C	PA, PD, PG, PJ	75	253

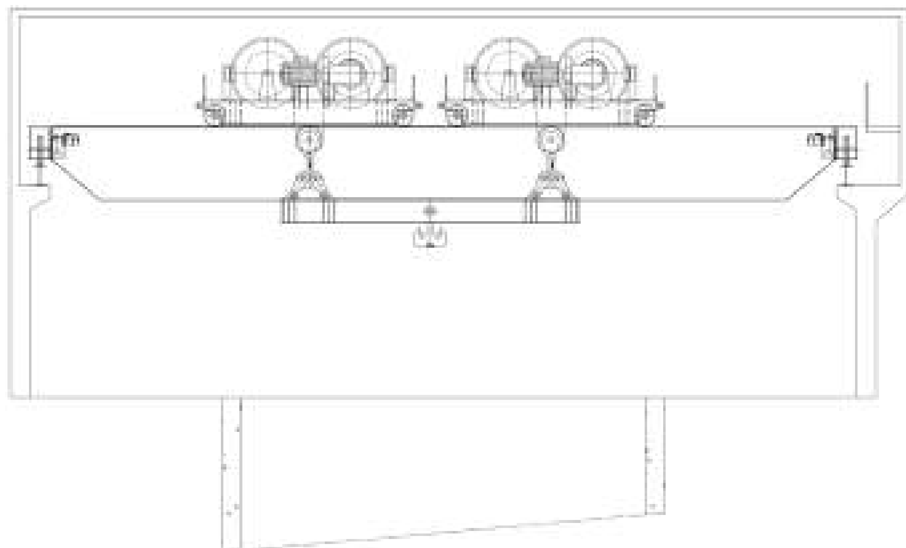

Fig. 8.88 Concept of shaft crane

Each building layout will ensure safe access to the cranes during preventive and corrective maintenance (e.g., a walkway at the side of the railway). Access to any position where the crane may stop in the event of a breakdown will be possible.

Shaft cranes The overhead cranes installed in the assembly halls and in the shaft-head buildings will require a bespoke design due to their particular lifting heights, as shown in Table 8.35. The overhead cranes in the SD buildings of the experiment points have a capacity of 75 t in order to allow the handling of the FCC-hh magnets in the future. This will avoid expensive modifications of the cranes and buildings arising from increasing the capacity from 25 t to 75 t.

To minimise the overall dimensions of the hoist while accommodating the required rope length, the cranes will be equipped with two trolleys, each capable of lifting approximately 55% of the crane's total capacity. When handling a full-capacity load, both trolleys will operate together, using a spreader beam (see Fig. 8.88).

Each trolley will house two independent hoisting units (motor – gearbox – rope drum) that support the hook block. Under normal operating conditions, both hoists will function simultaneously, with the rope winding evenly across both drums.

This configuration provides mechanical redundancy in the event of a hoist component failure. If any component of one hoist malfunctions and prevents normal operation, the other hoist will still be able to complete the lifting operation. In such a scenario, the rope will be wound on the functioning drum in a double-layer configuration, ensuring continued operation and safety.

The design of the shaft cranes will also include the following specific features:

- Emergency brake on each rope drum to avoid dropping the load should any element of the hoisting drive chain fail;
- FEM classification of the hoist gearboxes: M8
- Hoisting speed at full load: 15 m/min - hoisting speed without load: 30 m/min
- Laser sensors, encoders and a programmable logic controller (PLC) to control the hook position at any moment.

The cranes will also be equipped with a dedicated monorail, installed below one girder, hosting a traversing trolley on which a platform is suspended. The platform allows personnel access inside the shaft in both the construction and operation phases to install or maintain the technical infrastructure (e.g., ventilation ducts).

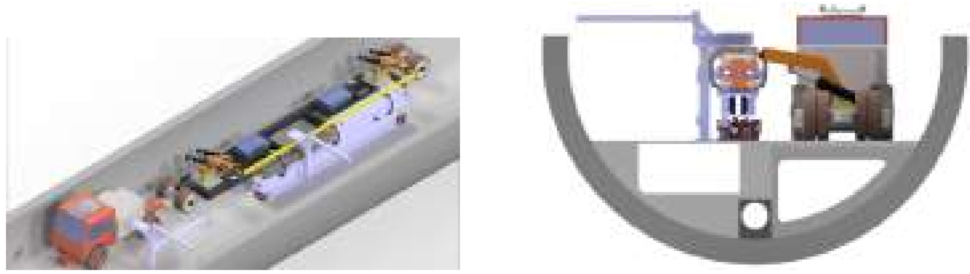

(a) (b)

Fig. 8.89 Transport and installation of a QSS unit

In the coming five years, CERN will also test a new technology for the lifting ropes, based on textile ropes instead of steel ropes, which reduces the overall weight suspended from the structure of the crane and, therefore, optimising the overall crane design and cost.

Underground transport vehicles The diversity of magnets to be transported creates a number of different requirements for the transport and handling technology in the tunnel. The basic principle will consist of two types of trailers, which are specially equipped with the technology required for the particular magnet transport and magnet handling. A detailed study is accessible in Ref. [394], based on QSS units of 11 t and dipoles of 3.7 t. In 2024 the design of the magnet has been updated with QSS units of 14.5 t and dipoles of 5 t, however, this change does not have a significant influence on the design of the vehicle, the main outcome being that the outer width may increase by 200 mm maximum, which still fits inside the transport volume.

The underground transport vehicles will be composed of convoys, each consisting of two tractors that can move in both directions and a specialised trailer designed for transporting and handling magnets within the regular arcs. There are two main categories of magnets and assemblies to be transported, both for the collider and the booster, each with specific weight distribution characteristics requiring adapted trailers. The dipole magnets are long and relatively light, with a unit weight of 5 t and 12 m long, whereas the QSS units are shorter and heavier, weighing up to 14.5 t and 7 m long.

The tractors and all actuators on the trailers will be fully electric, eliminating exhaust gas emissions and reducing noise in the tunnel during magnet assembly. The tractors and trailers will be powered by battery systems, requiring the installation of charging stations in the service caverns to allow recharging during vehicle downtime periods, such as magnet loading and maintenance. The battery-powered approach is preferred compared to a conductor rail system, as it provides greater flexibility, requires no additional tunnel infrastructure, and enhances safety by eliminating exposed live electrical components. Additionally, battery technology is expected to improve in capacity and reliability in the coming years, further strengthening this choice.

The specialised trailers will be loaded with magnets at the base of the service cavern shafts, which will be equipped with the necessary infrastructure for lowering them into the tunnel. Autonomous driving will be implemented for the journey from the shaft/loading area to the installation points in the tunnel, minimising personnel requirements and improving operational efficiency.

To accommodate vehicle movements, enlargements are planned at every alcove, following a fixed pattern determined by the alcove locations. These enlargements will allow vehicles to pass or overtake when necessary, and can also serve as evacuation points in case of an emergency. However, the baseline approach for magnet transport is to operate overnight without personnel present in the tunnel, thereby avoiding co-activity with workers. While interventions by personnel during magnet transport have not been entirely ruled out, additional compensatory safety measures would need to be implemented to ensure proper evacuation procedures in such cases.

The handling technique relies on three-axis movement. First, the components are lifted vertically from the trailer. Once at the required height, a movable arm equipped with gripping technology places the components onto jacks. Finally, a fine longitudinal adjustment can be made using the gripper, ensuring precise positioning of the magnets.

Transport of quadrupoles and sextupoles The QSS unit represents the biggest weight requirement for the equipment. The special trailer (shown in Fig. 8.89) which has the capability to carry the QSS unit is equipped with a damping system that protects the load from small bumps in the surface of the carriageway during travel through the tunnel. Hydraulic cylinders (alternatively electric cylinders) will be used by the handling system to generate the necessary force to move the load to its final destination. The hydraulic cylinders perform the main movements while placing the steel girder on top of alignment blocks.

Motors on the gripping system will allow the final fine adjustment longitudinally, due to the limitation in accuracy of the positioning of the whole convoy (as shown in Fig. 8.90).

(a) (b)

Fig. 8.90 Detail of the gripping system

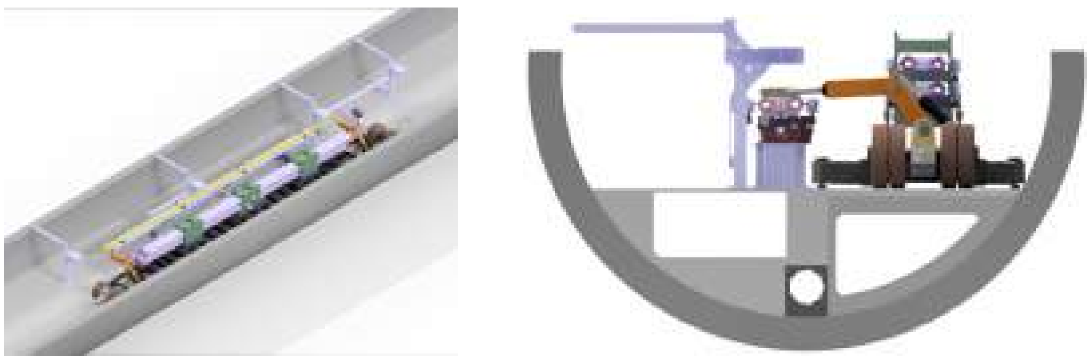

(a) (b)

Fig. 8.91 Transport and installation of 3 dipoles

Transport of dipoles The dipoles are nearly 12 m long and are the longest items to be transported; they require dedicated equipment for their transport and handling. The trailer which is planned for carrying the dipoles has the capability to carry three dipoles at one time, thereby increasing transport efficiency (see Fig. 8.91).

To enable the transport of three dipoles as a single load, the dipoles will be stored in a specially designed rack. The rack can be raised and lowered by the spindle lifting gear so that the handling system can always pick up the dipoles and place them in their final destination from one position.

Transport of booster ring components The components of the booster ring are mounted above the collider ring. The trailers for the dipoles can install magnets on both the collider and the booster, the same strategy applies for trailers dedicated to the QSS units.

Lifts The lifts will comply with the relevant European Directives (currently 2014/33/EU [395]) as well as CERN Safety Rules and EN standards. The lifts will use state-of-the-art technologies like those used in high-rise buildings, which already cover heights of up to 450 m. Two lifts will be installed at the technical points in each of the four shaft-head buildings, while four lifts will be installed at the experiment points within the service shafts in each of the four shaft-head buildings. Lifts are the only authorised means of personnel access to and from the underground areas, making their reliability and safety critical. To enhance safety, the lift shaft concrete modules will be overpressurised, preventing the ingress of contaminants or smoke in the event of an emergency.

The lifts will be powered by the secure power network, ensuring they remain fully operational even in the event of a failure of the standard electrical network. To further improve safety, operational efficiency, and maintenance availability, each lift shaft module will be equipped with two lifts, providing redundancy and easing access and maintenance operations.

The lift capacity and speed have been determined based on the results of evacuation simulations [396]. A maximum cycle time of 4 minutes has been defined, covering the entire process from people entering the lift, travelling from underground to the surface, and exiting the lift. This calculation assumes a shaft depth of 400 m and a lift speed of 4 m/s.

During the LHC programme, approximately 80% of the non-machine components were transported using lifts, suggesting that a similar proportion will apply to FCC. After evaluating different options, lifts with a 3 t capacity

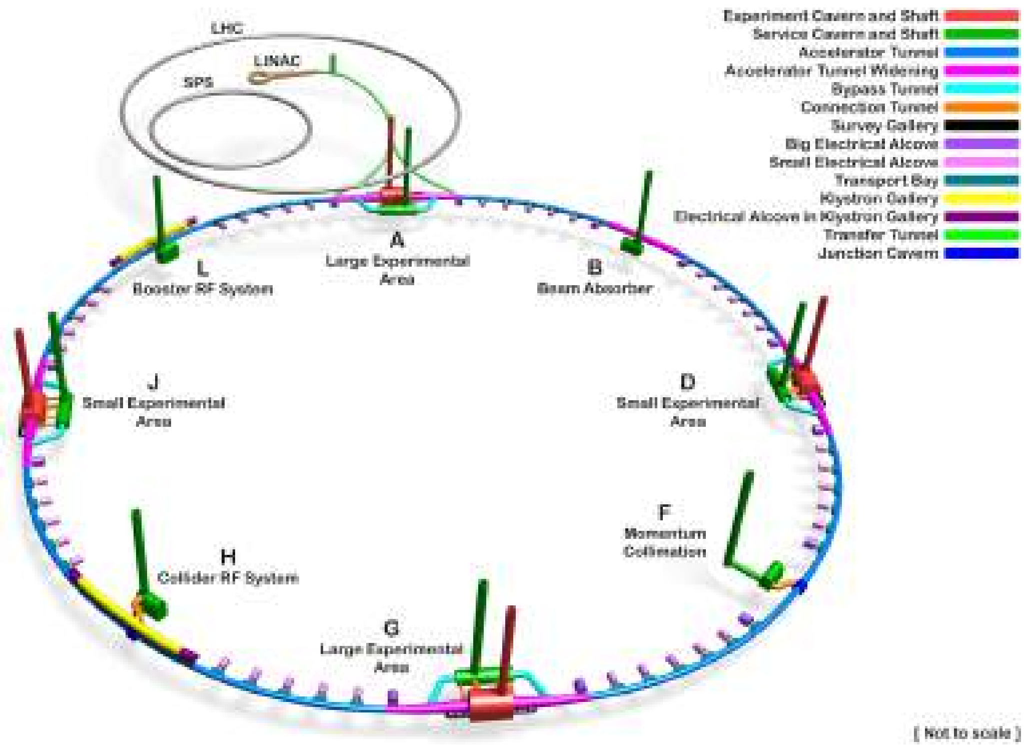

Fig. 8.92 FCC-ee Layout including machine tunnel widening areas

were chosen as the baseline solution, as they offer the best cost-to-capacity ratio while meeting the project's operational and logistic requirements.

The main characteristics of a lift are:

- Speed: 4 m/s;
- Capacity: 3000 kg/38 persons;
- Shaft height: (up to) 400 m;
- Car (length × width × height): 2700 mm × 1900 mm × 2700 mm;
- Door (width × height): 1900 mm × 2700 mm;
- Shaft width: 2750 mm;
- Shaft length: 3750 mm;
- Headroom: 7700 mm;
- Pit depth: 5900 mm.

Preliminary detailed handling studies in LSS sections in PA and PB The underground areas, identified as 'Machine tunnel widening' areas in Fig. 8.92, are zones where handling processes will be studied in detail since the configuration of the machine elements is different from the regular arcs. The input from the beam optics induces tunnels with specific configuration and handling challenges.

Studies based on the preliminary design of the beamstrahlung dump system, located 500 m away from the interaction point on each side of each experiment cavern, have been performed to determine the possible handling process and equipment to install it. The same conceptual study was performed for PB, hosting the beam dump system of the collider and the booster. Details can be found in Ref. [397]. The handling and installation of the beamstrahlung dump system is feasible using a mobile crane and a standard electric tractor pulling a trailer. This avoids the installation of an overhead crane above each system, allows the reuse of the mobile crane for the installation of several systems, and helps reduce the size of the cavern required to install this system (see Fig. 8.93).

Due to the limited space between beam lines in the area, the handling and installation of components in PB will be done by overhead cranes above the beam lines and beam dumps. Specific overhead cranes with a capacity of 20 t will be installed above each beam dump system to allow their installation and maintenance, as their weight is significantly higher than the elements of the beam lines estimated to be up to 5 t (see Fig. 8.94).

Once the final design of the machine components in this area is available, a detailed handling study will be performed in order to determine the most optimised handling strategy both for the installation and operation phase.

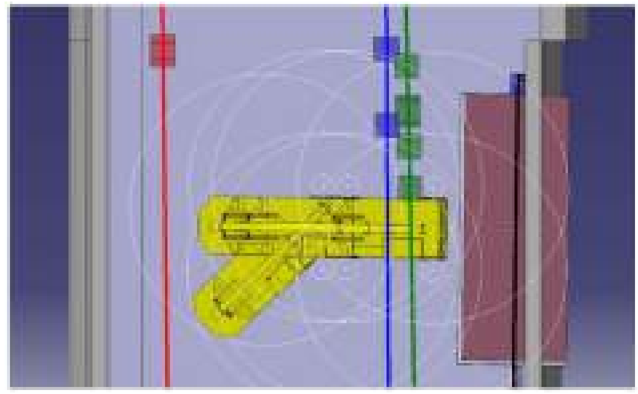

Fig. 8.93 Handling study for the beamstrahlung dump system

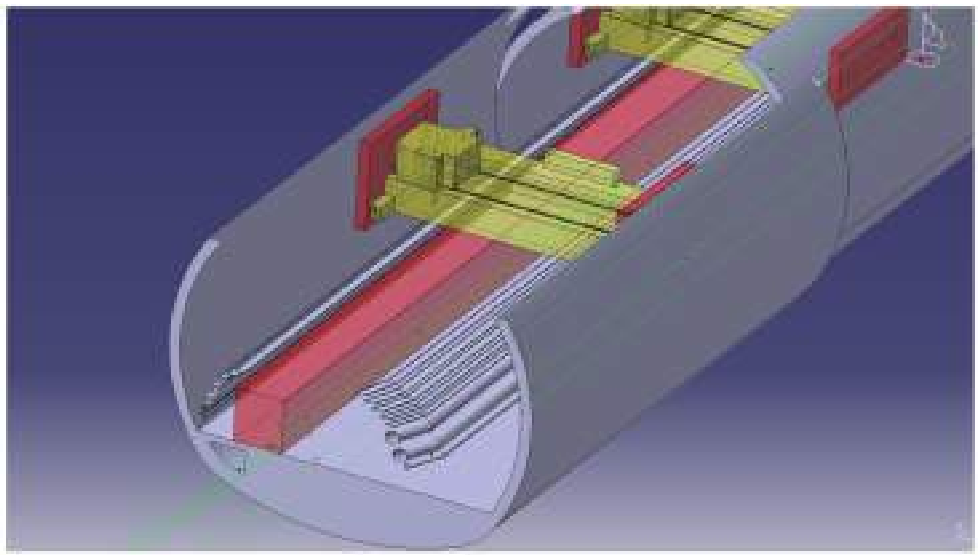

Fig. 8.94 Handling study in point PB, beam lines are highlighted in green

8.6.2 Logistics

Material flow simulation Logistics is of great importance for the construction, assembly, and operation of the FCC. An event-discrete material flow simulation study has been conducted to integrate all the dynamic interdependencies to create a robust schedule, identify bottlenecks and potential improvements, and estimate the resources required. Figure 8.95 shows the tunnel model which was developed. In addition, the corresponding necessary process flows and dependencies were defined and abstracted so that they could be integrated into the digital model. The simulation was run using Tecnomatix Plant Simulation©.

The underlying input parameters and handling strategy are described in Ref. [394]. Several sets of simulations were developed, allowing the identification of the optimised scenario: the dipole magnets will be handled through the experiments point service shafts, the QSS units will be handled through the technical points service shafts. This allows the workload of the shaft cranes to be balanced and optimisation of the overall arc transport time.

The main final outcome is that the effort required to handle the dipole magnets from experiment points to their final location in the arcs is 1200 man-hours or 75 days working in two shifts. The effort required to handle the QSS assemblies from the technical points is 1392 man-hours or 87 days working in two shifts. This result is compatible with the original assumption of 100 days duration and provides contingency in case of failure or logistic chain discontinuity. The workload of the shaft cranes allows the installation of two arcs from the same surface point to be performed in parallel, if the final schedule requires doing so. At the beginning of the simulation, it is assumed that the tunnel civil engineering has been completed and the general services technical infrastructure (cooling and ventilation, cabling, supporting jacks etc.) is installed so that the tunnel is ready for magnet transport. The logical flow of the programmed process is illustrated in Fig. 8.96.

The quadrupoles and sextupoles are pre-aligned on the girder and assembled into transport units. As described earlier, three dipoles can be grouped and transported simultaneously as a dipole pack. The magnet transport vehicle is designed to carry one QSS unit or one dipole pack at a time. During magnet transport operations, no other traffic will be present in the tunnel to ensure safety and efficiency.

Fig. 8.95 Tunnel model developed for logistics studies

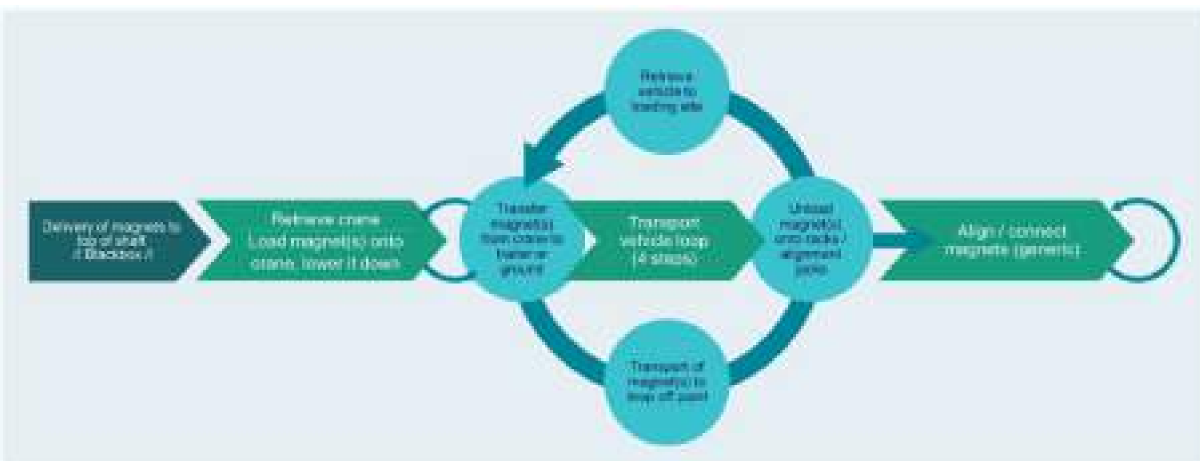

Fig. 8.96 Programmed logistic process

To enable continuous transport operations, a variable number of magnets can be stored underground at the bottom of the shafts. Simulations indicate that a buffer of three QSS units or three dipole packs in the underground service cavern allow smooth operation. Expanding this buffer to 16 dipole packs and 8 QSS units would provide a one-day operational margin, mitigating potential disruptions in the surface logistics chain.

Magnet transports will not be scheduled to pass through areas where installation teams are actively aligning and connecting the magnets, as this approach optimises transport times. While co-activity of simultaneous transport and installation could be possible by reducing convoy speed to enhance safety, it is not included in the baseline plan due to its impact on efficiency.

The collider ring and booster ring can be installed simultaneously during the same installation phase, thanks to the flexibility of the trailers. On the surface sites, storage areas are planned near each shaft, with a capacity of two days (equivalent to 32 dipole packs or 16 QSS units) to facilitate direct crane loading.

It is important to note that the time required for aligning and connecting the magnets remains an estimate at this stage. As a result, any conclusions drawn based on this parameter should be interpreted with caution.

Magnet production flow simulations As detailed in Ref. [398], the anticipated manufacturing timelines for dipoles, quadrupoles, and sextupoles are aligned with the current FCC-ee installation schedule. By targeting an average production throughput of 18 magnets per day, manufacturing and installation can proceed in parallel, ensuring timely deliveries while allowing sufficient time for R&D and procurement activities prior to full-scale production. This assessment confirms that the planned manufacturing rates are adequate to support the on-time installation phase, demonstrating the overall feasibility of the FCC-ee magnet production strategy.

Surface transport of 240 t transformers and 60 t magnets The transport of equipment exceeding 24 t in a single unit requires an exceptional convoy and, in some cases, modifications to public roads to ensure feasibility. The heaviest piece of equipment identified in the project is the high-voltage transformers to be installed at sites PA, PD, and PH. A study [399] has confirmed that these transformers can be transported to site PH via four different routes with exceptional convoy procedures and limited modifications to public roads.

The second heaviest equipment in the project consists of the cryo-dipoles for the FCC-hh machine, which have according to today's estimates a unit weight of approximately 60 t and a length of 15 m. A separate study [400] demonstrated the feasibility of transporting these magnets to their final destination along the last kilometres leading to sites PA, PD, PG, and PJ, where service shafts are sufficiently wide to accommodate the handling of 15 m-long magnets.

Overall surface road transport volumes for FCC-ee installation The scenario involves logistical planning for the transport of equipment on public roads. A key consideration is limiting the potential impact of daily transport operations. The most transport-intensive phase will be the magnet installation, during which the daily traffic per site is expected to remain below 10 trucks per day under the current schedule. This corresponds to an average of approximately one truck per hour, ensuring a steady, manageable flow of transport. Further details on transport logistics and planning can be found in Ref. [401].

Handling for experiments Handling activities in the experiment caverns will be conceptually similar to those currently carried out for the LHC Experiments. Detector components will be lowered to the cavern from the assembly hall through the shaft directly connecting the two facilities; this will be done with the overhead cranes installed in the surface hall. The components will then be handled with two overhead cranes installed inside the experiment cavern; each of them will have a capacity of 20 t. These overhead cranes will have the same characteristics as described in Sect. 8.6.1 plus the additional features listed below:

- the hoist gearbox will include a differential unit which allows the installation of a second hoist motor; this motor will be used for operations at very low speed (of the order of 0.3 m/min) which is usually requested for the precise assembly of detector components;
- an emergency brake on the rope drum to avoid dropping the load if any element of the hoisting drive chain fails.

Personnel access to the various parts of the detectors will be facilitated by mobile elevating working platforms (scissor and boom lifts).

8.6.3 Personnel transport

Requirements for personnel transport vehicle Throughout all stages of the life cycle, personnel will need to be transported from the vertical shafts to their designated workplaces. Following the handover of the shafts and tunnel from civil engineering, the installation of general infrastructure, such as electrical cabling, cooling, and ventilation, will take place, followed by the placement and connection of magnets. Various specialists will be required for these installation tasks, with the number of personnel varying depending on the specific phase of the project.

Once the collider is in operation, there will be technical and unplanned stops during which maintenance teams will enter the tunnel for repairs, inspections, and system upgrades. The safety requirements for personnel transport are outlined in Sect. 9.4.1, and further details can be found in Ref. [394].

The maximum distance between two shafts is 11 km, meaning that when some shafts are closed for access, the longest round-trip distance for personnel transport could be 22 km. To ensure efficient transport and minimise travel time, vehicles should be capable of speeds up to 30 km/h.

Fire doors installed in the tunnel define the maximum permissible vehicle size. Personnel transport vehicles should be able to pass each other to avoid blockages during evacuations and provide operational flexibility. The maximum driveway width is 2.2 m, and the maximum allowable vehicle height is 2.25 m. This allows vehicles to have a maximum width of 0.8 m, ensuring a 0.2 m clearance between vehicles as they pass, as well as between the vehicles and tunnel walls or machine equipment (see Fig. 8.97).

Based on these requirements, a design of a vehicle for four people has been established (see Fig. 8.98), the other constraint being the length of the vehicle to ensure maneuverability inside the tunnel (see Fig. 8.99).

The vehicles should be capable of autonomous driving using contour navigation, minimising the need for additional infrastructure. However, manual steering should remain an option for emergencies, maintenance, and

Fig. 8.97 Concepts of vehicle circulation in the regular arc

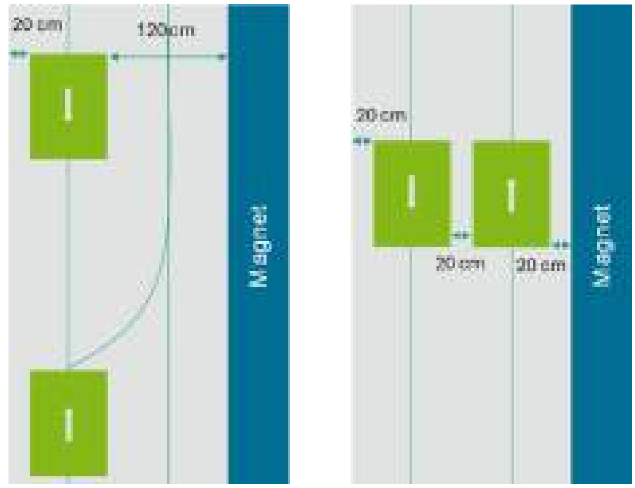

(a) (b)

Fig. 8.98 Dimensions of the conceptual design of the personnel transport vehicle

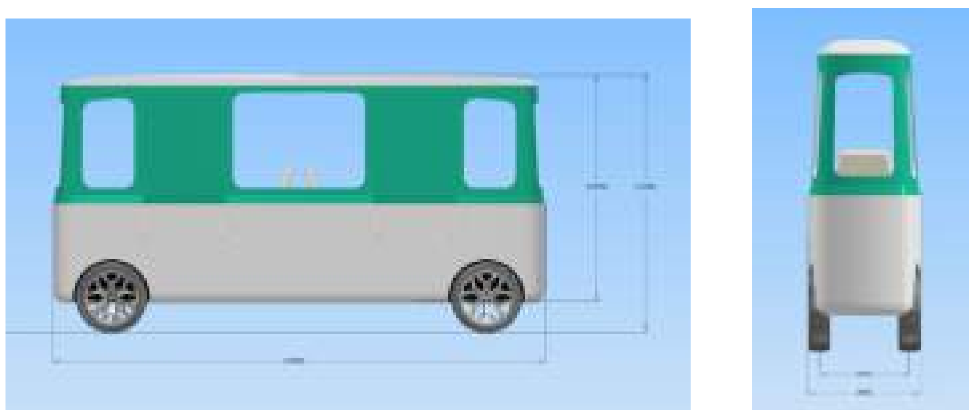

(a) (b)

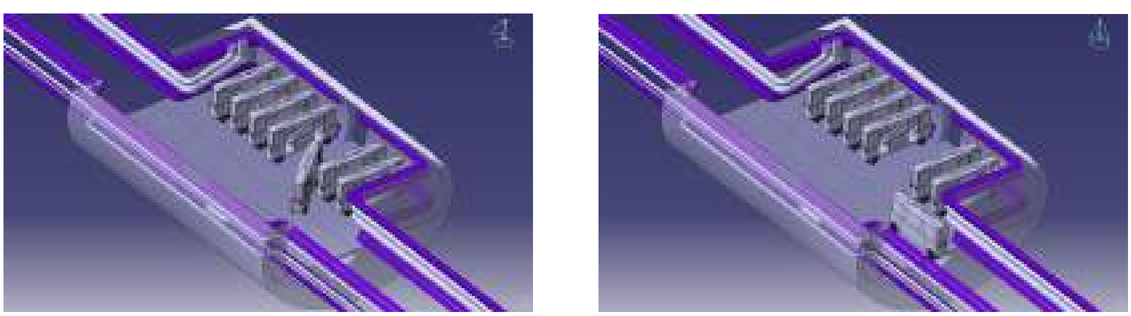

(a) (b)

Fig. 8.99 Illustration of manoeuvre of personnel transport vehicles in and out parking place

operational flexibility. The vehicles will be battery-powered, with an estimated range of approximately 200 km based on an available volume of 216 L. This autonomy is sufficient, allowing for over six hours of continuous operation at full speed or nine round trips along the maximum distance of 22 km. During peak times, up to 200 people may be present in a single sector, requiring 50 vehicles per arc, with designated parking positions in each alcove (see Fig. 8.99).

Fig. 8.100 Obstacle detection systems

Operation concept The concept of operation requires a distinction between the installation and operation phases of the accelerator, as each has distinct conditions. During installation, large quantities of materials must be transported to specific work sites, following a clear workflow. In contrast, the operation phase involves maintenance and other tasks distributed throughout the entire tunnel.

The main challenge during the installation phase is the simultaneous transport of materials and personnel within the tunnel. To minimise interference, the most effective approach is to prevent intersections of material flow. The baseline strategy for the magnet installation phase - the most transport-intensive phase - is to schedule material transport operations overnight while installation work takes place during the day. This method ensures better coordination and reduces congestion in the tunnel.

This night-time transport strategy can also be selectively applied to other phases where material movement is expected to be significant, such as the delivery of cables and pipes before their installation. However, in some cases, the presence of personnel near moving vehicles will be unavoidable during installation activities.

To enhance safety, personnel transport vehicles will be equipped with collision avoidance systems to detect and prevent accidents involving workers and obstacles within the transport zone. These systems will account for potential hazards, including toolboxes, materials, or personnel, ensuring safe and efficient tunnel operations (see Fig. 8.100).

The speed of the vehicles will be reduced in zones where activity is detected, ensuring safe coexistence of movement and ongoing work. For both the installation and operation phases, two scenarios for personnel transport can be defined:

- Groups of people use a vehicle assigned to them, after drop-off the vehicle will park in the closest alcove during the whole stay in the tunnel;
- Groups of people use a vehicle to get to their place of work, the vehicle then moves somewhere else to pick up the next team.

The two scenarios will be used depending on the type of work to be performed. The first scenario will be typically the one used for punctual work in several locations, the second being more dedicated to teams working in a fixed place.

Evacuation concept The personnel transport vehicles will be parked in the lay-by zones of the alcoves. The maximum number of workers per arc is limited to 200, meaning that up to 50 vehicles may be required per arc, ensuring that each worker always has an assigned seat in a vehicle for evacuation purposes. Figure 8.99 illustrates how seven vehicles can be parked in the small lay-by zones, providing a storage capacity of 49 vehicles per arc. Additionally, 20 vehicles can be parked in the service caverns at each point, offering contingency parking spaces to support traffic management.

The current installation schedule foresees work being carried out simultaneously in all eight arcs, requiring a maximum of 400 personnel transport vehicles across the entire accelerator. However, further studies on detailed installation scenarios may help optimise this number, particularly if it is possible to reduce the number of personnel present in a single arc during certain phases. Such an optimisation would require a real-time personnel and vehicle tracking system, ensuring that each worker always has a seat available in an evacuation scenario.

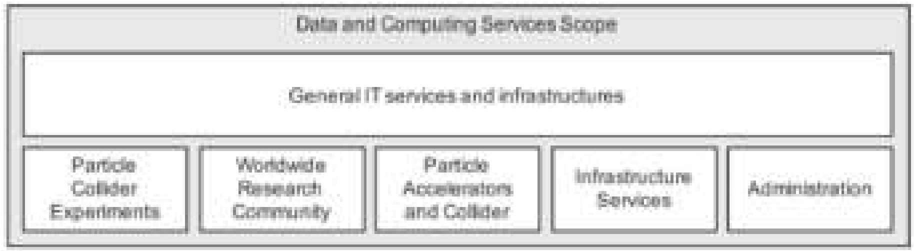

Fig. 8.101 Users and services of communication services

Current state of investigation Ongoing studies have led to the design of a vehicle that meets all dimensional, manoeuvrability, and autonomy requirements. The main challenges associated with these vehicles are their autonomous driving capabilities and the management of the fleet, both for daily operations and emergency evacuations.

CERN has prior experience with autonomous driving technologies. In addition, the industry has made significant advances in autonomous vehicle technology, with some manufacturers offering autonomous forklifts capable of operating safely alongside personnel. Modern factories, such as for example car manufacturing plants, are today typically deploying autonomous vehicles alongside human personnel. The challenge will be to integrate this autonomous functionality into a custom-designed personnel transport vehicle.

Fleet management presents another key challenge, as it requires integrating data from multiple systems, including safety systems, personnel tracking, and vehicle localisation. This integration will allow a centralised system to issue real-time instructions to each vehicle, ensuring efficient operations under normal conditions and coordinated response in case of evacuation. The development of this system will be addressed in a later phase.

8.7 Communications, computing and data services

The following sections outline the key components required for the computing infrastructure of the FCC, based on the Future Circular Collider Conceptual Design Report, Volume 3 [10]. These sections detail the equipment and infrastructure necessary to support data, voice, and radio communications, as well as the broader computing infrastructure. The document has been developed drawing on experience from previous colliders, particularly the LHC, to ensure a robust and efficient design.

The set of services and users was introduced in Ref. [10]. For completeness, it is depicted in Fig. 8.101.

8.7.1 Communication services

The FCC will require the same communication services portfolio as provided at the LHC. These services include:

- The site-wide campus network, including Wi-Fi coverage,
- The high-performance data centre network,
- The dedicated technical network supporting accelerator operations and control networks for experiments,
- CERN's fixed and mobile telephony services,
- The TETRA digital radio service for the Fire Brigade and site guards, and
- Support for IoT devices, including a LoRaWAN infrastructure.
- WhiteRabbit network for timing distribution and synchronisation of all accelerator machines.
- Access control and video surveillance systems
- CERN Safety Alarms Monitoring (CSAM) system

To support the diverse services and technologies required for communications, three independent infrastructures will be deployed within the FCC facilities to enable data, telephony, and radio networks. While these three communication systems operate on separate network equipment, they will all rely on a shared fibre infrastructure that will interconnect the FCC's surface and underground facilities with the rest of CERN.

It is important to note that the choice of fibre infrastructure will have a significant impact on the equipment and associated costs required to implement data, telephony, and radio services.

The following sections present the fibre infrastructure solutions currently under consideration for the FCC, along with the requirements for data, telephony, and radio networks.

8.7.2 Fibre network deployment

Three different possibilities are being evaluated:

- Deploy the cables on the surface. This might be very complicated, given the size of the FCC and the distances between the points. Laying the cable on the surface will require agreements with multiple entities.
- Deploy the cables underground using the tunnel. The main issue with this approach is the level of radiation that will affect the cable. Presently, there are two types of fibre optic channels: the standard one and a more radiation tolerant version. The price difference is very significant; therefore, placing standard cables and shielding them behind concrete might be more economical.
- Rely on existing telecommunication operators. This approach has issues regarding the management of the network. The planning of interventions will also be more cumbersome. Moreover, there is the risk of locking in with a single operator.

Another key aspect under study is the network topology. In the LHC, a star topology is used, where each point has direct and redundant access to the CERN Computer Centre. This design provides a resilient and efficient architecture, simplifying traffic exchange at the data centre, which serves as the central hub for all infrastructures, including the internet, WLCG, experiments, and GPN. While this star topology remains the preferred design for the FCC, the final decision will depend on the optical fibre deployment strategy and whether the fibre infrastructure will be owned by CERN or an external entity.

Additionally, the connections between the alcoves and access points are being carefully designed. In the LHC, each alcove is directly connected to the two access points of its sector. However, in the FCC, with seven alcoves per sector, an alternative approach is being considered: a daisy-chain topology, where each alcove is connected only to its two nearest alcoves or access points. This solution would significantly reduce the number of fibres required but would come at the cost of reduced resilience in case of network failures.

8.7.3 Telephony and radio networks

This section covers the voice and radio communication services requirements for FCC's facilities and experiments. The 'red phones' currently installed in the LHC are required, and a radiation resistance study should be carried out. The fixed telephony [402] is currently based on IP phones on the surface and the CERNPhone application [403].

In the LHC, CERN IT provides a mobile voice and data services [404], a TETRA [405] radio network for the fire brigade, and a LoRaWAN network [406] for battery-powered wireless sensors to the accelerator chain and the experiments via a radiating cable. WiFi is only available on the surface, the alcoves and certain areas of the experiments, such as the WiFi access points, are not radiation-free, and the WiFi frequencies are too high to be injected in the radiating cable.

The deployment of the radiating cable is essential to ensure the availability of mobile and TETRA services in the accelerators and experiment areas. Since the FCC environment may expose the cables to higher radiation levels than those currently supported, a study is underway to assess their long-term durability. The cable must be installed in a way that provides a direct line-of-sight for service users—such as personnel, robots, and sensors—while also optimising its placement to extend its lifespan.

By the time the FCC could become operational, telecommunications technologies will have evolved further. Current trends suggest a convergence of mobile telephony, TETRA, and IoT services into future mobile network generations (5G and beyond). While the specific technologies may change, the core services - including mobile data, voice communication, IoT connectivity, and safety functions - will remain fundamental.

From a deployment point of view, there are three points to be assessed:

- Interconnection:
  - Fibres between one or several central points, today Meyrin and Prévessin, and all the FCC access points.
  - Fibres between each FCC access point and its adjacent alcoves.
- Radio equipment:
  - Mobile/TETRA/LoRaWAN radio emitters: 1 rack per access point, 1 per alcove and probably 1 extra for each large experiment.
  - If safety is a concern for these services (as is the case today for TETRA), the racks should have a secure supply with backup from diesel generator sets and/or UPS.
- Antennae to emit the radio signals:
  - Radiating cable in all the tunnels and experiments.

8.7.4 Data network

The data network design of the FCC will follow the same approach as the LHC, as described in the LHC Computing TDR [407]. It is based on a tiered structure, with CERN being the Tier-0, several remote sites, or Tier-1s, connect directly to CERN and store, analyse and redistribute the data to other Tier-2 institutes. Connectivity from CERN to Tier-1's and other WLCG members is established through the national research and education networks, and the FCC will not impact its structure, apart from the foreseeable increase in capacity and members.

The networks at CERN are composed of several independent infrastructures. Following today's LHC design, the FCC network will need to offer user connectivity to:

- General Purpose Network (GPN): CERN's Campus Network offering Internet access, wired and wireless connectivity to users.
- Technical Network (TN): Control network critical for the management and operation of the accelerators.
- FCC Computing Grid (equivalent to today's LCG): High-bandwidth network connecting the server farms in the FCC experiments to the datacentres for data storage at the Tier-0 and communication with the Tier-1 and Tier-2 centres.

The FCC network will be composed of passive and active equipment. The passive equipment, providing the physical media to support data communication (mostly fibre and UTP), will include around 260 starpoints with racks, patch panels, patches, and the fibre infrastructure to connect each starpoint to the upper element in the topology, either FCC points or the datacentres. The starpoints will also house the active network equipment.

The active equipment, enabling data communication, will mainly include switches, wireless access points and routers. Based on today's LHC scale and user density, 300 and 280 switches will be needed for TN and GPN respectively. Around 600 access points will be needed to provide wireless coverage in the surface buildings, underground facilities and alcoves. To interconnect all FCC facilities to both TN and GPN networks, 34 routers will be required. While today the GPN and TN infrastructures are completely separated and use different passive and active equipment, some economies could be made in the future by sharing the equipment and using virtualisation to implement the separation.

As mentioned in Sect. 8.7.2, the fibre network deployment will have an important impact on the way the network topology is built and how alcoves, buildings and FCC points will be interconnected.

- Starpoints in the alcoves should, ideally, be connected to their closest FCC points to provide redundant TN and GPN access. Fibres could be direct to the points or patched between alcoves.
- Starpoints in the surface buildings and underground facilities will use internal fibres to connect the wired and wireless network to GPN and TN.
- FCC points will need redundant fibre connectivity to the datacentres to have access to GPN, TN and, in the case of experiments, to LCG.

To ensure redundancy and fault tolerance of the FCC network, the backbone equipment interconnecting all FCC points will be distributed between the datacentres in Building 513 (Meyrin) and Building 775 (Prévessin). The Second Network Hub (Building 773) in Prévessin will also offer possibilities for increased resiliency.

8.7.5 IT infrastructure

As described in the previous section, the FCC will combine computing resources distributed all over the world. CERN will be the Tier-0. By the time the FCC starts, CERN will have two datacentres: one in Meyrin and a second one in Prévessin. This redundancy will help with business continuity and disaster recovery. The Prévessin datacentre is currently being built [408]. During 2025, it will provide 12 megawatts of computing resources. It will use the latest cooling technologies, and it will recuperate heat for other buildings. The power usage effectiveness (PUE) is expected to be 1.1. For comparison, the current PUE of the Meyrin datacentre is 1.5.

The LHC experiments follow the CERN Open Data Policy [409], which ensures a consistent approach towards the openness and preservation of experiment data. The experiments at the FCC will continue in this direction, ensuring the use cases of re-interpretation and re-analysis of physics results are available to the public. The Data Preservation and Long Term Analysis in High Energy Physics Project (DPHEP) [410] identified four levels of data (published results, outreach and education, reconstructed and raw data). This goes in the direction of Open Science, which applies to multiple areas of the FCC and this Feasibility Study.

Given the distributed nature of the collaboration, cyber-security plays a critical role in the whole infrastructure. It is of vital importance that all the components are secured from the first day and that they can withstand the constant cyber attacks that target scientific infrastructures. Ensuring security, data resilience and protection, and long-term data accessibility requires dedicated organisation from the beginning of the project.

8.8 Robotics

The fourth industrial revolution drives automation and data interconnection across industries, including space, warehouses, and harsh environments. Industry 4.0's pillars are IoT, Wireless Sensors, Cloud Computing, AI, ML, and Robotics. Robots are vital for tasks humans avoid due to danger, size constraints, or extreme environments. CERN has developed robots for accelerator maintenance, reducing risk and enhancing uptime. Envisioning advances over two decades, robots could revolutionise FCC tunnel interventions, replacing manual work or risky interventions.

8.8.1 Robotic impact

Robotics can enhance machine availability by improving maintainability through both corrective and preventive maintenance, as well as by increasing reliability with predictive maintenance. Additionally, robotics improves operational safety by reducing the need for workers to perform hazardous tasks and improves emergency safety with fast interventions by readily available robotic systems in the underground facilities, able to provide situational awareness and support rescue teams [411].

The potential impact of robotics on the availability can be demonstrated by looking at the luminosity of the particle accelerator, a metric that can be approximated as the volume of physics data it generates within a given time frame. To reach the luminosity targets [13] of the FCC, the machine availability must reach a minimum of 80%, see Sect. 8.10. Recent studies, based on expert interviews and historical LHC data, have shown that this target can only be achieved by a 15-fold increase of the mean time between failures of certain critical systems. Introducing a readily available robotic system in the accelerator and thus reducing the drive time to intervention locations, allows to relax this constraint by a 10-fold, see Sect. 8.10.

As part of the safety concept for the FCC, robotics will enhance infrastructure and personnel safety during emergency scenarios within the 91 km long FCC tunnel. A three step emergency response strategy including robotics has been proposed by the CFRS [412]:

1. Response by trained workers on site
2. Emergency response robots
   (a) Situation awareness
   (b) First intervention (fire fighting, search and rescue)
3. Professional human responders
   (a) Verify situation
   (b) Second intervention (finalise situation awareness and fire fighting, specific damage control)

8.8.2 Level of robotic automation

Automation has the potential to be a primary driver of cost reduction across all stages of the accelerator's lifecycle, particularly in sustaining high availability throughout years of operation - directly influencing the organisation's data output and, consequently, its value and profit. It is therefore essential to determine the optimal level of automation that maximises benefits, while identifying the point beyond which additional automation leads to diminishing economic returns. The level of automation throughout the accelerator life cycle has to be identified in upcoming studies.

8.8.3 Standards, conventions, and guidelines towards efficient robotic automation

It is essential to emphasise that effective and economical robotics depends on incorporating automation requirements from the earliest design stages. Hardware and software components must adhere to well-defined standards, norms, and conventions, ensuring seamless integration of robotic automation. In the near future, a central point of contact or service needs to provide guidance, support, and oversight on implementing the conventions and guidelines for infrastructure and intervention procedures.

8.8.4 Robotic R&D required

The initial focus of the robotic development will be on a system with the greatest potential to enhance availability and safety, targeting the largest area of the FCC complex—the main tunnel. Previous studies [413] have identified a rail-based robotic system installed on the ceiling as the most efficient and robust solution for the accelerator tunnel. However, robotic systems covering other areas are expected to further enhance machine availability and safety. The necessary developments for a rail-based robotic system for the FCC tunnel area can be split into four phases:

1. **Definition of procedures and conventions**
   (a) Defining required tasks and intervention procedures
   (b) Defining remote maintenance code of practice
2. **Integration**
   (a) Define rail placement in regular tunnel cross section and parking locations
   (b) Design radiation safe spaces for parking and robot maintenance
   (c) Tool manager
   (d) Design of automated hatches in fire doors

3. **Technology R&D**
   (a) Infrastructure (Energy management, logistics)
   (b) Locomotion
   (c) Manipulator
   (d) Control (Motion, grasping)
   (e) Human-robot interfaces (Tele-operation, proprioception, haptics, collaboration)
   (f) Recovery scenarios and emergency interventions
   (g) Tool manager
   (h) Localisation, mapping & perception
   (i) Cognition
4. **Proof of concept**
   (a) Inspection and measurements in full autonomous mode
   (b) Teleoperation mode
   (c) Collaborative mode
   (d) Dipole alignment
   (e) Vacuum leak detection
   (f) Reconnaissance

The plan establishes progressive levels of capability:

1. **BASIC**: Full operation with limitations in automation and safety, requiring substantial tele-operation.
2. **BASIC+**: Emergency intervention capabilities added.
3. **MEDIUM**: Tool Manager, improved Human-Robot Interface, and higher efficiency.
4. **ADVANCED**: Semi-autonomy achieved, enabling collision avoidance and human-robot collaboration.
5. **ADVANCED+**: Full autonomy attained, introducing cognition and unforeseeable interventions.

This roadmap outlines the journey towards a comprehensive robotic solution for FCC. It addresses various technical challenges while highlighting the potential for enhanced safety, efficiency, and required innovation in maintenance operations.

8.8.5 Development status

The study on a rail-based robotic system for the FCC tunnel area departed from the first phase of the implementation plan outlined in the previous section. This rail-based robotic system, referred to as FCC robotic system, consists of two subsystems: the Remote Maintenance and Inspection System (RMIS) and the Surveillance and Emergency Shuttle (SES). The RMIS is designed to enhance machine availability and operational safety, while the SES focuses on improving emergency safety.

In Phase 1, requirements were gathered from stakeholders to enhance machine availability and operational safety [414], as well as emergency safety [415]. The requirements for emergency safety have reached a high level of maturity, while those for machine availability and operational safety are still in progress, as they are closely tied to the infrastructure design. Additionally, a draft for a Remote Maintenance Code of Practice has been developed, outlining conventions for infrastructure design and guidelines for intervention procedures [416].

In Phase 2, the integration of the rails beneath the ceiling of the accelerator has been finalised. A designated area within the tunnel's cross-section has been allocated for the robotic system, and radiation-shielded parking locations in the service caverns have been identified.

In Phase 3, a prototype of the 11-degree-of-freedom Remote Maintenance and Inspection System (RMIS) has been developed for proof-of-concept experiments in the FCC tunnel mock-up, with installation scheduled for 2025. The design of the Surveillance and Emergency Shuttle (SES) remains at the conceptual stage. The current baseline designs for both the RMIS and SES are illustrated in Fig. 8.102.

Phase 4, which begins in end of 2025, will focus on tests with functional infrastructure in the FCC tunnel mock-up.

8.9 Geodesy

Since the FCC-ee will extend well beyond the current CERN site, spanning both Switzerland and France across areas with diverse topographical and geological characteristics, an enhanced and extended geodetic infrastructure will be required. This will include an evolution of existing reference frames and an updated gravity field model to ensure precise positioning throughout the project.

A robust geodetic foundation will support the planning, construction, alignment, and operation of the FCC-ee, accommodating different levels of accuracy. These range from the initial large-scale placement studies to the final

Fig. 8.102 The current baseline of the rail-based FCC robotic system with one RMIS and two SES systems

sub-millimetric precision alignment, which will continue to be refined throughout the accelerator's lifetime. The geodetic infrastructure will be adaptable to meet the needs of each project phase.

During the preparatory phase, a primary geodetic network will be established as early as possible to provide a stable reference frame for all subsequent activities, including civil engineering. Once the FCC-ee layout is finalised and construction begins, the geodetic network will be extended underground through the shafts, forming a dedicated underground geodetic network to ensure precise alignment of the infrastructure.

This section describes the core components of the geodetic infrastructure, while the alignment strategy for the accelerator components and detectors is detailed in Sect. 3.5.

8.9.1 Geodesy

Definition of the coordinate reference systems for the FCC-ee A key component of the geodetic infrastructure will be a static coordinate reference system, established through the CERN Terrestrial Reference Frame (CTRF), along with a kinematic model (CKM) that represents the temporal evolution of the CTRF's reference points. This system will enable connections between CERN's existing reference frames and international, national, and local reference frames, ensuring compatibility and long-term stability. Additionally, it will serve as a foundation for analysing crustal deformations in the region.

For civil engineering works, a compound Coordinate Reference System (CRS) will be used, consisting of a projected CRS for horizontal positioning and a vertical CRS for gravity-related height determination. The horizontal coordinates will be defined through a CERN Projected Frame (CPF), while the Vertical Reference Frame (CVF) will provide height information consistent with the gravitational field.

For alignment purposes, the CERN Coordinate System (CCS) - which is currently used for all CERN machines - will remain in use. This will ensure a consistent and reliable link between the FCC infrastructure and the existing CERN facilities.

Since the FCC is a cross-border project, existing geo-referenced data such as geological maps, digital terrain models, and aerial imagery are expressed in different geodetic horizontal and vertical datums. To ensure compatibility, these datasets will be harmonised and transformed into the CTRF. Transformation models and their associated uncertainties will be carefully computed to maintain consistency across all datasets. Additionally, dedicated geodetic transformation software will be developed and made available to stakeholders to facilitate seamless integration.

Figure 8.103 shows the connection amongst the different parts of the reference system infrastructures. A detailed description of the coordinate reference systems is provided in Ref. [417].

Implementation of the surface geodetic network Since it will be the reference for all survey and civil engineering work, a primary surface geodetic network (P-SGN) will have to be created as soon as possible to implement the CTRF (see [418]). During the period of the FCC Feasibility Study, IGN and Swisstopo increased the density of their national geodetic network (Réseau de Base Français and Points fixes planimétriques, respectively) over the FCC area and built new geodetic pillars and installed a new continuously operating global navigation satellite system (GNSS) reference station at locations suitable for the FCC-ee (see Fig. 8.104). The coordinates of the P-SGN will be determined and tied in the latest implementation of the European Terrestrial Reference Frame using simultaneous GNSS observations, ensuring absolute accuracy of 3 to 5 mm.

During the tunnel construction, the P-SGN would increase its density with auxiliary points, and a portal network would be created at each shaft to define the orientation of the tunnel. A surface levelling network will also be created, linking the eight surface sites and access shafts.

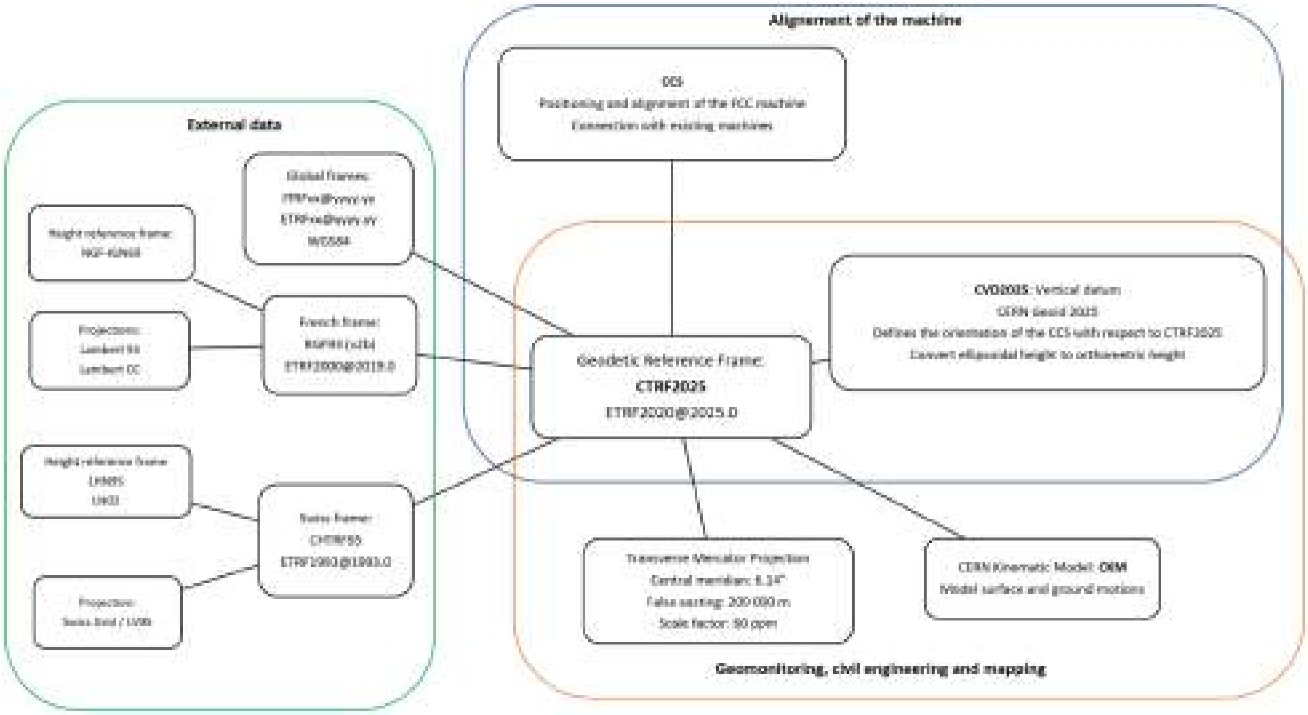

Fig. 8.103 Graphical outline of the coordinate reference systems for the FCC-ee

Gravity field model To meet the vertical alignment accuracy requirements and to overcome the differences between the French and the Swiss altimetric systems, the local variations of the gravity field must be known or modelled with high accuracy and resolution (i.e., at a very short wavelength).

A centimetric (1 cm) accuracy could be achieved for the civil engineering and tunnelling work and as a basis for computing the gravity field model at the tunnel level. The latter is required to align the machine in an Euclidean plane. The computation of these models will require additional R&D.

A control profile, composed of GNSS-levelling and astrogeodetic observations, has already been determined to control the different geoid solutions that will be computed [419].

Underground geodetic network Once the tunnel shafts have been excavated, the coordinate reference system will be transferred underground. At this stage, the coordinates of reference markers regularly spaced on the floor and on the wall of the tunnel will be computed (see Fig. 8.105).

The underground geodetic network will be the reference for all automatic or manual alignment activities. Systems and instruments detecting the movements of the reference markers will be developed and installed to permanently or periodically monitor the stability of the reference network.

The development of the optimum methodology for the determination and monitoring of the underground geodetic network will require additional R&D efforts.

A geodetic reference frame that includes the nominal beamline must be established for each of the FCC-ee experiment caverns. To achieve this, geodetic reference points will be installed within the experiment caverns, typically implemented using wall brackets, nests, permanent tripods, or ground inserts equipped with CERN standard survey reference sockets. The entire geodetic network will be defined within the CERN Coordinate System (CCS) as part of the broader underground geodetic network. The network will be measured using high-precision instrumentation, including laser trackers, total stations, and direct levelling techniques. To maintain accuracy and stability, the geodetic networks of the experiment caverns will be regularly updated, ensuring that alignment remains consistent throughout the lifetime of the FCC-ee.

Calibration, checking and testing of the geodetic instruments To meet surveying and alignment requirements, geodetic instruments, sensors, and tools used during the construction, installation and operation of the FCC must be regularly tested. A concept for calibration, checking, and testing (CCT) of geodetic instruments for the FCC has been developed (see Ref. [420]). A mix of in-house activities and facilities as well as outsourcing to external service providers would cover the needs. Dedicated spaces must be allocated at strategic locations for checking

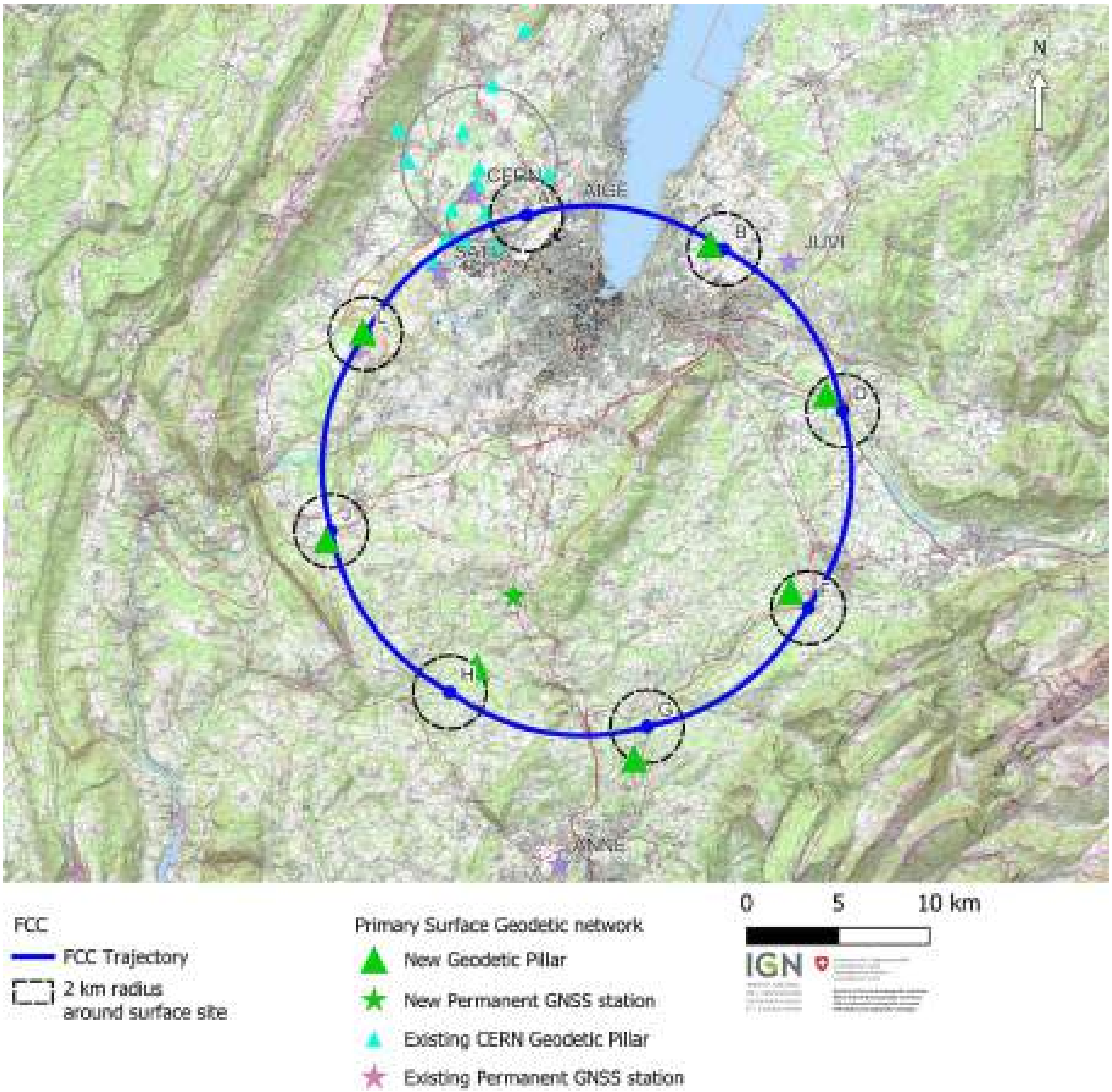

Fig. 8.104 Primary Surface Geodetic Network for the Future Circular Collider

instruments like total stations, levels, laser trackers, 3D scanners prior usage. External service providers can be in charge of yearly maintenance and fixing identified defects.

8.10 Availability

This section details results from the enhanced Monte Carlo simulation environment for FCC-ee availability described in Sect. 2.4, focusing on systems specific to the Technical Infrastructure serving the collider and booster. Infrastructure serving the injector complex is detailed in Sect. 7.9.

8.10.1 Contributing systems

The same general framework for availability approximation was applied to the collider systems, described in Sect. 2.4.1. Specifics of this process used for each technical infrastructure system are described in the following paragraphs. Only faults leading to downtime in the representative system were considered, thereby assuming a similar degree of redundancy for each basic component family as currently exists in the working accelerator.

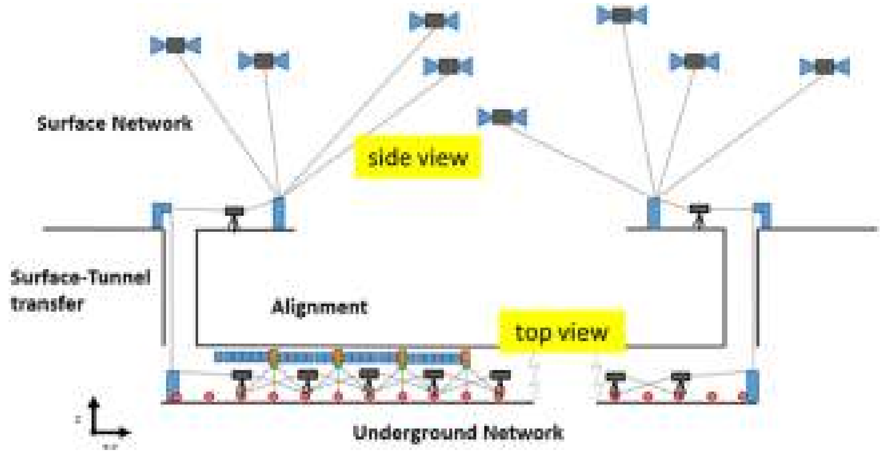

Fig. 8.105 Schematic representation of the coordinate transfer

Details of subsystems and scaling numbers are provided in Tables 8.36 and 8.37. Fault data was taken from CERN's Accelerator Fault Tracking (AFT) database [234] and is specific to the LHC physics operation 2015-2024, unless otherwise stated.

1. **Cooling & Ventilation:** Fault rate was scaled using the number of critical circuits at each access point, which is similar to the LHC (160 in LHC, 168 in FCC-ee). This does not consider the overall volume served by these critical circuits, which is significantly larger in the FCC-ee.
2. **Electrical Network:** The FCC-ee is connected to the PA, PD and PH external grid. The distribution between PA and PD is connected such that one can power the other in the event of failure with approximately 15 minutes of changeover time following beam dump. At PH, there is no backup reconfiguration option due to the high power demand in the collider RF system. Any electrical network failure at PH will, therefore, block the beam until failed hardware is restored. Two types of faults are categorised:
   (a) External network perturbations are a high contributor to downtime in the LHC, as they can trigger child faults in sensitive hardware across the complex. Failure rate and downtime from this category are applied without scaling to each of the three access points, assuming the same resilience to glitches as the LHC.
   (b) Internal network faults occur due to hardware failure in the electrical distribution designed and managed by CERN. This is scaled according to the number of substations at each location (PA: 4, PD: 3, PH: 1). This excludes the parallel power line feeding the collider RF at PH, which has not yet been modelled. A study to optimise the reliability of this parallel line against cost factors will take place in the pre-TDR phase.
3. **Cryogenics:** The FCC-ee requires only two cryoplants to serve the collider and booster superconducting RF systems at PH and PL, respectively. In the absence of a detailed design to indicate the number of components, the failure rate at each point is assumed to scale with the reference 4.5 K power level relative to one LHC cropland at 144 kW. This is constant for lower energy modes (Z, W, ZH) at 80 kW (collider) and 9 kW (booster). During the long shutdown prior to $t\bar{t}$ operation, each cryoplant is upgraded to 168 kW and 53 kW, respectively.

8.10.2 Simulation results

The breakdown of unavailability and lost luminosity contribution from each technical infrastructure system is shown in Fig. 8.106. The electrical network has the largest contribution to lost luminosity in Z, WW, and ZH operation due to its more frequent and shorter duration fault types. Cryogenics is the most significant contributor to unavailability and lost luminosity in $t\bar{t}$ mode due to the energy upgrade required for additional cavities in the superconducting RF system.

8.10.3 R&D opportunities

Several areas for improvement are identified:

Internal electrical network faults The internal electrical network significantly contributes to lost luminosity despite a 15-minute changeover redundancy between PA and PD. Designs must incorporate a more robust redundant connection between these two points. An automatic switch could significantly reduce the changeover time. However,

Table 8.36 Parameters used to simulate the availability of systems and subsystems in the collider Technical Infrastructure

System	Subsystem	LHC #	FCCee Z, WW, ZH / $t\bar{t}$ #	Location	Group MTBF Z, WW, ZH / $t\bar{t}$ days
Cooling & Ventilation	Critical circuits:				
	PA	200	30	PA	111.3
	PB	200	20	PB	166.9
	PD	200	30	PD	111.3
	PF	200	20	PF	166.9
	PG	200	30	PG	111.3
	PH	200	25	PH	133.6
	PJ	200	30	PJ	111.3
	PL	200	25	PL	133.6
Electrical Network	Internal Network:				
	PA	1	4	PA	3.6
	PD	1	3	PD	4.8
	PH	1	1	PH	14.3
	External Glitch	1	3	PA, PD, PH	7.7
Cryogenics (collider)	Tunnel:				
	Instrumentation	144	80 / 168	PH	70.6 / 33.6
	PLC	144	80 / 168	PH	352.9 / 168.1
	Production:				
	Temperature	144	80 / 168	PH	47.1 / 22.4
	Controls	144	80 / 168	PH	470.6 / 224.1
	Instrumentation	144	80 / 168	PH	74.3 / 35.4
	PLC	144	80 / 168	PH	235.3 / 112.0
	Vacuum	144	80 / 168	PH	352.9 / 168.1
	Operation:				
	PNO-SAM	144	80 / 168	PH	352.9 / 168.1
	PNO-BSCR	144	80 / 168	PH	235.3 / 112.0
	PNO-REF	144	80 / 168	PH	282.3 / 134.5
	PNO-DFB	144	80 / 168	PH	17.9 / 8.5
	PNO-HF	144	80 / 168	PH	282.3 / 134.5
	Other	144	80 / 168	PH	117.6 / 56.0
	Specific Operation	144	80 / 168	PH	176.5 / 84.0
	Users	144	80 / 168	PH	282.3 / 134.5

the largest gains would be made by avoiding beam dumps altogether, as this eliminates lost luminosity due to turnaround time in the initial operation phases (see Sect. 2.3.2).

Reliability must get particular attention at PH, as this cannot be reconfigured to draw power from another access point. Further, this means the parallel power line feeding the collider RF must be designed to a particularly high-reliability target.

External electrical perturbations The simulation assumes that the same resilience to external network perturbations will occur in the FCC-ee as currently appears in the LHC. This is a coarse assumption, as the resulting downtime is most commonly due to child faults in sensitive accelerator systems, e.g., high-precision power converters, RF, etc.; the number of which could be significantly higher in FCC-ee. Learning from LHC experience, all FCC-ee systems must be designed according to an established standard for resilience to electrical glitches.

Table 8.37 Parameters used to simulate availability of systems and subsystems in the booster

System	Subsystem	LHC #	FCCee Z, WW, ZH / $t\bar{t}$ #	Location	Group MTBF Z, WW, ZH / $t\bar{t}$ days
Cryogenics (booster)	Tunnel:				
	Instrumentation	144	9 / 53	PL	627.4/ 106.5
	PLC	144	9 / 53	PL	3137 / 532.7
	Production:				
	Temperature	144	9 / 53	PL	418.3/ 71.0
	Controls	144	9 / 53	PL	4183 / 710.3
	Instrumentation	144	9 / 53	PL	660.5 / 112.2
	PLC	144	9 / 53	PL	2091 / 355.2
	Vacuum	144	9 / 53	PL	3137 / 532.7
	Operation:				
	PNO-SAM	144	9 / 53	PL	3137 / 532.7
	PNO-BSCR	144	9 / 53	PL	2091 / 355.2
	PNO-REF	144	9 / 53	PL	2510 / 426.2
	PNO-DFB	144	9 / 53	PL	158.8/ 27.0
	PNO-HF	144	9 / 53	PL	2510 / 426.2
	Other	144	9 / 53	PL	1046/ 177.6
	Specific Operation	144	9 / 53	PL	1569/ 266.4
	Users	144	9 / 53	PL	2510 / 426.2

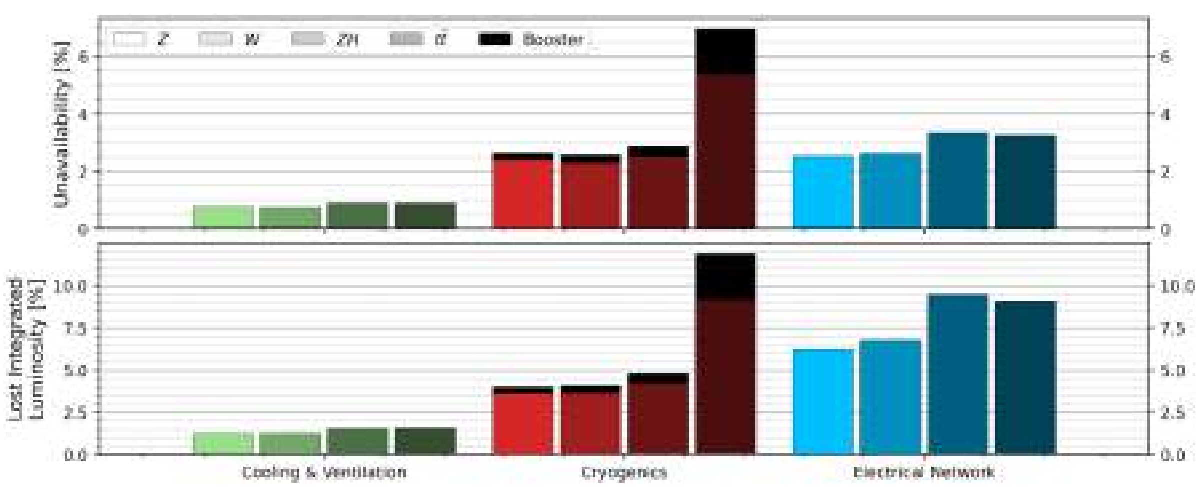

Fig. 8.106 Contribution of technical infrastructure subsystems to unavailability and lost luminosity. Systems are ordered according to Z mode lost luminosity contribution

Cryogenics Despite the significantly smaller cryogenic load compared to LHC, this is the highest contributor to downtime from the technical infrastructure systems. As designs develop, special consideration must be given to ensure availability.

8.10.4 Outlook

Technical infrastructure availability is of particular importance in the next phase as many of these systems have significant footprints on the civil engineering layout, e.g., the size of alcoves and caverns, routing and location of cables and equipment, radiation protection, access, etc. The coming years must see a thorough reliability/availability analysis of these high-priority systems to ensure performance ahead of civil engineering procurements.

Chapter 9

FCC safety concepts

9.1 Introduction

This chapter outlines the safety concept for FCC. Given the intricate nature of particle accelerators, which involve high-energy beams, radio frequency cavities, cryogenic systems, and sophisticated electromagnetic equipment, a comprehensive safety strategy is essential to ensure operational integrity.

Key safety considerations include identifying the scope of the concept, its objectives, as well as the underlying impact of domains such as deep underground siting, radiation protection, structural integrity, fire and oxygen deficiency, and emergency response protocols. Integrating safety measures into the FCC design has an impact on the layout of the facilities. This chapter underlines the specific strategies and technologies employed, demonstrating our commitment to creating a safe and efficient research environment.

9.1.1 Safety considerations

The geographical distribution of surface sites and the time required to reach each site by road, the challenges linked to the underground working conditions, and the diverse composition of technical equipment at surface sites require the systematic development of an integrated safety concept.

The results presented in this chapter are based on work that assumes the *baseline* layout and parameters outlined in this report. If future phases of the study introduce deviations from the *baseline*, their impact on the safety concept will have to be assessed. Certain safety systems form the foundation of the safety concept; therefore, any modifications to these systems may necessitate the development of an entirely new safety concept (see Sect. 9.3.4).

9.2 Safety goals & objectives

9.2.1 Regulatory framework

CERN, an intergovernmental organisation established under international law by its Convention (1 July 1953, amended 16 June 1972), is headquartered in Geneva and operates across the Franco-Swiss border.

Under its regulatory framework, CERN establishes safety rules as necessary for its functioning. The CERN Safety Policy [421] defines the overarching principles governing safety at CERN and is complemented by CERN-specific rules tailored to its operational requirements. Where specific rules are not established, national laws apply within their respective territories. This framework ensures that the rules are uniform throughout the site and adapted to the specific (particularly technical) requirements of the organisation.

CERN collaborates with the Host States under domain-specific treaties and tripartite agreements, e.g., in efforts to minimise environmental impact and uphold best practices in radiation protection. While the Host States facilitate its operations, CERN remains committed to limiting its impact on their territories and ensuring its activities do not compromise their security.

This regulatory framework reflects the current perspective and serves as the foundation for developing this safety concept.

9.2.2 CERN safety policy

CERN has a safety policy [421] in place that defines the safety objectives for every project and activity in order of priority:

1. *Life safety*: ensure the best possible protection according to CERN's Safety Rules in health and safety matters of all persons, irrespective of their status, participating in the organisation's activities or presence on its site, as well as of the population living in the vicinity of its installations.
2. *Environment protection*: limit the impact of the organisation's activities on the environment.

3. *Asset protection and business continuity*: guarantee the use of best practices in matters of safety.

The FCC feasibility study covers all these objectives, although the scope of the safety concept, developed at this stage, focuses on the life safety objective. The environmental protection aspects are covered in a dedicated stand-alone document, which is equally referenced in the third volume of the Feasibility Study Report.

Although the safety concept described focuses on the FCC-ee accelerators (injector, booster, and collider), possible incompatibilities with the civil engineering layout for FCC-hh are highlighted and integrated based on the requirements for the feasibility study. Modifications to the technical infrastructure needed for FCC-hh but which are not yet included in the design will be integrated in the safety concept when the infrastructure is being designed.

The transfer tunnels from the injector chain are not included in this concept, since safety aspects can only be studied for those elements once a design baseline is developed. The impact on safety of this part of the infrastructure would therefore be analysed in the next phase of the project.

9.2.3 Lifecycle phases

The Safety concept covers the following lifecycle phases:

- Construction phase.
- Installation phase.
- Operation phase, including maintenance periods and repair activities.

Each phase is characterised by different safety aspects, associated with the safety systems deployed and available, and with the time occupants are exposed to those conditions. The development of the safety concept described in this section is based on analysis of the *operation phase* of the FCC.

9.2.4 Safety organisation & management plan

A safety management plan is required to ensure the safe operation of such a large research infrastructure. This plan will not be limited to the respect of safety objectives but also safeguard the long-term viability of the facility by fostering a culture of safety, compliance, and continuous improvement. Through risk assessment, planning, and the establishment of clear procedures, a management plan ensures that safety is prioritised in all phases of the infrastructure.

The safety regulation on the ‘Responsibilities and organisational structure in matters of safety at CERN’ (SR-SO) [422] is based on the CERN Safety Policy [421].

Current practice at CERN foresees that the appointed project leader (PL) is responsible for safety within the project [422]. The PL may decide to appoint a project safety officer (PSO) with the mandate to support the project leader in meeting the obligations in matters of safety [423]. At the end of the project phase, safety responsibilities are transferred from the project leader to the organic units in charge of the operation.

9.3 Planning for safety

9.3.1 Hazard register

A *hazard register* is the result of systematic identification of activities, equipment, and substances with their associated hazards for workers, the public, or the environment. A systematic inventory of hazards serves as a support not to overlook any danger and unifies the terminology among different assessors. Such lists are available from different occupational safety organisms (see for example Ref. [424]). As they target manufacturing and services, they must be modified for particle accelerators and for research infrastructures in general to include hazards unique to these environments. Table 9.1 shows the headlines of a hazard register for particle accelerators. Ref. [425] provides a hazard list, tailored to particle accelerators. The adaptation of the hazard list to the local workplace by adding or suppressing hazardous equipment, activities, or substances precedes establishing the register.

The focus of the hazard register depends on the phase of the lifecycle. In the planning stage, it identifies hazards which can be controlled by design, for example, by adopting standards. In this early stage, organisational and psychosocial hazards and risks have not yet been assessed. In the installation and operational phase, workplace hazards become more important, for example, related to the organisation of work or physiological constraints.

The equipment, activities, and substances are identified by location (surface site and building or underground areas) and lifecycle phase. The hazards emerging from each equipment, activity, and substance are identified with a specific list of hazards based on Ref. [424], modified and complemented for accelerator facilities, and published

Table 9.1 Hazard domains for a hazard register, with examples

Hazard Domain	Examples
External	Earthquake, climate, malicious action, cyber criminality
Physical	Temperature, noise, electromagnetic fields
Ionising Radiation	Particle beam, stray radiation, activation
Non-ionising radiation	Static magnetic fields, UV light, microwaves, lasers, RF
Noxious substances	Chemically or biologically harmful substances
Fire	Ignition sources, flammable materials
Mechanical	Cutting, crushing, collision, fall of object
Electrical	Electrical shock, electrical arc
Working conditions	Temperature, lighting
Physiological	Working posture, vibration, manual handling
Unexpected events	Loss of control, loss of power
Organisation	Constraining schedule, lack of information
Psycho-social	Incomplete and monotonous activities

in Ref. [425]. The hazard description links to relevant sources of standard practice (see Sect. 9.3.2) at the time of the Feasibility Study. These sources must be updated regularly during the project life cycle.

In a large particle accelerator, most equipment, activity, and substance and their associated hazards occur repetitively at various locations and in different phases. To avoid tedious and error-prone updates of a written document, the hazard register is kept in a relational database where every piece of information needs to be updated only at a single location and is automatically propagated. Different types of database reports produce documents and reports summarising the hazards for a specific location and phase or the recommended sources of appropriate standard practice (Sect. 9.3.2). Hazards for which no standard practice exists (or where standard practice from *conventional* industry is not applicable) require a detailed risk assessment and identification of mitigation measures (see Sect. 9.3.3).

9.3.2 Standard practices

Standard practices are based on hazard identification, risk descriptions, and mitigating measures applying to technologies and related activities in industry that are similar to those encountered in an accelerator. Examples are electrical distribution of standard current and voltage and transport.

Suitable sources of standard practice are national and international legislation on hazardous equipment, activities, and substances. These documents are prescriptive, and their application is usually mandatory. A hazard is often considered under control when such mandatory regulations are implemented and applied.

CERN's safety policy [421] is to apply European Directives and associated standards where available. Numerous types of consumer and industrial products are subject to European Directives, which include chapters on Essential Health- and Safety Requirements (EHSR). Their purpose is to guarantee equal safety standards for workers and for consumers (who purchase and use products) throughout the member states of the European Union. Only under this condition can goods be freely traded within the European Economic Area (EEA). Suppliers from third countries must also apply the European safety standards to introduce their products into the common market.

Another source of standard practice is the publications by occupational health and safety organisations, e.g., *SUVA*,[12] *INRS*,[13] *HSE UK*,[14] *CTPI-AEAI CH*,[15] and of industrial associations e.g., *BG ETEM*.[16] Their recommendations provide the practical elements required to meet the legal prescriptions at the workplace. They are often borne from common sense and may be easy to apply, effectively eliminating the hazard and making further risk assessment superfluous.

Product documentation by manufacturers is another source of standard practice. The manufacturer, having designed the equipment so that it meets legal requirements, gives the necessary information for safe use in the

[12] https://www.suva.ch/.

[13] https://www.inrs.fr/.

[14] https://www.hse.gov.uk/.

[15] www.bsvonline.ch/fr/publications/det.

[16] https://www.bgetem.de/.

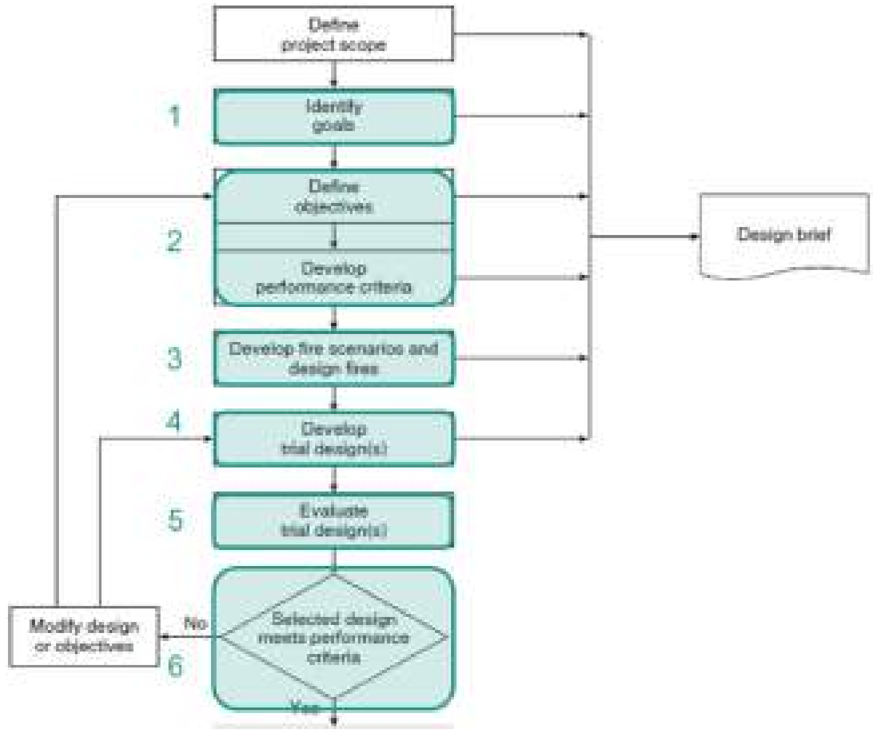

Fig. 9.1 Performance-based design flowchart. Example for fire scenarios from SFPE [427]

form of user manuals, video tutorials, and other training materials. Over time, CERN has accumulated a wealth of knowledge about safety, based on the experience gained from operating the existing infrastructure. The source material defining standard practices is assembled and classified in the hazard register.

9.3.3 Performance-based design

For hazards for which standard practices are not available or are not fully applicable to the particularities of an underground accelerator complex, the study follows a performance-based design (PBD) approach.

PBD is a state-of-the-art risk assessment approach, which is used in areas such as fire safety and introduced in national legislation in several countries, including Switzerland [426]. It is a process of defining alternative design options iteratively and assessing their impact against a predefined set of safety objectives. For this study, a PBD methodology introduced by the Society of Fire Protection Engineers (SFPE) [427] was adopted. According to SFPE, the PBD process can be divided into 6 steps (see Fig. 9.1) after having defined the scope of the assessment:

1. Identify the safety goals (see Sect. 9.2.2).
2. Define the design objectives and develop the performance criteria (i.e., safety requirements).
3. Develop the accident scenarios based on the system-level risk assessment.
4. Develop the trial design with the proposed safety systems.
5. Evaluate the trial design against the performance criteria.
6. Create new trial designs until they meet the criteria - (iterative process).

The process ends when a trial design that meets the safety objectives is retained as the baseline solution.

Different methodologies can be used for the evaluation of trial designs, ranging from simple assessments to highly complex algorithms [428] and numerical simulations. A qualitative analysis was performed during the conceptual study phase (2014 to 2018). For the feasibility study, a more in-depth evaluation was performed using quantitative (i.e., worst credible scenarios) and probabilistic approaches.

9.3.4 Safety systems

For the safety concept described in this document, a *safety system* refers to a set of engineering controls aimed primarily at ensuring life safety by incorporating both preventive and protective measures during normal and accident scenarios. A system that is used primarily for technical purposes but also performs safety functions can be considered a safety system, provided that it adheres to the required safety standards.

The following Sections 9.4 and 9.5 provide a brief summary of the safety systems proposed as a result of the study. Additional details are provided as references to reports, notes, etc.

9.4 Safety concept for the operation phase

As mentioned in Sect. 9.2.1, the strategy is to cover conventional hazards with standard practices and integrate accelerator-specific hazards in a performance-based design approach. The outcome is an integrated approach towards safety for the project.

9.4.1 Safety systems supporting the concept

The combination of the safety systems described hereafter constitutes the present safety concept. The suppression and/or major modification of any given safety system will have an impact on the global safety concept, which might require partial or total redesign of the concept.

The Safety concept is built on the following main pillars:

- Static confinement.
- Air management & dynamic confinement.
- Personnel transport.
- Emergency response.
- Secure power network.
- Access control.

In addition to these pillar systems, several high-integrity safety systems complement the safety concept. They permanently monitor the safety conditions and trigger appropriate safety actions from other systems or personnel.

- Access Safety System.
- Hazard detection.
- Emergency call.
- Evacuation alarm.

The particle accelerators have the following modes:

- Run mode: the beam is circulating or could be circulating; personnel can only be present in very limited areas of the facility.
- Access mode: beam cannot circulate. Personnel are authorised to access the facility. There are different types of access periods:
  - Short access: for interventions over a period of typically one hour or more and less than a day.
  - Technical stop: for planned interventions over a period of several days up to a few months.
  - Long shutdown: for planned interventions lasting several years for major consolidation and upgrade works.

Compared to other phases, the operation phase constitutes the longest part of the project's lifetime and during which the majority of occupational hazards (see Sect. 9.3.1) are present simultaneously. Depending on the state of the accelerators, the occupants may be exposed to different hazards. The average occupancy density in underground facilities is low, although occupancy during technical stops and long shutdowns can be comparable to that of the installation phase.

Static confinement (compartmentalisation) The fire safety concept relies on passive fire compartments as the principal strategy to sectorise the fire load and prevent fire and smoke propagation across the facility whilst enabling safe evacuation of occupants and intervention of the emergency teams.

The concept has partitions along the main tunnel and in all areas with a specific fire risk (e.g., electrical alcoves), using a dedicated fire-resistant partition. Moreover, protected areas for evacuation (e.g., safe areas[17]) will also be compartmentalised. Doors, dampers, and hatches installed in the compartment must also be fire-resistant and match the same resistance level as the fixed partition. For services penetration of those partitions (e.g., pipes, cable trays), the openings must be effectively sealed, following safety standards, to match the fire resistance required.

As a fundamental part of the fire safety concept, the fire rating of the compartments must guarantee that the fire and smoke are contained for the time needed to enable safe evacuation and intervention. Moreover, to limit property losses and recovery time, the integrity of the compartments must withstand all foreseeable fire scenarios. For this, the rating will be based on various factors: the fire load, the possibility of reaching flashover conditions in the affected compartments, and the time needed to ensure safe evacuation and emergency teams intervention. The

[17] Areas free from smoke and hazardous gases as a buffer for occupants to wait for the lift, *not to be confused with a temporary refuge shelter or equivalent.*

Table 9.2 Overview of distances between emergency exits in transport, technical, and accelerator tunnels. EU Regulation 1303/2014/EC and Directive 2004/54/EC apply to EU network of rail and road tunnels, respectively. XFEL compartments are made of solid fire-proof walls with a triple water mist enclosing system instead of a fire door

Source	Length [m]	Comment
EU road tunnels [431]	500	Between emergency exits (if required)
EU railway tunnels [432]	500	Between connections to adjacent tube
OLT4 [433]	500	Between access shafts in non-frequented technical galleries
NFPA 520 [434]	610	To reach a safe exit, refuge, or portal
XFEL [435]	600	Between two compartments (wall + water curtain)
ILC [436]	500	Passage connecting the two galleries

fire rating must also be consistent with the minimum structural fire resistance requirements assigned by standard practices and Host State regulations (see Table 9.6).

The following fire-resistance rating is proposed as a baseline for the feasibility study of the underground infrastructure. The resistance stated below is based on ISO 834 curves [429] for design purposes as defined in EN-13501-2 [430]. Section 9.4.3 provides more information on the difference between standard and natural curve-based fire resistance.

- Accelerator tunnel (arc and straight sections): EI90 partition (every 400 m) with interlocked door normally open.
- RF sector - connection between klystron gallery and accelerator tunnel: EI90 partition at the bottom and top of connection staircases.
- Service caverns - safe area (lift shaft): EI120 partition.
- Connection tunnels - connections between experiment and service caverns: EI120.
- Alcoves - connection to the accelerator tunnel: EI120 partition.
- Other underground spaces with specific risks (UPS, transformers): EI120.

In the accelerator tunnel, fire compartments also serve as an important element of the evacuation strategy by limiting the distances travelled within the affected compartment, and they allow occupants to quickly move into an adjacent (non-affected) compartment which serves as a safe area (free from smoke, gas and fire consequences) to continue the evacuation until reaching the safe area joined to the pressurised lift shaft and, ultimately, the assembly point at the surface.

Different requirements in terms of evacuation distances exist for tunnels. Table 9.2 provides references for railway and road infrastructures in Europe, as well as for other particle accelerator infrastructures.

These requirements are understood to be the distance to reach an area of relative safety where the occupants are no longer exposed to untenable conditions. Moreover, once the occupants reach the adjacent (unaffected) compartments, the remaining length needed to evacuate using motorised means is not considered in the maximum distance requirement. This is the case of the Gotthard and Lyon-Turin base tunnels [437] where evacuation is guaranteed through the adjacent (non-affected) double-tube concept.

The distance between two compartments must consider the maximum acceptable length (Table 9.2), as well as the layout constraints and practical aspects of the facility. For the FCC, this can be summarised as:

$$\begin{cases} d \leq 500\text{ m} \\ d = \text{distance between alcoves } \div \text{integer number of compartments between two alcoves} \end{cases}$$

Solving the system with 1600 m between two alcoves results in 4 compartments, hence one every 400 m. With this layout, each alcove will house safety-related systems for two compartments to the left and two to the right. The final implementation of each individual compartment will depend on the exact location of the beamline elements of both the collider and the booster. For example, one should avoid the installation of a compartment in the middle of a quadrupole girder, or close to a radiation absorber. A compartment assembly is planned to be included in the arc half-cell mockup to test and identify the best location. Figure 9.2 shows a possible integration layout of such a partition. The challenges emerging from integrating such a compartment around different services, including the hatches for overhead robots, need to be considered. A subsequent design phase has to develop detailed plans.

Air management & dynamic confinement (ventilation) Due to the nature of underground facilities, adequate indoor air quality is required for both the occupants and the equipment. A robust ventilation system ensures the

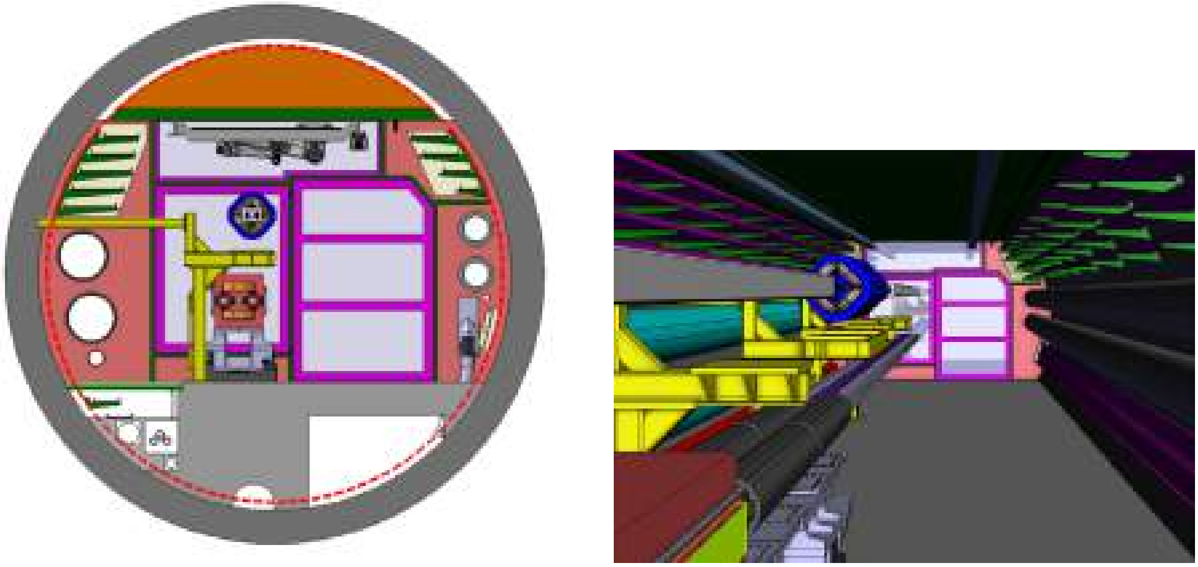

(a) 2D view (b) 3D view

Fig. 9.2 Illustration of the integration of a fire compartment in the cross-section of the FCC tunnel. Light red: fixed partition walls; Purple: frames with grey fill: movable parts - fire door, robot hatch, installation hatch

appropriate temperature and humidity conditions in the tunnel during operation and when people are present. During access mode, it provides a supply of fresh air for occupants with an appropriate air exchange rate.

Five different working modes for the tunnel ventilation are envisaged:

- *Run mode*: the accelerators are in operation and most electrical systems are powered; a heat load is transferred to the air in this mode; radiation protection aspects are taken into account for the air flow. No personnel are present in the main tunnel, the alcoves, and the experiment caverns.
- *Access mode*: the accelerators are not operational. Personnel can access and work in the tunnels. Occupational health & safety requirements must be considered.
- *Flushing mode*: Completely renew the air underground when moving from the Run to Access mode. Personnel are not present in underground structures.
- *Economy mode*: Reduced airflow for energy-saving reasons in situations other than Access mode, reducing the air exchange to a minimum. The presence of personnel is not foreseen in any underground structures.
- *Emergency mode*: activated in the event of a fire or gas release to guarantee dynamic confinement between the affected and adjacent compartments.

Tunnel arcs For tunnel arcs, two technical solutions were studied [438]:

1. *Semi-transverse* ventilation scheme where the air is supplied to each sector from both endpoints via a specific duct throughout the sector below the transport zone, supplied to each compartment transversely by air diffusers, and extracted either through the tunnel itself or by an emergency extraction duct on the ceiling of the tunnel;
2. *Longitudinal ventilation* scheme where the air is supplied at one end of the sector and extracted at the other end.

In addition to air management during nominal situations, an emergency extraction system is proposed for the main underground areas. This system will be activated in case of fire or cryogenic gas leak to:

- Allow safe evacuation from the affected compartment while providing enough safety margin (Sect. 9.4.3).
- Create a dynamic confinement to prevent smoke from spreading to adjacent compartments.
- Remove heat and smoke in the affected compartment, reducing the risk of structural damage and reinforcing property protection.
- Allow for a safe and efficient intervention from the emergency teams, allowing emergency responders the ability to manipulate and control the system to their advantage.

Since there are still two concepts for the ventilation system being considered, there are also two different concepts for the emergency extraction system under consideration, one for each ventilation scenario (semi-transverse & longitudinal).

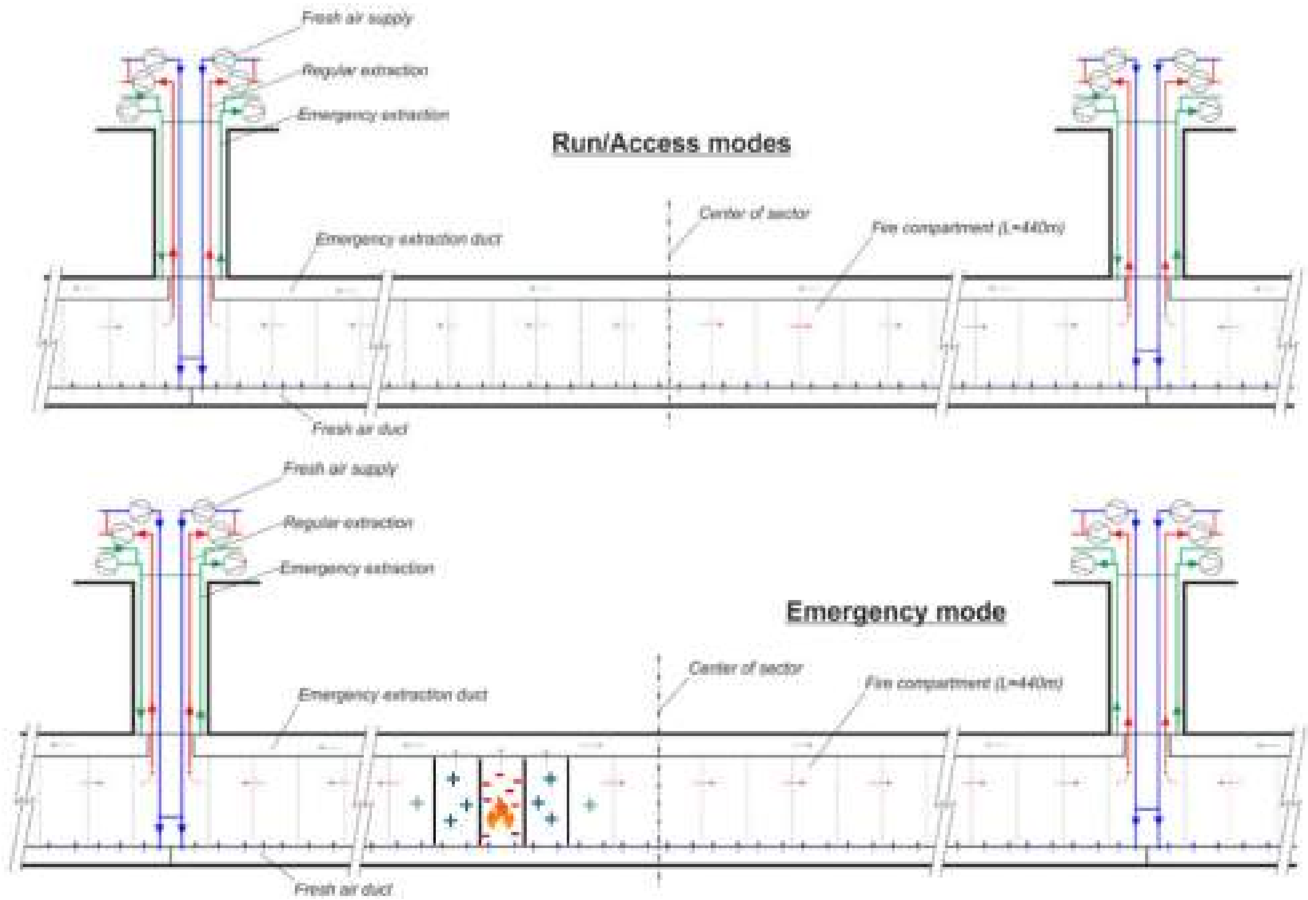

Fig. 9.3 Semi-transversal ventilation mode (top) and emergency mode (bottom). The + and − signs illustrate the pressure cascade in the affected compartment and the adjacent ones

In the semi-transverse ventilation concept, the sector between the two shafts is considered to be split in the middle. Air is supplied to the tunnel through four wall-mounted air diffusers in each compartment. During access mode 54,000 m^3h^{-1} ($2 \times 27{,}000$ m^3h^{-1}) of fresh air is supplied to both halves of the sector. In the event of a fire, the smoke and hot air are extracted from both ends of the sector and exhausted to the outside. In such emergency mode, the extraction dampers located under the ceiling of the tunnel are open in all three compartments (affected + two adjacent). The air in the affected compartment will be extracted at a flow rate of 10,000 m^3h^{-1} and 3500 m^3h^{-1} in the adjacent compartments, which yields a total extraction flow rate of 17,000 m^3h^{-1}. In the event of an emergency (e.g., fire), the fire doors of the affected compartment and the two adjacent ones are closed. Hence, to compensate for the extracted volume, an equal amount of fresh air (*make-up air*) is ensured via the nominal supply diffusers connected to the slab duct (Fig. 9.3). This concept creates a pressure difference between the different compartments, ensuring that smoke and gas are confined, providing enough time for the occupants to evacuate (see Sect. 9.4.3).

In the case of longitudinal ventilation (Fig. 9.4), under nominal conditions 54,000 m^3h^{-1} of fresh air is supplied to the tunnel from one end of the sector and extracted at the other. In the event of an emergency, the same extraction flow rates as per the semi-transverse are used in the affected and adjacent compartments. The fire doors of the affected compartment and the two adjacent ones are also closed, but in this case, the make-up air is supplied from both ends of the sector towards the adjacent compartments (2×8500 m^3h^{-1}), ensured via bidirectional dampers installed on the walls of the compartment. These dampers allow make-up air to enter the affected compartment, sweeping the smoke towards open extraction dampers located under the vault, providing the necessary compensation. The isolation of the compartments creates a pressure difference, ensuring the confinement of smoke/gas and providing enough time for the occupants to evacuate.

Regardless of the ventilation concept adopted, it is important to consider the full operability of the fire compartment doors at all times. The risk of overpressure due to nominal, emergency or degraded modes will be carefully studied to ensure that the evacuation concept is not compromised if these doors cannot be opened normally by

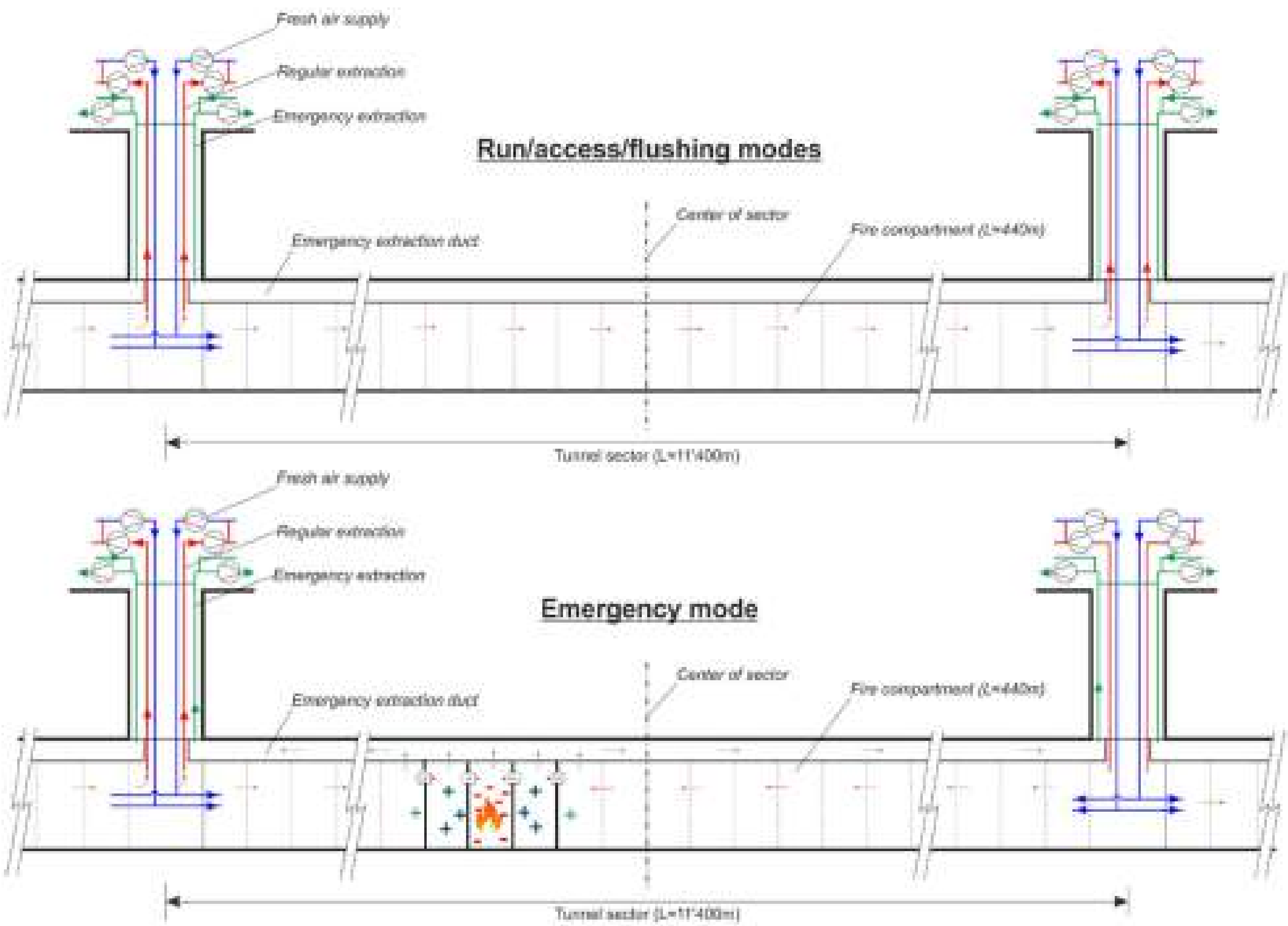

Fig. 9.4 Longitudinal ventilation mode (top) and emergency mode (bottom). The + and − signs illustrate the pressure cascade in the affected compartment and the adjacent ones

applying a force less than 70 N. Compensatory measures, such as installing pressure-breaking systems, sliding fire doors, etc., must be considered if such a risk is non-negligible.

A comparison of smoke extraction system performance with respect to life safety of occupants is discussed in Sect. 9.4.3.

Alcoves The electrical alcoves are ventilated through dedicated ducts, utilising the same system as the main tunnel. Emergency extraction is also available in these areas to support evacuation and intervention. However, due to the reduced evacuation distance inside the alcove, this system is not deemed necessary for the life safety of occupants; hence, it is not expected to be triggered automatically. However, in case of a fire, the smoke dampers must isolate the normal ventilation to prevent any propagation outside the compartment.

Experiment caverns The experiment caverns are ventilated by a dedicated system that also ensures dynamic confinement between the experiments and the accelerator tunnel, as well as providing the necessary airflow to ensure hygienic conditions and proper indoor air quality.

Several Computational Fluid Dynamics (CFD) analyses of CMS and ATLAS [439, 440], experiment detectors at the present LHC, have proven that the evacuation in experiment caverns can be safely performed without any active smoke extraction system due to their large volumes and relatively short evacuation distances. The FCC experiment caverns will be even larger, hence an active emergency extraction system for smoke is not required for life safety. However, the ventilation system should be able to support the extraction of cold smoke. In the case of particle (sub)detectors that require non-negligible amounts of cryogenic fluids, a risk assessment will be performed to determine if a dedicated gas extraction system is needed to cope with the Oxygen Deficiency Hazard (ODH).

Service caverns Service caverns are ventilated with a dedicated system that ensures dynamic confinement between the experiment cavern and the accelerator tunnel, as well as providing the necessary airflow to ensure hygienic

(a) Transport vehicle with 4 seats.

(b) Cross-section layout with the two vehicles passing each other within the 2.20 m transport zone.

Fig. 9.5 Personnel transport system [444]

conditions. Like the experiment caverns, a smoke extraction solution is required to support intervention and recovery time after a fire, but it is not deemed necessary for the occupants' life safety.

Safe areas & protected staircases As a basis for the safety concept, certain areas must be kept smoke-free. Consequently, safe areas, protected lift shafts, klystron gallery staircases, and personnel tunnels connecting service and experiment caverns will benefit from independent dynamic confinement. This over-pressurising system will, in general,[18] be fed fresh air and designed to guarantee its performance throughout the duration of the worst credible intervention case. Among other requirements, this implies that such a system must be supplied by a safety power network with fire-rated cables and redundant fans.

Surface buildings The surface buildings are ventilated by dedicated air handling units designed according to state-of-the-art best practices. Smoke extraction systems will be required for rooms with a floor area exceeding 300 m^2 (in France according to the 'Code de Travail' [441]) or 600 m^2 (in Switzerland according to AEAI DPI 21-15 [442]), in application of prescriptive design standards.

Personnel transport Due to the distances between the access shafts (11.4 km), occupants need to rely on a dedicated transport system to commute and evacuate the tunnel in an emergency. At any given time, the capacity of the personnel transport system available underground must ensure the evacuation of all occupants. The same transport system can be used during normal conditions for safe and efficient transport from the service caverns to workplaces along the arcs, with the possibility of parking the vehicles at the entrance of the alcoves and in the service caverns. In some situations, autonomous vehicles can go directly to the location of the workplace, drop-off the occupants (and material) before driving to the nearest alcove where it will stay parked until the end of the shift/activity. In contrast to the nominal scenario, during an emergency (i.e., evacuation alarm), the occupants are requested to walk towards the nearest safe alcove and take a seat in one of the parked vehicles.

The parking capacity for these vehicles will be ensured by the lay-by zones at the entrance of the alcoves. The baseline layout has parking spaces for up to 7 vehicles per alcove.

The simultaneous circulation of pedestrians and vehicles in the transport zone requires robust detection systems (e.g., stop in case of an obstacle or reduce speed near people or other vehicles) and a centralised communication system to ensure full autonomous driving.

The study included the feasibility assessment of an autonomous vehicle (Fig. 9.5) with a bi-directional drive. It is narrow enough to allow meeting traffic and bypassing of other vehicles within the 2.20 m wide transport zone of the cross-section [443].

The space on either side of a vehicle in the transport zone is ≈ 70 cm left and right. However, when two vehicles overtake or pass, the margin reduces to ≈ 20 cm [444].

[18] Alternative solutions might be studied case-by-case, such as using air from adjacent areas.

Personnel transport to and from the surface is ensured by at least two independent lifts situated in an overpressured elevator and stair compartment of the shafts. In the experiment points, two sets of two lifts are planned to provide the necessary reliability and ensure safe evacuation (see Sects. 9.4.1 and 9.4.4). As requested by the European Lift Directive and the associated harmonised standard [445], access hatches connecting a staircase to the lift shaft must be installed every 11 m for rescue purposes. The lifts must also conform with ISO 8100-1 [446].

Means of emergency response A simple scale-up of the current emergency response strategy in place for the LHC is not feasible due to the size of the infrastructure. A dedicated emergency preparedness and intervention concept will need to be developed in a subsequent design phase as well as a further extension of the existing Mutual Assistance Agreements with the Host States [447]. The feasibility study provided the basis and carried out an initial analysis of the concept. It consists of the following approach (see also Sect. 9.4.5):

1. A central emergency response coordination team.
2. First response from trained personnel.
3. Robotic intervention with firefighting capabilities.
4. On-site support from local emergency services, particularly for surface incidents.
5. Intervention from CERN Fire & Rescue Service (CFRS) and if relevant, other appropriately trained emergency services.

A dedicated approach is proposed for the installation and construction phases (see Sects. 9.5.2 and 9.5.3).

Secure power network Safety systems must maintain their functions at all times. A loss of the general electrical network, e.g., due to a power cut, would lead to a loss of electrically powered safety systems, hence the need for a secured power network to ensure the availability of safety systems at all times.

The secured power network is part of the global electrical network powered with backup sources in case the main power supply is lost, to allow the critical and safety-related loads to be powered at all times. To avoid duplicating medium voltage (MV) lines in the tunnel, it is proposed to optimise the infrastructure using the same MV link in the tunnel for powering general services and the secured network, applying a logic of load shedding in case of a power outage. The aim is to minimise the impact in the tightly integrated area and to avoid distributing the power at Low Voltage (LV), dedicated to safety systems, from the surface to the middle of the tunnel, due to the large cable distances that can induce high power losses and critical voltage drops [448].

Two backup sources are planned for the secured power network:

- A connection to an alternative public electrical utility.
- Emergency power supplies on each surface site.

In case of a failure, maintenance, or any other unavailability of the general service network, the electrical network is supplied using the backup power sources mentioned above. In this case, the couplings between the secured network and the general services network are automatically disconnected when the voltage from the main sources is no longer available. This logic of load shedding is used on the surface and underground, all the way down to the electrical alcoves, providing power only to the safety systems, leaving the other loads de-energised.

All active and passive components involved in the load shedding must be properly designed, maintained, inspected, and tested regularly to ensure a level of reliability which is consistent with that of the safety systems it serves. A description of the network and the single-line diagram is available in Ref. [448].

Access control Control of access to the installations at CERN today is based on several layers of protection, each one only allowing a more restricted number of people to enter. On-site access is permitted for identified affiliated personnel; entering a surface building housing an accelerator access point requires special authorisations, and finally, entering a beam facility is subject to the most rigorous control.

Before granting access to a beam facility, and once a user is identified, several database verifications are performed, which include:

- Authorisation is granted by the facility responsible to a person recognised by the organisation and with a professional need to access this facility.
- All mandatory and specific Safety training for the facility is valid.
- The activity has been declared and approved; the organisational unit in charge of works' coordination keeps a detailed list of planned and approved activities together with the assigned personnel, as well as a list of on-call personnel likely to intervene at short notice.

Access control, therefore, constitutes the first element in the chain of personnel safety systems, installed to protect the personnel and guarantee that only identified, trained, and authorised personnel enter the underground premises.

Access control is also used to ensure that the number of persons accessing the facility does not exceed the maximum number that has been set for safety or operational reasons. For example, the pressurised safe zones at the bottom of the shafts can only host a limited number of people in case of emergency. Therefore, once this number is reached, further access is blocked until some personnel leave the facility. Similarly, the limited capacity of the underground vehicle fleet limits the number of people allowed to enter, and this limit is also ensured by the access control system.

Access control is formed by two sets of access points; one at the surface and one underground.

Surface access points The access points at the surface, installed just before reaching the pressurised lifts, give access to the underground areas that are accessible in both beam and access modes, i.e., the service caverns and the klystron galleries.

These access points are composed of one or several personnel access devices (PAD) and a material access device (MAD). The devices are linked with commercial access control products, such as access rights and biometry databases, using computer networks and state-of-the-art human-computer interfaces.

A personnel access device (PAD) performs all the checks in one place. It is an inviolable barrier that guarantees that only one identified person can enter at a time. The user's identity is confirmed by a biometric check, relevant access authorisations are verified, and equipment checks (for example, possession of passive or active dosimeters) are performed. All these actions take place while the user is inside the PAD.

The PADs are built using commercial-off-the-shelf components, integrated to form one system, following the same principles that have been applied throughout the CERN accelerator complex for almost 20 years. Future PADs, although conceptually similar to the PADs of existing CERN accelerators, will leverage technological advances that can be seen, for example, in the domain of border control, with similar airlock-like booths installed in recent years at major international airports.

In addition to the PAD(s), each access point is equipped with at least one MAD. This device allows a safe way to bring bulky material in and out of the accelerator premises. The current concept uses a booth of the same size as the lift in the shaft. Its doors can only be operated from outside. After opening the doors on one side, the material is placed inside the device, the doors are closed and locked, and a scanning process ensures that no one is present within the device. Once scanning is completed successfully, the door on the other side of the MAD can be opened and the material removed. The MADs at existing CERN facilities are equipped with a combination of standard volumetric detectors and custom image processing algorithms. The MADs for a future project will certainly also benefit from technological advances, especially in the field of image processing.

Underground access points The service caverns are sufficiently shielded from radiation emitted, while the collider is operated with beams. However, access to the accelerator tunnels and experiment caverns requires passing through additional access points, which are interlocked with the presence of beams and other specific hazards. Constructed with the same components as their surface counterparts, the underground access points leading to areas subject to the presence of beams will thus form part of the Access Safety system.

Given the size of the FCC and the distance between two adjacent sites, the granularity of the access control system needs further enhancements. Having a detailed count of people inside the facility, as well as a good vision of their location within the facility, is important for safety. Individual tracking devices will be worn by all personnel entering the underground premises. Antennas distributed at regular intervals (in each alcove and throughout the access tunnels and service caverns) will allow the emergency response team to locate people within the underground complex.

Access safety system The Access Safety System is an interlock mechanism that acquires the status of and acts on elements important for safety (EIS) of two types: EIS-access and EIS-beam. It prevents the beam from being present at the same time as personnel. The EIS-access consists of the personnel and material access devices (access control components), emergency exit doors, movable shielding walls etc. The EIS-beam consists of accelerator components that can stop the circulation and the injection of beams. These components will include the beam dumps of the collider and the booster. Additional EIS-beam devices will allow redundancy for each interlock chain with technological diversity (e.g., a bending magnet or a moving stopper obstructing the beam aperture). A functional safety approach, e.g., following the IEC 61511 [449] standard, will be used throughout the lifecycle of the system.

The main functions of the Access Safety System include the following:

Search mechanism. After a prolonged operation with access, the machine volumes must be visually inspected for the absence of human presence. To facilitate this task, each site is divided with doors into smaller, more manageable units called access sectors. Once the patrol is completed, the search memory of each access sector is armed. The division of the FCC into access sectors takes into account the civil engineering constraints, accessibility of equipment, etc. Short accesses are thereafter permitted as long as personnel members are in possession of a safety token. Should an intrusion occur or unauthorised access take place without a token, the search of the corresponding access sector is disarmed, and a new patrol is required. Unlike the preceding accelerators, the patrol will be largely automated, with the long portions of the tunnel swept by a robot equipped with a camera. Algorithms to detect the presence of humans, combined with remote supervision, allow unambiguous confirmation of the absence of personnel.

Monitoring of *safe for beam* conditions. Whenever equipment is powered and there is ongoing or imminent injection or circulation of beams, the system monitors the state of all EIS-access. The moment the EIS-access quit their safe state, or there is a detected failure of the EIS-access equipment, the EIS-beam of the corresponding interlock chain is systematically and automatically activated to stop the beam.

Establishing *safe for access* conditions. Prior to permitting access to the FCC, the accelerator equipment is stopped using its conventional control system. The role of the access safety system is then to inhibit the possibility of starting the beam by interlocking the EIS-beam. Access can begin only when the interlock actions have been confirmed.

Monitoring of *safe for access* conditions. When access to the FCC is allowed, the safety system continuously monitors the state of the EIS-beam. Degradation of the protection barriers results in actions ranging from blocking access to launching evacuation and requesting the stoppage of an upstream accelerator that could potentially inject a beam in a downstream accelerator.

Establishing *safe for beam* conditions. In order to permit the operation of the FCC with beam, it must be empty of personnel and its search memories armed. To further secure the transition from access to beam operation, an audible warning signal will sound to announce the imminent injection of beams. The personnel are trained to press emergency power cut buttons if there is an audible beam imminent warning signal. Only once the warning has correctly sounded and no abnormal presence in the facility is detected will the conditions for removing the inhibition from EIS-beam be established.

Hazard detection The access safety system prevents any human entry into certain zones in case of radiation and electrical hazards by blocking access while the accelerators are operated or are about to be operated with beam. Access is only allowed when the beam is not present and when the pre-conditions for access are met. In addition, the access safety system monitors its own elements and launches evacuation alarms should a hazardous situation occurs.

However, even with a complete stop of beam operation, it is important to monitor the situation for other hazards. The principal ones identified for the FCC accelerator are fire, oxygen deficiency, and ionising radiation.

Fire detection system The Fire Detection (FD) system must satisfy the requirements resulting from fire risk studies. These imply generalised early fire detection. Several fire detection technologies meet this requirement, e.g., smoke detection with opacimeters or with laser beams. However, not all are well suited to be deployed in the FCC tunnel (low height, material obstructing lines of sight, electronics sensitive to ionising radiation). The baseline solution consists of equipping each alcove with aspirating smoke detectors (ASD). A variant – long range ASD (L-ASD) - which is suitable for the FCC, has been put in service at CERN in the SPS ring. It is capable of detecting aspirated smoke with a 100 m long sampling segment that can be extended by up to 700 m of non-sampling tube.

With the proposal of having alcoves every ∼1600 m, it is possible to install 16 L-ASDs in each alcove and aspirate air samples from the 800 m left and right of the alcove. Additional ASDs will be installed for detection within the alcoves themselves, as well as within the service and experiment caverns. Control and monitoring equipment racks, interconnected with optical fibres, will be installed in each alcove. All components of the fire detection system must meet the requirements of the applicable European standard, EN 54 [450].

It should be noted that this solution requires about 400 km of aluminium aspirating tubes. Should further analysis prove that having thermal detection is sufficient in terms of performance, newer technologies, more suited for long tunnels, will be considered. The thermal detection method most adapted to the accelerator environment consists of using distributed temperature sensing (DTS). It is based on optical fibre line-type temperature variation detection. This solution is particularly well-suited for long tunnel sections, where an integrator unit connected to an optical fibre pulled inside the 11.4 km tunnel segment can be installed in each service area. The spatial resolution of the detection is of the order of a few metres and the algorithms can trigger an alarm both in case of a temperature rise (fire) or a temperature drop (e.g., due to cryogenic leak) of a few degrees. However, the suitability of the technology in an environment with high levels of ionising radiation must first be proven.

Oxygen deficiency hazard The two technical sites PH and PL, where the superconducting RF cavities are located, require particular attention due to the presence of cryogenic coolants. Commercial oxygen deficiency hazard (ODH) detectors that are installed today in the LHC complex can be used to monitor the oxygen level in the vicinity of cryogenic installations at the two RF points of the FCC. They are based on electrochemical cell sensors installed inside the tunnel, connected to detector electronics which can be housed up to 900 m away. Signals from several detectors are then fed to the control and monitoring equipment rack.

Alternative detection techniques can be used (aspirating detector, fibre sensors etc.). In addition to oxygen level monitoring in precise locations, larger parts of the FCC could be monitored for a sudden temperature drop using the fibre-based distributed temperature sensing.

Radiation monitoring system A radiation monitoring system will be installed to measure prompt radiation levels at the interfaces to the accelerator tunnel, the experiment caverns, and the injector complex. These detectors are equipped with alarm functions that will signal any increased ambient dose equivalent rates. Radiation detectors will be installed at strategic locations in the tunnel and experiments to continuously measure residual ambient dose equivalent rates after beam stop.

Detectors will be installed to monitor the activation levels in the air of the tunnel. The radioactivity in the water circuits is expected to be negligible and will be checked during regular sampling campaigns. Air and water releases, radioactivity in the environment, and levels of stray radiation on surface sites will be surveyed by an environmental monitoring system with real-time monitoring where required.

Emergency call points

Manual call points Manual call points (break-the-glass devices) are installed throughout the facility. They will be on each side of an alcove entry door, as well as on each side of the fire partition doors in the tunnel. In addition, CERN best practices require placing manual call points at regular intervals in the tunnels, grouped with other safety equipment: emergency lights, evacuation loudspeakers, etc., fixed on easily identifiable modular panels.

Emergency communication system In the past, the CERN underground facilities have been equipped with emergency telephone sets (known as red-telephones). Based on analogue technology, the devices contain no active electronic components and could, therefore, be even placed permanently in areas possibly exposed to high levels of ionising radiation. Mobile phones come with more functions, for instance, precise localisation and video transmission, but they rely on a communication infrastructure that comprises electronic equipment, which is not radiation-hard.

Although the need for reliable, safe communication is clear throughout the complex, no decision has been made as to which specific technology is the most appropriate. The installation of fixed red-telephones could be one of the solutions. Having a leaky feeder cable with a fire-resistant jacket and circuit integrity properties (P_{ca}90-PH90, [451]), and fed by a secure power network, would allow emergency communication with mobile telephony services throughout the subsurface infrastructure. Today, this seems to be the most viable option. Such an approach could benefit from the developments required to provide secure data communication means to control autonomous vehicles as well as emergency surveillance robots. Moreover, this might also respond to the need for safe communication for interventions. In this case, its performance and reliability must be compatible with the intervention time (see Sect. 9.4.1), and some adaptations would be necessary (double loop, additional fire rating, etc.).

Evacuation alarms Whenever a hazardous situation (fire, oxygen deficiency, possible problem with access safety system) is detected, the concerned zones of FCC are evacuated. To this end, the FCC tunnel will be equipped with loudspeakers placed every $\sim$25 m connected to amplifier racks of a voice alarm system located in the alcoves.

The choice of voice alarm system is dictated by the added possibilities for emergency response teams to play pre-recorded messages or directly address the personnel underground with ad hoc instructions. An alternative solution, based on using more sparsely installed sirens, exists. Although less versatile, allowing only an evacuation siren with no accompanying voice messages, this solution is more suited to very large (e.g., experiment caverns) or noisy (e.g., compressor room) locations.

The system control and monitoring equipment racks, installed at regular intervals, acquire evacuation requests from the detection systems. The racks are connected by optical fibre and configured with appropriate evacuation matrices. Thus, in case of a hazardous event, evacuation is launched not only in the same location but also at other sites, as required by the evacuation matrices. This is possible as the control racks communicate between themselves. The components of the evacuation system must be compliant with the appropriate European standard EN 54 [450].

Due to the circular shape of the underground structure, most locations can be evacuated in two directions. However, in emergency situations, evacuating personnel can often use only one of the two possible escape routes. Despite the fact that most personnel movements (including evacuation) will be made using autonomous vehicles, all alcoves and fire compartment doors will be equipped with adaptable direction signage. It must clearly indicate the direction in which to go to escape a detected danger.

Emergency lighting and route guidance All of the underground facility is equipped with emergency lighting as defined in the corresponding CERN safety guideline [452]. This includes:

- A general ambient safety lighting, ensuring at least 5 lux (lm/m^2) at floor level,
- Marked evacuation routes (exit ways, doors, direction) with illuminated and luminescent signs. This wayfinding (guidance) system will also be dynamic and inform occupants if an evacuation way is no longer safe (for example, smoke presents in adjacent compartment).